DEVELOPMENT OF AN ELECTROSTATIC LINEAR ION TRAP FOR TANDEM MASS SPECTROMETRY

by

Joshua T. Johnson

A Dissertation

Submitted to the Faculty of Purdue University

In Partial Fulfillment of the Requirements for the degree of

Doctor of Philosophy

Department of Chemistry

West Lafayette, Indiana

May 2020

THE PURDUE UNIVERSITY GRADUATE SCHOOL

STATEMENT OF COMMITTEE APPROVAL

Dr. Scott McLuckey, Chair

Department of Chemistry

Dr. Peter Kissinger

Department of Chemistry

Dr. Mingji Dai

Department of Chemistry

Dr. Julia Laskin

Department of Chemistry

Approved by:

Dr. Christine Hyrcyna

Dedicated to the friends and family who inspire me every day.

ACKNOWLEDGMENTS

I would first like to thank my family for providing me constant support and unconditional love. My parents, Sean and Shelley, and my sister, Jade, are a source of joy from which I can draw when things get tough. I want to thank my wife for standing by me during this journey. I would also like to thank the Grayson family who have been immensely kind to me and I am proud to be part of their family. My dog Luna also merits a thanks as she brings a smile to my face every day.

While at Purdue, I had the privilege to work with several great people and scientists. First and foremost, Professor Scott McLuckey provided me with a learning environment in which I could grow as both a professional and as a researcher. He supported my ideas and was always willing to provide feedback. His openness to talk and provide guidance was one of my favorite aspects of him as well as the group in general.

I want to offer a special thanks to the Jonathon Amy Facility for Chemical Instrumentation (JAFCI), and specifically, Mr. Gregory Eakins, Dr. Ryan Hilger, Ms. Cathy McIntrye, and Mr. Randy Replogle. Each of you played a crucial role in my research. The Amy facility is an integral part of the analytical program at Purdue and plays a large role in the success of the department.

Throughout my time in the McLuckey lab, I have worked with many gifted scientists and have created great friends. Dr. Eric Dziekonski was my mentor who taught me a lot about mass spectrometry and what it takes to be a good scientist. I was eager to jump into research when I first joined the group, and you patiently taught me the ropes and answered my questions. Your mentorship meant more than you know, and I am truly thankful. Congratulations and thanks to my fellow classmates, Dr. David Foreman, Dr. Chris Harrilal, and Dr. Elissia Franklin. You all are great scientists and friends who I will miss dearly. To those that came before me, Dr. Andrew DeBlase, Dr. Alice Newman (Pilo), Dr. Stella Bentacourt, Dr. Jiexun Bu, Dr. Mack Shih, Dr. Nan

Wang, and Dr. Feifei Zhao, I want to thank you for your helpful discussions and insight. To the younger students, John Lawler, Kenneth Lee, Anthony Pitts-McCoy, Caitlin Randolph, Abdirahman Abdillahi, Jay Bhanot, His-Chun Chao, Ian Carrick De'Shovon Shenault, Kimberly Fabijanczuk, Nicole Brundridge, Liangzuan Fu, and Sarah Nsiah, I have enjoyed watching each of you grow as scientists and wish you all the best of luck in graduate school. I urge you to embrace the learning process and to put your mark on the strong mass spectrometry tradition at Purdue.

I want to give a special thanks to Dave Foreman for being a genuinely good friend. He listened to me complain and gave me some great advice along the way. We have had some great scientific conversations in which we both come out of the conversation feeling smarter. We have also had some conversations after which we both questioned each other's intelligence. In the end, I could always count on you to talk and "go grab a bit to eat".

Special thanks should also go out to my good friends Chris Harrilal and Jeremy Manheim. Chris thanks for getting up early to lift and co-founding the field of flexomics. I'll see you at the tan and green benches in the Corec. I'll be with Dave. Jeremy, even though you lived in the attic and I in the basement during graduate school we remained great friends. You and Juliet are both awesome and have infectious personalities. Thanks for the game nights which were a welcomed distraction from lab.

TABLE OF CONTENTS

LIST OF FIGURES

LIST OF ABBREVIATIONS

AcOH	Acetic Acid
CDMS	Charge Detection Mass Spectrometry
CHEF	Correlated Harmonic Excitation Field
CID	Collision Induced Dissociation
CMOS	Complementary Metal-Oxide-Semiconductor
DC	Direct Current
DNA	Deoxyribonucleic Acid
EDTA	Ethylenediaminetetraacetate
eFT	Enhance Fourier Transform
ELIT	Electrostatic Linear Ion Trap
ESI	Electrospray Ionization
FT	Fourier Transform
FT-ELIT	Fourier Transform Electrostatic Linear Ion Trap
FT-ICR	Fourier Transform Ion Cyclotron Resonance
FT-MS	Fourier Transform Mass Spectrometry
FWHM	Full-Width at Half-Maximum
H_2O	Water
IC	Integrated Circuit
IRMPD	Infrared Multiphoton Photodissociation
JAFCI	Jonathon Amy Facility for Chemical Instrumentation
JFET	Junction Field Effect Transistor
KE	Kinetic Energy
LC	Liquid Chromatography
MCP	Microchannel Plate
MeOH	Methanol
MR-TOF	Multiple-Reflection Time-of-Flight
MS	Mass Spectrometry

MS/MS	Tandem Mass Spectrometry
m/z	Mass-to-Charge Ratio
nESI	Nanoelectrospray Ionization
PC	Phosphocholine
PEIT	Planar Electrostatic Ion Trap
QLIT	Quadrupole Linear Ion Trap
RF	Radio Frequency
SAM	Self-Assembled Monolayer
SID	Surface Induced Dissociation
SWIFT	Stored Waveform Inverse Fourier Transform
TFS	Time Focus Shifting
TOF	Time-of-Flight
TOF/TOF	Tandem Time-of-Flight
TTL	Transistor-Transistor Logic
UVPD	Ultraviolet Photodissociation

ABSTRACT

The electrostatic line ion trap (ELIT) is a relatively new type of mass analyzer in which ions are axially confined between two opposing ion mirrors. Image charge induced on a central pick-up electrode can be digitized, mass analyzed, and calibrated to produce a mass spectrum. Recent improvements to the ELIT and the development of a novel high resolution, high efficiency ion isolation method have given new life to the use of the ELIT as high-performance tandem mass spectrometer. This dissertation outlines advancements in all areas of tandem mass spectrometry (ion isolation, probing ions, and mass analysis) using an electrostatic linear ion trap.

An introduction to the ELIT and the analytical techniques associated with the device is discussed in Chapter 1. Next, Chapters 2 and 3 discuss innovations in the realm of mass analysis using an ELIT. Following discussion of the mass analyzer, Chapter 4 discusses a novel high resolution, high efficiency method for ion isolation. Chapter 5 then discusses an extension of the fore-mentioned ion isolation method in which multiple ions can be isolated simultaneously. Finally, Chapter 6 discusses tandem mass spectrometry experiments that have been done with the current iteration of the ELIT.

In Chapter 2, the ELIT was configured to allow for the simultaneous acquisition of mass spectra via Fourier transform (FT) techniques (frequency measurement) and via time-of-flight (TOF; time measurement). In the former case, the time-domain image charge derived from a pick-up electrode in the field free region of the ELIT is converted to frequency-domain data via Fourier transform (FT-ELIT MS). The ELIT geometry facilitates the acquisition of both types of data simultaneously because the detection schemes are independent and do not preclude one another. The two MS approaches exhibit a degree of complementarity. Resolution increases much faster with time with the MR-TOF approach, for example, but the closed-path nature of executing the

MR-TOF in an ELIT limits both the *m/z* range and the peak capacity. For this reason, the FT-ELIT MS approach is most appropriate for wide *m/z* range applications, whereas MR-TOF can provide advantages in a "zoom-in' mode in which moderate resolution ($M/\Delta M_{fwhm} \approx$ 10,000) at short analysis time (10 ms) is desirable.

In Chapter 3, the mass resolution of the FT-ELIT experiment is increased by reducing the axial length of the ELIT. Mass resolution increases linearly with frequency. For an equivalent transient length, which implies an equivalent path length, resolution is higher in a shorter ELIT. Relative changes in the *m/z* range were also explored. When trapping ions using mirror switching, the *m/z* range is determined by the time required for fast ions to enter and exit the trap (one reflection), and the time it takes slow ions to enter the trap. By reducing the length of the FT-ELIT mass spectrometer while maintaining a constant distance from the point ions are initially accelerated to the first ion mirror, only the low *m/z* limit is affected for a given mirror switching time. Both a 2.625" and a 5.25" trap will be examined and compared.

In Chapter 4, ion isolation was achieved via selective pulsing of the entrance and exit ion mirrors in an electrostatic linear ion trap mass spectrometer. In addition to ion capture, mirror switching can also be used as a method for ion isolation of successively narrower ranges of mass-to-charge (*m/z*) ratio. By taking advantage of the spatial separation of ions in an ELIT device, pulsing of the entrance and/or exit mirrors can release unwanted ions while continuing to store ions of interest. Furthermore, mirror switching can be repeated multiple times to isolate ions of very similar *m/z* values with minimal loss of the stored ions. As isolation is accomplished due to the spatial/temporal separation of ion packets within the ELIT, multiple MR-TOF spectra are shown to demonstrate separation in the ELIT at the time of isolation. An isolation resolution of greater than 36,000 is demonstrated here using a 5.25" ELIT. This resolution corresponds to the

fwhm resolution necessary to reduce contaminate overlap of an equally abundant adjacent ion to 1% or less of the isolated ion intensity.

In Chapter 5, advantage is taken of the ion overlapping phenomenon in an ELIT to enable the simultaneous isolation of ions of disparate *m/z* ratios using mirror switching. This process is demonstrated with minimal ion loss using the isotopologues of three carborane compounds ranging in *m/z* from 320 to 1020. Simultaneous isolation is demonstrated with the isolation of two and three peaks in separate isotopic distributions as well as with isolation of alternating isotopologues within the same distribution. Such simultaneous isolation experiments are particularly useful when conducting experiments in which a mass calibrant is needed or when multiplexing in a tandem MS workflow.

Chapter 6 discusses the use of the current ELIT as a tandem mass spectrometer. Tandem mass spectrometry (MS/MS or MS^n) is the sequential mass spectrometric analysis of analyte ions. Product ions are often informative and can provide information about the structure and identity of the precursor ion. The use of the electrostatic linear ion trap as both a tandem-in-space and tandem-in-time mass spectrometer is demonstrated. The quadrupole linear ion trap (QLIT) located colinear to the ELIT can be used for apex isolation, collision induced dissociation (CID), and ion acceleration for mass analysis in the ELIT. As a tandem-in-space device, isolation and CID are accomplished in the QLIT prior to product ion analysis in the ELIT. When operated as a tandem-in-time mass spectrometer, mirror switching can be used for high resolution, high efficiency isolation. Post-isolation, ions are subjected to surface induced dissociation using a gold disk placed directly behind plate 8. Ions still within the kinetic energy focusing range of the ELIT after fragmentation are re-trapped for product ion analysis.

CHAPTER 1. INTRODUCTION TO MASS SPECTROMETRY USING AN ELECTROSTATIC LINEAR ION TRAP

1.1 Background

Since the advent of mass spectrometry by Dr. JJ Thomson,[1,2] mass spectrometry has become increasingly important in many facets of analytical science. Much mass spectrometry (MS) research currently involves the analysis of biological ions with a wide variety of molecular weights. Mass analyzer research provides improved analytical figures-of-merit through technological advancement. Advances in many tangential fields such as electronics, precision machining, and computer sciences also impact MS advancement and thus the challenges that can be addressed using MS. Continuing to develop and implement new technologies and strategies surrounding the quality of mass measurement will ensure the growth of mass spectrometry and the problems that can be solved using MS for years to come.

1.2 Electrostatic Linear Ion Traps

The electrostatic linear ion trap was first developed as an alternative to heavy ion storage rings in 1997 by Dr. Daniel Zajfman at the Weizmann Institute.[3] In an electrostatic linear ion trap (ELIT), ions oscillate between two axially symmetric electrostatic ion mirrors in a manner analogous to the oscillation of light in an optical resonator such as those used in lasers. Dr. Zajfman's research using his electrostatic trapping device focused on measuring the neutralization of ions after collisions with a bath gas overtime. After neutralization ions would exit the ELIT and impinge open an external detector for measurement. Concurrently with the design of the ELIT designed by Zajfman, Dr. Henry Benner was utilizing an electrostatic storage device for the repeated measurement of *m/z* and charge for absolute mass determination.[4] His trap utilized a

central pick-up electrode for measurement of induced image charge and ion velocity. The Benner ELIT was being utilized for charge detection mass spectrometry (CDMS) a method useful for mass determination of large ion species. Zajfman later modified his ELIT to include a central pick-up electrode such that the image charge of ion populations could be measured overtime. The resulting spectrum of induced image charge as a function of time could then be fast Fourier transformed to produce a frequency spectrum. Since ions with different *m/z* produce different frequencies, the electrostatic linear ion trap can be used to analyzed mixtures of ions thus making it amenable to the field of mass spectrometry.

Since the advent of the dual-mirror electrostatic linear ion trap much research has been done on how this design can be utilized for both *m/z* and absolute mass measurement. Through the years this electrostatic storage device has gone by many names; however, in this discussion the device will be term an electrostatic linear ion trap (ELIT). An example of the device utilized throughout my research is shown below (Figure 1.1).

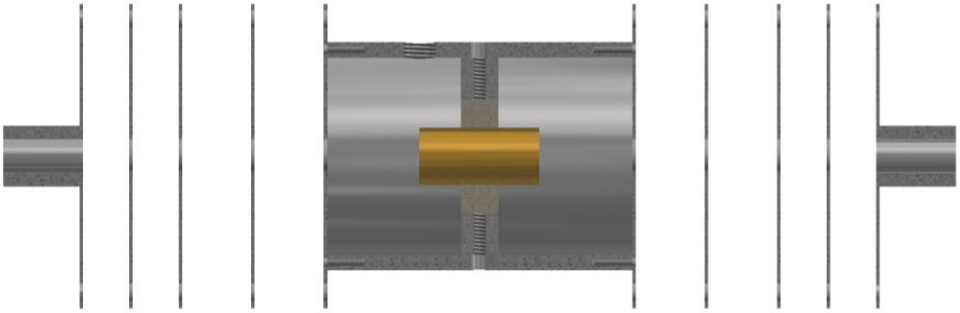

Figure 1.1. Dual-mirror electrostatic linear ion trap with parallel plate ion mirrors as introduced by Zajfman, et al. used in the McLuckey Lab.

This device allows for mass analysis using a variety of methods including, but not limited to, Fourier transform mass spectrometry (FT-MS), multiple-reflection time-of-flight mass spectrometry (MR-TOF), and charge detection mass spectrometry (CDMS). These traps are not limited to terminal mass analysis, however and recent advancement have been made in the realm of collisional cross section measurement, ion isolation, and tandem mass spectrometry. This chapter will act as a primer for the use and operation of the ELIT and should provide a theoretical basis for the rest of this dissertation.

1.3 Geometries

Figure 1.2 depicts a parallel plate, dual ion mirror, electrostatic linear ion trap with a central pick-up electrode for image charge detection.[4-10] This geometry has been widely adopted due to the ease in which the potential curvature can be adjusted by changing the individual plate voltages. The number and thickness of the electrodes can vary between devices. With the overall length ranging from 10 cm to 1 m. Using more plates allows for better approximation of an ideal parabolic field which is used to focus a range of ion kinetic energies into isochronous motion; however, as the number of electrodes increases, the complexity of tuning space also increases. The potential

surface for the ELIT used in much of the research presented in this thesis is shown in Figure 1.2. Ions are axially confined via the electrostatic retarding field; however, to due to the LaPlace condition, ions must be confined radially via an additional einzel element normally located between the central housing and the ion mirror. In order to maintain stable ion trajectories within the device the focal length set by the ion mirror and einzel elements must satisfy equation 1.1.[3,11]

$$\frac{L}{4} \leq f_L \leq \infty \qquad (1.1)$$

Where L is the length of the trap and f_L is the focal length.

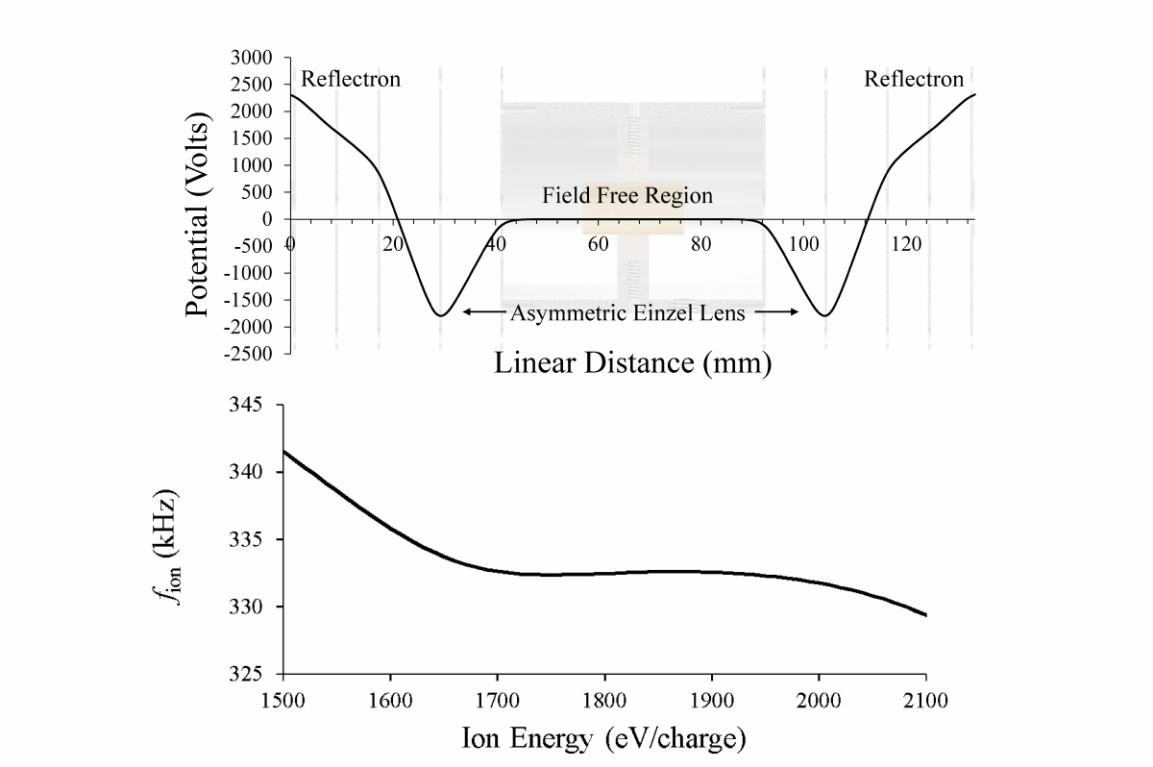

Figure 1.2. (A) Typical potential energy profile along the axis of the Fourier transform electrostatic linear ion trap utilized in the McLuckey Lab for high resolution mass analysis. (B) Simulated relationship between an ions kinetic energy and measured frequency in an ELIT. Ions in the ELIT have a nominal trapped kinetic energy of ~1960 eV/charge.

Another common ELIT geometry is the Conetrap which was introduced by Schmidt in 2001.[12] Each cone electrode is used to trap ions axially and the potential difference between the cone electrode and the central housing is used for radial trapping. Due to the reduced number of elements, this geometry is simpler to tune however the cone-trap suffers from lower ion frequencies and a lower accepted kinetic energy range. Conversely, the Conetrap has a wider accepted angular divergence upon ion injection.[13] The inability to tune the electric field near the ion turning point hamper the kinetic energy focusing of this device. By using a kinetic energy filter prior to ion introduction into the device, the small kinetic energy focusing range can be

circumvented. This type of ELIT is commonly used in charge detection mass spectrometry where a single energy selected ion is analyzed.[13-16]

Several atypical electrostatic ion trap geometries exist and have been used for a variety of reasons. A dual detector electrostatic linear ion trap has been used for frequency multiplying experiments. This geometry takes advantage of two off-axis detection electrodes which effectively quadrupled the detected ion frequencies, albeit with amplified harmonic overtones. Bent electrostatic ion trap also exist and have been used in measurements of both charged and neutral fragments as well as determination of the kinetic energy distribution released upon dissociation.

A planar electrostatic ion trap (PEIT) was recently introduced by Ding et. al. and functioned by taking the y-z plane of the ELIT and rotating it about the y-axis of the trap centered at the detector.[17,18] This trap was developed to reduce the magnitude of space charge conditions in a purely linear device by distributing ions in a plane. This dissertation will focus on electrostatic ion trap with a purely linear geometry.

1.4 Ion Injection

In order to analyze ions while utilizing the ELIT as a mass spectrometer, a narrow ion packet must be injected into the device. The optimal width of the ion packet depends on the application of the research as well as various other factors such as trap dimension, space charge limits, background noise, and required resolution.

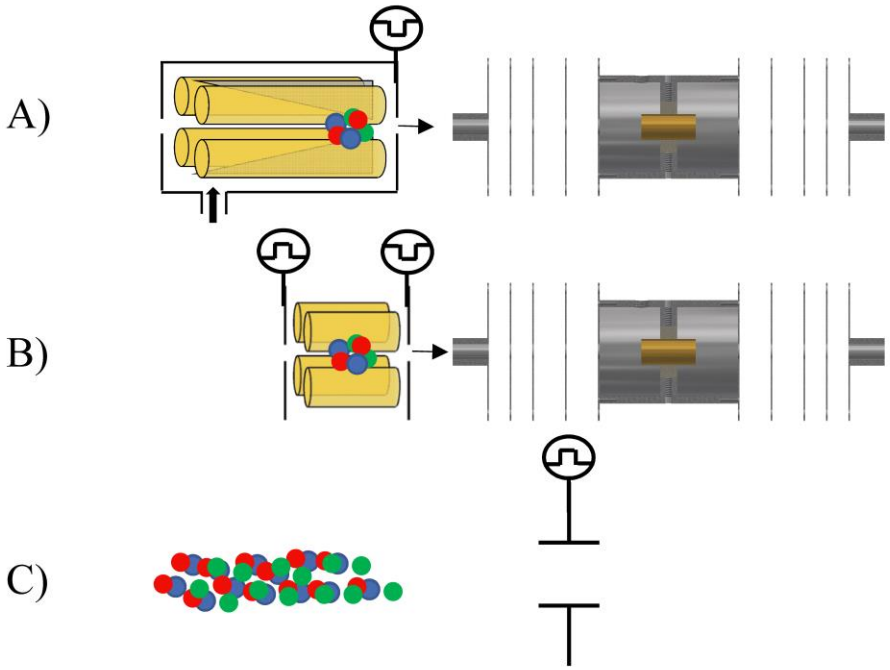

Figure 1.3. Methods in which ions can be injected as an ion packet into an ELIT. (A) Quadrupole with the ability to generate an axial field. (B) Brubaker lens using push-pull ion extraction. (C) Extraction of ion from a continuous ion beam using a pulsed drift tube.

Figure 1.3 illustrates three of the numerous different methods in which ions can be injected into the ELIT as a packet. (A) A quadrupole which can generate an axial field can also be used to spatially confine ions at one end of the trap.[19] Axial field can be generated in a quadrupole using several methods including tilted rods, segmented quadrupoles, wire electrodes, and LINAC II electrode[8,9,20-29] (used throughout this dissertation). By gating the endcap lens the ion packet can be injected into the ELIT with a full-width at half-maximum (FWHM) of 100 nanoseconds to microseconds. (B) Ions can also be trapped and thermalized in a short quadrupole also known as a Brubaker lens or a three-dimensional ion trap.[30] Due to the short geometry of these traps, ion packets can be extracted in a push-pull manner. This method provides a high degree of flexibility in the kinetic energy and temporal width of the injected ion packet. Push-pull injection is

commonly used in the MR-TOF community to generate very narrow ion packets (10-50 nanoseconds)[10, 31-38], thus generating high resolution mass spectra very rapidly. (C) A pulsed drift tube can be used to generate ion packets by puling from ground to a higher voltage while a continuous beam of ions is travelling through the drift tube. In this way, a narrow section (~100 ns) of the beam can be cut out of and accelerated to the trapping region.[39]

1.5 Methods for Ion Capture

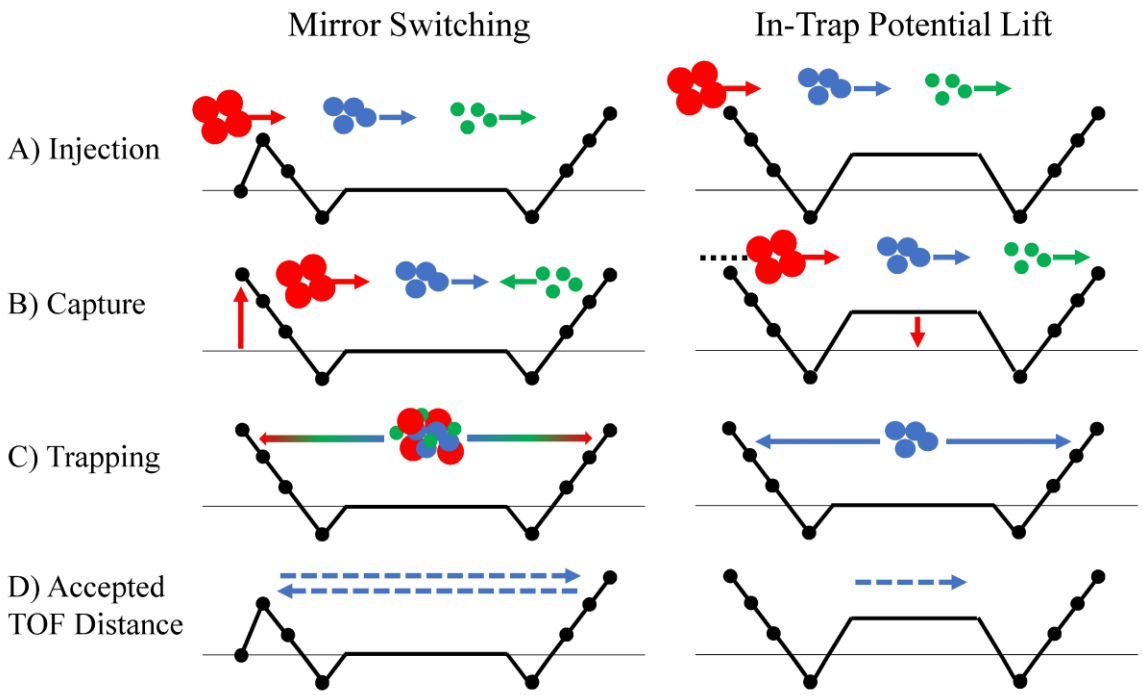

Figure 1.4. Representation of ion capture using a parallel plate electrostatic linear ion trap via mirror switching (left) and potential lift (right). The y-axis is total energy (potential + kinetic) and the x-axis is axial position. The black dots represent the potentials applied to each plate of the ion mirrors. The red, green, and blue dots represent ions of different *m/z*. Only ions within the accepted time-of-flight region (blue dashed arrow) when either mirror switching, or potential lifting occurs are trapped.

There are currently two methods for capturing externally generated ion packets in an ELIT (Figure 1.4): mirror switching[8,15,25,34,40] and in-trap potential lift[23,32,41,42]. To trap ions using mirror switching, ions must be injected with an energy less than that of the rear ion mirror (A). One or more of the entrance mirror electrodes are held at a voltage lower than that of the ions such that once the ion-of-interest are within the device, the entrance electrodes can be pulsed to their nominal trapping potentials (B) after which they remain trapped (C) until they are lost due to ion-neutral collisions. To capture ions via in-trap potential lift, all plate voltages are held at the trapping potentials and ions are injected with enough energy to overcome the electrostatic barrier of the plates (A). When the ion-of-interest is within the region of some internal lift electrode the potential is switched to ground such the energy of the ion of interest is lowered such that it is no longer able to overcome the electrostatic barrier of the ion mirror (B) where it remains trapped (C) until it is lost due to ion-neutral collisions. The accepted time-of-flight length of each capture method is indicative of the mass range for each method and it is clear even from the cartoon illustration of the two methods that mirror switching has a larger accepted time-of-flight given traps of similar geometries (D). This results in a larger *m/z* range when using mirror switching when compared to in-trap potential lift. An extensive *m/z* range is particularly important when looking at biological samples with multiple charge states. However, potential lift has it's uses as it does not suffer from capacitive loading that occurs in mirror switching experiments.[9,23,32,41]

1.6 Ion Isolation

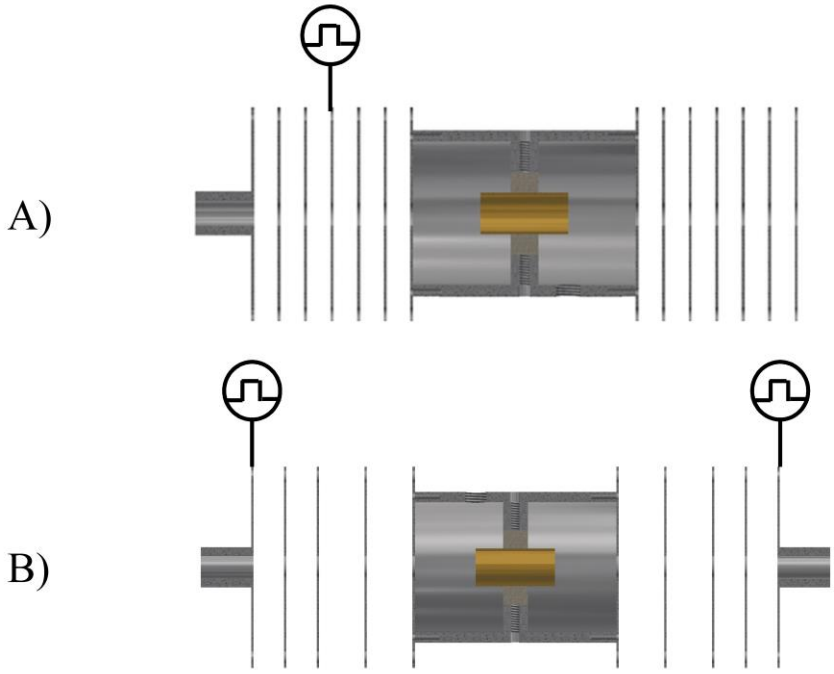

Figure 1.5. Two methods of in-trap ion isolation are possible using an ELIT, frequency modulation (A) and mirror switching (B). Shown here are two ways in which these methods have been implemented on the ELIT in the McLuckey lab.

1.6.1 Frequency Modulation

A variety of isolation methods can be utilized using an ELIT. These methods take advantage of either ion frequency differences or spatial separation. While inherently related, frequency modulation utilizes nominal differences overtime while spatial separation isolates ions based on instantaneous temporal differences. In 2009, Zajfman introduced kick-out mass selection using an internal electrode pulsing from ground to 100V at the frequency of the ion-of-interest and phase locked to the ion injection.[32,35,43] In this way, ions that were outside of the frequency of the ion-of-interest are eventually subjected to the pulsed potential and therefore are moved outside of the kinetic energy focusing regime of the trap. When the ion-of-interest passed through the pulsing

electrode, the nominal voltage was always ground and therefore this ion remained trapped for the duration of the experiment. Using this method, Zajfman achieved isolation resolution of approximately 100 after 19.3 ms. Using a similar motif, Dr. Ryan Hilger conducted ion isolation by frequency modulation in which an electrode that was grounded could be switch to 600V at the ion-of-interests lap frequency (Figure 1.5A).[24] Using this method, ions at different frequencies that were not sufficiently focused in the ELIT and therefore were no longer trapped. Using this frequency modulation of a single electrode, isolation resolutions of approximately 200 were achieved after 670 μs. Recently, Fischer et. al. demonstrated isolation resolutions of 40,000 using a dual deflector setup in which two cylindrical electrodes where modulated at the frequency of an ion-of-interest.[44,45]

Another method by which ions can be isolated is via the re-trapping in an external quadrupole in which the m/z acceptance window of the external quadrupole is dictated by the potential well ions experience when exiting the ELIT.[46] Using this method isolation resolution of 70,000 resolution were achieved albeit with 35% efficiency. Once isolated by recapture, ions can be thermalized and re-injected into the ELIT for post-isolation mass analysis.

1.6.2 Mirror Switching and Gating Methods

Alternatively, ions can be isolated based on their instantaneous temporal separation at any point during trapping.[28,29] The linear geometry of the device is convenient, as ion injection and release can occur via the same or opposite ion mirrors (Figure 1.5B). In this way, the range of trapped *m/z* values within the device can be dynamically reduced such that only a single ion species remains trapped. Isolation resolution of up to 36,000 with high efficiency (>90%) have been demonstrated using this method and will be discussed further in Chapter 3. Alternatively, ions can be separated temporally and released from the device, where they are then isolated using an external deflector.[8] The ion-of-interest is then re-trapped in the accumulation quadrupole before being re-injected into the device.

1.7 Tandem Mass Spectrometry and Dissociation Methods

The ELIT has the capability to act as either a stand-alone tandem mass spectrometer (tandem-in-time) or as coupled system in which ion isolation and dissociation occur in a quadrupole and mass analysis is done in using the ELIT (tandem-in-space). Thus, making the ELIT amenable to a variety of methods to probe ion species and produce structurally informative product ion species. The ways in which an ELIT can be utilized as a tandem mass spectrometer will be discussed in detail in Chapter 6.

1.8 Mass Analysis

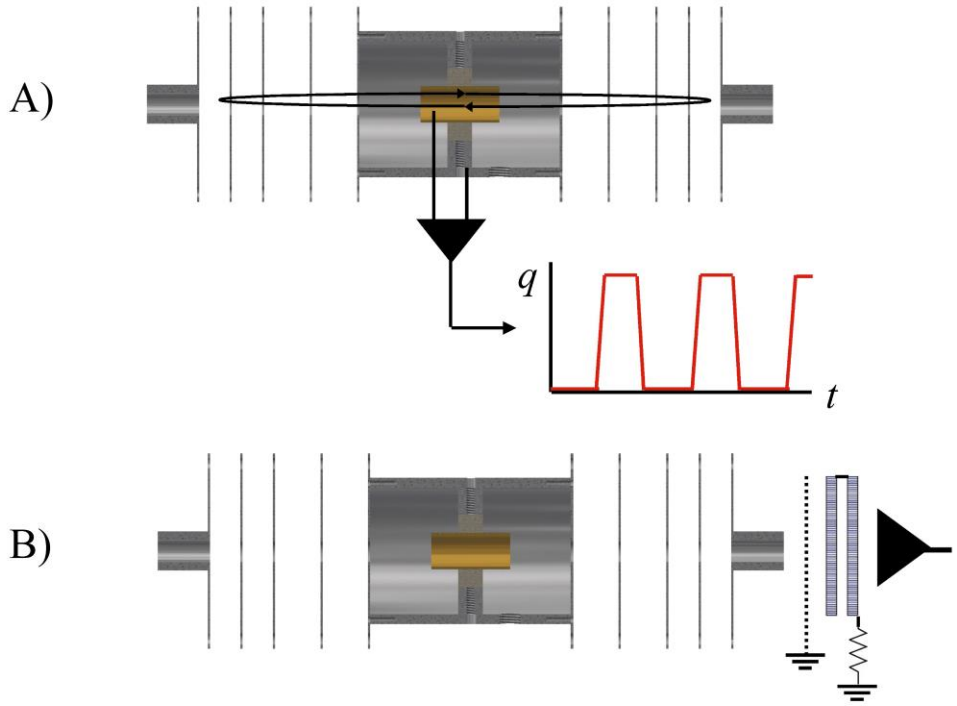

Figure 1.6. Methods used to detect ions in an ELIT. (A) Image charge or image current detection on a central pick-up electrode. When ion trajectories and trap geometry are considered, the generated signal corresponds to a trapezoidal pulse train rather than a sinusoid. (B) External detection using a microchannel plate detection. This method can be used for time-of-flight measurements.

1.8.1 The Fourier Transform

Using the Fourier transform any smooth, periodic, time-domain signal can be decomposed into its individual frequency components along with each component's amplitude and phase.[47] The continuous Fourier transform is expresses via equation 1.2

$$f(\omega) = \int_{-\infty}^{\infty} F(t) \cdot e^{-i2\pi pt} dt \qquad (1.2)$$

where $f(\omega)$ is the complex, frequency domain Fourier transform of the time domain signal $F(t)$, i the imaginary unit, and p is the real frequency. Because in the time domain signal in FT-MS is sampled at fixed interval f_s, the discrete Fourier transform can be used and is defined below.

$$f(\omega) = \sum_{n=0}^{N-1} F(t) \cdot e^{\frac{i2\pi pn}{N}} \tag{1.3}$$

Where n is the time point and N_s is the number of time domain sampling points. The frequency bin spacing is determined by the transient length (sampling time), the number of time domain samples, the sampling interval T, and the sampling frequency f_s. This is expressed in equation 1.4 and is directly related to the Fourier transform uncertainty principle shown in equation 1.5.

$$\Delta f = \Delta p = \frac{1}{T_0} = \frac{1}{N_s \cdot T} = \frac{f_s}{N_s} \tag{1.4}$$

By measuring more cycles of a waveform in time, the accuracy of the frequency measurement increases. The Fourier transform uncertainty principle, which shows the relationship between the frequency uncertainty (Δf) and time uncertainty (Δt) is shown below.

$$\Delta f \Delta t \geq 1 \tag{1.5}$$

To reach maximum resolutions in FT-MS, space charging and device pressure should be reduced such that ion signal can be detected for as long as possible. The maximum resolving power achievable in an ELIT for a given ion frequency is expressed in equation 1.6 and occur when a frequency can be perfectly measured from an undamped waveform. In this case the spectral linewidth is exactly equal to the bin spacing.[48]

$$R_{max} = \frac{m}{\Delta m_{50\%}} = \frac{1}{2}\frac{f}{\Delta f_{50\%}} = \frac{f}{2 \cdot (1/T_0)} = \frac{f \cdot T_0}{2} \tag{1.6}$$

The Fourier transform is a complex transformation that produces both real and imaginary components which are linear combinations of the absorption $(A(\omega))$ and dispersion $(D(\omega))$ mode spectra as defined below.[20]

$$Re[f(\omega)] = A(\omega) \cdot \cos[\varphi_0(\omega)] + D(\omega) \cdot \sin[\varphi_0(\omega)] \quad (1.7)$$

$$Im[f(\omega)] = D(\omega) \cdot \cos[\varphi_0(\omega)] - A(\omega) \cdot \sin[\varphi_0(\omega)] \quad (1.8)$$

Expressed this way, the rectangular coordinate shows initial phase as a function of angular frequency; however, this can be expressed in terms of the more recognizable polar coordinates magnitude $(M(\omega))$ and phase $(\Phi(\omega))$ as is shown below.

$$M(\omega) = \sqrt{(Re[f(\omega)])^2 + (Im[f(\omega)])^2} \quad (1.9)$$

$$\Phi(\omega) = tan^{-1}\left(\frac{Im[f(\omega)]}{Re[f(\omega)]}\right) \quad (1.10)$$

Many FT-MS spectra take advantage of only the magnitude information; however, resolution[49-52,] and mass accuracy[53,54] can be increased by utilizing the phase of the ions using absorption mode spectra which is expressed in equation 1.11.

$$A(\omega) = Re[f(\omega)] \cdot \cos[\varphi_0(\omega)] - Im[f(\omega)] \cdot \sin[\varphi_0(\omega)] \quad (1.11)$$

Difficulty arises when determining the initial phase of ions. Fourier transform – Ion cyclotron resonance (FT-ICR) mass spectrometry primarily relies on algorithms and experimental methods to determine phase as ions are excited in a sequential fashion.[49,52-58] Alternatively, in Orbitrap[59] and ELIT[20] experiments, ions are excited via injection and therefore the initial phase of ions is determined by the time at which they are injected for mass analysis. Determination of phase simply from injection time can be imperfect; however, due to deviation from linearity in ion extraction.

Because the Fourier transform assumes all frequencies are present at equal amplitudes, real-life measurements of exponential damped transients results in spectral leakage which manifests itself as side-lobes in absorption mode spectra. One method to circumvent spectral leakage while still obtaining the higher resolution of absorption mode spectra is a technique called enhanced Fourier transform (eFT).[59] Introduced by Lange et al, a synthetic spectrum is generated via a linear combination of the magnitude and absorption mode spectra. Thus, the resulting spectrum is more absorption mode on the top 50% of the peak and more magnitude mode on the bottom 50% of the peak.

1.8.2 Fourier Transform Mass Spectrometry

When compared to other mass analysis techniques, Fourier transform mass analysis provide unparalleled mass resolution. High mass resolution is particularly important when analyzing particularly complex mixtures such as crude oil or biological mixture which contain thousands of compounds with varying charge states, isotopes, adducts, and ion types. High mass resolution and mass accuracy can be used to determine molecular compositions using programs which consider mass defect and isotope ratios.

Fourier transform – Ion cyclotron resonance (FT-ICR) mass spectrometry offers the highest resolution of any mass spectrometer.[49,60-63] Invented in 1974[50,64], FT-ICR operates by ions within a magnetic field and measuring their inherent cyclotron frequency as a function of time. This cyclotron frequency is proportional to the magnetic field strength (equation 1.12)[65]

$$f_c = \frac{\omega_c}{2\pi} = \frac{q}{m}B \qquad (1.12)$$

Where f_c is the cyclotron frequency in Hz, ω_c is the ion cyclotron angular frequency, B is the magnetic field strength, m is the mass of an ion in kg, and q is ion charge in Coulombs. Due to

the large magnetic fields required to reach high mass resolution, most FT-ICRs require cryogenic cooling which is expensive.

A second type of FT-MS device is the Orbitrap™ which was invented in 2000 by Dr. Alexander Makarov.[66,67] In an Orbitrap ions undergo harmonic oscillation in a Quadro-logarithmic field. The harmonic oscillation is related to ion mass-to-charge by equation 1.13

$$f_z = \sqrt{k\frac{q}{m}} \tag{1.13}$$

In which f_z is the frequency of the harmonic oscillation of ions in Hz and *k* is the constant for field curvature based on the geometry of the device. The Orbitrap is compact and cheaper than an FT-ICR and although the mass resolution is not as high, the Orbitrap is widely used in lieu of an FT-ICR.

A third type of FT mass analyzer, and the subject of this dissertation, is the ELIT which traps ion axially between to ion mirrors.[21] Using a conductor within the device, ion image charge can be measured as a function of time to generate a mass spectrum. Like the Orbitrap, axial oscillations are measured which are inversely proportionally to square root of ion mass-to-charge.

1.8.3 Multiple-Reflection Time-of-Flight

The maximum resolving power achievable in a time-of-flight experiment is determined by the starting condition of the ion packet and the path length allowed for separation.[32] Although very long linear path length can be made, a more efficient solution is to reuse the same path length multiple times. This allows the user to set an arbitrarily long path length which is practically limited by the decay rate of the ion signal. The ELIT can be operated as a closed-path multiple reflection time-of-flight (MR-TOF) device; however due to the closed path nature, lighter ions can overlap larger ions after some time due to difference in relative ion velocities and the geometric constraints of the device. This property of ion overlap is known as the racetrack effect and is shown

in Figure 1.7. Since the time in which any particular ion is detected is dependent both the ion *m/z* and the number of laps undergone, neither of which are known prior to analysis, the resulting mass spectra are difficult to assign after ion overlap due to an ambiguous mass range.[32,33,68,69] However, if ion *m/z* is known a-prior, the racetrack effect can be used to isolate multiple ion simultaneously which will be discussed in detail in Chapter 5.

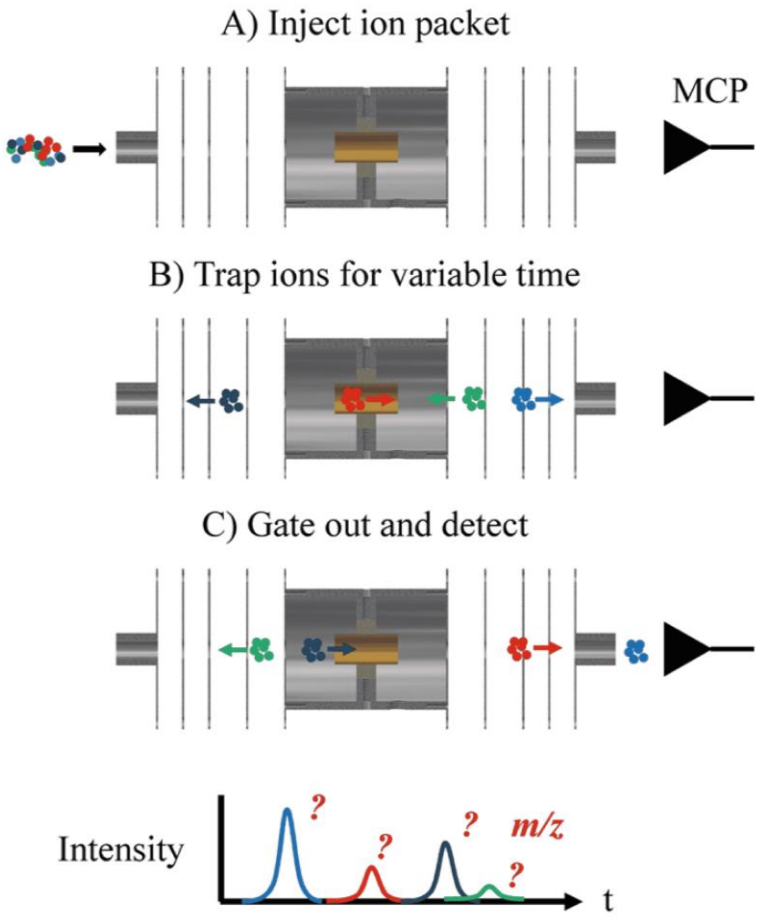

Figure 1.7. Illustration of the ambiguous mass range generated after the racetrack effect has taken place in a closed-path multiple-reflection time-of-flight device. After a given time the lap each ion is on becomes unknown and therefore the m/z cannot be directly determined for the time domain spectrum.

The unambiguous mass range can be expressed as a function of the number of laps completed by the ion population prior to analysis which is shown below. Where $(m/z)_{max}$ and $(m/z)_{min}$ define the unambiguous mass range after *N* number of laps. Conversely, a given mass range can be achieved after a certain number of laps equation 1.14. This relationship proves to be useful in determining appropriate ion isolation times as will be discussed in Chapter 4.[21,70]

$$\frac{(m/z)_{max}}{(m/z)_{min}} = \left(\frac{N_t + 1}{N_t}\right)^2 \tag{1.14}$$

$$N \approx \left(\left(\frac{(m/z)_{max}}{(m/z)_{min}}\right)^{\frac{1}{2}} - 1\right)^{-1} \tag{1.15}$$

As the number of laps increases, the unambiguous mass range decreases making closed-path MR-TOF mass analysis useful for simple mixtures or for zoom scans as a compliment to the FT-MS experiment. There are three way to generate an unambiguous mass measurement using in an MR-TOF experiment. The first, is to isolate a narrow mass range prior to mass analysis in the ELIT. Ions can then be detected after they have separated in the ELIT, but before they begin to lap one another. The second method is to gate out ions that are not on the same lap using a kick-out mass selector.[71] The third method is to repeat the mass analysis at multiple analysis times such that the ambiguous mass range can be disentangled using multiple equations.[21,72] This method become difficult for complex mixtures as the number of injection events increases with sample complexity.

The achievable mass resolution in an MR-TOF experiment is shown in equation 1.16 and will be discussed in more detail in Chapter 2.[31]

$$\frac{m}{\Delta m} = \frac{t_0 + N_t t_t}{2\sqrt{\Delta t_0^2 + (N_t \Delta t_t)^2 + [(t|\delta)_0 \delta + N_t (t|\delta)_t \delta]^2}} \tag{1.16}$$

Where t_0 is the time-of-flight from injection from the accumulation quadrupole to the detector, t_t is the time-of-flight for one lap in the analyzer, Δt_0 is the time-of-flight spread

resulting from initial injection conditions, Δt_t is the time-of-flight spread per lap due to field aberrations in the ion mirrors, δ is the kinetic energy spread, and $(t|\delta)_0$ and $(t|\delta)_t$ are the first-order dispersion coefficients with respect to kinetic energy spread for a single pass and for each lap.

Chapter 2 provides a detailed discussion comparing the use of the ELIT as a FT-MS and closed-path MR-TOF for mass analysis and therefore further discussion of the figures-of-merit for the MR-TOF will be postponed.

1.8.4 Charge Detection Mass Spectrometry

Charge detection mass spectrometry is commonly used to determine the absolute mass of large ions which are not amenable to analysis by other MS methods. In order to unambiguously assign molecular weight, two pieces of information are necessary, the ion mass-to-charge and the charge state. Charge state is normally determined by the spacing of isotopes, but with high molecular weight species (>1MDa), the inherent heterogeneity (isotopes, adducts, ion types, multiples charge states) of the analyte makes resolving isotopes very difficult, normally requiring high to ultra-high resolution. By using a charge sensitive detector, the number of charges on an ion can be determine thereby eliminating the need for ultra-high resolution. In a single ion analysis, the *m/z* can be determined by either a time-to-frequency or time-to-velocity measurement and thus with both *m/z* and *z*, molecular weight *m* can be easily determined. This has been demonstrated on a wide variety of analytes including but not limited to DNA[4,73-75], viruses[76-78], pyruvate kinase[79-82], and polymer.[83]

When an ion travels through the detection electrode two signals of opposite polarity are registered. The magnitude of the signal is proportional to the number of charges associated with ion, while the time between the signals is related to the ion's velocity. Due to experimental

variations, the uncertainty of the charge and velocity measurements decreases with the square root of the number of measurements. In a frequency measurement, the resolution increases linearly as a function of time and therefore uncertainty in the m/z measurement decreases linearly assuming the frequency of the ion remains constant and detectable for the duration of the experiment. The charge of ions can be very accurately assigned (error rate of 1 in 15,000) therefore the uncertainty in the mass measurement is limited by the uncertainty in the *m/z* measurement. [14]

1.9 Conclusion

The electrostatic linear ion trap is a low-cost instrument that provides a highly flexible mass spectrometry platform. The linear geometry ELIT provides an excellent tandem mass spectrometry platform from which ions can be isolated, probed, and mass analyzed in a variety of ways. The trap can be coupled to numerous ionization sources and can be made compact/portable. Ions can be isolated with high resolution and efficiency prior to being probed in a number of ways. The ELIT also enables mass analysis via both Fourier transformation (broad-band) or closed path multiple-reflection time-of-flight (narrow-band). The rest of this thesis focuses on each aspect of developing the ELIT into a high-performance tandem mass spectrometer.

1.10 References

1. Thomson, J. J. XLVII. On rays of positive electricity. *The London, Edinburgh, and* Dublin Philosophical Magazine and Journal of Science, **1907,** 13, 561-575.

2. Thomson, J. J. XXVI. Rays of positive electricity. *The London, Edinburgh, and Dublin Philosophical Magazine and Journal of Science,* **1911,** *21,* 225-249.

3. Zajfman, D.; Heber, O.; Vejby-Christensen, L.; Ben-Itzhak, I.; Rappaport, M.; Fishman, R.; Dahan, M. Electrostatic bottle for long-time storage of fast ion beams. *Phys. Rev. A,* **1997,** *55,* R1577-R1580.

4. Benner, W. H. A gated electrostatic ion trap to repetitiously measure the charge and m/z of large electrospray ions. *Anal. Chem.,* **1997,** *69,* 4162-4168.

5. Ring, S.; Pedersen, H. B.; Heber, O.; Rappaport, M. L.; Witte, P.; Bhushan, K. G.; Altstein, N.; Rudich, Y.; Sagi, I.; Zajfman, D. Fourier transform time-of-flight mass spectrometry in an electrostatic ion beam trap. *Anal. Chem.,* **2000,** *72,* 4041-4046.

6. Zajfman, D.; Rudich, Y.; Sagi, I.; Strasser, D.; Savin, D. W.; Goldberg, S.; Rappaport, M.; Heber, O. High resolution mass spectrometry using a linear electrostatic ion beam trap. *Int. J. Mass Spectrom.,* **2003,** *229,* 55-60.

7. Doussineau, T.; Bao, C. Y.; Clavier, C.; Dagany, X.; Kerleroux, M.; Antoine, R.; Dugourd, P. Infrared multiphoton dissociation tandem charge detection-mass spectrometry of single megadalton electrosprayed ions. *Rev. Sci. Instrum.,* **2011,** *82,* 084104.

8. Hilger, R. T.; Santini, R. E.; McLuckey, S. A. Nondestructive Tandem Mass Spectrometry Using a Linear Quadrupole Ion Trap Coupled to a Linear Electrostatic Ion Trap. *Anal. Chem.,* **2013,** *85,* 5226-5232.

9. Dziekonski, E. T.; Johnson, J. T.; Hilger, R. T.; McIntyre, C. L.; Santini, R. E.; McLuckey, S. A. Voltage-induced frequency drift correction in fourier transform electrostatic linear ion trap mass spectrometry using mirror-switching. *Int. J. Mass Spectrom.,* **2016,** *410,* 12-21.

10. Plaß, W. R.; Dickel, T.; Czok, U.; Geissel, H.; Petrick, M.; Reinheimer, K.; Scheidenberger, C.; Yavor, M. I. Isobar separation by time-of-flight mass spectrometry for low-energy radioactive ion beam facilities. *Nucl. Instrum. Meth. B,* **2008,** *266,* 4560-4564.

11. Pedersen, H. B.; Strasser, D.; Heber, O.; Rappaport, M. L.; Zajfman, D. Stability and loss in an ion-trap resonator. *Phys. Rev. A,* **2002,** *65,* 042703.

12. Schmidt, H. T.; Cederquist, H.; Jensen, J.; Fardi, A. Conetrap: A compact electrostatic ion trap. *Nucl. Instrum. Meth. B,* **2001,** *173,* 523-527.

13. Elliott, A. G.; Merenbloom, S. I.; Chakrabarty, S.; Williams, E. R. Single Particle Analyzer of Mass: A Charge Detection Mass Spectrometer with a Multi-Detector Electrostatic Ion Trap. *Int. J. Mass Spectrom.,* **2017,** *414,* 45-55.

14. Keifer, D. Z.; Jarrold, M. F. Single molecule mass spectrometry. *Mass Spectrom. Rev.,* **2016,** 1-19.

15. Contino, N. C.; Jarrold, M. F. Charge detection mass spectrometry for single ions with a limit of detection of 30 charges. *Int. J. Mass Spectrom.,* **2013,** *345,* 153-159.

16. Contino, N. C.; Pierson, E. E.; Keifer, D. Z.; Jarrold, M. F. Charge detection mass spectrometry with resolved charge states. *J. Am. Soc. Mass Spectrom.,* **2013,** *24,* 101-108.

17. Ding, L.; Badheka, R.; Ding, Z.; Nakanishi, H. A simulation study of the planar electrostatic ion trap mass analyzer. *J. Am. Soc. Mass Spectrom.,* **2013,** *24,* 356-364.

18. Knapp, D. R. Planar geometry inertial electrostatic confinement fusion device. Journal of Physics: Conference Series, IOP Publishing, **2015**, pp. 012018.

19. Thomson, B. A.; Jolliffe, C. L.; Spectrometer with axial field, US5847386 A; **1998**.

20. Hilger, R. T.; Wyss, P. J.; Santini, R. E.; McLuckey, S. A. Absorption mode Fourier transform electrostatic linear ion trap mass spectrometry. *Anal. Chem.,* **2013,** *85,* 8075-8079.

21. Hilger, R. T.; Santini, R. E.; McLuckey, S. A. Tandem Mass Spectrometry in an Electrostatic Linear Ion Trap Modified for Surface-Induced Dissociation. *Anal. Chem.,* **2014,** *86,* 8822-8828.

22. Dziekonski, E.; Johnson, J. T.; McLuckey, S. A. Utility of Higher Harmonics in Electrospray Ionization Fourier Transform Electrostatic Linear Ion Trap Mass Spectrometry. *Anal. Chem.,* **2017,** *89,* 4392-4397.

23. Dziekonski, E. T.; Santini, R. E.; McLuckey, S. A. A dual detector Fourier transform electrostatic linear ion trap utilizing in-trap potential lift. *Int. J. Mass Spectrom.,* **2016,** *405,* 1-8.

24. Hilger, R. T.; Santini, R. E.; McLuckey, S. A. Square wave modulation of a mirror lens for ion isolation in a Fourier transform electrostatic linear ion trap mass spectrometer. *Int. J. Mass Spectrom.,* **2014,** *362,* 1-8.

25. Hilger, R. T.; Dziekonski, E. T.; Santini, R. E.; McLuckey, S. A. Injecting electrospray ions into a Fourier transform electrostatic linear ion trap. *Int. J. Mass Spectrom.,* **2015,** *378,* 281-287.

26. Hilger, R. T.; Santini, R. E.; Luongo, C. A.; Prentice, B. M.; McLuckey, S. A. A method for isolating ions in quadrupole ion traps using an excitation waveform generated by frequency modulation and mixing. *Int. J. Mass Spectrom.,* **2015,** *377,* 329-337.

27. Johnson, J. T.; Lee, K. W.; Bhanot, J. S.; McLuckey, S. A. A Miniaturized Fourier Transform Electrostatic Linear Ion Trap: Mass Range and Resolution *J. Am. Soc. Mass Spectrom*. 2019, 30, 588−594.

28. Johnson, J. T.; Carrick, I. J.; Eakins, G. S.; McLuckey, S. A. Mirror Switching for High Resolution Ion Isolation in an Electrostatic Linear Ion Trap. *Anal. Chem.* 2019, 91, 8789-8794.

29. Johnson, J. T.; Carrick, I. J.; Eakins, G. S.; McLuckey, S. A. Simultaneous Isolation of Non-Adjacent m/z Ions Using Mirror Switching in an Electrostatic Linear Ion Trap. *Anal. Chem.*2019, 91, 12574-12580.

30. Brubaker, W. M. An improved quadrupole mass analyzer. *Adv. Mass Spectrom,* **1968,** *4,* 293-299.

31. Plaß, W.; Dickel, T.; Petrick, M.; Boutin, D.; Di, Z.; Fleckenstein, T.; Geissel, H.; Jesch, C.; Scheidenberger, C.; Wang, Z. An RF quadrupole–time-of-flight system for isobar-separation and multiplexed low-energy Rare-Isotope Beam experiments. *The European Physical Journal-Special Topics,* **2007,** *150,* 367-368.

32. Plaß, W. R.; Dickel, T.; Scheidenberger, C. Multiple-reflection time-of-flight mass spectrometry. *Int. J. Mass Spectrom.,* **2013,** *349,* 134-144.

33. Dickel, T.; Plaß, W. R.; Lang, J.; Ebert, J.; Geissel, H.; Haettner, E.; Jesch, C.; Lippert, W.; Petrick, M.; Scheidenberger, C. Multiple-reflection time-of-flight mass spectrometry for in situ applications. *Nucl. Instrum. Meth. B,* **2013,** *317,* 779-784.

34. Yavor, M. I.; Plaß, W. R.; Dickel, T.; Geissel, H.; Scheidenberger, C. Ion-optical design of a high-performance multiple-reflection time-of-flight mass spectrometer and isobar separator. *Int. J. Mass Spectrom.,* **2015,** *381-382,* 1-9.

35. Jesch, C.; Dickel, T.; Plaß, W. R.; Short, D.; San Andres, S. A.; Dilling, J.; Geissel, H.; Greiner, F.; Lang, J.; Leach, K. G. The MR-TOF-MS r separator for the TITAN facility at TRIUMF. *Hyperfine Interact.,* **2015,** 1-10.

36. Dickel, T.; Yavor, M. I.; Lang, J.; Plaß, W. R.; Lippert, W.; Geissel, H.; Scheidenberger, C. Dynamical time focus shift in multiple-reflection time-of-flight mass spectrometers. *Int. J. Mass Spectrom.,* **2017,** *412,* 1-7.

37. Dickel, T.; Plaß, W. R.; Lippert, W.; Lang, J.; Yavor, M. I.; Geissel, H.; Scheidenberger, C. Isobar Separation in a Multiple-Reflection Time-of-Flight Mass Spectrometer by Mass-Selective Re-Trapping. *J. Am. Soc. Mass Spectrom.,* **2017,** 1-12.

38. Grinfeld, D.; Giannakopulos, A. E.; Kopaev, I.; Makarov, A.; Monastyrskiy, M.; Skoblin, M. Space-charge effects in an electrostatic multireflection ion trap. *Eur. J. Mass Spectrom.,* **2014,** *20,* 131-142.

39. Wolf, R. N.; Eritt, M.; Marx, G.; Schweikhard, L. A multi-reflection time-of-flight mass separator for isobaric purification of radioactive ion beams. *Hyperfine Interact.,* **2011,** *199,* 115-122.

40. Breitenfeldt, C.; Froese, M. W.; Blaum, K.; George, S.; Grieser, M.; Lange, M.; Menk, S.; Repnow, R.; Schwalm, D.; Schweikhard, L. Spreading times of ionbunches in the Cryogenic Trap for Fast ion beams. *Int. J. Mass Spectrom.,* **2016,** *396,* 1-4.

41. Wolf, R. N.; Marx, G.; Rosenbusch, M.; Schweikhard, L. Static-mirror ion capture and time focusing for electrostatic ion-beam traps and multi-reflection time-offlight mass analyzers by use of an in-trap potential lift. *Int. J. Mass Spectrom.,* **2012,** *313,* 8-14.

42. Wolf, R. N.; Wienholtz, F.; Atanasov, D.; Beck, D.; Blaum, K.; Borgmann, C.; Herfurth, F.; Kowalska, M.; Kreim, S.; Litvinov, Y. A. ISOLTRAP's multireflection time-of-flight mass separator/spectrometer. *Int. J. Mass Spectrom.,* **2013,** *349,* 123-133.

43. Toker, Y.; Altstein, N.; Aviv, O.; Rappaport, M. L.; Heber, O.; Schwalm, D.; Strasser, D.; Zajfman, D. The kick-out mass selection technique for ions stored in an electrostatic ion beam trap. *J. Instrum.,* **2009,** *4,* P09001.

44. Fischer, P.; Knauer, S.; Marx, G.; Schweikhard, L. In-depth study of in-trap high-resolution mass separation by transversal ion ejection from a multi-reflection time-of-flight device. *Rev. Sci. Instrum.* 2018, 89, 015114.

45. Fischer, P.; Marx, G.; Schweikhard, L. Multiple ion capture and separation in an electrostatic storage device. *Int. J. Mass Spectrom.* 2019, 435, 305−314.

46. Dickel, T.; Plaß, W. R.; Lippert, W.; Lang, J.; Yavor, M. I.; Geissel, H.; Scheidenberger, C. Isobar separation in a multiple-reflection time-of-flight mass spectrometer by mass-selective re-trapping. *J. Am. Soc. Mass Spectrom.* 2017, 28, 1079−1090.

47. Marshall, A. G.; Verdun, F. R., Fourier Transforms in NMR, Optical, and Mass Spectrometry: A User's Handbook, Elsevier Science and Technology, Oxford, UK, 1990.

48. Perry, R. H.; Cooks, R. G.; Noll, R. J. Orbitrap mass spectrometry: instrumentation, ion motion and applications. *Mass Spectrom. Rev.,* **2008,** *27,* 661-699.

49. Qi, Y.; Witt, M.; Jertz, R.; Baykut, G.; Barrow, M. P.; Nikolaev, E. N.; O'Connor, P. B. Absorption_mode spectra on the dynamically harmonized Fourier transform ion cyclotron resonance cell. *Rapid Commun. Mass Spectrom.,* **2012,** *26,* 2021-2026.

50. Comisarow, M. B.; Marshall, A. G. Fourier transform ion cyclotron resonance spectroscopy. *Chemical physics letters,* **1974,** *25,* 282-283.

51. Marshall, A. G.; Comisarow, M. B.; Parisod, G. Relaxation and spectral line shape in Fourier transform ion resonance spectroscopy. *J. Chem. Phys.,* **1979,** *71,* 4434-4444.

52. Vining, B. A.; Bossio, R. E.; Marshall, A. G. Phase correction for collision model analysis and enhanced resolving power of fourier transform ion cyclotron resonance mass spectra. *Anal. Chem.,* **1999,** *71,* 460-467.

53. Xian, F.; Hendrickson, C. L.; Blakney, G. T.; Beu, S. C.; Marshall, A. G. Automated broadband phase correction of Fourier transform ion cyclotron resonance mass spectra. *Anal. Chem.,* **2010,** *82,* 8807-8812.

54. Qi, Y.; Barrow, M. P.; Li, H.; Meier, J. E.; Van Orden, S. L.; Thompson, C. J.; O'Connor, P. B. Absorption-mode: the next generation of Fourier transform mass spectra. *Anal. Chem.,* **2012,** *84,* 2923-2929.

55. Kilgour, D. P.; Wills, R.; Qi, Y.; O'Connor, P. B. Autophaser: an algorithm for automated generation of absorption mode spectra for FT-ICR MS. *Anal. Chem.,* **2013,** *85,* 3903-3911.

56. Kilgour, D.; Nagornov, K. O.; Kozhinov, A. N.; Zhurov, K. O.; Tsybin, Y. O. Producing absorption mode Fourier transform ion cyclotron resonance mass spectra with non-quadratic phase correction functions. *Rapid Commun. Mass Spectrom.,* **2015,** *29,* 1087-1093.

57. Beu, S. C.; Blakney, G. T.; Quinn, J. P.; Hendrickson, C. L.; Marshall, A. G. Broadband phase correction of FT-ICR mass spectra via simultaneous excitation and detection. *Anal. Chem.,* **2004,** *76,* 5756-5761.

58. Qi, Y.; Li, H.; Wills, R. H.; Perez-Hurtado, P.; Yu, X.; Kilgour, D. P.; Barrow, M. P.; Lin, C.; O'Connor, P. B. Absorption-mode Fourier transform mass spectrometry: the effects of apodization and phasing on modified protein spectra. *J. Am. Soc. Mass Spectrom.,* **2013,** *24,* 828-834.

59. Lange, O.; Damoc, E.; Wieghaus, A.; Makarov, A. Enhanced Fourier transform for Orbitrap mass spectrometry. *Int. J. Mass Spectrom.,* **2014,** *369,* 16-22.

60. Hendrickson, C. L.; Quinn, J. P.; Kaiser, N. K.; Smith, D. F.; Blakney, G. T.; Chen, T.; Marshall, A. G.; Weisbrod, C. R.; Beu, S. C. 21 Tesla Fourier Transform Ion Cyclotron Resonance Mass Spectrometer: A National Resource for Ultrahigh Resolution Mass Analysis. *J. Am. Soc. Mass Spectrom.,* **2015,** *26,* 1626-1632.

61. Shaw, J. B.; Lin, T.-Y.; Leach, F. E.; Tolmachev, A. V.; Tolić, N.; Robinson, E. W.; Koppenaal, D. W.; Paša-Tolić, L. 21 Tesla Fourier Transform Ion Cyclotron Resonance Mass Spectrometer Greatly Expands Mass Spectrometry Toolbox. *J. Am. Soc. Mass Spectrom.,* **2016,** *27,* 1929-1936.

62. Kostyukevich, Y. I.; Vladimirov, G. N.; Nikolaev, E. N. Dynamically harmonized FT-ICR cell with specially shaped electrodes for compensation of inhomogeneity of the magnetic field. Computer simulations of the electric field and ion motion dynamics. *J. Am. Soc. Mass Spectrom.,* **2012,** *23,* 2198-2207.

63. Popov, I. A.; Nagornov, K.; Vladimirov, G. N.; Kostyukevich, Y. I.; Nikolaev, E. N. Twelve million resolving power on 4.7 T Fourier transform ion cyclotron resonance instrument with dynamically harmonized cell—observation of fine structure in peptide mass spectra. *J. Am. Soc. Mass Spectrom.,* **2014,** *25,* 790-799.

64. Comisarow, M. B.; Marshall, A. G. Frequency-sweep Fourier transform ion cyclotron resonance spectroscopy. *Chemical Physics Letters,* **1974,** *26,* 489-490.

65. Marshall, A. G.; Hendrickson, C. L.; Jackson, G. S. Fourier transform ion cyclotron resonance mass spectrometry: a primer. *Mass Spectrom. Rev.,* **1998,** *17,* 1-35.

66. Makarov, A. Electrostatic axially harmonic orbital trapping: a high-performance technique of mass analysis. *Anal. Chem.,* **2000,** *72,* 1156-1162.

67. Hu, Q.; Noll, R. J.; Li, H.; Makarov, A.; Hardman, M.; Graham Cooks, R. The Orbitrap: a new mass spectrometer. *J. Mass Spectrom.,* **2005,** *40,* 430-443.

68. Yavor, M., Optics of charged particle analyzers, Academic Press, 2009.

69. Casares, A.; Kholomeev, A.; Wollnik, H. Multipass time-of-flight mass spectrometers with high resolving powers. *Int. J. Mass Spectrom.,* **2001,** *206,* 267-273.

70. Dziekonski, E.T., Johnson, J.T., Lee, K.W., McLuckey, S.A.: Fourier transform MS and closed-path multireflection time-of-flight MS using an electrostatic linear ion trap. Anal. Chem. 89, 10965–10972 (2017)

71. Dickel, T.; Plaß, W.; Becker, A.; Czok, U.; Geissel, H.; Haettner, E.; Jesch, C.; Kinsel, W.; Petrick, M.; Scheidenberger, C. A high-performance multiplereflection time-of-flight mass spectrometer and isobar separator for the research with exotic nuclei. *Nucl. Instrum. Meth. A,* **2015,** *777,* 172-188.

72. Schury, P.; Ito, Y.; Wada, M.; Wollnik, H. Wide-band mass measurements with a multi-reflection time-of-flight mass spectrograph. *Int. J. Mass Spectrom.,* **2014,** *359,* 19-25.

73. Fuerstenau, S. D.; Benner, W. H. Molecular weight determination of megadalton DNA electrospray ions using charge detection time_of_flight mass spectrometry. *Rapid Commun. Mass Spectrom.,* **1995,** *9,* 1528-1538.

74. Doussineau, T.; Paletto, P.; Dugourd, P.; Antoine, R. Multiphoton dissociation of electrosprayed megadalton-sized DNA ions in a charge-detection mass spectrometer. *J. Am. Soc. Mass Spectrom.,* **2015,** *26,* 7-13.

75. Doussineau, T.; Antoine, R.; Santacreu, M.; Dugourd, P. Pushing the limit of infrared multiphoton dissociation to megadalton-size DNA ions. *J. Phys. Chem. Lett.,* **2012,** *3,* 2141-2145.

76. Pierson, E. E.; Keifer, D. Z.; Selzer, L.; Lee, L. S.; Contino, N. C.; Wang, J. C. Y.; Zlotnick, A.; Jarrold, M. F. Detection of late intermediates in virus capsid assembly by charge detection mass spectrometry. *J. Am. Chem. Soc.,* **2014,** *136,* 3536-3541.

77. Keifer, D. Z.; Motwani, T.; Teschke, C. M.; Jarrold, M. F. Acquiring Structural Information on Virus Particles with Charge Detection Mass Spectrometry. *J. Am. Soc. Mass Spectrom.,* **2016,** *27,* 1028-1036.

78. Keifer, D. Z.; Motwani, T.; Teschke, C. M.; Jarrold, M. F. Measurement of the accurate mass of a 50 MDa infectious virus. *Rapid Commun. Mass Spectrom.,* **2016,** *30,* 1957-1962.

79. Pierson, E. E.; Keifer, D. Z.; Contino, N. C.; Jarrold, M. F. Probing higher order multimers of pyruvate kinase with charge detection mass spectrometry. *Int. J. Mass Spectrom.,* **2013,** *337,* 50-56.

80. Keifer, D. Z.; Shinholt, D. L.; Jarrold, M. F. Charge detection mass spectrometry with almost perfect charge accuracy. *Anal. Chem.,* **2015,** *87,* 10330-10337.

81. Pierson, E. E.; Keifer, D. Z.; Contino, N. C.; Jarrold, M. F. Probing higher order multimers of pyruvate kinase with charge detection mass spectrometry. *Int. J. Mass Spectrom.,* **2013,** *337,* 50-56.

82. Pierson, E. E.; Contino, N. C.; Keifer, D. Z.; Jarrold, M. F. Charge detection mass spectrometry for single ions with an uncertainty in the charge measurement of 0.65 e. *J. Am. Soc. Mass Spectrom.,* **2015,** *26,* 1213-1220.

83. Doussineau, T.; Bao, C. Y.; Antoine, R.; Dugourd, P.; Zhang, W.; D'Agosto, F.; Charleux, B. Direct molar mass determination of self-assembled amphiphilic block copolymer nanoobjects using electrospray-charge detection mass spectrometry. *ACS Macro Letters,* **2012,** *1,* 414-417.

CHAPTER 2. FOURIER-TRANSFORM MS AND CLOSED-PATH MULTIREFLECTION TIME-OF-FLIGHT MS USING AN ELECTROSTATIC LINEAR ION TRAP

Adapted with permission from Dziekonski, E. T., Johnson, J. T., Lee, K. W., McLuckey, S. A. *Anal. Chem.* **2017**, 89, 10965-10972.

2.1 Introduction

Devices capable of trapping gaseous ions have become common-place in analytical mass spectrometry (MS) both as ion storage devices and as mass analyzers. Electrodynamic ion traps, such as the Paul trap[1] and linear quadrupole ion traps,[2,3] are commonly used as mass spectrometers and as devices for conducting multistage MS experiments (i.e., MS^n, where $n > 1$). In most cases, mass analysis is conducted using a form of mass-selective instability[4] whereby ions are scanned out of the ion trap in an *m/z*-dependent fashion with external detection via an electron multiplier. The ion cyclotron resonance (ICR) ion trap, which combines trapping in the x and y-dimensions using a strong magnetic field with electrostatic trapping in the z-dimension, can provide unparalleled mass resolution via Fourier transformation of time-domain signals generated by the detection of image currents on opposing electrodes to the frequency domain via Fourier transformation.[5,6] The ICR cell was the first to employ Fourier transform techniques for mass spectrometry and forms the basis for FT-ICR mass spectrometers.[7] A purely electrostatic ion trap based on orbital trapping,[8,9] referred to as the Orbitrap, was introduced by Makarov[10,11] that is also capable of FT-MS.[12] The generation of a differential time-domain image current on an outer electrode that is split into two halves facilitates Fourier-transformation to generate a mass spectrum. The Orbitrap, operated in the FT-MS mode, is also capable of generating very high mass resolution and is now widely used in applications that require high resolution and high mass measurement accuracy. A conceptually very simple form of electrostatic ion trapping can be effected via the

reflection of ions between two opposing ion mirrors, in analogy with an optical resonator. Such devices, referred to here as electrostatic linear ion traps (ELITs), have been used for mass analysis, although they are not as fully developed for mass spectrometry as the other forms of ion trapping devices mentioned above. A particularly prominent application of an ELIT is found in so-called charge detection mass spectrometry (CDMS) in which both the charge and the *m/z* ratio of a single ion are measured to determine ion mass. This application, first described by Benner[13,14] and further developed by Jarrold et al.,[15–17] Dugourd et al.,[18,19] and Williams et al.,[20] relies on image charge measurements as individual large multiply charged ions pass through one or more central pick-up electrodes in the field-free region of an ELIT. The *m/z* ratio of the individual ion can be determined either via measurement of the time the ion takes to pass through a pickup electrode[21] (i.e., an ion velocity measurement) or via Fourier transformation of the time-domain signal generated by the pick-up electrode (i.e., a frequency measurement). Zajfman et al. first described FT-ELIT MS on populations of ions,[22,23] in analogy with the FT-ICR and Orbitrap experiments. A parallel line of work with ELITs has involved a time measurement in which ions undergo multiple reflections in an ELIT,[24,25] followed by destructive detection typically using a microchannel plate detector. The latter work falls into the general category of closed-path multireflection time-of-flight mass spectrometry (MR-TOF MS), which has also been effected using electrostatic sectors[26] rather than ion mirrors. Several closed-path MR-TOF devices have been constructed for the purpose of high resolution mass selection and mass analysis for the study of short-lived nuclei[27–29] in radioactive beam facilities. However, a relatively compact MR-TOF designed for use as an analytical mass spectrometer has been described.[30] We have been exploring the ELIT geometry as a component in a platform for MS^n experiments for several reasons. These include, for example, the facility with which a device with a linear geometry can be coupled with other ion optical elements and the

relative simplicity of a purely electrostatic ion trap. We have demonstrated, for example, nondestructive tandem mass spectrometry in a combined ELIT/quadrupole linear ion trap instrument, whereby ions were passed back and forth between the ion traps without an intervening ionization step. Mass analysis of the precursor ions and the product ions were carried out via FT-ELIT MS, whereas ion dissociation was conducted in the quadrupole ion trap.[31] We subsequently demonstrated ion isolation within the ELIT via modulation of one of the trapping electrodes[32] and surface-induced dissociation[33] at the end of the ELIT. The latter two developments enabled the execution of a tandem MS experiment using the ELIT for mass selection, dissociation, and mass analysis of the products. In the course of this work, we have expended effort to optimize the FT-ELIT mass measurement in our apparatus.[34–37] However, a particularly attractive feature of the ELIT is that it is amenable to both FT-MS and closed-path MR-TOF MS measurements. Both forms of mass analysis can be performed simultaneously on the same population of ions as the two types of measurements are independent. In this work, we have adapted our current ELIT instrument for MR-TOF MS measurements while retaining the FT-MS capability. Each MS approach has its own relative strengths and weaknesses. While the MR-TOF measurement is as yet not fully optimized in this instrument, many of the key considerations in comparing time-based versus frequency-based measurements can be illustrated and point to the degree to which these approaches can be used to complement one another.

2.2 Experimental Section

2.2.1 Materials

Bromazepam, chlorprothixene HCl, gadolinium- (III) chloride hexahydrate, and insulin (from bovine pancreas) were purchased from Sigma-Aldrich (St. Louis, MO, U.S.A.). Methanol (MeOH) was purchased from Thermo Fisher Scientific (Waltham, MA, U.S.A.). Glacial acetic

acid (AcOH) was purchased from Mallinckrodt (Phillipsburg, NJ, U.S.A.). HPLC-grade water (H_2O) was purchased from Fisher Scientific (Pittsburgh, PA, U.S.A.). The mixture of bromazepam (100 μM) and chlorprothixene HCl (5 μM) was prepared using 50/ 50 v/v MeOH/H_2O. Insulin was prepared to a final concentration of 100 μM in 49.5/49.5/1 v/v/v MeOH/H_2O/AcOH. Gadolinium(III) chloride hexahydrate was prepared to a concentration of 15 mM (49.5/49.5/1 v/v/v MeOH/H_2O/AcOH).

2.2.2 Mass Spectrometry

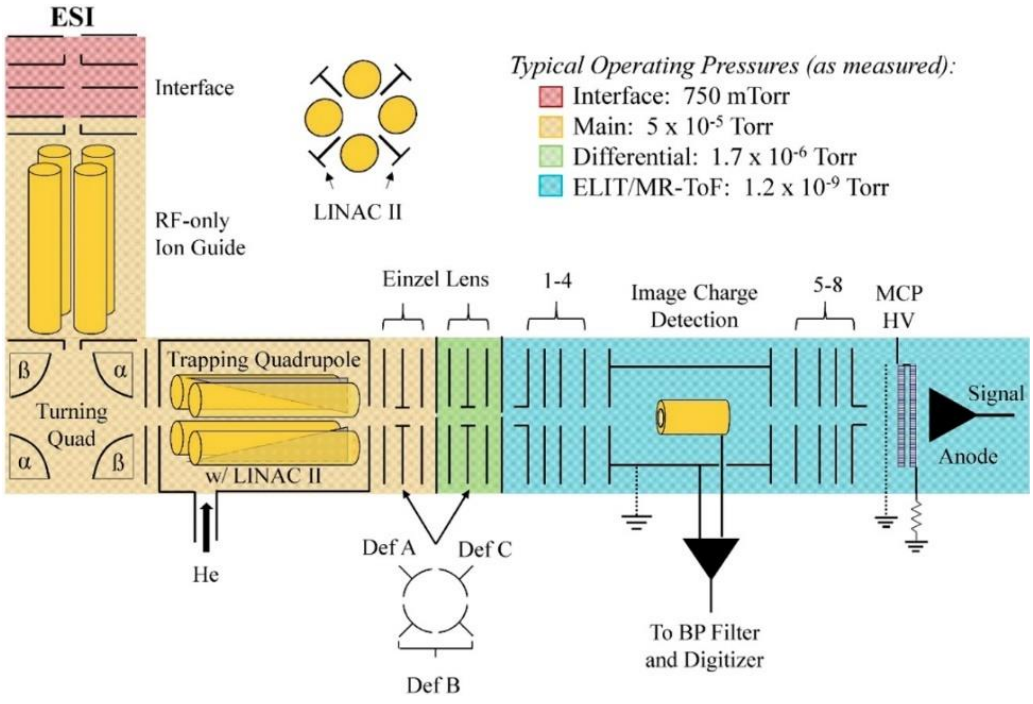

Figure 2.1. Instrument schematic.

All experiments were carried out on a home-built mass spectrometer depicted in Figure 2.1 The ELIT captures ions via mirror switching and detects the resulting image charge using a central electrode. The trap itself is made up of 10 parallel stainless steel plates (5.08 cm x 5.08 cm x 0.635 mm thick, Kimball Physics, Wilton, NH) with holes 6.48 mm in diameter drilled thorough the

center; eight of the plates control ion acceleration, deacceleration, and radial focusing (plate 1-8) while the other two are used to enclose the grounded housing for the detector. The spacing between elements (plates 1 to 3 = 7.62 mm, plate 3 to central housing 11.43 mm) is maintained by alumina spacers (Kimball Physics). The copper pick-up tube used for image charge detection (8.26 mm i.d, 9.53 mm o.d., 3 cm long) is centered within the grounded housing (50.8mm long, 33.02 mm i.d.) by poly ether ketone (PEEK) spacers. Stainless steel tubes (6.35 mm i.d., 10.16 mm o.d, 19.05 mm long) were welded to plates 1 and 8 to make the electric fields in both ion mirrors identical. To trap positive ions plate 1 is pulsed from ground to 2356 V (ORTEC Model 556, Advanced Measurement Technology, Oak Ridge, TN) using a fast, high-voltage switch (HTS 31-03-GSM, Behlke Power Electronics, Billerica, MA) at a time defined relative to the ejection of the ion packet, containing those ions of nominally lower kinetic energy, were within the changing electric field, imparting additional kinetic energy, thereby minimizing band broadening due to kinetic energy distribution. All other plate potentials are generated by additional ORTEC 556 power supplies with typical potentials being 2364 (plate 8), 1646 V (plates 2 and 7), 1047 V (plates 3 and 6), and -2106 V (plates 4 and 5) as measured with a calibrated 1000x probe and a HP 34401A multimeter. Frequency shifts arising from the transient voltage recovery of the pulsed power supply are minimized by utilizing the ORTEC 556 as the power supply for plate 1 and 8. Daily variation in the output voltages of the power supplies were minimized by leaving the ORTEC's on. With the detailed trap dimensions, ion energy (nominally 1960 eV/charge), and trapping voltages, typical ion frequencies are between 400 kHz and 100 kHz for m/z 100 and 1500, respectively. With the differential region installed and the collision gas on, the base pressure of the ELIT chamber was measured to be 1.2×10^{-9} Torr using a Granville Phillips 355001-YF ion gauge.

A differentially pumped region was installed between the accumulation quadrupole and the ELIT chamber to lower the overall background pressure in the presence of a continuous buffer gas, thereby increasing the duty cycle of the mass analysis. The differential region is housed within a hollow 6" double faced conflat (0.78" thick) that is pumped on by a Pfeiffer TMH 261 turbomolecular pump (210 L/s, N_2) through two independent 0.5" stainless steel tubes with KF25 fittings. It includes a carbon copy of the differential aperture, einzel lenses, and deflection electrodes, that have been installed in the accumulation quadrupole for all past experiments. Briefly, the four deflection (Def) are 0.344" long and have an inscribed diameter of 0.394" with a 0.025" gap between each quadrant. On either side of the deflection electrodes (0.05" gap) is a flat electrode (0.0063" thick) with a center hole that is 0.188" in diameter. PEEK spacers were included to center the differential apertures on the conflats. The deflection electrodes were individually biased to steer the beam and maximize the transfer efficiency through both differential apertures. All parts in the differential region are made of stainless steel, Teflon PTFE), ceramic, or polyether ketone (PEEK), and are therefore ultra-high vacuum compatible.

The nanoelectrospray ionization (nESI) source and the method by which ions are concentrated and injected into the electrostatic linear ion trap (ELIT) have been described.[31,38] Breifly, the sample was loaded into a pulled glass capillary and placed in front of the sampling orifice. High voltage was applied to a platinum wire in contact with the solution to generate and electrospray. Ions generated via nESI were transported to a trapping quadrupole equipped with LINAC II electrodes, where their accumulation and collisional cooling was facilitated by the continuous introduction of either helium or nitrogen gas. Descriptions of the mass analysis approaches are provided below. Once cooled, ions-of-interest could be isolated (apex) after which the voltage applied to all quadrupole elements were ramped to their injection potentials where the

kinetic energy (KE) of the ions is set by the rod offset. An RF phase-locked circuit was used to trigger both the injection of the bunched ion packet and the start of data collection at the zero crossing of the trapping RF such that a consistent ion energy was sampled. Nominally, the ions were trapped with a kinetic energy of 1960 eV/charge, referenced to the field free region of the ELIT.

2.2.2.1 Fourier Transform Ion Detection and Signal Processing

The charge sensitive detection electronics have been described previously.[33,36] The preamplifier JFET was changed from a NTE452 to a BF862, resulting in a signal-to-noise enhancement factor of 1.9. The output of the charge sensitive preamplifier (A250, Amptek) was filtered (band-pass, Krohn-Hite Model 3940, Brockton, MA) and amplified (gain = 5) prior to digitization by a PCI-based digitizer (CS1621, 16-bit, Gage Applied Technologies, Lanchine, Quebec, Canada) at a rate of 10 MS/s (AC coupled, 1 MΩ input impedance, 25 MHz lowpass filter enabled). A program written in LabVIEW 13.0 (National Instruments, Austin, TX) was used to acquire each transient for FT analysis. A custom program, written in MATLAB 2015, was used to process the transients using the enhanced Fourier transform (eFT).[39]

2.2.2.2 Multiple-Reflection Time-of-Flight

Dynamical time focus shifting (TFS)[40] was used on plates 8 and 1 (~2200 V) to shift the time focus of the ions to the center of the ELIT and the plane of the detector, respectively, thereby increasing the observed mass resolution. The TFS voltages were applied and pulsed using additional ORTEC 556 power supplies and solid-state switches (HTS 31-03-GSM). When ions were to be detected, plate 8 was pulsed from its nominal trapping potential to ground, allowing all ions to exit the ELIT and impinge upon a microchannel plate detector (MCP, APD 2 MINITOF 8/6/ 5/12 D 60:1 EDR SE, PS34049) manufactured by Photonis (Sturbridge, MA, U.S.A.). To

detect positive ions, the input voltage lead was biased to −2200 V and the output voltage lead was connected to ground through a series 20 MΩ resistor to operate the SMA signal lead at ground. The signal was amplified by a Keithly Instruments (Cleveland, OH, U.S.A.) 108 wideband amplifier (50 Ω termination, 20 dB gain) prior to digitization by channel 2 of the CS1621 (50 Ω, 100 MS/s, DC coupled, 25 MHz low-pass filter enabled). All MR-TOF data were collected using the GaGeScope software provided with the digitizer and analyzed without further processing.

2.3 Results and Discussion

Each mass analysis approach is considered using a set of common mass analyzer figures of merit.[41] Results and commentary are provided here regarding mass resolution, mass measurement accuracy, *m/z* range, "peak capacity", and speed.

2.3.1 Mass Resolution

Mass resolution, *R*, using the definition of $R = M/\Delta M_{fwhm}$[42] in an ELIT is given by $f/2\Delta f$ in the FT-ELIT experiment and $t/2\Delta t$ in the MR-TOF experiment, where f is ion frequency, Δf is the width of the peak at half height in the frequency domain signal, t is the ion flight time, and Δt is the width of the peak at half-height in the flight time spectrum. In the frequency measurement, in the absence of any ion loss or dephasing mechanisms, *R* increases linearly with acquisition time, T_{acq}, and decreases with the square root of the *m/z* of the ion according to

$$R = CT_{acq}/(m/z)^{1/2} \qquad (2.1)$$

where *C* is a proportionality constant that depends on the apparatus. In practice, the useful T_{acq} is limited by the damping constant, τ, which is the time for the time-domain signal to decay to $1/e \approx 0.368$ of its original amplitude. The major contributor to the damping constant in our apparatus is

collisions with background gas. The point is that *R* increases with measurement time until the signal is lost due to collisions/dephasing. (Based on a previously reported *R* = 36900 at the fundamental frequency for ions at m/z 173.9 (i.e., the base peak of the GdO^+ isotopic envelope) at a T_{acq} = 300 ms,[37] *C* can be estimated to be 1.622 × 10^6 for the present apparatus.) Figure 2.2 includes plots of *R* versus time for various scenarios. The dashed blue line represents *R* versus time up to 300 ms for anion of *m/z* 316 under the FT-MS conditions used in our apparatus. We note that *R* has been observed to increase with the order of the detected harmonic, at least up to the third harmonic, in our apparatus,[37] which increases the slope of the resolution versus time relationship by a corresponding factor. In the case of the MR-TOF experiment, *R* is approximately given by[43,27]

$$R = \frac{t_0/N + t_a}{2\sqrt{\left(\frac{\Delta t_0}{N}\right)^2 + (\Delta t_a)^2}} \tag{2.2}$$

where t_0 is the flight time for a single pass from the ion injector to the detector, *N* is the number of passes through the ELIT, t_a is the flight time for a single lap in the ELIT, Δt_0 is the initial time spread, which largely arises from the turn-around time associated with ion injection, as well as any spatial spread in the injection quadrupole, and Δt_a is the additional time spread (i.e., dispersion) that occurs on each turn. The latter arises from imperfections in the performance of the mirrors and trajectory variations. For our system, t_a is approximately given by

$$t_a = 2(m/z)^{1/2} \,/\, K \tag{2.3}$$

where *m/z* is the numerical value of the mass-to-charge ratio (unitless) and *K* = 3848700 Hz. Note that, in the absence of Δt_a, R increases linearly with flight time with no limit. In any real device, Δt_a is nonzero such that, as $N \rightarrow \infty$:

$$R \rightarrow t_a/2\Delta t_a \tag{2.4}$$

Figure 2.2 compares the dependence of resolution on storage time for an MR-TOF MS experiment (red data points), derived from relations 2.2 and 2.3, with that of an FT-ELIT MS experiment (blue data points), derived from relation 2.1, for an ion of *m/z* =316 using values that apply, at least approximately, to the conditions used in these studies (viz., t_0 = 10 μs, Δt_0 = 110 ns, Δt_a = 50 ps, *K* = 3858700, *C* = 1.622 × 10^6). In the case of the MR-TOF experiment, resolution approaches the maximum value of roughly 92000 within about 100 ms under these conditions. It is clear from Figure 2.2 that *R* increases much more rapidly in the MR-TOF experiment relative to the FT-MS experiment during the first 50 ms of storage time.

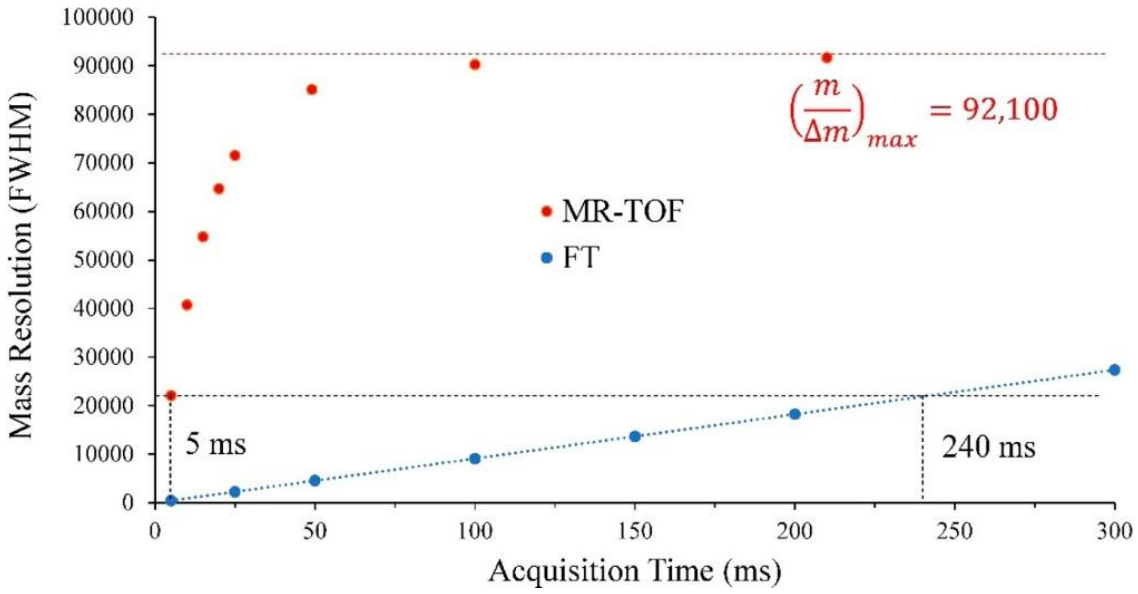

Figure 2.2. Mass resolution versus acquisition (storage) time for the MR-TOF experiment (red data points) and the FT-ELIT experiment (blue datapoints) for an ion of m/z 316

The figure indicates that a resolution slightly in excess of 20000 can be achieved in 5 ms in the MR-TOF mode, whereas an equivalent resolution at the first harmonic in FT-ELIT mode for an ion of m/z 316 requires a 240 ms transient. It is worthy of note that the performance of the MR-TOF experiment is more sensitive to injection conditions than the FT-ELIT experiment. The initial slope of the resolution versus time curve for the MR-TOF experiment is strongly dependent upon injection pulse width, Δt_0 (see relation 2.2). In the case of the FT-ELIT experiment, on the other hand, as long as an ion yields a time varying signal at the pick-up electrode, the resolution of the FT-ELIT experiment is independent of pulse width.

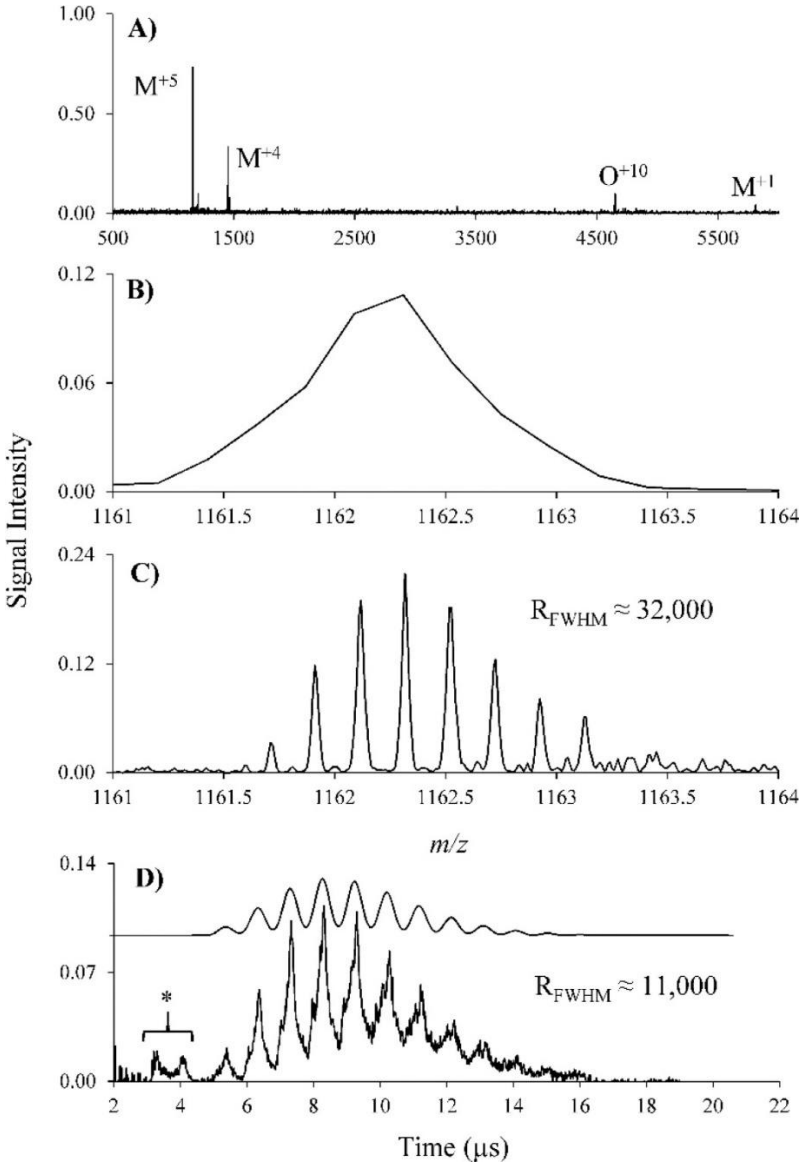

Figure 2.3 (A) eFT mass spectrum of insulin using a 250 ms transient (100 AVGS) that was truncated to 75 ms to observe the larger m/z ions. (B) eFT mass spectrum of insulin+5 using a 11.0913 ms transient (100 AVGS, 3rd harmonic). (C) eFT mass spectrum of insulin+5 using the full 250 ms transient (100 AVGS, 3rd harmonic). (D) MR-TOF mass spectrum of insulin+5 at 11.0913 ms (1000 AVGS). The theoretical isotopic distribution at a mass resolution of 11000 is shown for comparison. The * indicates peaks that arise from ions believed to be present in the region between plates 7 and 8 when plate 8 is pulsed down.

Figure 2.3 compares insulin data acquired via nESI under various mass analysis conditions. Figure 2.3a shows the broadband FT-ELIT mass spectrum obtained over the first 75 ms of a 250 ms transient (100 averages, first harmonic). The data were restricted to the first 75 ms because the higher *m/z* ion signals decay relatively quickly. This spectrum shows an *m/z* range in excess of 5000. Figure 2.3b shows the eFT mass spectrum encompassing the isotopes of the 5+ charge state of bovine insulin derived from an 11.0913 ms transient (100AVGS, third harmonic). This spectrum shows no evidence for the individual isotopes. Figure 2.3c shows the eFT mass spectrum of the 5+ charge state of insulin derived from the full 250 ms transient (100 AVGS, third harmonic), which results in a mass resolution of 32000. Figure 2.3d shows the MR-TOF MS over the narrow *m/z* range of the 5+ insulin isotopes after a storage time of 11.0913 ms (1000 AVGS). This spectrum reflects a mass resolution of roughly 11000 and should be compared directly with the spectrum of Figure 2.3b. This comparison demonstrates experimentally that mass resolution increases more quickly with time in the MR-TOF measurement, at least at short times, than does the FT-ELIT measurement. (We note that a reviewer asked if the predicted maximum resolution is achieved at longer storage times. We believe so. However, it is not trivial to demonstrate. A major point of the paper is that the *m/z* range decreases with the number of laps (see relation 2.6 and Figure 2.4, below). For the nominal m/z 316 ion used for the various figures, a storage time of 200 ms (>21000 laps) that leads to a resolution of 92000 results in an un-lapped *m/z* range of 20−30 milli-mass units. We cannot demonstrate such a resolution with the isobaric drugs used here because they differ in mass by a little over 80 milli-mass units.

2.3.2 Mass Measurement Accuracy

The main limitation to mass measurement accuracy in our ELIT device is likely to arise from instabilities in the power supplies used to trap the ions. Such instabilities affect both the ion

frequency and flight-time measurements. Assuming both detection methods employ data acquisition rates sufficient to define the position of a peak, both approaches are ultimately limited by resolution and counting statistics according to the relationship:

$$\frac{\delta M}{M} = \frac{k}{R\sqrt{n}} \tag{2.5}$$

where δM is the difference between the measured mass and the true mass, k is a factor that has been reported to be approximately unity,[44] R is mass resolution as defined above, and n is the number of detected ions. This relationship has been used in the context of frequency measurements in a Penning trap[41] and time measurements made via MR-TOF.[45] Another report indicated a k value of $1/(2(2\ ln\ 2)1/2)$ for the MR-TOF approach, assuming a Gaussian peak shape. In any case, with careful calibration of the mass scale, both FT-MS and approaches have demonstrated sub-ppm mass measurement accuracies.

While we have not attempted to optimize mass measurement accuracy in the development of this instrument to date, we have observed mass measurement accuracies on the order of 10 ppm or less when using internal standards in our FT-ELIT measurements. Based on relation 2.5 and the results and discussion regarding mass resolution above, given the same number of ions per injection, mass measurement accuracy would be expected to improve faster with the MR-TOF measurement than with the FT-MS method such that high mass measurement accuracies would be expected to be achieved faster with MR-TOF. Indeed, the speed and accuracy of the MR-TOF measurement enabled the accurate mass measurement of short-lived calcium isotopes under conditions in which Penning trap measurements were too slow.[43] Alternatively, with the higher speed of the MR-TOF measurement, it should be possible to achieve better ion statistics than the FT-MS experiment at the same mass resolution due to the greater number of measurement cycles that can be executed over a given time-scale.

2.3.3 *m/z* Range

For all practical purposes, there is no upper or lower *m/z* limit for trapping and storing ions in an ELIT. There are constraints associated with detection methods for factors such as the minimum number of charges, in the case of image charge/current measurements, and the minimum ion velocity, in the case of electron multipliers. These factors can play a role in limiting the mass range but are not addressed here. The range of *m/z* values that can be studied for a given ion injection event into the ELIT for an FT-ELIT experiment has been discussed for both the in-trap potential lift approach to ion capture[36] and for the mirror switching approach for ion capture,[35] as used here. Briefly, for mirror switching, the *m/z* range that can be captured is constrained by the flight time associated with a single reflection for the fastest ion of interest (i.e., the ion of lowest *m/z* ratio). The entrance gate must be closed before the fastest injected ion can reflect back and escape the ELIT via the entrance mirror. Any ion too slow (i.e., of *m/z* too high) to enter the ELIT during this gating window is prevented from entering the ELIT. For a given injection energy and set of trapping conditions, the *m/z* range of captured ions can be varied via the delay time between ion ejection from the accumulation quadrupole and the closing of the entrance mirror. For example, an *m/z* range of 500−5800 for a single set of ion injection conditions is demonstrated in Figure 2.3a. In the case of closed-path MR-TOF, the *m/z* range over which unambiguous mass assignments can be made is severely constrained by the so-called "race track effect", whereby fast ions lap slower ions.[47] The ratio of highest *m/z* ion to the lowest *m/z* ion that can be stored without lapping in an ELIT as a function of the number of turns (laps), *N*, is approximately[48]

$$\frac{m/z_{max}}{m/z_{min}} \approx \left(\frac{N+1}{N}\right)^2 \tag{2.6}$$

There is clearly a trade-off between resolution and *m/z* range for unambiguous mass assignment in the MR-TOF experiment. Figure 2.4 shows a plot of $m/z_{max}/m/z_{min}$ versus lap

number (blue line, left y-axis) and mass resolution for an ion of *m/z* 316, using the parameters given for Figure 2.2, versus lap number (right axis, red line). This plot clearly demonstrates how rapidly the unambiguous *m/z* range narrows with lap number. The potential for ambiguity in mass assignment at high resolution is usually minimized by injecting ions within a narrow distribution of *m/z* values and ejecting the trapped ions before lapping can take place for the mass-selected ion population. A simple example illustrating the trade-off between resolution and *m/z* range is given in Figures 2.5a,b, which compare MR-TOF data for a mixture of cations derived from the nESI of the drugs bromazepam ($C_{14}H_{11}N_3OBr$, monoisotopic *m/z* = 316.0085) and chlorprothixene ($C_{18}H_{19}NSCl$, monoisotopic *m/z* = 316.0921) at storage times of 1.1595 and 4.730 ms, respectively. For reference, the eFT mass spectrum obtained from a 150 ms transient is shown in Figure 2.5c. (The tailing in the MR-TOF data is believed to result from an asymmetric trapped ion kinetic energy distribution resulting from the nonlinear extraction field of our injection method. This is not a fundamental characteristic of MR-TOF, as this would probably be eliminated if we were to use a push−pull technique for extracting the ions. We do not claim to have achieved a state-of-the-art approach to MR-TOF. However, it is certainly good enough to illustrate the relative strengths of MR-TOF vs FT-ELIT.) The monoisotopic drug ions are labeled as 1 and 2, while the single ^{13}C-containing ions are labeled 3 and 4, the ^{81}Br- and ^{37}Cl-containing ions are labeled 5 and 6, respectively, and the ^{13}C, ^{81}Br- and ^{13}C, ^{37}Cl-containing ions are labeled 7 and 8, respectively. In Figure 2.5a, the signals for these ions are observed in the order expected for ions that undergo the same number of laps. In Figure 2.5b, however, the pairs of ions (viz., 1 and 2, 3 and 4, 5 and 6, 7 and 8) are observed in the reverse order, while the correct order within each pair is preserved. The *m/z* range estimated for the 1.1595 ms storage time (126 laps) is 5 *m/z* units assuming *m/z* min = 316.

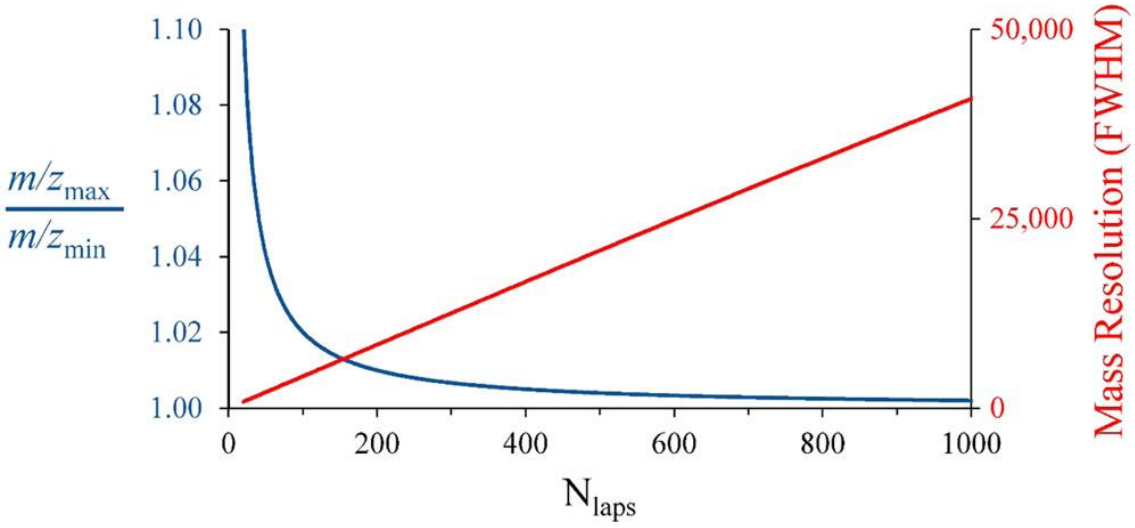

Figure 2.4. Unambiguous mass range and theoretical mass resolution as a function of the number of laps (N) for an ion of m/z 316. The parameters are as follows: t_0 = 10 μs, Δt_0 = 110 ns, K = 3858700, and Δt_a = 50 ps.

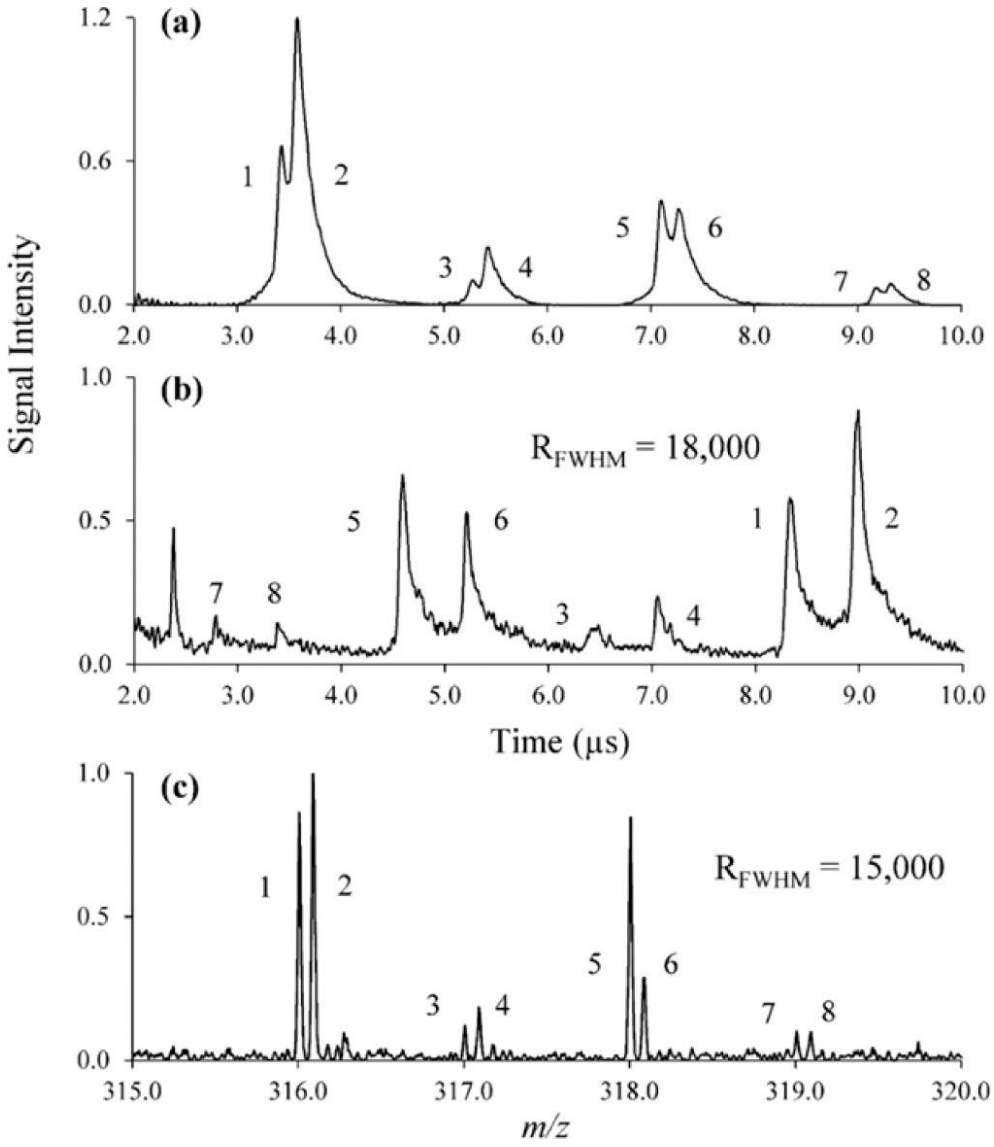

Figure 2.5. Mixture of bromazepam and chlorprothixene HCl cations detected at 1.1595 (a) and 4.730 ms (b) using MR-TOF. The eight isotopes are numerically labeled. (c) eFT mass spectrum of the same mixture at the fundamental frequency using a 150 ms transient (100AVGS).

The *m/z* range for an ion of *m/z* = 316 stored for 4.73 ms (513 laps) is roughly 1 *m/z* unit. This is consistent with ions of each nominal *m/z* ratio (e.g., the two monoisotopic ions 1 and 2 at nominal *m/z* 316) undergoing the same number of laps but each successive pair of peaks undergoing one less cycle than the ions one unit lower in *m/z* (i.e., the ions at nominal *m/z* 317 undergo 512 laps). Hence, the pairs of ions within each *m/z* unit appear in the correct order in Figure 2.5b but the ions of each successive nominal *m/z* ratio undergo one less lap than the ions of the preceding *m/z* ratio and are therefore detected in reverse order. While there are approaches that can mitigate the complications from fast ions lapping slow ions, such as mass selection prior to injection of ions into the trap, the race-track effect places a severe constraint on the use of a closed-path MR-TOF device for general usage as a mass spectrometer for a wide range of applications. The *m/z* window for un-lapped ions can be moved over a very wide range via an ion isolation step but it will be quite narrow at high resolution.

2.3.4 Peak Capacity

The term "peak capacity" is usually encountered within the context of chromatography and refers to the number of peaks that can be resolved with a particular column.[49] It is an idealized figure of merit in that is assumes that the peaks are optimally distributed across the separation space. The actual number of peaks that are resolved in the nonideal (i.e., "real-world") situation is usually much lower.[50] Within the context of mass analysis, peak capacity is equal to the number of resolution elements (*RE*) across the accessible m/z range, which is given by[51]

$$RE = \int_{m/z_{min}}^{m/z_{max}} \frac{R}{(m/z)} d(m/z) \qquad (2.7)$$

where R is the mass resolution defined above and m/z_{max} and m/z_{min} define the upper and lower limits to the *m/z* range. In the case where R is independent of *m/z*, such as the MR-TOF experiment,[30] the number of resolution elements is given by

$$RE = R \ln \frac{m/z_{max}}{m/z_{min}} \tag{2.8}$$

If the *m/z* range is restricted to non-lapped ions and $N \geq 1$, relation 8 can be rewritten based on relations 2 and 6 as

$$RE \approx \frac{t_0/N + t_a}{2\sqrt{\left(\frac{\Delta t_a}{N}\right)^2 + (\Delta t_a)^2}} \ln\left(\frac{N+1}{N}\right)^2 \tag{2.9}$$

In the case where R is inversely related to $(m/z)^{1/2}$, which applies to the FT-ELIT experiment, the number of resolution elements is given by

$$RE = CT_{acq}\left(\left(\frac{1}{\sqrt{m/z_{min}}}\right) - \left(\frac{1}{\sqrt{m/z_{max}}}\right)\right) \tag{2.10}$$

where C and T_{acq} have been defined in relation 2.1. For any mass spectrometry experiment, peak capacity is determined by both the width of the resolution element(s) and the total width of the separation space (i.e., the *m/z* range). In the case of the FT-ELIT experiment, these two factors are independent of one another, whereas they are inversely related in the closed cycle MR-TOF experiment. The result is that peak capacity increases linearly with resolution in the FT-MS experiment because the *m/z* range does not change. It is this characteristic of FT-ICR, for example, that makes it so well suited to applications like petroleomics,[52] which places a high premium on peak capacity. An example of increasing peak capacity with storage (transient) time in the FT-ELIT experiment with the present instrument is given in Figure 2.6 with mass spectra derived from the electrospray of a solution of $GdCl_3$ hexahydrate, which is dominated by GdO^+ ions and their adducts. All spectra were derived from different time segments (viz., (a) 4, (b) 15, (c) 25, and (d) 75 ms) of the same 75 ms transient.

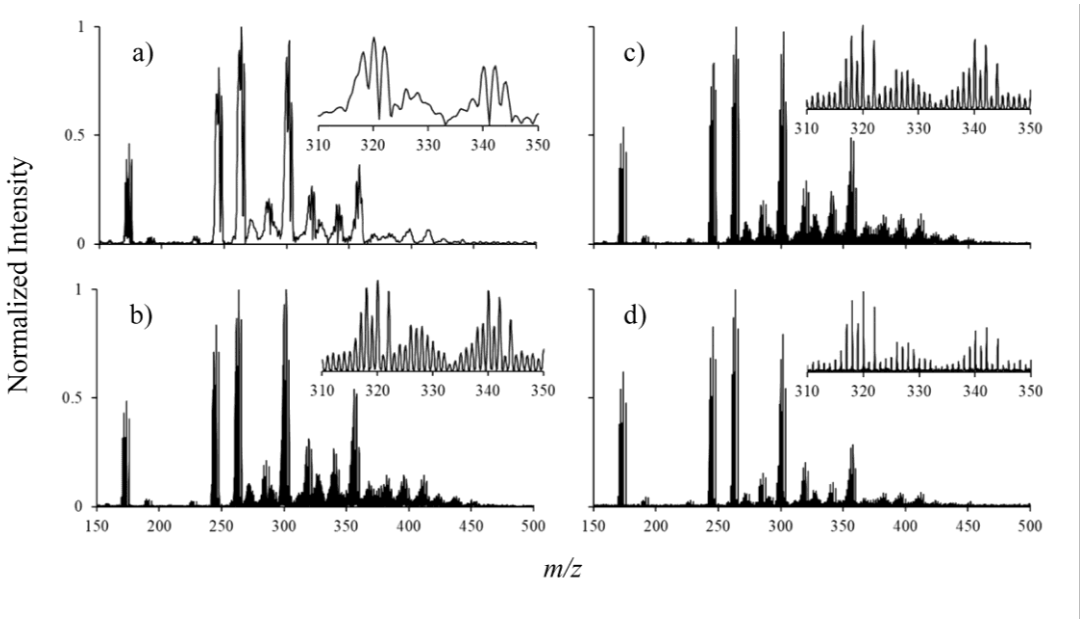

Figure 2.6: FT-ELIT MS of (a) 4 ms, (b) 15 ms, (c) 25 ms, and (d) 75ms of the same 75ms transient.

The *m/z* range for this figure is arbitrarily restricted to m/z 150 - 500 due to the absence of ions at higher *m/z* ratios. The point is that the peak capacity, even at T_{acq} = 4 ms, is already in excess of 200 and reaches nearly 5000 at T_{acq} = 75 ms within this *m/z* range. The case is dramatically different in the closed-path MR-TOF experiment.

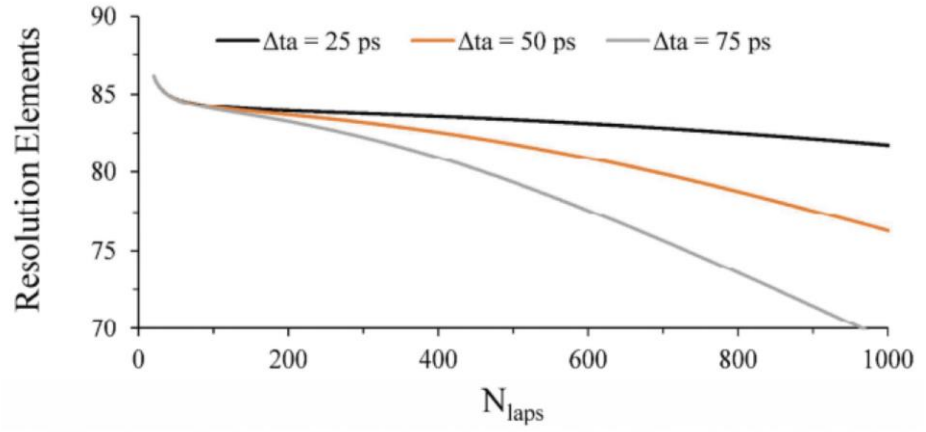

Figure 2.7: Number of resolution elements as a function of the number of laps completed (N). The parameters are as follows: t_0 = 10 μs, Δt_a = 110 ns, *m/z* = 316, k = 3858700, t_a = 9.21 μs, and Δt_a = 25 (black), 50 (orange) and 75 (grey) ps

Figure 2.7 shows plots of *RE* versus *N* for anion of *m/z* = 316 using approximate values for the current apparatus. Unlike the case with the FT-MS experiment, the number of resolution elements tends to decrease with storage time. Over the period in which the resolution continues to increase linearly with time, the number of resolution elements remains roughly constant. However, when the resolution begins to level off, the number of resolution elements decreases increasingly rapidly. The point at which this decrease becomes significant is largely determined by the dispersion term (i.e., Δt_a). The major point here is that the peak capacity of the MRTOF

measurement is relatively modest due to the rapidly decreasing *m/z* range with lap number (storage time), whereas it increases linearly with storage time in the FT-MS experiment.

It is also worth considering the case when m/z is not restricted to unlapped ions (e.g., all ions in the trap are collected during the full time range for dropping the exit lens until the last ion is detected, which is close to the time for one reflection of the slowest ion in the trap). Operating in the way presumes some means for dealing with the race-track effect. In this scenario, relation (2.9) is no longer applicable as all ions within the range of trapped ions can give rise to signals in the final MR-TOF spectrum. An estimate of the peak capacity in this situation can be made by dividing the time-window for the TOF detection, t_{TOF}, (i.e., roughly t_a in the present apparatus, which depends in part on the slowest and fastest ions in the trap) by the time-width of a peak. The maximum peak capacity would be determined by Δt_0, the initial time-width of the injected ions. If we take Δt_0 to be roughly 110 ns and the time read-out for the ion, t_{TOF}, to be roughly 10 μs, a peak capacity of roughly 90 results. The point is that the peak capacity cannot be improved with increasing N via increasing the storage time, in contrast with the FT-MS, even when the criterion for unlapped ions is lifted. This difference is due to the fact that peak width decreases in frequency-space with storage time in the FT-MS experiment whereas peak width in time does not decrease with time in the TOF experiment. Improvement in resolution with time in the TOF experiment takes place when the flight time differences between ions of different mass increase faster than the peak width. When ions are allowed to lap one another, however, flight time difference in the final t_{TOF} loses its relevance. Approaches to improve peak capacity would include narrowing t_0 and/or adding additional flight time to the t_{TOF} by injecting the ions into, for example, a linear TOF of reTOF.

2.3.5 Speed

The foregoing results and discussion provide context for considering the relative analysis times for the MR-TOF and FT experiments in an ELIT. The MR-TOF approach can provide moderate resolution at significantly shorter analysis times than the FT approach but with a limited *m/z* range. Furthermore, it is generally necessary to prevent ions from outside of the *m/z* range of interest from being injected into the ELIT in the MR-TOF experiment as such ions will appear in the mass spectrum at locations that are inconsistent with the mass calibration for the ions of interest. In order to generate data with the *m/z* range and peak capacity afforded by the FT experiment using MR-TOF, it is necessary to piece together a spectrum using multiple injections of isolated segments of the overall spectrum. In this scenario, the speed advantage of the MR-TOF is seriously compromised.

2.4 Conclusions

The linear electrostatic ion trap geometry allows for a straightforward combination of a frequency-based mass measurement (e.g., FT-ELIT MS) and a time-based measurement (e.g., MR-TOF MS). The FT-ELIT MS experiment affords a much larger *m/z* range, increasing peak capacity with time, and is less sensitive to initial injection pulse width. It can also provide superior mass resolution at long storage times, provided sufficiently long transients can be achieved. Mass resolution decreases with the inverse square root of ion *m/z* ratio with the FT experiment and tens to hundreds of charges are needed for image charge/current detection. With the MR-TOF experiment, mass resolution increases faster with storage time and is less strongly dependent upon *m/z*. Furthermore, in principle, it is possible to detect a single charge with a channel plate detection scheme. However, the race-track effect associated with a closed-path MR-TOF experiment severely limits the *m/z* range for unambiguous mass measurement and also limits peak capacity.

Taken collectively, the relative merits of these mass analysis approaches point to the use of the FT-ELIT MS scheme as most appropriate for broad *m/z* range mass analysis and the MR-TOF MS scheme as a complementary approach for "zoom-in" targeted applications that can benefit from faster measurements focused on a very narrow *m/z* range for the separation of isobaric ions, for example.

2.5 References

1. March, R. E., Todd, J. F. J. Quadrupole Ion Trap Mass Spectrometry, 2nd ed. *John Wiley & Sons, Inc.*: Hoboken, NJ, **2005**.

2. Schwartz, J. C.; Senko, M. W.; Syka, J. E. P. A two-dimensional quadrupole ion trap mass spectrometer. *J. Am. Soc. Mass Spectrom.* **2002**, 13, 659−669.

3. Hager, J. W. A new linear ion trap mass spectrometer. *Rapid Commun. Mass Spectrom*. **2002**, 16, 512−526.

4. Stafford, G. C., Jr.; Kelly, P. E.; Syka, J. E. P.; Reynolds, W. E.; Todd, J. F. J. Recent improvements in and analytical applications of advanced ion trap technology. *Int. J. Mass Spectrom. Ion Processes* **1984**, 60, 85−98.

5. Marshall, A. G.; Hendrickson, C. L.; Jackson, G. S. Fourier transform ion cyclotron resonance mass spectrometry: a primer. *Mass Spectrom. Rev.* **1998**, 17, 1−35.

6. Marshall, A. G.; Hendrickson, C. L.; Shi, S. D.-H. Scaling MS Plateaus with High-Resolution FT-ICRMS. *Anal. Chem.* **2002**, 74, 252A−259A.

7. Comisarow, M. B.; Marshall, A. G. Fourier transform ion cyclotron resonance spectroscopy. *Chem. Phys. Lett.* **1974**, 25, 282−283.

8. Kingdon, K. H.: A method for the neutralization of electron space charge by positive ionization at very low gas pressures. *Phys. Rev.* **1923**, 21, 408−418.

9. Knight, R. D. Storage of ions from laser-produced plasmas. *Appl. Phys. Lett.* **1981**, 38, 221−223.

10. Makarov, A. Electrostatic axially harmonic orbital trapping: a high-performance technique of mass analysis. *Anal. Chem.* **2000**, 72, 1156−1162.

11. Eliuk, S.; Makarov, A. Evolution of orbitrap mass spectrometry instrumentation. *Annu. Rev. Anal. Chem.* **2015**, 8, 61−80.

12. Scigelova, M.; Hornshaw, M.; Giannakopulos; Makarov, A. Fourier transform mass spectrometry. *Mol. Cell. Proteomics* **2011**, 10, 1−19.

13. Benner, W. H. A Gated Electrostatic Ion Trap to Repetitiously Measure the Charge and m/z of Large Electrospray Ions. *Anal. Chem.* **1997**, 69, 4162−4168.

14. Schultz, J. C.; Hack, C. A.; Benner, W. H. Mass determination of megadalton-DNA electrospray ions using charge detection mass spectrometry. *J. Am. Soc. Mass Spectrom.* **1998**, 9, 305−313.

15. Pierson, E. E.; Keifer, D. Z.; Contino, N. C.; Jarrold, M. F. Probing higher order multimers of pyruvate kinase with charge detection mass spectrometry. *Int. J. Mass Spectrom.* **2013**, 337, 50−56.

16. Pierson, E. E.; Contino, N. C.; Keifer, D. Z.; Jarrold, M. F. Charge detection mass spectrometry for single ions with an uncertainty in the charge measurement of 0.65 e. *J. Am. Soc. Mass Spectrom.* **2015**, 26, 1213−1220.

17. Keifer, D. Z.; Shinholt, D. L.; Jarrold, M. F. Charge detection mass spectrometry with almost perfect charge accuracy. *Anal. Chem.* **2015**, 87, 10330−10337.

18. Doussineau, T.; Kerleroux, M.; Dagany, X.; Clavier, C.; Barbaire, M.; Maurelli, J.; Antoine, R.; Dugourd, P. Charging maegadalton poly(ethylene oxide)s by electrospray ionization. A charge detection mass spectrometry study. *Rapid Commun. Mass Spectrom.* **2011**, 25, 617−623.

19. Doussineau, T.; Antoine, R.; Santacreu, M.; Dugourd, P. Pushing the limit of infared multiphoton dissociation to megadalton-size DNA ions. *J. Phys. Chem. Lett.* **2012**, 3, 2141−2145.

20. Elliott, A. G.; Merenbloom, S. I.; Chakrabarty, S.; Williams, E. R. Single particle analyzer of mass: a charge detection mass spectrometer with a multi-detector electrostatic ion trap. *Int. J. Mass Spectrom.* **2017**, 414, 45−55.

21. Wuerker, R. F.; Shelton, H.; Langmuir, R. J. Electrodynamic containment of charged particles. *Appl. Phys.* **1959**, 30, 342−349.

22. Ring, S.; Pedersen, H. B.; Heber, O.; Rappaport, M. L.; Witte, P.; Bhushan, K. G.; Altstein, N.; Rudich, Y.; Sagi, I.; Zajfman, D. Fourier transform time-of-flight mass spectrometry in an electrostatic ion beam trap. *Anal. Chem.* **2000**, 72, 4041−4046.

23. Zajfman, D.; Rudich, Y.; Sagi, I.; Strasser, D.; Savin, D. W.; Goldberg, S.; Rappaport, M.; Heber, O. High resolution mass spectrometry using a linear electrostatic ion beam trap. *Int. J. Mass Spectrom.* **2003**, 229, 55−60.

24. Wollnik, H.; Przewloka, M. Time-of-flight mass spectrometers with multiply reflected ion trajectories. *Int. J. Mass Spectrom. Ion Processes* **1990**, 96, 267−274.

25. Wollnik, H.; Casares, A.; Radford, D.; Yavor, M. Multi-pass time-of-flight mass spectrometers of high resolving power. *Nucl. Instrum. Methods Phys. Res., Sect. A* **2004**, 519, 373−379.

26. Toyoda, M. Development of a multi-turn time-of-flight mass spectrometers and their applications. *Eur. Mass Spectrom.* **2010**, 16, 397−406.

27. Plaβ, W. R.; Dickel, T.; Scheidenberger, C. Multiple-reflection time-of-flight mass spectrometry. *Int. J. Mass Spectrom.* **2013**, 349, 134−144.

28. Schury, P.; Okada, K.; Shchepunov, S.; Sonoda, T.; Takamine, A.; Wada, M.; Wollnik, H.; Yamazaki, Y. Multi-reflection time-of-flight mass spectrograph for short-lived radioactive ions. *Eur. Phys. J. A* **2009**, 42, 343−349.

29. Wolf, R.; Errit, M.; Marx, G.; Schweikhard, L. A multi-reflection time-of-flight mass separator for isobaric purification of radioactive ion beams. *Hyperfine Interact*. **2011**, 199, 115−122.

30. Dickel, T.; Plaβ, W. R.; Lang, J.; Ebert, J.; Geissel, H.; Haettner, E.; Jesch, C.; Lippert, W.; Petrick, M.; Scheidenberger, C.; Yavor, M. I. Multiple-reflection time-of-flight mass spectrometry for *in situ* applications. *Nucl. Instrum. Methods Phys. Res., Sect. B* **2013**, 317, 779−784.

31. Hilger, R. T.; Santini, R. E.; McLuckey, S. A. Nondestructive tandem mass spectrometry using a linear quadrupole ion trap coupled to a linear electrostatic ion trap. *Anal. Chem.* **2013**, 85, 5226−5232.

32. Hilger, R. T.; Santini, R. E.; McLuckey, S. A. Square wave modulation of a mirror lens for ion isolation in a Fourier transform electrostatic linear ion trap mass spectrometer. *Int. J. Mass Spectrom.* **2014**, 362, 1−8.

33. Hilger, R. T.; Santini, R. E.; McLuckey, S. A. Tandem mass spectrometry in an electrostatic linear ion trap modified for surface-induced dissociation. *Anal. Chem.* **2014**, 86, 8822−8828.

34. Hilger, R. T.; Wyss, P. J.; Santini, R. E.; McLuckey, S. A. Absorption mode Fourier transform electrostatic linear ion trap mass spectrometry. *Anal. Chem.* **2013**, 85, 8075−8079.

35. Dziekonski, E. T.; Santini, R. E.; McLuckey, S. A. A dual detector Fourier transform electrostatic linear ion trap utilizing in-trap potential lift. *Int. J. Mass Spectrom.* **2016**, 405, 1−8.

36. Dziekonski, E. T.; Johnson, J. T.; Hilger, R. T.; McIntyre, C.; Santini, R. E.; McLuckey, S. A. Voltage-induced frequency drift correction in Fourier transform electrostatic linear ion trap mass spectrometry using mirror -switching. *Int. J. Mass Spectrom*. **2016**, 410, 12−21.

37. Dziekonski, E. T.; Johnson, J. T.; McLuckey, S. A. Utility of higher harmonics in electrospray ionization Fourier transform electrostatic linear ion trap mass spectrometry. *Anal. Chem.* **2017**, 89, 4392−4397.

38. Hilger, R. T.; Dziekonski, E. T.; Santini, R. E.; McLuckey, S. A. Injecting electrospray ions into a Fourier transform electrostatic linear ion trap. *Int. J. Mass Spectrom.* **2015**, 378, 281−287.

39. Lange, O.; Damoc, E.; Wieghaus, A.; Makarov, A. Enhanced Fourier transform for Orbitrap mass spectrometry. *Int. J. Mass Spectrom.* **2014**, 369, 16−22.

40. Dickel, T.; Yavor, M. I.; Lang, J.; Plaß, W. R.; Lippert, W.; Geissel, H.; Scheidenberger, C. Dynamical time focus shift in multiple-reflection time-of-flight mass spectrometers. *Int. J. Mass Spectrom.* **2017**, 412, 1−7.

41. McLuckey, S. A.; Wells, J. M. Mass analysis at the advent of the 21st century. *Chem. Rev.* **2001**, 101, 571−606.

42. Murray, K. K.; Boyd, R. K.; Eberlin, M. N.; Langley, G. J.; Li, L.; Naito, Y. Definitions of terms relating to mass spectrometry (IUPAC Recommendations 2013). *Pure Appl. Chem.* **2013**, 85, 1515−1609.

43. Wolf, R. N.; Wienholtz, F.; Atanasov, D.; Beck, D.; Blaum, K.; Borgmann, Ch.; Herfurth, F.; Kowalska, M.; Kreim, S.; Litvinov, Yu. A.; Lunney, D.; Manea, V.; Neidherr, D.; Rosenbusch, M.; Schweikhard, L.; Stanja, J.; Zuber, K. Mass and lifetime measurements of exotic nuclei in storage rings. *Int. J. Mass Spectrom.* **2013**, 349−350, 123−133.

44. Bollen, G. Mass measurements of short-lived nuclides with ion traps. *Nucl. Phys. A* **2001**, 693, 3−18.

45. Schury, P.; Wada, M.; Ito, Y.; Naimi, S.; Sonoda, T.; Mita, H.; Takamine, A.; Okada, K.; Wollnik, H.; Chon, S.; Haba, H.; Kaji, D.; Koura, H.; Miyatake, H.; Morimoto, K.; Morita, K.; Ozawa, A. A multi-reflection time-of-flight mass spectrograph for short-lived and super-heavy nuclei. *Nucl. Instrum. Methods Phys. Res., Sect. B* **2013**, 317, 537−543.

46. Wienholtz, F.; Beck, D.; Blaum, K.; Borgmann, Ch.; Breitenfeldt, M.; Cakirli, R. B.; George, S.; Herfurth, F.; Holt, J. D.; Kowalska, M.; Kreim, S.; Lunney, D.; Manea, V.; Menéndez, J.; Neidherr, D.; Rosenbusch, M.; Schweikhard, L.; Schwenk, A.; Simonis, J.; Stanja, J.; Wolf, R. N.; Zuber, K. Masses of exotic calcium isotopes pin down nuclear forces. *Nature* **2013**, 498, 346−349.

47. Schury, P.; Ito, Y.; Wada, M.; Wollnik, H. Wide-band mass measurements with a multi-reflection time-of-flight mass spectrograph. *Int. J. Mass Spectrom.* **2014**, 359, 19−25.

48. Yavor, M. I.; Plaβ, W. R.; Dickel, T.; Geissel, H.; Scheidenberger, C. Ion-optical design of a high-performance multiple-reflection time-of-flight mass spectrometer and isobar separator. *Int. J. Mass Spectrom.* **2015**, 381−382, 1−9.

49. Giddings, J. C. Maximum number of components resolvable by gel filtration and other elution chromatographic methods. *Anal. Chem.* **1967**, 39, 1027−1028.

50. Davis, J. M.; Giddings, J. C. Statistical theory of component overlap in multicomponent chromatograms. *Anal. Chem.* **1983**, 55, 418−424.

51. Liu, J.; Chrisman, P. A.; Erickson, D. E.; McLuckey, S. A. Relative information content and top-down proteomics by mass spectrometry: utility of ion/ion proton-transfer reactions in electrospray-based approaches. *Anal. Chem.* **2007**, 79, 1073−1081.

52. Marshall, A. G.; Rodgers, R. P. Petroleomics: Chemistry of the underworld. *Proc. Natl. Acad. Sci. U. S. A.* **2008**, 105, 18090−18095.

CHAPTER 3. A MINIATURIZED FOUIER TRANSFORM ELECTROSTATIC LINEAR ION TRAP MASS SPECTROMETER: MASS RANGE AND RESOLUTION

Adapted with permission from Johnson, J. T., Lee, K. W., Bhanot, J. S., McLuckey, S. A. *J. Am. Soc. Mass Spectorm.* **2019**, 30, 588-594.

3.1 Introduction

In Fourier transform mass spectrometry (FT-MS), mass resolution ($M/\Delta M_{FWHM}$) is directly related to the frequencies of detected ions. Increased mass resolution results in increased spectral peak capacity and potentially higher mass measurement accuracy making high resolution mass spectrometers particularly useful for complex mixture analysis.[1-4] Existing methods to increase mass resolution relative to magnitude mode FT-based mass analysis include: data processing techniques that consider phase information,[5-8] extending data acquisition times,[9, 10] and increasing the detection frequencies.[11-13] Increasing detection frequencies can be achieved by increasing the number of detection events,[11, 12, 14] increasing the magnetic field strength in Fourier transform ion cyclotron resonance mass spectrometers (FT-ICR),[15] or by increasing the number of axial oscillations per unit time in electrostatic traps such as the Orbitrap™ and electrostatic linear ion traps (ELIT).[13, 16, 17] Alternatively, detection at higher harmonics using multiple detection electrodes, which was first demonstrated in the FT-ICR community,[11, 18-21] can lead to resolution increases in proportion to the number of detection electrodes. Use of frequency multiplying traps has been limited, however, largely due to the complex nature of the frequency spectra (fractional harmonics) that can arise from imperfectly positioned electrodes. Harmonic overtones naturally exist in many FT-MS devices due to signal deviation from an ideal sine-wave. Naturally occurring harmonics are often regarded as spectral artifacts and are widely considered a nuisance as they complicate spectral interpretation.[22] Under conditions in which transient length is pressure-limited,

however, resolution increases linearly with harmonic order.[23, 24] Multiple detectors have been used in charge detection mass spectrometry (CDMS) to measure the mass of large ion species. CDMS using multiple detectors was initially done using array detection systems such as those developed by Jarrold et al.,[25] Austin et al.,[26] and Gamero-Castaño.[27] In addition to array detection, measuring induced ion signal multiple times, using an ELIT or Conetrap, has also been used to increase the accuracy of *m/z* and charge measurements in CDMS.[28] Furthermore, the Williams group has implemented a trapping device that also utilizes an array detection scheme.[29] Whereas CDMS analyzes single ion species and focuses primarily on multiply-charged megadalton ions, electrostatic linear ion traps are also used as conventional mass spectrometers by injecting ion bunches.[30] Introducing multiple detectors in ensemble measurements using an FT-ELIT necessitates precise alignment else fractional harmonic are manifested.[12] By reducing the axial length of an ELIT, frequencies and thus resolution are increased at equivalent transient lengths. The introduction of the high-field Orbitrap™ allowed for higher detected frequencies by reducing the dimensions of the mass analyzer and thereby increasing the electric field strength between the inner spindle and outer electrode.[13] Reducing the size of the Orbitrap™ resulted in a frequency increase of ~ 1.8-fold when compared to the standard Orbitrap™. In much the same way, detected ion frequencies in a FT-ELIT can be increased by simply reducing the spaces between opposing ion mirrors. Herein, the performance of a miniaturized ELIT is described to demonstrate the influence of reducing the trap axial dimension on mass resolution and mass/charge range. Comparisons to a previously used ELIT are drawn to demonstrate the relative performance differences between each device. The miniaturized ELIT has been modified by reducing the spacing between the electrodes making up the ion mirrors and by reducing the space separating the ion mirrors. The properties and operation of the previous ELIT have been discussed at length

elsewhere[3] and are mentioned here only as means of comparison with the smaller ELIT discussed here.

3.2 Experimental Section

3.2.1 Materials

Bradykinin acetate salt and insulin (from bovine pancreas) were purchased from Sigma-Aldrich (St. Louis, MO, USA). Methanol (MeOH) was purchased from Thermo Fisher Scientific (Waltham, MA, USA). Glacial acetic acid (AcOH) was purchased from Mallinckrodt (Phillipsburg, NJ, USA). HPLC grade water (H_2O) was purchased from Fisher Scientific (Pittsburgh, PA, USA). LC/MS tuning mix for ESI (G2421A) was purchased from Agilent Technologies (Santa Clara, CA, USA). Insulin was prepared to a final concentration of 100 μM in 49.5/49.5/1 v/v/v MeOH/H_2O/AcOH. Bradykinin was prepared to a final concentration of 20 μM in 49.5/49.5/1 v/v/v MeOH/H_2O/AcOH.

3.2.2 Mass Spectrometry

All experiments were carried out on a home-built mass spectrometer. The ELIT described previously has been replaced with a shorter trap in which the spacings between electrodes have been reduced by a factor of 2 (plates 1 to 3 = 3.81mm, plate 3 to central housing = 5.715 mm). Spacings are maintained using alumina spacers (Kimball Physics). In addition, the length of the central housing was reduced from 50.8 to 25.4 mm. The nano-electrospray ionization (nESI) source and the method by which ions are concentrated and injected into the electrostatic linear ion trap (ELIT) have been described.[30] The electrostatic linear ion traps described in this work are 2.625″ and 5.25″ in length measured from the beginning of the first trapping electrode to the end of the last trapping electrode.

The charge-sensitive detection electronics have been described previously.[31, 32] The in-vacuum electronics for the 2.625" ELIT were altered due to spatial restrictions within the vacuum chamber. Thus, the detection electronics were moved onto a printed circuit board to reduce the dimensions of in-vacuum electronics. A side effect of moving to a PCB detection scheme is a reduction in the total dielectric noise of the circuit including detector (capacitance between the detector electrode and the JFET) and stray (capacitance between elements within the detection electronics) capacitance. The housing used to mount the in-vacuum electronics for the 2.625" trap is shown in Figure 3.1a along with the associated PCB and surface mount elements for the in-vacuum circuit (Figure 3.1b). The schematics for the in-vacuum portion of the detection circuitry are shown in Figure 3.1c.

The output of the charge sensitive preamplifier (A250, Amptek) was filtered (band-pass, Krohn-Hite Model 3945, Brockton, MA) and amplified (gain = 5) prior to digitization by a PCI-based digitizer (CS1621, 16-bit, Gage Applied Technologies, Lanchine, Quebec, Canada) at a rate of 10 MS/s (AC coupled, 1 MΩ input impedance, 25 MHz low-pass filter enabled). A program written in LabVIEW 13.0 (National Instruments, Austin, TX) was used to acquire each transient for FT analysis. A custom program, written in MATLAB 2017a, was used to process the transients using the enhanced Fourier transform (eFT).[8]

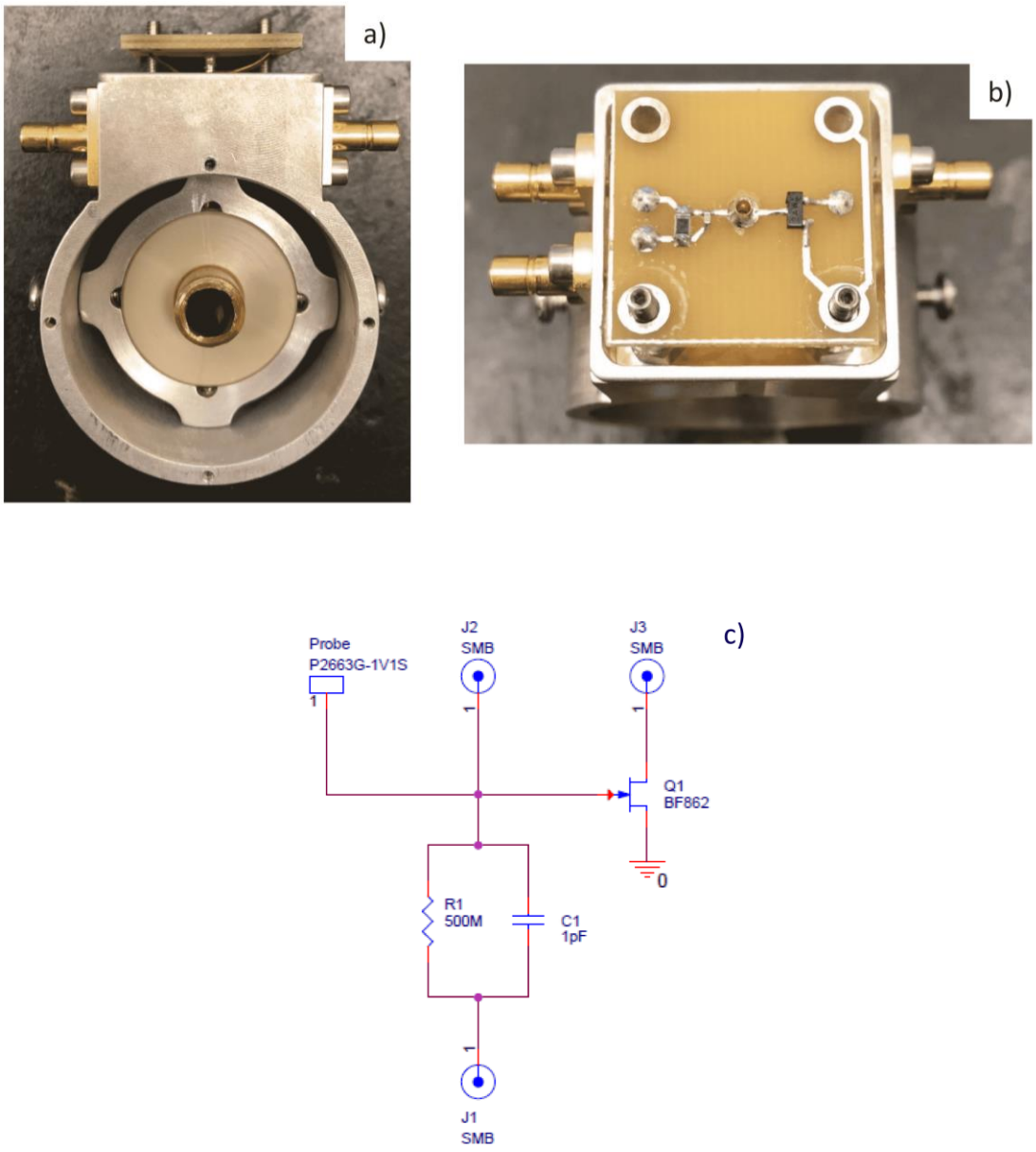

Figure 3.1. The in-vacuum detector housing (a) attached to the field free region of the ELIT and the associated PCB detection electronics (b). The pickup electrode is connected to the detection PCB via a spring-loaded push pin. The schematics for the in-vacuum electronics (c) are relatively simple and include a JFET, feedback resistor, and a capacitor.

3.2.3 Ion Optical Simulations

A model of the trapping quadrupole, intermediate lenses, differential pumping region, and 2.625″ ELIT was constructed in SIMION v8.1. An additional model using the 5.25″ ELIT was also constructed for theoretical frequency and mass range comparisons. For mass range simulations, ions were initialized within a cylindrical distribution (radius = 0.1 mm, length = 1 mm) located near the end exit of our trapping quadrupole with kinetic energies uniformly distributed between of 0.01 and 0.02 eV. Collisional cooling using nitrogen gas was simulated via a hard-sphere collision model that was included in the SIMION software. The trapping quadrupole was operated at 816 kHz with the RF amplitude set such that the m/z being trapped had a q value of 0.4 on the Matheiu stability diagram. The LINACII electrodes, rod offset, and exit lens were held at 700 V, 1990 V, and 1978 V during the 2 ms ion thermalization step. Ions were ejected from the trapping quadrupole by pulsing the exit lens from 1978 to 1500 V at a zero crossing of the RF. After ion injection, the background pressure was set to zero to avoid unstable trajectories caused by ion/neutral collisions. Mass/charge range simulations for Figures 4 and 5 were done by injecting 100 ions of each mass-to-charge ratio from *m/z* 100 to 8000 in 50 *m/z* unit increments. Low *m/z* limit simulations were done with 100 ions of each mass-to-charge ratio from *m/z* 100 to 1500 in 10 *m/z* unit increments in order to better approximate the low m/z limits of the 2.625″ and 5.25″ ELIT.

3.3 Results and Discussion

3.3.1 Mass Resolution

Reduction in the axial dimension of an ELIT at constant trapping voltages can be used to increase the detected frequencies of ions in the device thereby increasing mass resolution per unit acquisition time. Reducing the length of our ELIT by a factor of 2 resulted in a ~ 90% increase in oscillation frequencies. The frequency increase and the resulting resolution increase are demonstrated using ions of the + 5 charge state of bovine insulin in Figure 3.2. After a 250 ms data acquisition time, the isotopes of $[insulin+5H]^{5+}$ are not fully resolved in the 5.25″ ELIT; however, in the 2.625″ ELIT, the + 5 charge state is baseline resolved with a resolution increase equal to the observed frequency increase. Peak shifting on the right side of the red spectra in Figure 3.2 is a result of space charge due to high ion densities. We have demonstrated previously that at lower ion densities (i.e., shorter accumulation times), peaks remain uncoalesced.[23] Theoretical fits for the +5 charge state of insulin are shown in Figure 3.3.

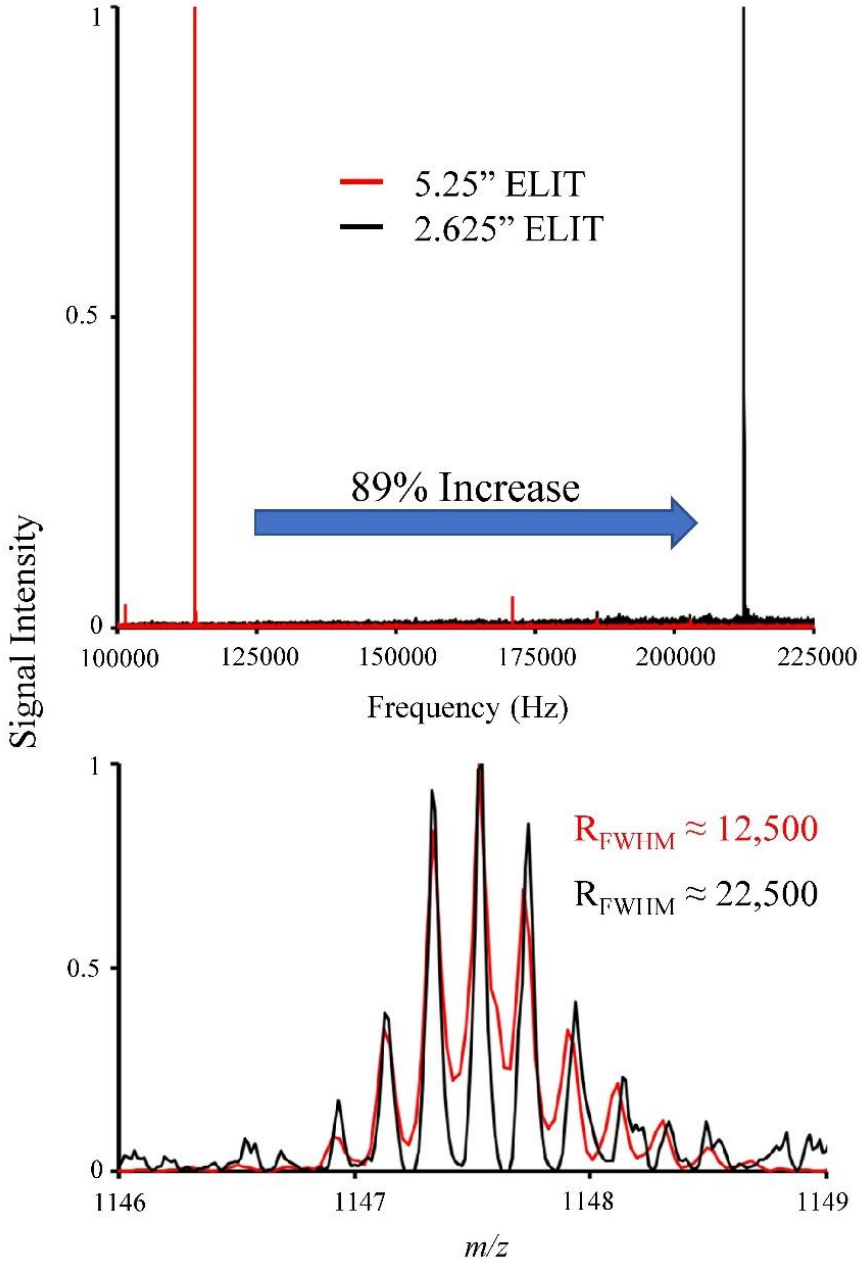

Figure 3.2. (top) Detected ion frequencies for [insulin+5H]$^{5+}$ ions in the 5.25″ (red) and 2.625″ (black) ELITs. eFT mass spectra of [insulin+5H]$^{5+}$ ions for a 250 ms transient using the 5.25″ (red) and 2.625″ (black) ELITs.

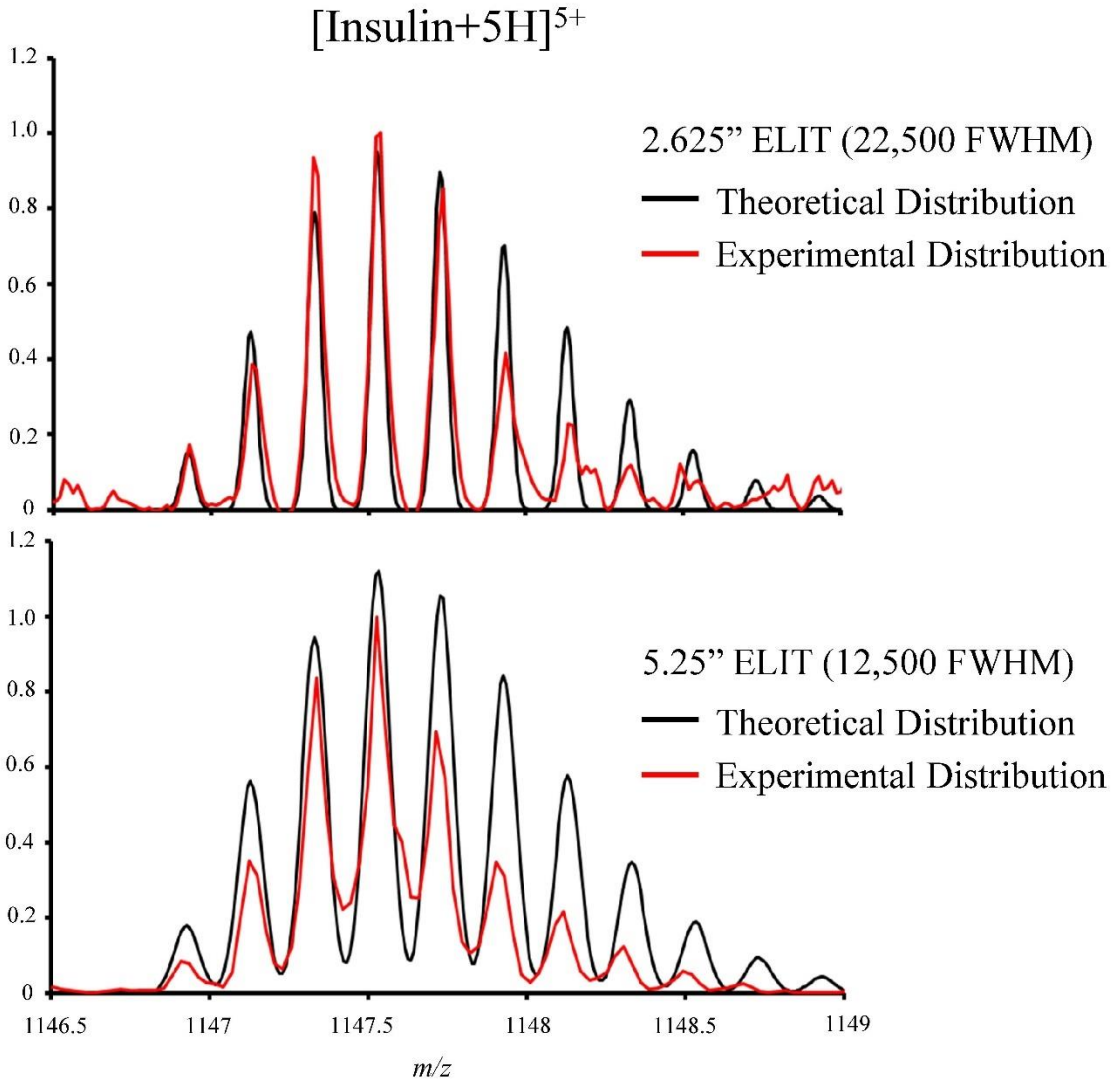

Figure 3.3. Experimental (red) and theoretical (black) mass spectra of [Insulin+5H]$^{5+}$ in the 2.625” (top) and 5.25” (bottom) ELIT.

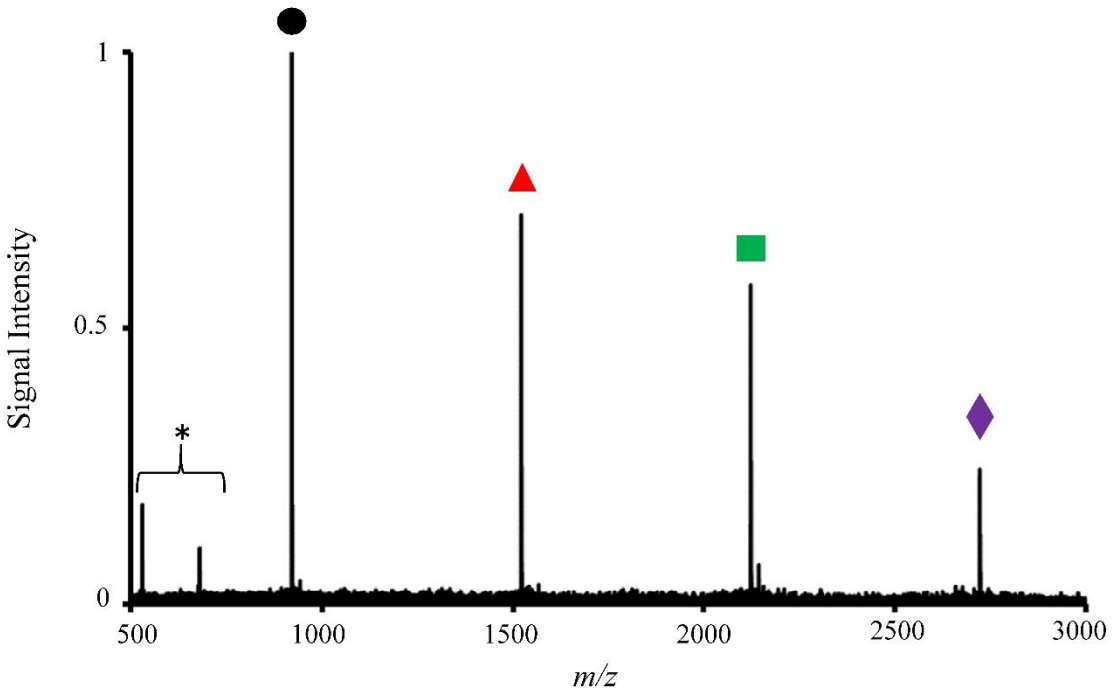

m/z	R_{FWHM} (150ms Transient)	C-Value
922.01 ●	15,300	3.10×10^6
1521.97 ▲	11,500	2.99×10^6
2121.93 ■	9,800	3.01×10^6
2721.89 ♦	8,550	2.97×10^6

Figure 3.4. eFT mass spectrum of Agilent ESI Tuning Mix (G2421A) from 500 to 3000 *m/z* (150 ms transient, 100 averages) with corresponding m/z values, resolutions (FWHM), and calculated instrument proportionality constants. The * indicates higher harmonics.

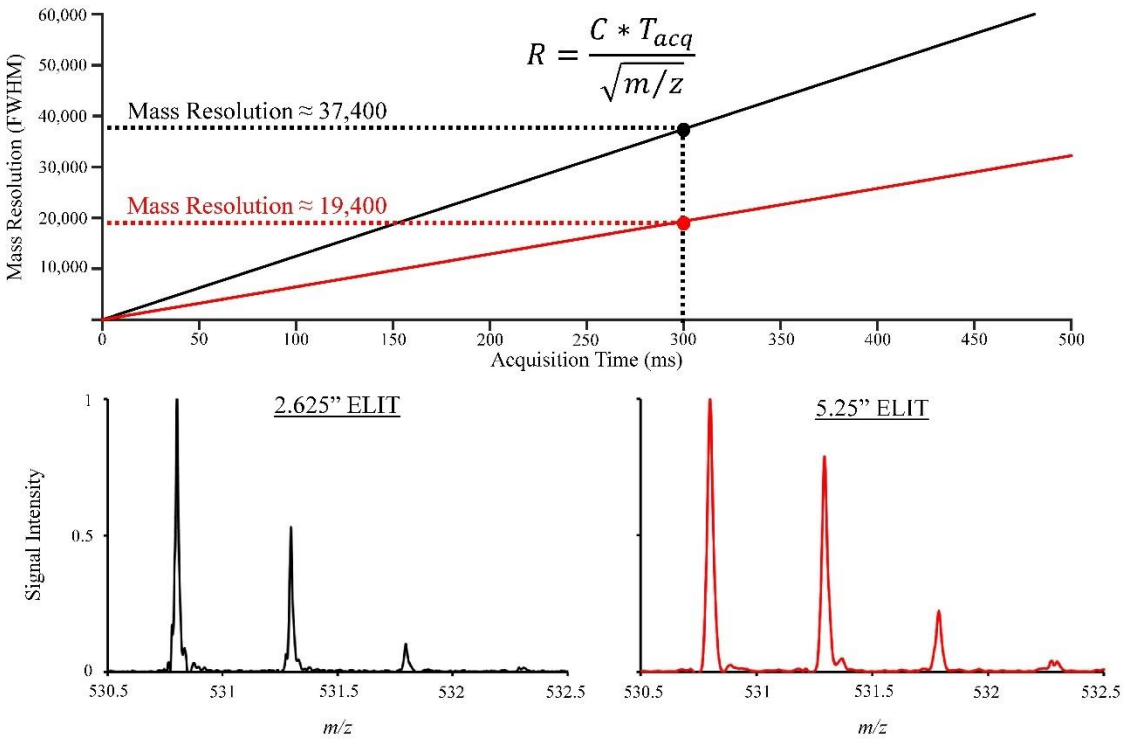

Figure 3.5. Theoretical resolution trends for the 2.625″ (black) and 5.25″ (red) FT-ELIT mass analyzers at *m/z* 530.8 based on the average proportionality constant calculated using eFT mass spectra of bradykinin^{2+} from 100, 150, 200, 250, and 300 ms transients in either device

In an FT-ELIT, resolution, *R*, increases linearly with acquisition time, T_{acq}, and decreases with the square root of *m/z*. In the absence of dephasing, resolution follows the equation below:

$$R = CT_{acq}/(m/z)^{1/2} \quad (3.1)$$

where *C* is a proportionality constant that depends on the device. This proportionality constant is directly related to mass resolution and should be independent of mass/charge value provided detected ion signals persist over the duration of the acquisition time. In Figure 3.4, measured proportionality constants are reported over a range of *m/z* values (~ 1800 *m/z*) produced using Agilent LC/MS tuning mix for ESI (G2421A). The consistency of the proportionality constants over a wide m/z range demonstrates that the increased mass resolution in the miniaturized device applies for a wide range of masses under a single fixed set of trapping conditions, which demonstrates the ability of the FT-ELIT to operate as a broadband mass spectrometer. A mass resolution of ~ 37,400 FWHM was achieved for the + 2 charge state of bradykinin at *m/z* 530.8 using a 300 ms acquisition time in the 2.625″ ELIT. For comparison, an equivalent acquisition time on the 5.25″ FT-ELIT yielded a resolution of roughly 20,050 FWHM for the same *m/z* value (see Figure 3.5). Alternatively, in the 2.625″ ELIT, a resolution of approximately 20,050 FWHM can be reached after only 154 ms of data acquisition. Using the proportionality constant calculated for the $[\text{bradykinin+2H}]^{2+}$ ions in the 5.25″ and 2.625″ ELITs, theoretical resolutions for different acquisition times were calculated and plotted in Figure 3. Such plots illustrate the relative resolution performance of the two analyzers and can be used to predict resolution for different acquisition times.

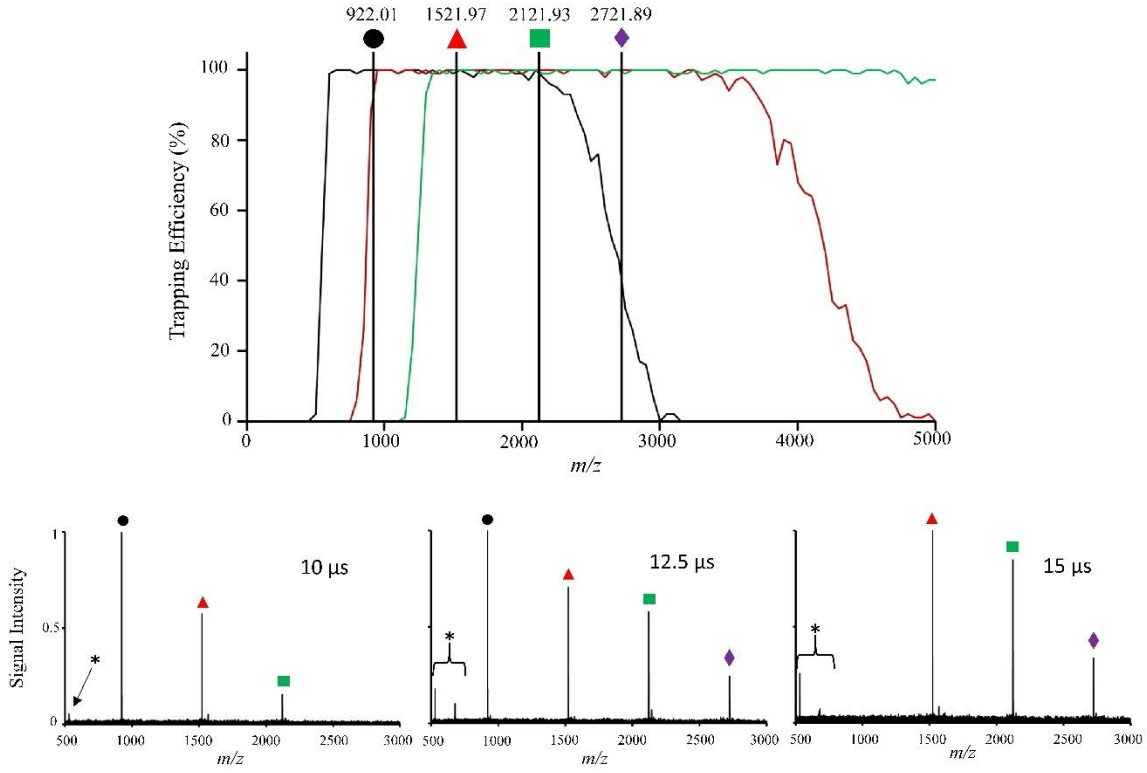

Figure 3.6. Mass/charge range simulated as a function of mirror switching time (µs). Agilent ESI tuning mix (G2421A) from *m/z* 500 to 3000 (150 ms transient, 100 averages). The * indicates higher harmonics.

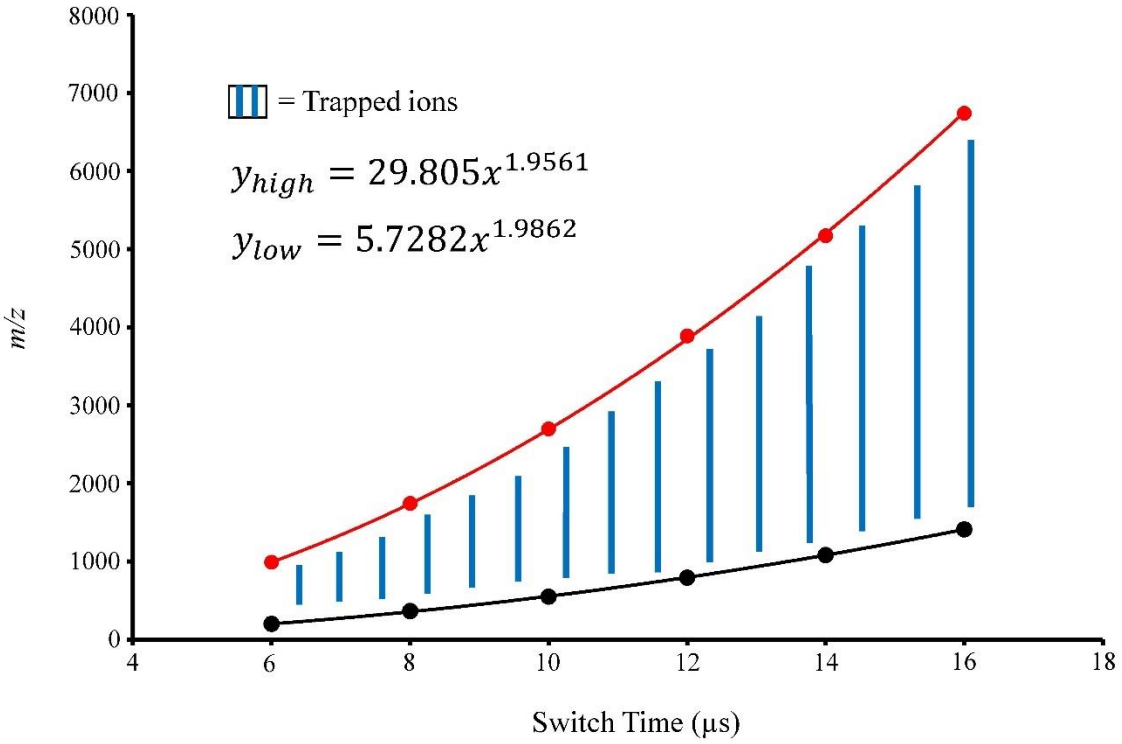

Figure 3.7. Ions trapped with an efficiency of at least 50% for mirror switching times from 6 to 16 µs in the 2.625″ ELIT. Trapping efficiencies were determined using SIMION v8.1. Ions between the m/z_{high} (red) and the m/z_{low}(black) are stably trapped for a given mirror switching time.

3.3.2 *m/z* Range

Ion capture in an ELIT can be affected by either potential lift or mirror switching approaches, both of which have been described previously.[33] Of the two techniques, mirror switching offers larger mass/charge ranges and is used in the current work. Mirror switching involves the release of ions from an accumulation quadrupole while the entrance mirror voltage is low enough to allow ions to enter the ELIT with a subsequent increase in the entrance mirror voltage (i.e., mirror switching) to capture the ions that are in the ELIT. The time between dumping the ions from the accumulation quadrupole and the switching of the entrance mirror voltage to capture ions in the ELIT, referred to herein as the mirror switching time, determines the mass/charge range of the ions captured in the ELIT. Ions with flight times from the accumulation

quadrupole to the entrance mirror that are roughly equal to or longer than the mirror switching time are too slow to enter the ELIT, which establishes the upper *m/z* limit. The lower *m/z* limit coincides with ions with flight times from the exit of the accumulation quadrupole to the far mirror and back out of the ELIT that are roughly equal to or less than the mirror switching time. Experimental mass/charge ranges are demonstrated in Figure 3.6 using Agilent LC/MS tuning mix for ESI (G2421A).

Upper and lower *m/z* limits of the 2.625″ ELIT were calculated using various mirror switching times in SIMION v8.1 for the geometries and voltages relevant to the experiments of Figure 3.6 and the results were consistent with the experimental observations for the tuning mix. In Figure 3.7, trapped *m/z* values between 6 and 16 μs switch times are used to illustrate the relationship between mirror switching time and *m/z* range for the 2.625″ ELIT using a 50% trapping efficiency as an arbitrary working regime to define the upper and lower *m/z* limits. Fits of the lower (m/z_{low}) and upper (m/z_{high}) *m/z* limits as functions of the mirror switching time are shown as black and red lines, respectively. The data approximately follow a power-of-2 relationship which is consistent with the relationship between ion velocity and *m/z*. The ratio of the coefficients in the two fits can be used to estimate the mass range at any mirror switching time (i.e., $m/z_{high} = 5.2 * m/z_{low}$). For comparison, in the 5.25″ ELIT, an analogous simulation exercise yielded the relationship $m/z_{high} = 8.9 * m/z_{low}$. Hence, for a given low *m/z* limit, the longer ELIT yields a roughly 71% larger upper *m/z* limit. Alternatively, for a given upper *m/z* limit, which corresponds to a given mirror switching time, the lower *m/z* limit for the 2.625″ ELIT is 1.71× greater than that of the 5.25″ ELIT.

3.4 Conclusions

Reducing the length of FT-ELIT mass spectrometers offers a simple way to enhance mass resolution albeit with a proportionally reduced mass range. Mass resolution increases linearly with frequency. For an equivalent transient length, which implies an equivalent path-length, resolution is higher in a shorter ELIT. Mass resolution in a 2.625″ ELIT increased by ~ 90% when compared to a 5.25″ ELIT. Although a shorter trap has higher mass resolution, it has a smaller mass/charge range. For mirror switching at a fixed distance from the ion accumulation quadrupole to the entrance mirror and a fixed mirror switching time, the upper *m/z* limit is independent of the length of the ELIT. Only the low *m/z* limit is affected by reducing the length of the ELIT. For the instrument geometry used in this work, the *m/z* range for the 5.25″ ELIT was reduced from ($m/z_{low} - 8.9\, m/z_{high}$) to ($m/z_{low} - 5.2\, m/z_{high}$) when reducing the trap length to 2.625″. However, the *m/z* range is readily adjusted by changing the mirror switching time. Hence, it is possible, in principle, to access a practically unlimited *m/z* range by stitching together spectra obtained at different mirror switching times.

3.5 References

1. Kim, S., Rodgers, R.P., Marshall, A.G. Truly exact mass: elemental composition can be determined uniquely from molecular mass measurement at ~0.1 mDa accuracy for molecules up to ~500 Da. *Int. J. Mass Spectrom.* **2006**, 251, 260–265.

2. Smith, D.F., Podgorski, D.C., Rodgers, R.P., Blakney, G.T., Hendrickson, C.L. 21 tesla FT-ICR mass spectrometer for ultrahigh-resolution analysis of complex organic mixtures. *Anal. Chem.* **2018**, 90, 2041– 2047.

3. Dziekonski, E.T., Johnson, J.T., Lee, K.W., McLuckey, S.A. Fourier transform MS and closed-path multireflection time-of-flight MS using an electrostatic linear ion trap. *Anal. Chem.* **2017** 89, 10965–10972.

4. Marshall, A.G., Hendrickson, C.L., Jackson, G.S. Fourier transform ion cyclotron resonance mass spectrometry: a primer. *Mass Spectrom. Rev.* **1998**, 17, 1–35.

5. Comisarow, M.B., Marshall, A.G. Selective-phase ion cyclotron resonance spectroscopy. *Can. J. Chem.* **1974**, 52, 1997–1999.

6. Marshall, A.G., Comisarow, M.B., Parisod, G. Relaxation and spectral line shape in Fourier transform ion resonance spectroscopy. *J. Chem. Phys.* **1979**, 71, 4434–4444.

7. Hilger, R.T., Wyss, P.J., Santini, R.E., McLuckey, S.A. Absorption mode Fourier transform electrostatic linear ion trap mass spectrometry. *Anal. Chem.* **2013**, 85, 8075–8079.

8. Lange, O., Damoc, E., Wieghaus, A., Makarov, A. Enhanced Fourier transform for Orbitrap mass spectrometry. *Int. J. Mass Spectrom.* **2014**, 369, 16–22.

9. Comisarow, M.B., Marshall, A.G. Theory of Fourier transform ion cyclotron resonance mass spectroscopy. I. Fundamental equations and low-pressure line shape. *J. Chem. Phys.* **1976**, 64, 110–119.

10. Boldin, I.A., Nikolaev, E.N. Fourier transform ion cyclotron resonance cell with dynamic harmonization of the electric field in the whole volume by shaping of the excitation and detection electrode assembly. *Rapid Commun. Mass Spectrom.* **2011**, 25, 122–126.

11. Nikolaev, E.N., Rakov, V., Futrell, J.H. Analysis of harmonics for an elongated FTMS cell with multiple electrode detection. *Int. J. Mass Spectrom. Ion Process.* **1996**, 157, 215–232.

12. Dziekonski, E.T., Santini, R.E., McLuckey, S.A. A dual detector Fourier transform electrostatic linear ion trap utilizing in-trap potential lift. *Int. J. Mass Spectrom.* **2016**, 405, 1–8.

13. Denisov, E., Damoc, E., Lange, O., Makarov, A. Orbitrap mass spectrometry with resolving powers above 1,000,000. *Int. J. Mass Spectrom.* **2012**, 325, 80–85.

14. Shaw, J.B., Gorshkov, M.V., Wu, Q., Paša-Tolić, L. High speed intact protein characterization using 4X frequency multiplication, ion trap harmonization, and 21 tesla FTICR-MS. *Anal. Chem.* **2018**, 90, 5557–5562.

15. Marshall, A.G., Guan, S. Advantages of high magnetic field for Fourier transform ion cyclotron resonance mass spectrometry. *Rapid Commun. Mass Spectrom.* **1996**, 10, 1819–1823.

16. Zajfman, D., Rudich, Y., Sagi, I., Strasser, D., Savin, D.W., Goldberg, S., Rappaport, M., Heber, O.: High resolution mass spectrometry using a linear electrostatic ion beam trap. *Int. J. Mass Spectrom.* **2003**, 229, 55–60.

17. Ring, S., Pedersen, H.B., Heber, O., Rappaport, M.L., Witte, P., Bhushan, K.G., Altstein, N., Rudich, Y., Sagi, I., Zajfman, D. Fourier transform time-of-flight mass spectrometry in an electrostatic ion beam trap. *Anal. Chem.* **2003**, 72, 4041–4046.

18. Pan, Y., Ridge, D., Wronka, J., Rockwood, A.L., Marshall, A. Resolution improvement by using harmonic detection in an ion cyclotron resonance mass spectrometer. *Rapid Commun. Mass Spectrom.* **1987**, 1, 120–121.

19. Pan, Y., Ridge, D., Rockwood, A.L. Harmonic signal enhancement in ion cyclotron resonance mass spectrometry using multiple electrode detection. *Int. J. Mass Spectrom. Ion Process.* **1998**, 84, 293–304.

20. Nikolaev, E., Gorshkov, M. Dynamics of ion motion in an elongated cylindrical cell of an ICR spectrometer and the shape of the signal registered. *Int. J. Mass Spectrom. Ion Process.* **1985**, 64, 115–125.

21. Limbach, P.A., Grosshans, P.B.,Marshall, A.G. Harmonic enhancement of a detected ion cyclotron resonance signal by use of segmented detection electrodes. *Int. J. Mass Spectrom. Ion Process.* **1993**, 123, 41–47.

22. Mathur, R., O'Connor, P.B. Artifacts in Fourier transform mass spectrometry. *Rapid Commun. Mass Spectrom.* **2009**, 23, 523–529.

23. Dziekonski, E.T., Johnson, J.T., McLuckey, S.A. On the utility of higher harmonics in electrospray ionization Fourier transform electrostatic linear ion trap mass spectrometry. *Anal. Chem.* **2017**, 89, 4392–4397.

24. Grosshans, P.B., Marshall, A.G. Can Fourier transform mass spectral resolution be improved by detection at harmonic multiples of the fundamental ion cyclotron orbital frequency? *Int. J. Mass Spectrom. Ion Process.* **1991**, 107, 49–81.

25. Smith, J.W., Siegel, E.E., Maze, J.T., Jarrold, M.F. Image charge detection mass spectrometry: pushing the envelope with sensitivity and accuracy. *Anal. Chem.* **2011**, 83, 950–956.

26. Barney, B.L., Daly, R.T., Austin, D.E. A multi-stage image charge detector made from printed circuit boards. *Rev. Sci. Instrum.* **2013**, 84, 114101.

27. Gamero-Castaño, M. Induction charge detector with multiple sensing stages. *Rev. Sci. Instrum.* **2007**, 78, 043301.

28. Hogan, J.A., Jarrold, M.F. Optimized electrostatic linear ion trap for charge detection mass spectrometry. *J. Am. Soc. Mass Spectrom.* **2018**, 29, 1–10.

29. Elliott, A.G., Merenbloom, S.I., Chakrabarty, S., Williams, E.R. Single particle analyzer of mass: a charge detection mass spectrometer with a multi-detector electrostatic ion trap. *Int. J. Mass Spectrom.* **2017**, 414, 45–55.

30. Hilger, R.T., Dziekonski, E.T., Santini, R.E., McLuckey, S.A. Injecting electrospray ions into a Fourier transform electrostatic linear ion trap. *Int. J. Mass Spectrom.* **2015**, 378, 281–287.

31. Hilger, R.T., Santini, R.E., McLuckey, S.A. Square wave modulation of a mirror lens for ion isolation in a Fourier transform electrostatic linear ion trap mass spectrometer. *Int. J. Mass Spectrom.* **2014**, 362, 1–8.

32. Hilger, R.T., Santini, R.E., McLuckey, S.A. Tandem mass spectrometry in an electrostatic linear ion trap modified for surface-induced dissociation. *Anal. Chem.* **2014**, 86, 8822–8828.

33. Dziekonski, E.T., Johnson, J.T., Hilger, R.T., McIntyre, C.L., Santini, R.E., McLuckey, S.A. Voltage-induced frequency drift correction in Fourier transform electrostatic linear ion trap mass spectrometry using mirror-switching. *Int. J. Mass Spectrom.* **2016**, 410, 12–21.

CHAPTER 4. MIRROR SWITCHING FOR HIGH RESOLUTION ION ISOLATION IN AN ELECTROSTATIC LINEAR ION TRAP

Adapted with permission from Johnson, J. T., Carrick, I. J., Eakins, G. S., McLuckey, S. A. *Anal. Chem.* **2019**, 91, 8789-8794.

4.1 Introduction

The efficiency and resolution with which precursor ions can be selected for subsequent interrogation are important figures of merit in any tandem mass spectrometry (MS/MS) experiment.[1] Various precursor ion selection approaches have been used in the many MS/MS platforms that have been developed over the past several decades. A particularly common approach in many commercial platforms, for example, is the use of a quadrupole mass filter for precursor ion isolation. In the case of most tandem time-of-flight (TOF/TOF) instruments, a single-pass TOF process is used to separate precursor ions for subsequent activation.[2] Improved precursor ion isolation resolution can be achieved using multiple reflection TOF (MR-TOF) via a significant extension in ion flight path, as demonstrated with the commercially available spiralTOF, an open-path MR-TOF/TOF mass spectrometer that offers a fixed path length of 17 m for precursor ion isolation and a single reflection TOF for mass analysis.[3,4]

A high degree of selectively in ion flight length can be achieved via ion storage time in a closed-loop MR-TOF device.[5] After a given storage time, ions can be released for detection or to an external device for subsequent processing. A deflector, such as a Bradbury-Nielsen gate, is commonly used to selectively pass ions within a small m/z range after a MR-TOF separation.[6–12] Similarly, isolation by in-trap potential lift ejection has also been demonstrated.[13] Alternatively, a trapping plate can be modulated such that unwanted ions become unstable over time to accomplish ion isolation within MR-TOF devices.[14,15] Recently, authors using a MR-TOF device with a single

in-trap deflector consisting of two electrodes quoted an ion selection resolution of 40,000 using square wave modulation using low voltages.[16,17] Ions can also be selectively retrapped in an injection region then sequentially reinjected into the MRTOF.[18] Isolation is accomplished due to the small acceptance window of the retrapping field. Using this technique isolation, resolutions up to 70,000 were quoted with trapping efficiencies of up to 35%.

The electrostatic linear ion trap (ELIT), which consists of two ion mirrors facing each other and separated by a field free region, is a common platform for MR-TOF measurements.[19–21] The linear geometry is convenient for ion isolation because ion injection and release can occur via the same ion mirror or via opposite mirrors. Ions are introduced axially at a fixed energy and are trapped between the two ion mirrors. Although there is no inherent limit to the *m/z* values that can be trapped in an ELIT device, the physical dimensions of the trap and trapping method (e.g., mirror switching[22] or potential lift[13,23–25]) limit the maximum achievable mass range for a given injection of ions. It has been demonstrated, however, that use of multiple injection events can be used to partially overcome this limitation.[17] Mass analysis can be achieved via MR-TOF using an external detector following release from the ELIT or by Fourier transform mass spectrometry (FTMS),[26] using a pick-up electrode within the ELIT for image current detection, or both.[27] A serious potential complication for both mass analysis and ion isolation using a closed-path MR-TOF device, however, is the so-called "racetrack effect"[28] whereby fast ions lap slow ions leading to ambiguity in mass selection/determination. Herein, we describe and demonstrate a general approach to achieving high-resolution (>10,000) ion isolation with high efficiency (i.e., little or no ion loss) using multiple mirror switching pulses with an ELIT. Isolation resolution is defined here as the full width at half-maximum (fwhm) resolution necessary to reduce peak overlap from an equally abundant adjacent ion to 1% or less of the amplitude of the ion of interest. This approach

has been implemented on an ELIT of relatively modest length (5.25 in.) but applies to any closed-loop MR-TOF device.

4.2 Experimental Section

4.2.1 Materials

L-Lysine monohydrochloride, L-glutamine, and ammonium acetate were purchased from Sigma-Aldrich (St. Louis, MO). [PC P-18:0/22:6] and [PC 19:0/19:0] were purchased from Avanti Polar Lipids (Alabaster, AL). Methanol was purchased from Thermo Fisher Scientific (Waltham, MA). HPLC-grade water was purchased from Fisher Scientific (Pittsburgh, PA). The LC/MS tuning mix for ESI (G2421A) was purchased from Agilent Technologies (Santa Clara, CA). The mixture of L-lysine (100 μM) and L-glutamine monohydrochloride (1 mM) was prepared using 50/50 v/v MeOH/H_2O. The mixture of [PC P-18:0/22:6] (100 μM) and [PC 19:0/19:0] (100 μM) was prepared using 99/1 v/v MeOH/1 mM ammonium acetate.

4.2.2 Mass Spectrometry

All experiments were carried out on a home-built 5.25 in. ELIT that has been described previously.[27] The nano-electrospray ionization (nESI) source and the method by which ions are concentrated and injected into the ELIT have been described previously.[29] Procedures for obtaining mass spectra via Fourier transformation and via MR-TOF with this device have been described previously as well.[25] It is important to note that the MR-TOF spectra shown here provide an estimate of the time separation of the ions in the ELIT at the time of ejection; however, peaks are broadened due to the mirror foci (temporal focusing) being at the center of the trap for FT measurements and not at the face of the MCP.

4.2.3 Ion Isolation

Ion isolation was performed by pulsing of the first plate of the ELIT (plate 1) or the last plate (plate 8) (or both) from their nominal trapping potentials (~2360 V) to ground at some specified time after ion injection. It is important to note that the voltage necessary for ion ejection needs only to be lower than the nominal ion energy (~1960 eV/charge). The time in which the electrodes are pulsed and the duration they are held at ground was set by a pulse/delay generator (model 575, Berkeley Nucleonics, San Rafael, CA). A home-built digital signal joiner was developed for combining waveforms from multiple signal sources such that a single mirror could be pulsed multiple times by coupling up to four input TTL signals. The digital signal joiner and its associated schematics are shown in Figure 4.1. This device allowed for high accuracy control over multiple mirror switching events using the BNC 575 pulse/delay generator. Each signal drives a high impedance input that prevents interference or signal degradation of adjacent channels. By utilizing high-speed CMOS technology, the circuit was configured such that the propagation delay stays within an 8.5 ns window. Mirror switching was done using ORTEC 556 power supplies and solid-state switches (HTS 31-03-GSM, Behlke Electronics GMBH, Kronberg, Germany).

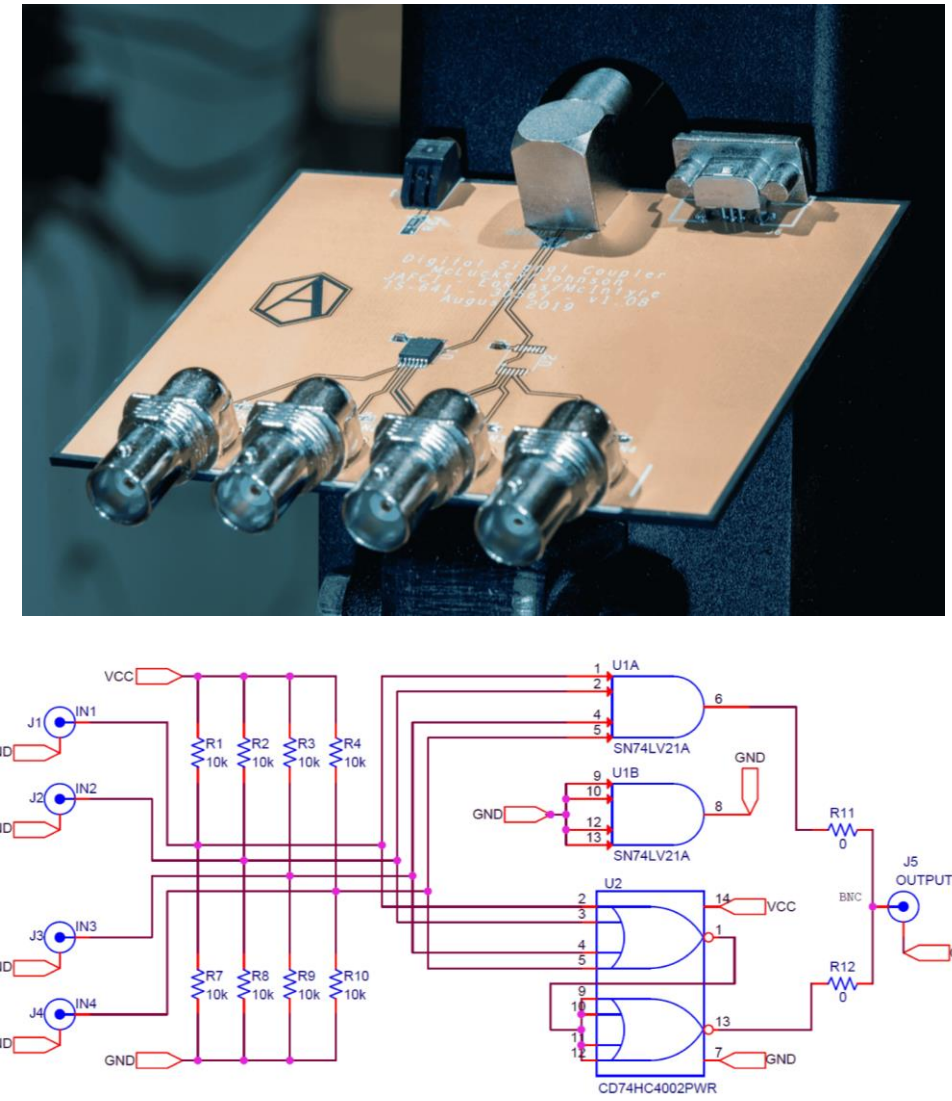

Figure 4.1. The digital signal joiner circuit used for coupling TTL signals for mirror switching isolation experiments. This circuit is operational as either a NAND or OR logic based on how the elements are populated. To operate the circuit in a NAND configuration populated R1, R2, R3, R4, R11, and U1. To operate the circuit in an OR configuration populate R7, R8, R9, R10, R12, and U2.

4.3 Results and Discussion

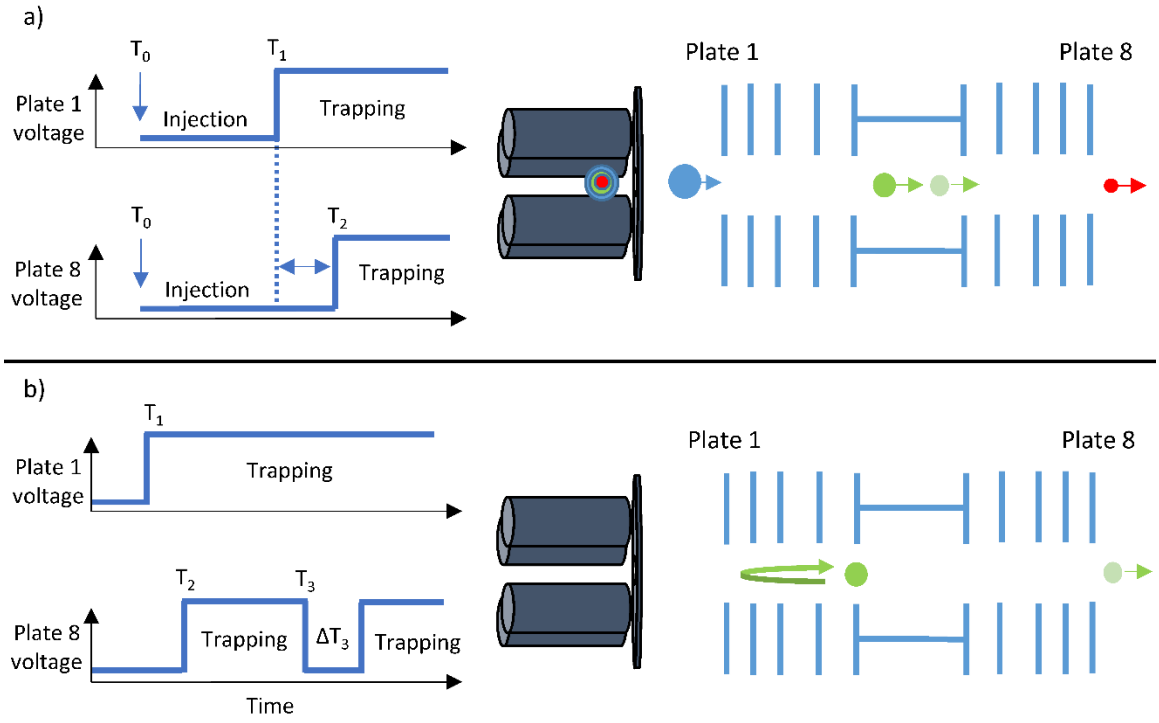

Figure 4.2. Illustration of techniques used in mirror switching isolation. (a) Selection of a restricted mass range by pulsing plates 1 (T1) and 8 (T2) after ion injection (T0). (b) High-resolution ion selection after adequate separation time using a third pulse (T3) of a given width (ΔT3).

In an ELIT device, ions separate in time until some maximum separation is achieved based on the relative ion velocities and dimensions of the mass analyzer, after which fast ions overtake slow ions (i.e., the racetrack effect). The racetrack effect must be avoided to achieve ion isolation without contamination due to ion lapping. For the separation of ions of very similar *m/z* ratio, long flight times/distances are required. It is therefore important to be able to dynamically control the *m/z* range of the ions stored in the ELIT, which can be achieved via the appropriately timed release of ions that might otherwise lap or be lapped by the ions of interest. By progressively reducing the range of masses trapped in the device, high spatial separation can be achieved for ions of very similar *m/z* ratios, as illustrated schematically in Figure 4.2 for a simple four-component mixture.

The accepted m/z range for an ion population released from the accumulation ion trap at T_0 in the present device is determined by the timing of raising the voltage applied to plate 1 (entrance mirror) from 0 V to the value used to store ions at T_1.[25] High *m/z* ions too slow to enter the ELIT prior to T_1 are precluded from being trapped and low *m/z* ions that bounce from the opposing mirror (plate 8) and exit through plate 1 before T_1 are also precluded from being trapped. The ions at the lower end of the trapped *m/z* range can begin to lap the ions at the upper end of the *m/z* range after the low *m/z* ions have undergone a single lap. To avoid such a scenario, it is desirable to limit the initial *m/z* range of trapped ions to allow for ions to separate in time while avoiding any ion lapping. It is straightforward to restrict the *m/z* range of trapped ions in the initial ion injection step (i.e., a low resolution selection step) by using two timed mirror switches, as illustrated in Figure 4.2a. One of several ways to do this is to time the gating of plates 1 and 8 such that only ions with flight times between the two gates pulse are stored. In the schematic of Figure 4.2a, plate 1 is gated up at T_1 to prevent (blue) ions of *m/z* higher than those of interest from entering the trap while plate 8 is gated up at T_2 just before the ions of interest can exit, thereby allowing faster (red), lower *m/z* ions to pass through the trap. The trapped (green) ions of a relatively narrow *m/z* range can then be allowed to further separate in time to the point at which another mirror switch at T_3 with a given pulse width (ΔT_3) can be used to allow unwanted (lighter green) ions to escape the ELIT. This is illustrated in Figure 4.2b.

The initial mass selection step illustrated in Figure 4.2a, in which T_1 determines the high *m/z* cutoff and T_2 determines the low *m/z* cutoff, is relatively crude because it depends on the degree of separation that takes place during the short time-of-flight associated with the initial injection step from the trapping quadrupole. Nevertheless, it prevents the immediate onset of ion lapping when ions of widely different *m/z* values are initially stored in the ELIT. The unlapped

m/z-range in a MR-TOF, expressed as the ratio of the upper $(m/z)_{max}$ and lower $(m/z)_{min}$ *m/z* limits, is approximated by[30]

$$\frac{(m/z)_{max}}{(m/z)_{min}} \approx \left(\frac{N+1}{N}\right)^2 \tag{4.1}$$

Based on this relationship, it is possible to estimate the number of laps (N), as determined by the storage time, that can be allowed before the ions in the initially selected ion population can begin to undergo ion lapping:

$$N \approx \left(\left(\frac{(m/z)_{max}}{(m/z)_{min}}\right)^{1/2} - 1\right)^{-1} \tag{4.2}$$

At any point prior to the time that ion lapping can occur, one or more subsequent mirror switching events can be used to release unwanted ions in a selective fashion. A series of appropriately timed mirror switches can be used to provide precursor isolation at a resolution related to the temporal/spatial separation obtainable via a MR-TOF experiment. Isolation performance can also be impacted by the speed with which the mirror electrodes can be switched and any associated ringing, which has been discussed for the present apparatus and is shown experimentally in Figure 4.3.[25,27]

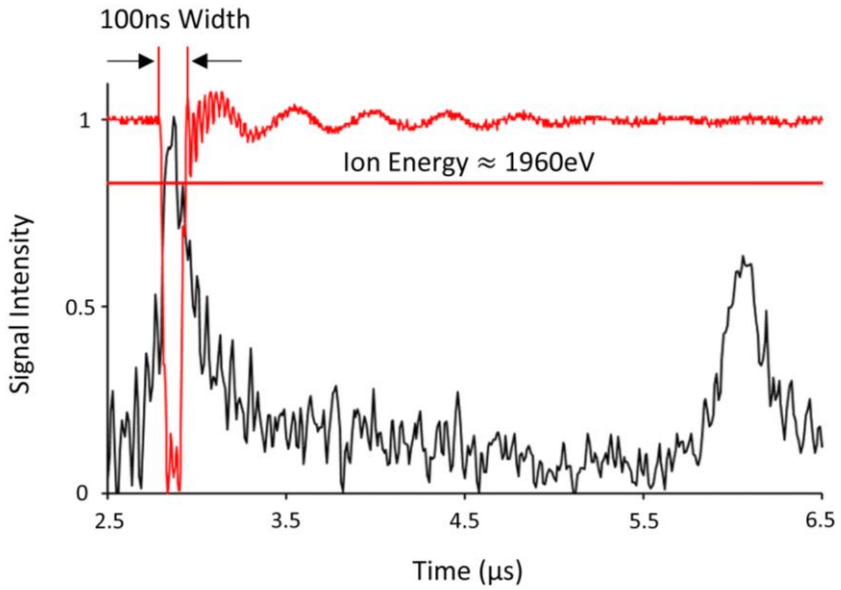

Figure 4.3. MR-TOF mass spectrum of protonated glutamine and lysine with an overlay of the narrowest plate pulse event achievable using our current electronics. The y-axis is scaled to the measure plate 8 trapping voltage (~2360 V). The plate voltage is only low enough to eject ions during the set isolation event. Rippling after the isolation event is likely due to parasitic capacitance on the output of the high voltage switch. This ripple was likely exacerbated by measuring the signal output and therefore this is a worst-case scenario.

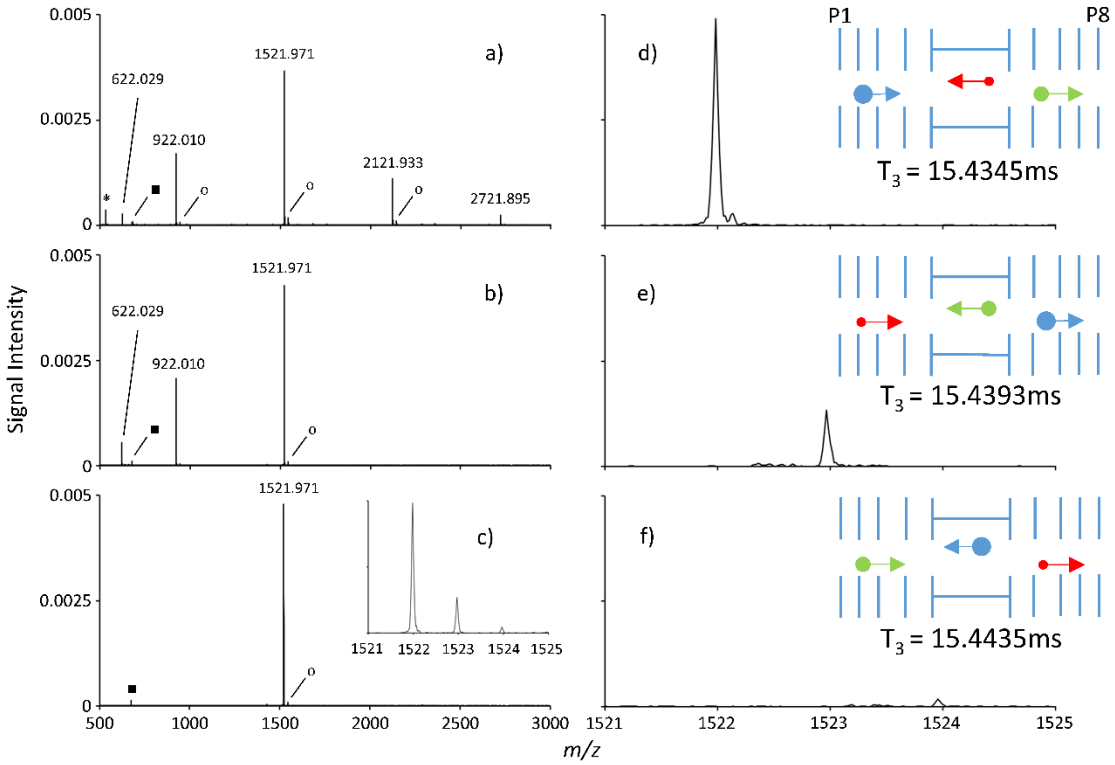

Figure 4.4. eFT mass spectra of Agilent ESI tuning mix. (a) Tuning mix with wide m/z range acceptance (T_1 = 20 μs). (b) Reduction of the *m/z* range at the high end by use of T_1 = 13.5 μs. (c) Isolation of the 1521.97 peak and its isotopes by use of T_1 = 13.5 μs (plate 1) and T_2 = 19 μs (plate 8). (d−f) Isolation of successive isotopes at different T_3 values (96.7% efficient) (see inserts). Intensity scales are the same for each eFT spectra, and efficiencies are within the experimental reproducibility for this device. All mass spectra are averages of 100 spectra. All transients are 300 ms in length. The * indicates background noise. The ○ represents sodiated peaks. The ■ represents peaks associated with harmonics.

An ion isolation process for ions derived from the Agilent tuning mix is illustrated in Figure 4.4. The enhanced Fourier transform (eFT) mass spectrum of the tuning mix obtained after a single mirror switching event for plate 1 (T_1 = 20 μs) is shown in Figure 4.4a. Figure 4.4b shows the spectrum obtained using T_1 = 13.5 μs, which prevents the higher *m/z* ions from entering the ELIT. Figure 4.4c shows the mass spectrum obtained using a plate 1 mirror switch at T_1 = 13.5 μs and a plate 8 mirror switch at T_2 = 18.5 μs. This process prevents the higher *m/z* ions from entering the

ELIT while it allows the lower *m/z* ions to pass through the ELIT. The time-of-flight separation in the single pass through the ELIT is insufficient for the isolation of the isotopologues of protonated hexakis(1H,1H,5H-octafluoropentoxy)phosphazine (monoisotopic ion = *m/z* 1521.971). During the storage time between T_2 and T_3 (15.47 ms and 761 laps), the isotopologues separate further such that they are spaced roughly 5 μs apart in-flight time shown below in Figure 4.5. A third, 12 μs long mirror switch (plate 8) to ground (i.e., T_3) can be used to release two of the three isotopic peaks (d−f) remaining in the ELIT. For example, at T_3 = 15.43 ms, the locations of the isotopes in the trap are such that the two heavier isotopes are in line to reach plate 8 before the lightest isotope (see insert to Figure 4.4d) such that the 12 μs plate 8 pulse to ground is sufficiently long to release the two heavier isotopic ions. The order in which the three isotopic peaks reach plate 8 can be adjusted via T_3, thereby allowing for the selective release of two of the three isotopic ions (see also the insets to Figure 4.4e,f). The isolation resolution demonstrated for Figure 4.4d−f is approximately 3700 fwhm based on the resolution necessary to reduce peak overlap to 1% of the ion of interest. (We assume a Gaussian peak shape, which approximates the shapes of the peaks we generally observe in the MR-TOF experiment.) The ion path length in the 5.25 in. ELIT was estimated to be 124 mm using a simulated model of the device in SIMION v8.1 (Scientific Instrument Services, Ringoes, NJ). A trapping time of 15.47 ms in the 5.25 in. ELIT results in 761 laps for ions of m/z 1521.971 (lap time ≈ 20.3 μs) and a time-of-flight path length of 188.7 m prior to isolation.

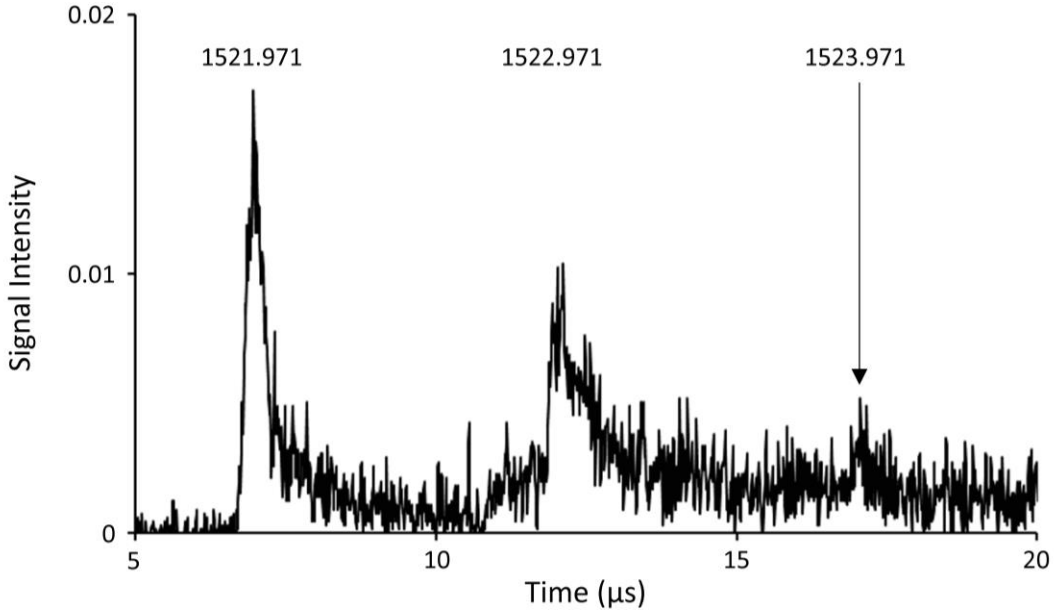

Figure 4.5. MR-TOF mass spectrum of protonated hexakis(1H,1H,5H-octafluoropentoxy)phosphazine and its associated isotopologues after low resolution isolation via mirror switching. Ions were detected after 15.43 ms of separation resulting in a spacing of approximately 5 μs between the isotopolouges.

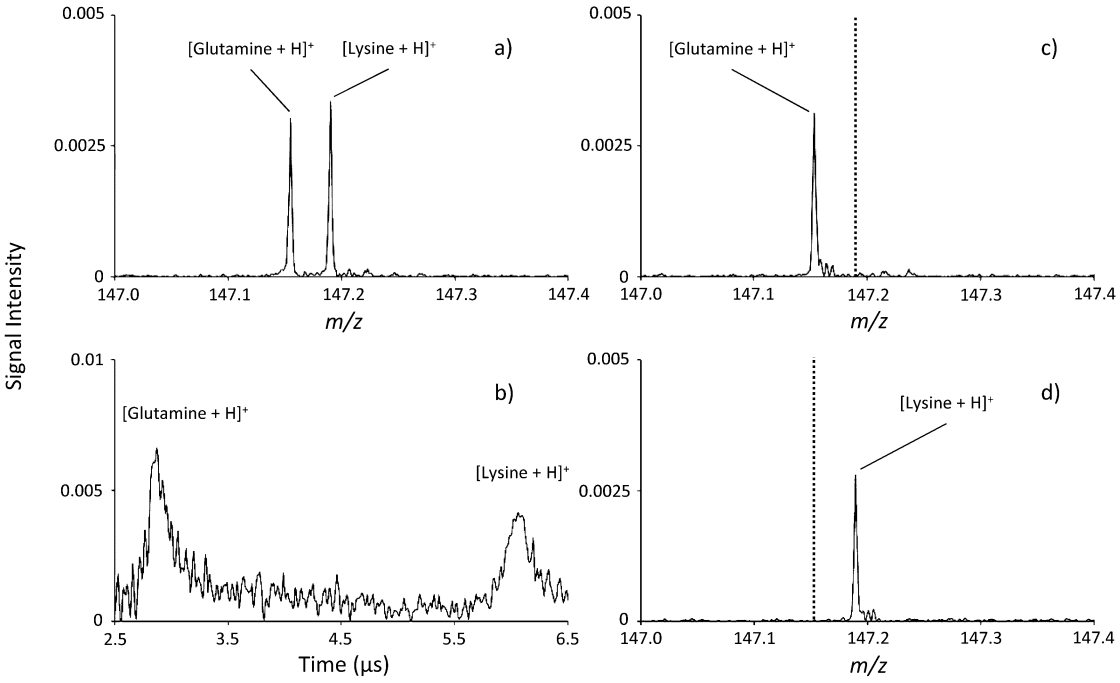

Figure 4.6. eFT mass spectra and MR-TOF of protonated L-glutamine (*m/z* 147.0764) and L-lysine (*m/z* 147.1128). (a) Pre-isolation eFT mass spectrum. (b) MR-TOF spectrum of protonated L-glutamine (left) and L-lysine (right) after 25.65 ms. (c) Isolated L-glutamine (101% efficient) after 25.65 ms. (d) Isolated L-lysine (85.9% efficient) after 25.65 ms using isolation pulse widths of 1.5 μs. Intensities scales are the same for all eFT spectra and efficiencies are within the experimentally reproducibility for this device. All mass spectra are averages of 100 spectra. All transient are 200 ms in length.

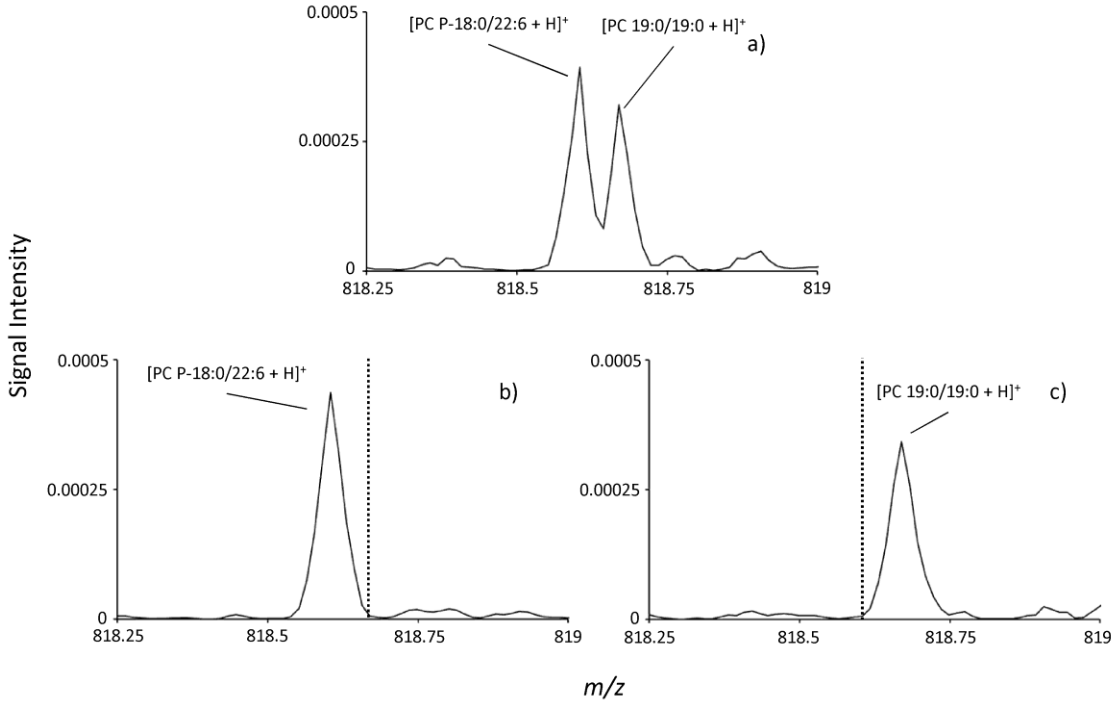

Figure 4.7. eFT mass spectra of protonated [PC P-18:0/22:6] (*m/z* 818.6063) and [PC 19:0/19:0] (*m/z* 818.6638). (a) eFT mass spectrum of the monoisotopic isolation of the two isobaric ions. (b) Isolated [PC P-18:0/22:6] (111% efficient) and (c) isolated [PC 19:0/19:0] (106% efficient) after 45.58 ms using a 2 μs pulse of plate 8. Intensities scales are the same for all eFT spectra, and efficiencies are within the experimentally reproducibility for this device. All eFT mass spectra are averages of 100 spectra. All transients are 300 ms in length.

Higher resolution ion isolations can be achieved by allowing longer separation times for closely spaced ions. This was demonstrated with a mixture of protonated L-lysine and L-glutamine, two isobaric species that are separated by *m/z* 0.0364 (Figure 3), and protonated [PC P-18:0/22:6] and [PC 19:0/19:0], which are also isobaric and are separated by *m/z* 0.0575 (Figure 4). As can be seen with the MR-TOF spectrum of the amino acid mixture near the isolation time, the ion packets for protonated L-lysine and L-glutamine are well separated in MR-TOF space (Figure 3b). Temporal and spatial separation demonstrated in the MR-TOF measurement allowed an experimental isolation resolution of at least 10,000 fwhm (i.e., the resolution needed to isolate one of the roughly equally abundant isobaric ions with less than 1% abundance of the other isobaric ion present after the isolation step) as illustrated in panels c and d in Figure 4.6. Ions underwent 4071 laps after the 25.65 ms separation time (lap time ≈ 6.3 μs) and thus had a final time-of-flight path length of 1009.6 m before ion isolation. Isolation resolutions of 38,000 fwhm were achieved for a fatty acid mixture of [PC P-18:0/22:6] and [PC 19:0/19:0] (Figure 4.7) after 48.58 ms of separation time (lap time ≈ 14.9 μs). After 3375 laps, ions experienced a final time-of-flight length of 837.0 m before isolation.

4.4 Conclusions

A novel ion isolation approach is demonstrated here with a device capable of MR-TOF and FT mass analysis. This isolation technique takes advantage of the spatial separation possible in a closed path MR-TOF device. The range of masses trapped within an ELIT is decreased successively to allow ions of very similar *m/z* to separate while avoiding the racetrack effect. In this work, ion isolation was demonstrated to different extents on Agilent ESI tuning mix, a mixture of two closely spaced amino acids (L-glutamine and L-lysine, Δ *m/z* = 0.0364), and a mixture of two isobaric fatty acids ([PC P-18:0/22:6] and [PC 19:0/19:0], Δ *m/z* = 0.0575). Furthermore, MR-TOF mass spectra were used to demonstrate the degree of spatial/temporal separation accomplished with a 5.25 in. ELIT. This spatial separation is due to the long flight paths achievable with a closed-loop trapping device and is related to the resolution with which ions of similar *m/z* can be isolated from one another. In all cases reported here, flight paths of greater than 100 m were achieved using a 13.33 cm (5.25 in.) long ELIT device. In the most extreme case, a path length of 1009.6 m was achieved. Mirror switching is demonstrated as a straightforward and effective method for high-resolution and high-efficiency ion isolation in an ELIT without the incorporation of any supplemental electrical elements, such as deflection plates.

4.5 References

1. Gross, J. H. Mass Spectrometry: A Textbook, 2nd ed.; *Springer: New York*, **2011**; pp 415−478.

2. Schey, K.; Cooks, R.; Grix, R.; Wollnik, H. A tandem time-of-flight mass spectrometer for surface-induced dissociation. *Int. J. Mass Spectrom. Ion Processes* **1987**, 77, 49−61.

3. Satoh, T.; Tsuno, H.; Iwanaga, M.; Kammei, Y. the design and characteristic features of a new time-of-flight mass spectrometer with a spiral ion trajectory. *J. Am. Soc. Mass Spectrom.* **2005**, 16, 1969−1975.

4. Satoh, T.; Sato, T.; Tamura, J. Development of a high-performance MALDI-TOF mass spectrometer utilizing a spiral ion trajectory. *J. Am. Soc. Mass Spectrom.* **2007**, 18, 1318−1323.

5. Okumura, D.; Toyoda, M.; Ishihara, M.; Katakuse, I. Application of a multi-turn time-of-flight mass spectrometer, MULTUM II, to organic compounds ionized by matrix-assisted laser desorption/ionization. *J. Mass Spectrom.* **2004**, 39, 86−90.

6. Bradbury, N. E.; Nielsen, R. Absolute values of the electron mobility in hygrogen. *A. Phys. Rev.* **1936**, 49, 388.

7. Plaß, W. R.; Dickel, T.; Czok, U.; Geissel, H.; Petrick, M.; Reinheimer, K.; Scheidenberger, C.; Yavor, M. I. Nucl. Instrum. Methods Phys. Res. B **2008**, 266, 4560−4564.

8. Toker, Y.; Altstein, N.; Aviv, O.; Rappaport, M.; Heber, O.; Schwalm, D.; Strasser, D.; Zajfman, D. J. Instrum. **2009**, 4, P09001.

9. Plaß, W. R.; Dickel, T.; Scheidenberger, C. Int. J. Mass Spectrom. 2013, 349, 134−144.

10. Wolf, R.N.; Beck, D.; Blaum, K.; Bohm, C.; Borgmann, C.; Breitenfeldt, M.; Herfurth, F.; Herlert, A.; Kowalska, M.; Kreim, S.; Lunney, D.; Naimi, S.; Neidherr, D.; Rosenbusch, M.; Schweikhard, L.; Stanja, J.; Wienholtz, F.; Zuber, K. On-line separation of short-lived nuclei by a multi-reflection time-of-flight device. *Nucl. Instrum. Methods Phys. Res. A* **2012**, 686, 82−90.

11. Wolf, R.N.; Wienholtz, F.; Atanasov, D.; Beck, D.; Blaum, K.; Borgmann, C.; Herfurth, F.; Kowalska, M.; Kreim, S.; Litvinov, Y. A.; Lunney, D.; Manea, V.; Neidherr, D.; Rosenbusch, M.; Schweikhard, L.; Stanja, J.; Zuber, K. ISOLTRAP's multi-reflection time-of-flight mass separator/spectrometer. *Int. J. Mass Spectrom.* **2013**, 349, 123−133.

12. Plaß, W. R; Dickel, T.; San Andres, S. A.; Ebert, J.; Greiner, F.; Hornung, C.; Jesch, C.; Lang, J.; Lippert, W.; Majoros, T.; Short, D.; Geissel, H.; Haettner, E.; Reiter, M. P; Rink, A.-K.; Scheidenberger, C.; Yavor, M. I. High-performance multiple-reflection time-of-flight mass spectrometers for research with exotic nuclei and for analytical mass spectrometry. *Phys. Scr.* **2015,** 2015, 014069.

13. Wienholtz, F.; Kreim, S.; Rosenbusch, M.; Schweikhard, L.; Wolf, R. Mass-selective ion ejection from multi-refelction time-of-flight devices via a pulsed in-trap lift. *Int. J. Mass Spectrom.* **2017**, 421, 285−293.

14. Hilger, R. T.; Santini, R. E.; McLuckey, S. A. Square wave modulation of a mirror lens for ion isolation in a Fourier transform electrostatic linear ion trap mass spectrometer. *Int. J. Mass Spectrom.* **2014**, 362, 1−8.

15. Hilger, R. T.; Santini, R. E.; McLuckey, S. A. Nondestructive tandem mass spectrometry using a linear quadrupole ion trap coupled to a linear electrostatic ion trap. *Anal. Chem.* **2013**, 85, 5226−5232.

16. Fischer, P.; Knauer, S.; Marx, G.; Schweikhard, L. In-depth study of in-trap high-resolution mass separation by transversal ion ejection from a multi-reflection time-of-flight device. *Rev. Sci. Instrum.* **2018**, 89, 015114.

17. Fischer, P.; Marx, G.; Schweikhard, L. Int. Multiple ion capture and separation in an electrostatic storage device. *J. Mass Spectrom.* **2019**, 435, 305−314.

18. Dickel, T.; Plaß, W. R.; Lippert, W.; Lang, J.; Yavor, M. I.; Geissel, H.; Scheidenberger, C. Isobar separation in a multiple-reflection time-of-flioght mass spectrometer by mass-selective re-trapping. *J. Am. Soc. Mass Spectrom.* **2017**, 28, 1079−1090.

19. Wollnik, H.; Przewloka, M. Time-of-flight mass spectrometers with multiply refelected ion trajectories. *Int. J. Mass Spectrom. Ion Processes* **1990**, 96, 267−274.

20. Benner, W. H. A Gated Electrostatic Ion Trap to Repetitiously Measure the Charge and m/z of Large Electrospray Ions. *Anal. Chem.* **1997**, 69, 4162−4168.

21. Zajfman, D.; Heber, O.; Vejby-Christensen, L.; Ben-Itzhak, I.; Rappaport, M. L.; Fishman, R.; Dahan, M. Electrostatic bottle for long-time storage of fast ion beams. *Phys. Rev. A: At., Mol., Opt. Phys.* **1997**, 55, R1577−R1580.

22. Dziekonski, E. T.; Santini, R. E.; McLuckey, S. A. A dual detector Fourier transform electrostatic linear ion trap utilizing in-trap potential lift. *Int. J. Mass Spectrom.* **2016**, 405, 1−8.

23. Wolf, R. N.; Marx, G.; Rosenbusch, M.; Schweikhard, L. Static-mirror ion capture and time focusing for electrostatic ion-beam traps and multi-reflection time-of-flight mass analyzers by use of in-trap potential lift. *Int. J. Mass Spectrom.* **2012**, 313, 8−14.

24. Knauer, S.; Fischer, P.; Marx, G.; Schabinger, B.; Schweikhard, L.; Wolf, R. Multi-reflection time-of-flight mass spectrometry with combined in-trap lift capture and mirror-switching ejection. *Int. J. Mass Spectrom.* **2017**, 423, 46−53.

25. Dziekonski, E. T.; Johnson, J. T.; Hilger, R. T.; McIntyre, C. L.; Santini, R. E.; McLuckey, S. A. Voltage-induced frequency drift correction in Fourier transform electrostatic linear ion trap mass spectrometry using mirror switching. *Int. J. Mass Spectrom.* **2016**, 410, 12−21.

26. Ring, S.; Pedersen, H. B.; Heber, O.; Rappaport, M.; Witte, P.; Bhushan, K.; Altstein, N.; Rudich, Y.; Sagi, I.; Zajfman, D. Fourier transform time-of-flight mass spectrometry in an electrostatic ion beam trap. *Anal. Chem.* **2000**, 72, 4041−4046.

27. Dziekonski, E. T.; Johnson, J. T.; Lee, K. W.; McLuckey, S. A. Fourier-transform MS and closed-path multireflection time-of-flight MS using a electrostatic linear ion trap. *Anal. Chem.* **2017**, 89, 10965−10972.

28. Schury, P.; Ito, Y.; Wada, M.; Wollnik, H. Wide-band mass measurement with a multi-reflection time-of-flight mass spectrograph. *Int. J. Mass Spectrom.* **2014**, 359, 19−25.

29. Hilger, R. T.; Dziekonski, E. T.; Santini, R. E.; McLuckey, S. A. Injecting electrospray ions into a Fourier transform electrostatic linear ion trap. *Int. J. Mass Spectrom.* **2015**, 378, 281−287.

30. Yavor, M. I.; Plaß, W. R.; Dickel, T.; Geissel, H.; Scheidenberger, C. Ion-optical design of a high-performance multiple-reflection time-of-flight mass spectrometer and isobar separator. *Int. J. Mass Spectrom*. **2015**, 381, 1−9.

CHAPTER 5. SIMULTANEOUS ISOLATION OF NON-ADJACENT *M/Z* IONS USING MIRROR SWITCING IN AN ELECTROSTATIC LINEAR ION TRAP

Adapted with permission from Johnson, J. T., Carrick, I. J., Eakins, G. S., McLuckey, S. A. *Anal. Chem.* **2019**, 91, 12574-12580.

5.1 Introduction

Applications for the simultaneous isolation of ions of non-adjacent (*m/z*) ratio include mass calibration[1,2] and multiplexing in tandem mass spectrometry.[3,4,5] Studies using simultaneous ion isolation have primarily used ion trapping instruments in conjunction with tailored waveforms such as correlated harmonic excitation fields (CHEF)[6] and stored waveform inverse Fourier transform (SWIFT)[7], broadband isolation techniques that operate by generating a tailored waveform that excites and ejects unwanted ions over time. Numerous techniques have been demonstrated for ion isolation within multiple reflection time-of-flight (MR-TOF) devices.[8-13] Of these methods, only one has demonstrated simultaneous isolation of multiple ion species of disparate *m/z*.[14] This isolation method uses selective modulation of an in-trap deflector consisting of two electrodes at the frequencies of the ions of interest. The deflector is at ground when the ions of interest are in the deflector region and at a low deflection voltage when the ions of interest are outside of the deflector region. This method, like SWIFT and CHEF, relies on frequency modulation to alter the trajectories of unwanted ions over time until they are ejected. Mirror switching has been demonstrated as a method for high resolution and high efficiency ion isolation in an electrostatic linear ion trap (ELIT).[8] In addition, this method can be used to selectively retain multiple ions of disparate *m/z* ratios based on their temporal/spatial overlap within the device. Unlike frequency modulation experiments, mirror switching relies solely on the instantaneous positions of ions in relation to the switching electrode. As a result, advantage can be taken of the

high spatial and temporal separation achieved in relatively short time scales in MR-TOF experiments. In this work, a method based on mirror switching for simultaneous isolation of ions of non-adjacent *m/z* ratios is described and demonstrated. Efficient isolation of a single isotope each from two and three isotopic distributions of a mixture of three carborane ion populations is demonstrated. Furthermore, a method for simultaneous isolation of equally spaced ions in a narrow *m/z* range is also described and illustrated using a carborane ion isotopic distribution. Finally, an internal mass calibration is demonstrated by simultaneously isolating three calibrant ions from a tuning mixture and a single charge state of insulin.

5.2 Experimental Section

5.2.1 Materials

A mixture of carboranes consisting of $AgCH_{11}H_5Cl_6$, $CsCHB_{11}Cl_{11}$, and $AgCHB_{11}Br_{11}$ (100μM each) was prepared in a solution using 50/50 v/v MeOH/H_2O. The carboranes were synthesized and provided by Professor C.A. Reed's group at the University of California Riverside, Department of Chemistry. Methanol was purchased from Sigma-Aldrich (St. Louis, MO, USA). Water was purchased from Malinckrodt (Phillipsburg, NJ, USA). Insulin (from bovine pancreas) was purchased from Sigma-Aldrich (St. Louis, MO, U.S.A.). Insulin was prepared to a final concentration of 20 μM in 49.5/49.5/1 v/v/v MeOH/H_2O/AcOH. LC/MS tuning mix for ESI (G2421A) was purchased from Agilent Technologies (Santa Clara, CA, USA).

5.2.2 Mass Spectrometry

All experiments were carried out on a home-built 5.25" ELIT that has been described previously.[15] The nano-electrospray ionization (nESI) source and the method by which ions are concentrated and injected into the electrostatic linear ion trap (ELIT) have been described

previously.[16] Procedures for obtaining mass spectra via Fourier transformation (FT) have been described.[15]

5.2.3 Ion Isolation

Ion isolation was performed by pulsing of the first plate of the ELIT (plate 1) or the last plate (plate 8) (or both) from their nominal trapping potentials (~2360 V) to ground at some specified time after ion injection. The time in which the electrodes were pulsed and the duration they were held at ground was set by a pulse/delay generator (model 575, Berkeley Nucleonics, San Rafael, CA). A home-built digital signal joiner (discussed in Chapter 4) was used to combine waveforms from multiple signal sources such that a single mirror could be pulsed multiple times by coupling up to three input TTL signals. Mirror switching was done using ORTEC 556 power supplies and solid-state switches (HTS 31-03-GSM, Behlke Electronics GMBH, Kronberg, Germany).

5.3 Results and Discussion

In a closed-loop MR-TOF device, such as an ELIT, all ions of a given *m/z* ratio either lap or are lapped by ions of other *m/z* ratios (i.e., the racetrack effect) given a sufficiently long storage time. To avoid ambiguities due to ion lapping in single ion isolation experiments using mirror switching, care must be taken to release potentially lapped or lapping ions while ions of very similar *m/z* ratio can continue to separate. This can be done via the judicious timing of ion release events to manage the trapped mass range inside the device. The racetrack effect can be exploited, however, if more than one ion species of disparate *m/z* ratios are to be isolated simultaneously as in, for example, a tandem MS workflow. In the following we describe and illustrate isolation of multiple ions in the general case, which makes no constraint on the difference in *m/z* ratios of the

selected ions, and in a special case in which multiple ions of a small relative Δm are to be selected simultaneously.

5.3.1 Timing of Ion Release Events for Multiple Ions of Arbitrary Δm

Prediction of ion position and direction in the ELIT is necessary in establishing the timing for ion release in a multiple ion isolation experiment. The instantaneous ion position and direction in the ELIT is related to the number of laps an ion has undergone after its initial entrance into the ELIT. This includes the number of laps after the plate 1 ion mirror is pulsed high to trap injected ions plus the fractional lap that each injected ion undergoes once it enters the ELIT and before plate 1 is pulsed high. Due to the *m/z* dependent flight time differences of the ions injected from the accumulation quadrupole, trapped ions of each *m/z* ratio undergo a unique fraction of one lap prior to the initial plate 1 mirror switch. When ions have experienced half a lap, they are positioned at the turning point near plate 8 and when ions have experienced an integer lap number they are located at the turning point near plate 1. The fractional lap value can be denoted as a position index in which ions at plate 8 have a position index of 0.5 and ions at plate 1 have a position index of 0 or 1 depending on whether they are travelling to or from plate 8. Position indices of 0.0-0.5 denote ions moving in the direction of plate 8 whereas position indices of 0.5-1.0 indicated ions moving in the direction of plate 1. Hence, determination of the fractional lap number from the instant an ion enters the ELIT as a function of time indicates the position and direction of the ion. A Matlab script (MATLAB 2019a) was written to calculate position indices as a function of time for multiple ions at the same time.

Figure 5.1 is provided to illustrate a pulse sequence that could be used to isolate simultaneously three ions from three distinct isotopic distributions using a plot of position index versus storage time (corrected for the fractional lap number for each *m/z* value of interest). The

position index versus time plots for *m/z* 350.99 (black line), *m/z* 522.76 (red line), and *m/z* 1012.21 (blue line) over a 20 μs time period is provided in the figure along with a diagram that relates the position index to plate locations in the ELIT. The schematic diagram of the ELIT plates on the left indicates that position indices of 0.0-0.5 relate to ions moving in the direction from plate 1 to plate 8 and that position indices of 0.5-1.0 relate to ions moving in the direction from plate 8 to plate 1. Three blue dots of small, medium, and large size represent the next smaller isotope (smallest dot) and next larger isotope (large dot) of the *m/z* 1012.21 ion (medium dot) at three distinct storage times. The solid horizontal line indicated at position index 0.5 represents the voltage applied to the plate 8 mirror. Black represents the full voltage of the mirror, which is effective at reflecting (storing) ions while green represents a potential that releases ions from the trap. This diagram shows that the plate 8 voltage can be dropped anywhere between the first intersection of the *m/z* 350.99 line with the 0.5 position index and corresponding intersection of the *m/z* 1012.21 line to release any ions that approach plate 8 during that period, including the lighter isotope of the *m/z* 1012.21 ion. To retain the three ions of interest, it is necessary to restore the plate 8 voltage to the trapping level prior to the first intersection of the blue line with position index 0.5 until just after the second intersection of the black line with 0.5 position index. Plate 8 can then be pulsed down to release ions until such time that the *m/z* 350.99 ion returns to plate 8. An analogous process can be repeated, as necessary, to remove any residual untargeted ions whenever the three ions of interest are in close proximity.

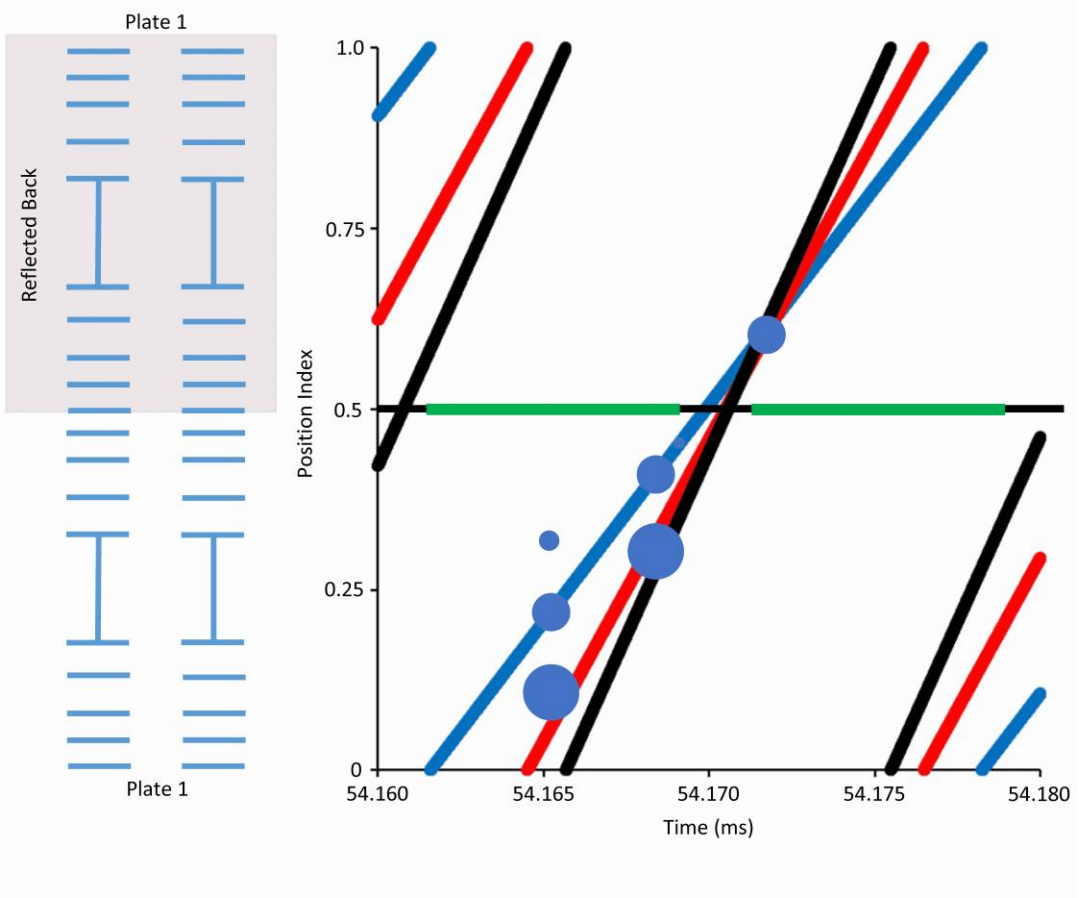

Figure 5.1. The trajectories of three ions are shown by lines (*m/z* 350.99 in black, 522.76 in red, and 1012.21 in blue). Neighboring isotopes of the 1012.21 ion are depicted as circles, with the lighter isotope ahead in position of the 1012.21 ion, and the heavier isotope lagging behind. A position index of 0.5 corresponds to an ion located at plate 8, while between 0.5 and 1.0, the ion is travelling from 8 back to plate 1 (grey area). A mirror switching pulse is depicted as a green window at plate 8, spanning the length of the isolation pulse. As long as plate 8 is pulsed back up to trapping voltage in time for the 1012.21 isotope to reach it (blue line), the light and heavy isotope of this distribution can be let out while the 1012.21, 522.76, and 350.99 *m/z* species are retained.

Simultaneous isolation is demonstrated in Figure 5.2 using centrally located isotopes of three carborane ion distributions ($CHB_{11}H_5Cl_6^-$ (349.70 average *m/z*), $CHB_{11}Cl_{11}^-$ (521.92 average *m/z*), and $CHB_{11}Br_{11}^-$ (1012.56 average *m/z*). The three distributions prior to ion isolation are shown in Figure 5.2a. Figure 5.2b shows the isolation of the *m/z* 350.99 and *m/z* 522.76 ions from the $CHB_{11}H_5Cl_6^-$ and $CHB_{11}Cl_{11}^-$ distributions, respectively, while Figure 5.2c shows the isolation of the *m/z* 522.76 and *m/z* 1012.21 ions from the $CHB_{11}Cl_{11}^-$ and $CHB_{11}Br_{11}^-$ distributions, respectively. These two spectra illustrate that ions of any two arbitrary *m/z* ratios can be isolated simultaneously. Simultaneous isolation of three ions-of-interest (*m/z* 350.99, *m/z* 522.76, and *m/z* 1012.21) is shown in Figure 5.2d. The isolation efficiency for each case is illustrated in Figures 5.2e-h, which compare the pre-isolation $CHB_{11}Cl_{11}^-$ distribution (Figure 5.2e) with the isolated *m/z* 522.76 ion following the three isolation experiments (Figures 5.2f-h). In all three cases, the pre- and post-isolation abundances of the *m/z* 522.76 ion are observed to be within the experimental variation of the carborane distribution signal. (The pre- and post-isolation results for all three carborane distributions associated with the experiment of Figure 5.2d are provided in Figure 5.3, again, showing ion isolation efficiency to be within the reproducibility of the abundance measurement.) A total storage time of 54.25 ms was used for all three isolation examples. In the case of the simultaneous isolation of three ions (Figures 5.2d and 5.2h), four ion overlap events were chosen and used for successive release (via plate 8) of unwanted isotopes and are shown in Table 5.1.

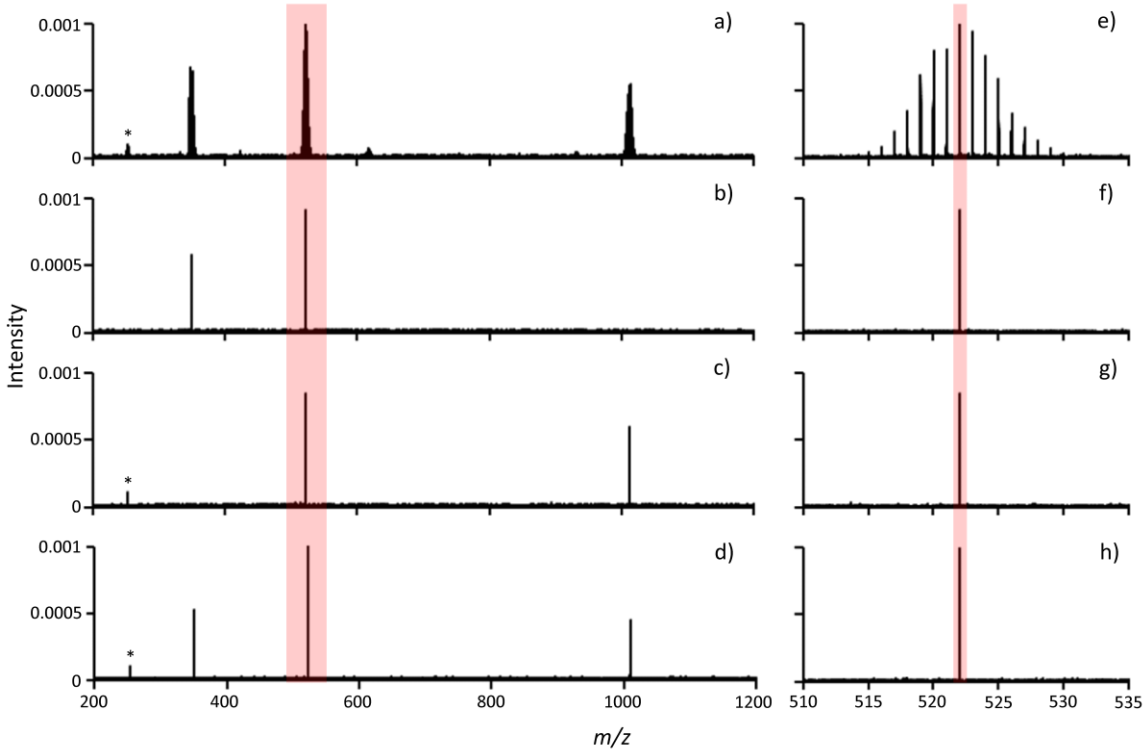

Figure 5.2. a) eFT mass spectrum of $CHB_{11}H_5Cl_6^-$ (349.70 average *m/z*), $CHB_{11}Cl_{11}^-$ (523.51 average *m/z*), and $CHB_{11}Br_{11}^-$ (1012.56 average *m/z*). b) Simultaneous isolation of *m/z* 350.99 and *m/z* 522.76. c) Simultaneous isolation of *m/z* 522.76 and *m/z* 1012.21. d) Simultaneous isolation of a single isotope from each of the three carborane distributions (*m/z* 350.99, *m/z* 522.76, and *m/z* 1012.21). Zoom-in of the $CHB_{11}Cl_{11}^-$ distribution (e-h) for each adjacent mass spectrum. All isolations were done after a separation time of 54.25 ms. All eFT spectra are averages of 100, 500 ms transients. The (*) denotes the second harmonic of $CHB_{11}Br_{11}^-$.

Table 5.1. Mirror switching isolation delay times and pulse widths used for the simultaneous isolation of *m/z* 350.99, 522.76, and 1012.21

Isolation Time (ms)	Isolation Pulse Width (μs)
4.161	5
14.098	5
22.346	2
54.25	3

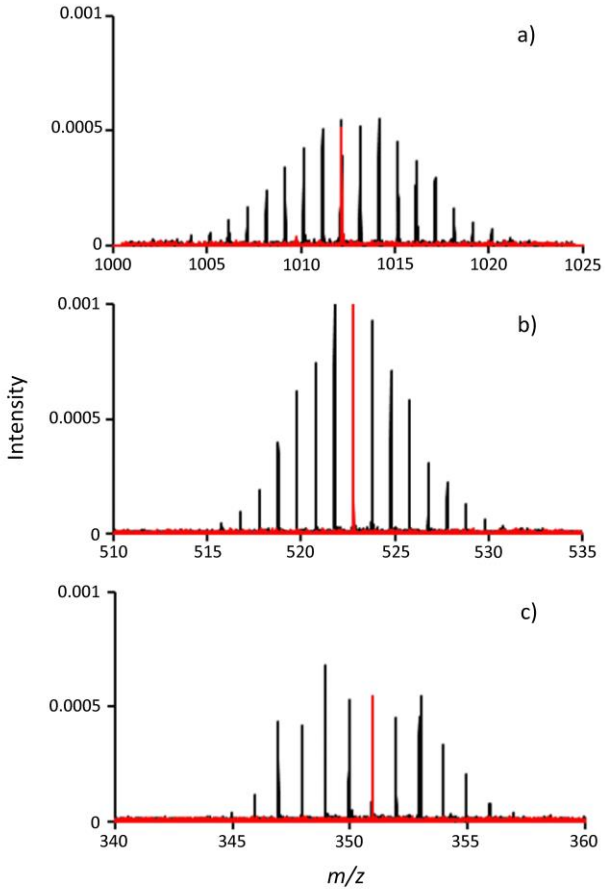

Figure 5.3. a) eFT mass spectra of $CHB_{11}Br_{11}^-$ before (black) and after (red) simultaneous isolation. b) eFT mass spectra of $CHB_{11}Cl_{11}^-$ before (black) and after (red) simultaneous isolation. c) eFT mass spectra of $CHB_{11}H_5Cl_6^-$ before (black) and after (red) simultaneous isolation. Isolation efficiencies were 89%, 95%, and 121%.

Figure 5.4 illustrates the step-wise release of ions resulting in simultaneous isolation of the *m/z* 520.76 and *m/z* 619.68 ions from a mixture containing $CHB_{11}Cl_{11}^-$ (521.92 average *m/z*), and $CHB_{11}H_5Br_6^-$ (616.40 average *m/z*). In this example, the *m/z* range is small enough to clearly see the individual isotopes of each distribution during the step-wise ion release process. Figure 5.4a shows the pre-isolation mass spectrum of the two isotopic distributions. Figures 5.4b-d shows the remaining ions after each ion release event (plate 8) with the timing of the steps shown in the figure. In this case, the isolation could be effected in slightly over 5 ms.

One of the applications for the simultaneous isolation of multiple ions of disparate m/z ratios is the inclusion of ions of known *m/z* for mass calibration associated with the measurement of the *m/z* of an analyte of interest. A simple example is provided in Figure 5.5, which shows the results for the simultaneous isolation of three calibrant ions (*m/z* 622.029, 922.010, and 1521.971) generated from a tuning mix supplied by Agilent for LC/MS calibration along with the $[M+4H]^{4+}$ ions generated by nano-ESI of bovine insulin (Figure 5.5a). Figure 5.5b shows a blow-up of the experimental insulin $[M+4H]^{4+}$ isotope distribution (black) with the theoretical isotope distribution in red. The mass calibration derived from the three tuning mix ions yielded mass measurements for the insulin isotopes with an average mass measurement error of 10 ppm.

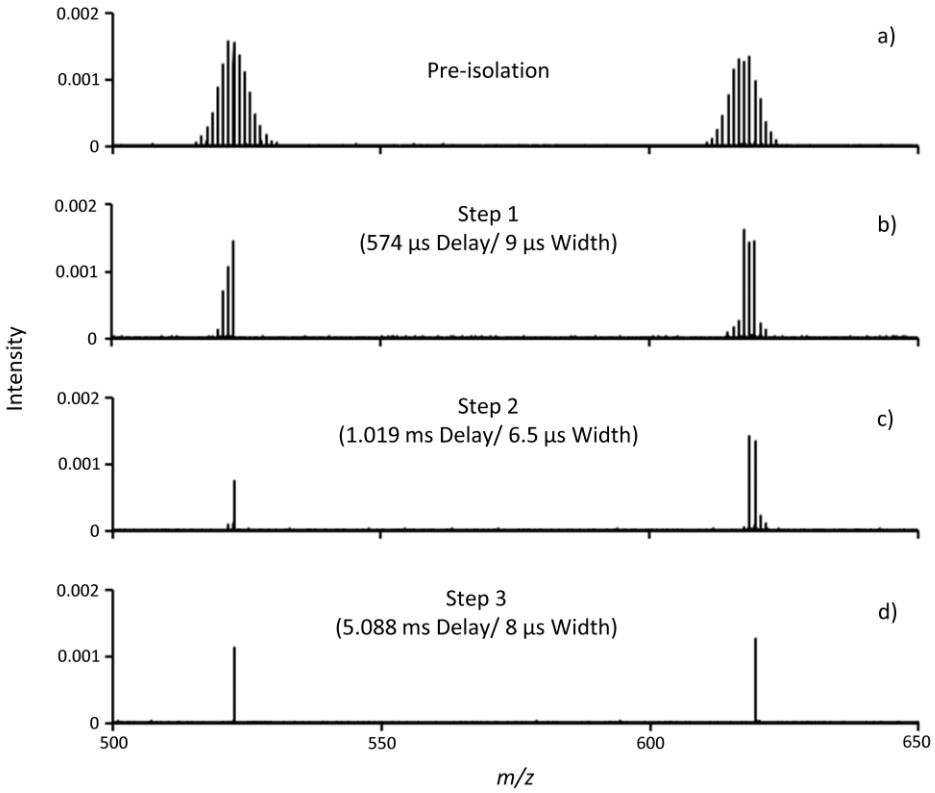

Figure 5.4. eFT mass spectra demonstrating step-wise simultaneous isolation of *m/z* 520.76 and *m/z* 619.68 from a mixture containing $CHB_{11}Cl_{11}^-$ (521.92 average *m/z*), and $CHB_{11}H_5Br_6^-$ (616.40 average *m/z*). a) Mass spectrum prior to any isolation steps. b) Mass spectrum after a single mirror switching isolation pulse after 574 µs of storage. c) Mass spectrum after adding a second mirror switching isolation pulse after 1.019 ms of storage. d) Mass spectrum after the addition of a third mirror switching isolation pulse after 5.088 ms of storage. These spectra are averages of 100, 500 ms transients.

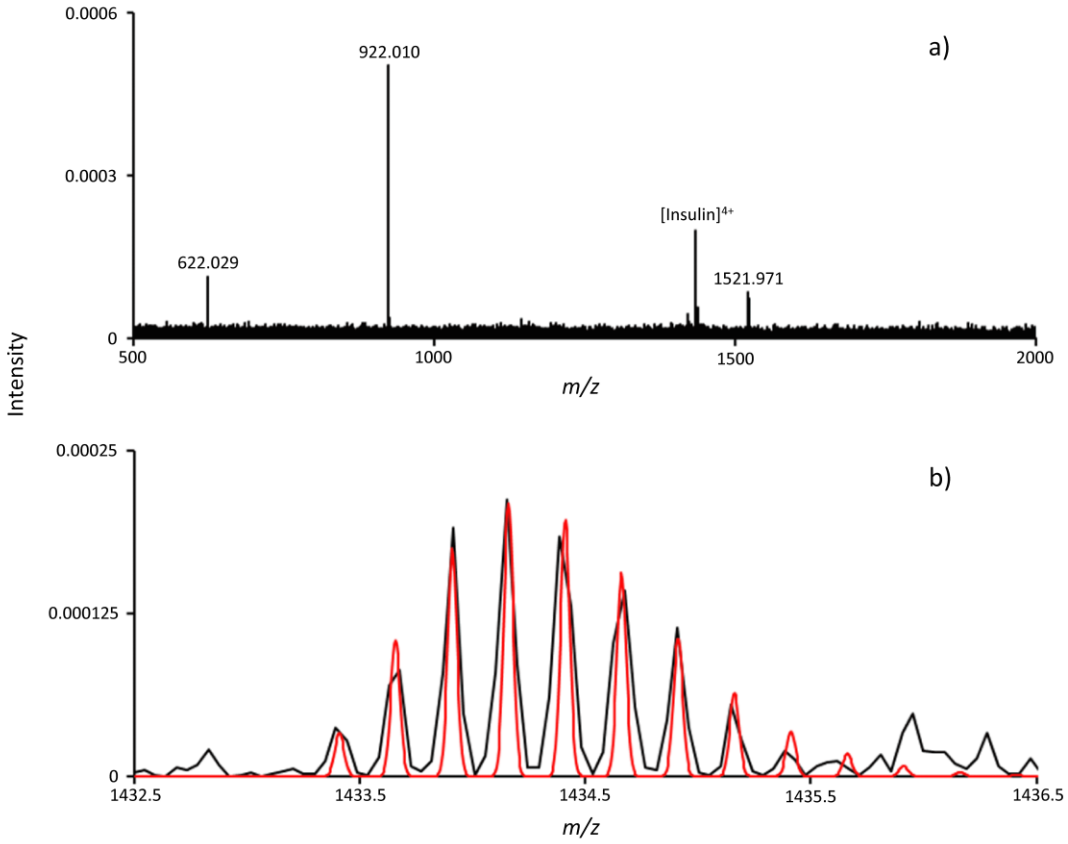

Figure 5.5. a) eFT mass spectrum of three calibrant ions and $[M+4H]^{4+}$ ion of bovine insulin simultaneously isolated from a mixture of ESI tuning mix and bovine insulin. b) Expanded region for the $[M+4H]^{4+}$ of bovine insulin (black) with simulated isotope distribution for the theoretical mass (red). All eFT spectra are averages of 100, 400 ms transients.

5.3.2 Timing of Ion Release Events for Multiple Ions of Fixed and Small Relative Δm

A special case for simultaneous ion isolation arises when there are multiple peaks with a small fixed mass spacing within a distribution of a much larger average mass (e.g., the isotope distribution of a relatively large molecule). In this scenario, closely and regularly spaced ions can be released in selective manner using a single ion release gate. We illustrate this capability in Figure 5.6 with the isotopes of a carborane anion distribution. Figure 5.6a shows the pre-isolation mass spectrum of the isotope distribution of $CHB_{11}Br_{11}^-$ (average *m/z* = 1012.56) while Figures 5.6b and 5.6c show post-isolation spectra of the even (Figure 5.6b) and odd (Figure 5.6c) isotopes following single plate 8 release pulses of 5 μs at 16.779 ms and 16.7765 ms, respectively. These multiple simultaneous isolation events are possible due to the periodicity that arises from regularly and closely spaced peaks within a distribution of relatively high *m/z* ions.

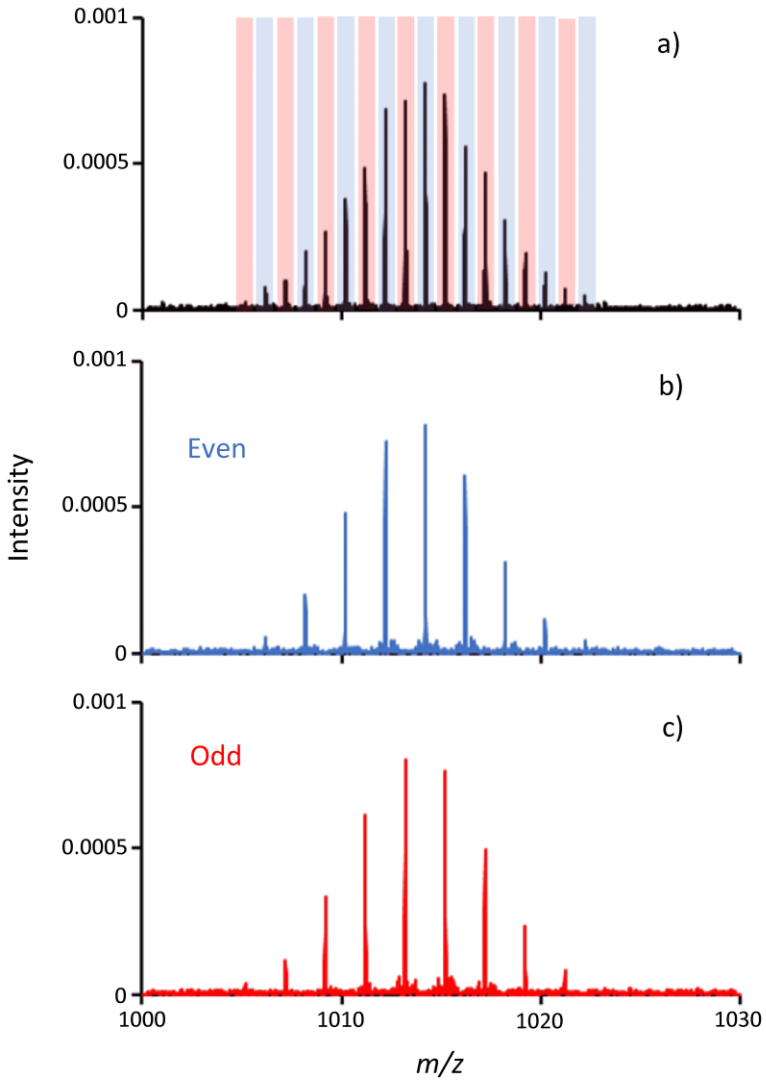

Figure 5.6. a) eFT mass spectrum of $CHB_{11}Br_{11}^-$ (1012.56 average *m/z*). b) Isolation of isotopes with an even nominal m/z using a 5 μs isolation window after 16.779 ms of separation. c) Isolation of isotopes with a nominal odd *m/z* using a 5 μs pulse after 16.7765 ms of separation. All eFT spectra are averages of 100, 500 ms transients. The phenomena underlying the isolation data of Figure 5.6 are described below for an isotopic distribution.

Consider an ion of mass m, with isotope spacing of 1 Da. The frequency with which adjacent isotopes will overlap in the ELIT (i.e., the beat frequency of the pair of ions) is given by the difference in the fundamental oscillation frequencies of the two ions, as indicated in equation 1, where c is the frequency-to-mass calibration for the ELIT.[17]

$$\Delta v_{1\mathrm{Da}} = \frac{c}{\sqrt{m}} - \frac{c}{\sqrt{m+1}} = \frac{c\left(\sqrt{m+1} - \sqrt{m}\right)}{\sqrt{m(m+1)}} \tag{5.1}$$

Similarly, the beat frequency between m and its isotope 2 Da away is given by:

$$\Delta v_{2\mathrm{Da}} = \frac{c}{\sqrt{m}} - \frac{c}{\sqrt{m+2}} = \frac{c\left(\sqrt{m+2} - \sqrt{m}\right)}{\sqrt{m(m+2)}} \tag{5.2}$$

The ratio of beat periods, given by the inverse of the ratio of beat frequencies, is shown by equation 3:

$$\frac{\text{beat period 1 Da}}{\text{beat period 2 Da}} = \frac{\Delta v_{2\mathrm{Da}}}{\Delta v_{1\mathrm{Da}}} = \frac{\sqrt{m(m+1)}}{\sqrt{m(m+2)}} * \frac{\sqrt{m+2} - \sqrt{m}}{\sqrt{m+1} - \sqrt{m}} \tag{5.3}$$

If m is large compared to the Δm (2 or 1 in this case), the term $\frac{\sqrt{m(m+1)}}{\sqrt{m(m+2)}}$ approaches 1 while $\frac{\sqrt{m+2}-\sqrt{m}}{\sqrt{m+1}-\sqrt{m}}$ approaches 2. Thus, to a first approximation, the beat period between an ion of mass m and an ion 1 Da away will be twice the beat period of the ion m and an isotope 2 Da away. Likewise, the beat period for the 1 Da spacing will be three times that for a spacing of 3 Da, and so forth. Defining the beat period between m and m+2 as T, the beat period between m and m+4 will be T/2, and between m and m+6 it will be T/3, etc. Therefore, after time T has passed, and if ion m is of even nominal mass, all even isotopes will be overlapping with the ion m (m+4 will have overlapped with m once already, m+6 twice, etc.). In contrast, the beat period between ion m and m+1 will be 2T; between m and m+3 it will be 2T/3, and between m and m+5 it will be 2T/5. Therefore, after time T has passed, these odd isotopes will have undergone N + 1/2 beat periods

(for example T/ (2T/3) = 1+1/2) with ion m and its corresponding set of even isotopes, which will all be overlapping. This means they will be almost perfectly separated by half the lap time of m from ion m and the set of even isotopes containing m. Thus, a single appropriately timed gate can allow for the simultaneous release of either all odd or all even isotopes. This can be extended to separate ions with a spacing of 3 Da as well, although in this case, at the beat period between m and m+3, the distribution will form three sets of ions, now separated by $1/3^{rd}$ the lap time of m. We further note that this technique is not necessarily limited for use with isotopic mass differences of 1 Da. For example, the mass of a protein may be large enough compared to masses associated with sodium and other adductions for this technique to be performed to isolate alternating degrees of adduction.

5.4 Conclusion

An approach for simultaneous isolation of multiple ions of disparate *m/z* ratios is demonstrated in an electrostatic linear ion trap. Simultaneous isolation takes advantage of both the rapid spatial separation of ions and the periodic nature of ion overlap in a closed path MR-TOF device. Mirror switching isolation pulses can be timed to coincide with overlapping events and because the ions of interest are spatially overlapped during the isolation event, they can be isolated from contaminant ions simultaneously. The time in which the overlap event occurs can be determined based on ion frequencies and beat periods within the device. Furthermore, the position and direction of ion motion can be predicted and used to optimize the timing of mirror switching isolation. To demonstrate simultaneous isolation, isotopes were selected from three carborane distributions and isolated in a combination of ways. This capability is useful for multiplexed MS/MS experiments and for inclusion of calibrant ions for high mass measurement accuracy applications. In addition, equally spaced ions with a small mass range can be simultaneously isolated if the *m/z* spacing is small compared to the nominal *m/z* of the isolated ions.

5.5 References

1. McDonald, L.A.; Barbieri, L.R.; Carter, G.T.; Kruppa, G.; Feng, X.; Lotvin, J.A.; Siegel, M.M. FTMS Structure Elucidation of Natural Products: Application to Muraymycin Antibiotics Using ESI Multi—CHEF SORI-CID FTMS^n, the top-Down/Bottom-Up Approach, and HPLC ESI Capillary-Skimmer CID FTMS. *Anal. Chem.* **2003**, 75, 2730-2739.

2. Wootton, C.A.; Sanchez-Cano, C.; Lopez-Clavijo, A.F.; Shaili, E.; Barrow, M.P.; Sadler, P.J.; O'Connor, P.B. Sequence-dependent attack on peptides by photoactivated platinum anticancer complexes. *Chem. Sci.* **2018**, 9, 2733-2739.

3. Kruppa, G.; Schnier, P.D.; Tabei, K.; Van Orden, S.; Siegel, M.M. Multiple Ion Isolation Applications in FT-ICR MS: Exact-Mass MS^n Internal Calibration and Purification/Interrogation of Protein-Drug Complexes. *Anal. Chem.* **2002**, 74, 3877-3886.

4. Wilson, J.; Vachet, R.W. Multiplexed MS/MS in a quadrupole ion trap mass spectrometer. *Anal. Chem.* **2004**,76, 7346-7353.

5. Ledvina, A.; Savitski, M.; Zubarev, A.; Good, D.; Coon, J.; Zubarev, R. Increased throughput of proteomics analysis by multiplexing high-resolution tandem mass spectra. *Anal. Chem.* **2011**, 83, 7651-7656.

6. O'Connor, P.B.; Little, D.P.; McLafferty, F.W. Isotopic Assignment in Large-Molecule Mass Spectra by Fragmentation of a Selected Isotope Peak. *Anal. Chem.* **1996**, 68, 542-545.

7. De Koning, L.; Nibbering, N.M.M.; Van Orden, S.; Laukien, F. Mass selection of ions in a Fourier transform ion cyclotron resonance trap using correlated harmonic excitation fields (CHEF). *Int. J. Mass Spectrom. Ion Processes.* **1997**, 165, 209-219.

8. Marshall, A.G.; Wang, T.C.L.; Ricca, T.L. Tailored excitation for Fourier transform ion cyclotron mass spectrometry. *J. Amer. Chem. Soc.* **1985**, 107, 7893-7897.

9. Johnson, J.T.; Carrick, I.J.; Eakins, G.S.; McLuckey, S.A. Mirror Switching for High-Resolution Ion Isolation in an Electrostatic Linear Ion Trap. *Anal. Chem.* **2019**, 91, 8789-8794.

10. Toker, Y.; Altstein, N.; Aviv, O.; Rappaport, M.; Heber, O.; Schwalm, D.; Strasser, D.; Zajfman, D. The kick-out mass selection technique for ions stored in an Electrostatic Ion Beam Trap. *J. Instrum.* **2009**, 4, P09001.

11. Hilger, R.T.; Santini, R.E.; McLuckey, S.A. Square wave modulation of a mirror lens for ion isolation in a Fourier transform electrostatic linear ion trap mass spectrometer. *Int. J. Mass Spectrom.* **2014**, 362, 1-8.

12. Wienholtz, F.; Kreim, S.; Rosenbusch, M.; Schweikhard, L.; Wolf, R. Mass-selective ion ejection from multi-reflection time-of-flight devices via a pulsed in-trap lift. *Int. J. Mass Spectrom.* **2017**, 421, 285-293.

13. Dickel, T.; Plaß, W.R.; Lippert, W.; Lang, J.; Yavor, M.I.; Geissel, H.; Scheidenberger, C. Isobar Separation in a Multiple-Reflection Time-of-Flight Mass Spectrometer by Mass-Selective Re-Trapping. *J. Am. Soc. Mass Spectrom.* **2017**, 28, 1079-1090.

14. Fischer, P.; Knauer, S.; Marx, G.; Schweikhard, L. In-depth study of in-trap high-resolution mass separation by transversal ion ejection from a multi-reflection time-of-flight device. *Rev. Sci. Instruments.* **2018**, 89, 015114.

15. Fischer, P.; Marx, G.; Schweikhard, L. Multiple ion capture and separation in an electrostatic storage device. *Int. J. Mass Spectrom.* **2019**, 435, 305-314.

16. Dziekonski, E.T., Johnson, J.T., Lee, K.W., McLuckey, S.A. Fourier-transform MS and Closed-Path Multireflection Time-of-Flight MS Using an Electrostatic Linear Ion Trap. *Anal. Chem.* **2017**, 89, 10965-10972.

17. Hilger, R.T.; Dziekonski, E.T.; Santini, R.E.; McLuckey, S.A. Injecting electrospray ions into a Fourier transform electrostatic linear ion trap. *Int. J. Mass Spectrom.* **2015**, 378, 281-287.

18. Johnson, J.T.; Lee, K.W.; Bhanot, J.S.; McLuckey, S.A. A Miniaturized Fourier Transform Electrostatic Linear Ion Trap Mass Spectrometer: Mass Range and Resolution. *J. Am. Soc. Mass Spectrom.* **2019**, 30, 588-594.

CHAPTER 6. TANDEM MASS SPECTROMETRY USING AN ELECTROSTATIC LINEAR ION TRAP

6.1 Introduction

Tandem mass spectrometry[1] (MS/MS or MS^n) is the sequential mass spectrometric analysis of analyte ions. MS/MS is primarily executed by conducting an initial MS experiment to identify potential precursor ion for subsequent MS/MS. In the MS/MS experiment, the first MS step involves the isolation of a precursor ion which is then subjected to some physiochemical process to produce new product ions which are analyzed in the second MS stage. Product ions are often informative and can provide information about the structure and identity of the precursor ion. Thus, tandem mass spectrometry is often used in the analysis of many classes of molecules including drugs,[2,3] proteins,[4,5] lipids,[6,7] carbohydrates,[8,9] and protein complexes.[10,11]

Tandem mass spectrometry can be performed in one of two ways: tandem-in-time or tandem-in-space.[12] A convenient aspect of the tandem-in-time approach is the ease (no hardware modifications required) in which multidimensional mass spectrometry (MS^n, where n >2) can be performed. MS^n involves the same steps as a tandem mass spectrometry experiment repeated multiple times. In this case the product ions of the previous experiment become the precursors for the next MS stage. This sequence of event can be repeated until the ion population is diminished due to charge partitioning among product ion and/or ion losses in each MS stage.

Since multidimensional mass spectrometry necessitates non-destructive ion detection, MS^n has been primarily been limited to magnetic/electrostatic (FT-ICR) and electrodynamic ion traps. One of the most prominent non-destructive mass analyzers is the Orbitrap however it is difficult to induce ion chemistry without losing ions and also difficult to extract ions from these devices. An alternative non-destructive electrostatic mass analyzer is the electrostatic linear ion trap (ELIT)

in which it is relatively straight forward to fragment ions within the device using SID [13] (tandem-in-time) and can also be used as a high-resolution terminal mass analyzer after quadrupole linear ion trap (QLIT) isolation and CID [14] (tandem-in-space).

In this work, we demonstrate the use of an electrostatic linear ion trap as both a tandem-in-space and tandem-in-time mass spectrometer. High resolution product ion spectra are demonstrated after apex ion isolation and fragmentation in QLIT. Finally, tandem-in-time mass spectrometry is demonstrated using mirror switching isolation and SID. Tandem-in-time is demonstrated on lipid mixtures and a protein complex.

6.2 Experimental Section

6.2.1 Materials

[PC P-18:0/22:6] and bovine heart extract were purchased from Avanti Polar Lipids (Alabaster, AL). Methanol was purchased from Thermo Fisher Scientific (Waltham, MA). HPLC-grade water was purchased from Fisher Scientific (Pittsburgh, PA). Triosephosphate isomerase, ethylenediaminetetraacetic acid (EDTA), 3,3,4,4,5,5,6,6,7,7,8,8,9,9,10,10,10-heptadecafluoro-1-decanethiol, sodium borohydride, ammonium iron(II) sulfate hexahydrate and reserpine was purchase from Sigma-Aldrich (St. Louis, MO). Glacial acetic acid, sodium hydroxide, and hydrogen peroxide (30% w/w) were purchased from Macron Fine Chemicals (Center Valley, PA). Ethanol was purchased from Decon Laboratories (King of Prussia, PA). The mixture of [PC P-18:0/22:6] (100 μM) was prepared using 99/1 v/v MeOH/1 mM ammonium acetate. Bovine heart extract (polar) was prepared to a final concentration of 100 μM in methanol with 100 mM ammonium acetate, assuming an average lipid molecular mass of 760 g/mol. Triosephosphate

isomerase was prepared to a final concentration of 50 μM in 100 mM ammonium acetate after buffer exchange and dialysis

6.2.2 Mass Spectrometry

All experiments were carried out on a home-built electrostatic linear ion trap mass spectrometer shown in Figure 6.1. The nano-electrospray ionization (nESI) source and the method by which ions are concentrated and injected into the electrostatic linear ion trap (ELIT) have been described.[15] The electrostatic linear ion trap described in this work is 5.25″ in length measured from the beginning of the first trapping electrode to the end of the last trapping electrode. The charge-sensitive detection electronics have been described previously.[16] The output of the charge sensitive preamplifier (A250, Amptek) was filtered (band-pass, Krohn-Hite Model 3945, Brockton, MA) and amplified (gain = 5) prior to digitization by a PCI-based digitizer (CS1621, 16-bit, Gage Applied Technologies, Lanchine, Quebec, Canada) at a rate of 10 MS/s (AC coupled, 1 MΩ input impedance, 25 MHz low-pass filter enabled). A program written in LabVIEW 13.0 (National Instruments, Austin, TX) was used to acquire each transient for FT analysis. A custom program, written in MATLAB 2019b, was used to process the transients using the enhanced Fourier transform (eFT).[17]

Ion Isolation

Ion isolation was performed by pulsing of the first plate of the ELIT (plate 1) from its nominal trapping potentials (~2360 V) to ground at some specified time after ion injection.[18] It is important to note that the voltage necessary for ion ejection needs only to be lower than the nominal ion energy (~1960 eV/charge). The time in which the electrodes are pulsed and the duration they are held at ground was set by a pulse/delay generator (model 577, Berkeley Nucleonics, San Rafael, CA). A home-built digital signal joiner was developed for combining

waveforms from multiple signal sources such that a single mirror could be pulsed multiple times by coupling up to three input TTL signals. This device allowed for high accuracy control over multiple mirror switching events using the BNC 577 pulse/delay generator. Each signal drives a high impedance input that prevents interference or signal degradation of adjacent channels. By utilizing high-speed CMOS technology, the circuit was configured such that the propagation delay stays within an 8.5 ns window. Mirror switching was done using ORTEC 556 power supplies and solid-state switches (HTS 31-03-GSM, Behlke Electronics GMBH, Kronberg, Germany).

Collision Induced Dissociation

Once injected ions are transported from the ion source to the quadrupole linear ion trap (QLIT) where they are thermalized. Ions can be isolated via apex isolation before being subjected to collision induced dissociation. This is done by triggering a function generator to produce a sinusoidal signal of proper amplitude and frequency across one of the rod pairs (dipolar excitation) using a transformer. The linear acceleration (LINAC) electrode can then be ramped to bunch the product ions before the exit lens is then pulsed down to inject ions into the ELIT for mass analysis.

Surface Induced Dissociation

The SID surface consisted of a polished gold disk (5mm outer diameter, 4mm thick, Pine Research Instrumentation, Durham, NC). The surface was first prepared by rinsing with ethanol followed by sonication for 10 min in cleaning solution followed by 10 min of sonication in ethanol. The surfaced was then rinsed with water. Nano-polishing was performed by placing the surface in 1 mM Fe^{2+}, 10 mM H_2O_2, an 1 mM acetate buffer (pH = 4.7) for 1 h followed by rinsing with water.[19] Oxides on the surface were reduced by placing the surface in 0.5 M $naBH_4$ in 1:1 ethanol/water for 10 min followed by rinsing with water followed by ethanol.[20] A self-assembled

monolayer (SAM) was added by placing the surface in a 1 mM solution of 3,3,4,4,5,5,6,6,7,7,8,8,9,9,10,10,10-heptadecaflouro-1-decanethiol in ethanol for 24 h. The surface was then sonicated in ethanol for 5 min three times. The surface was then air dried before being mounted 2 mm behind plate 8 to which it was electrically connected via a wire.

Since ions are injected at ~1960 eV, the energy imparted on the ions upon collision with the gold surface is the difference between the ion energy and the potential of the surface. The relationship between ion collision energies and the timing associated with SID in an ELIT has been discussed at depth previously by Hilger et. al..[13] Here we primarily discuss SID in an ELIT in relation to tandem mass spectrometry in which ions are isolated using mirror switching and subsequently fragmented to derive information about lipid class and higher order structure from the protein complex triose phosphate isomerase.

6.3 Results and Discussion

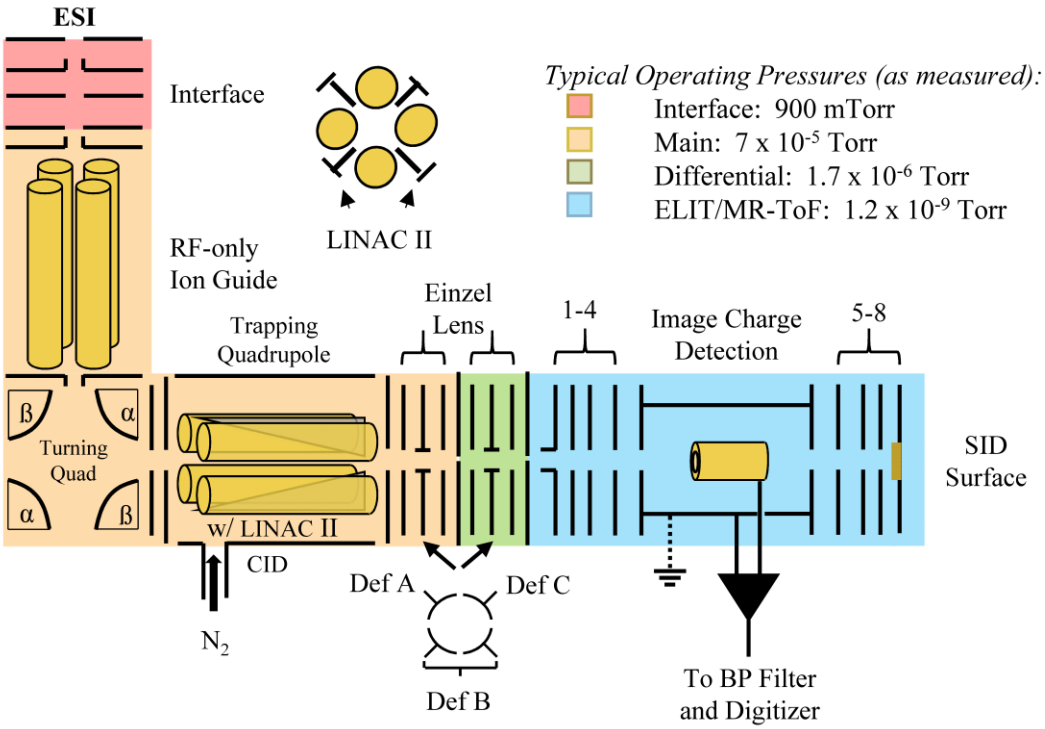

Figure 6.1. Instrument Schematic

6.3.1 Tandem-in-Space

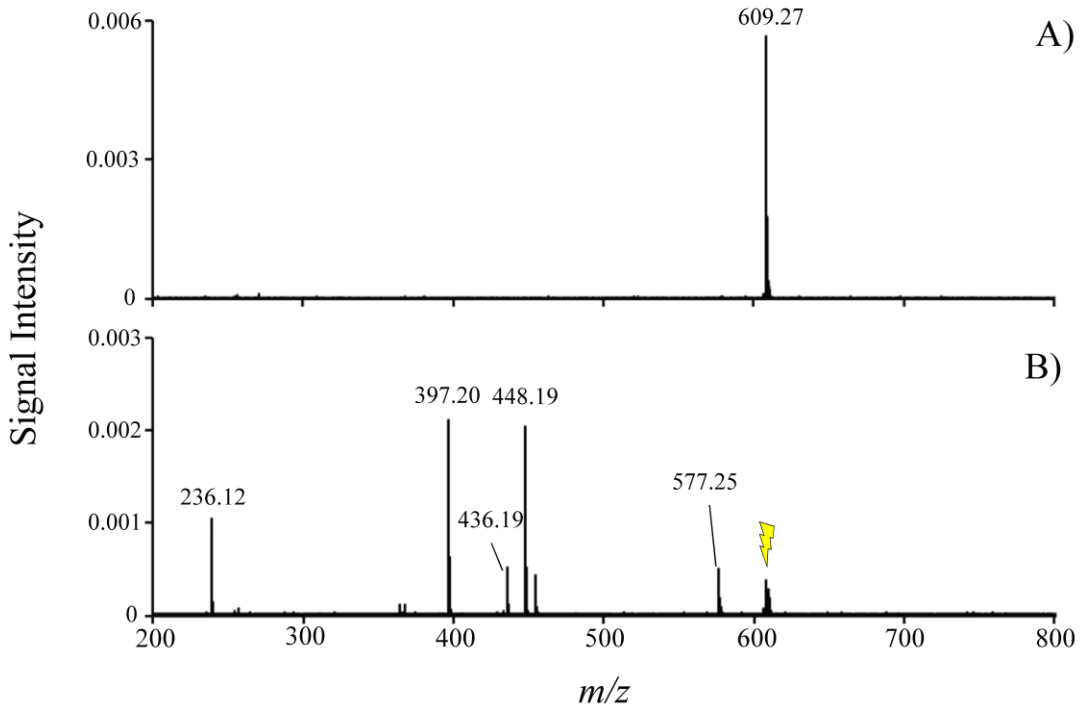

Figure 6.2. Collision induced dissociation of reserpine after being isolated using apex isolation.

When operated as a tandem-in-space mass spectrometer, ions are probed and analyzed in two separate devices.[12] In the device shown in Figure 6.1, ions can be apex isolated and fragmented via collision induced dissociation in the trapping quadrupole. Product ions generated are then injected into the ELIT for mass analysis. Figure 6.2 demonstrates tandem-in-space mass spectrometry of $[\text{reserpine} + \text{H}]^+$ in which the precursor ion at *m/z* 609 is isolated in the trapping quadrupole (A). Ions are then subjected to resonant excitation in which ions undergo collision induced dissociation. After CID ions are concentrated to the end of the quadrupole and injected into the ELIT for high resolution product mass analysis (B).

Tandem-in-space mass spectrometry can also be accomplished using the ELIT for ion isolation and mass analysis while still utilizing the trapping quadrupole for CID.[14] Ions are isolated either via frequency modulation with or mirror switching within the ELIT and subsequently transferred back into the trapping quadrupole for CID. Once product ions are generated, ions can be concentrated near the exit electrode of the trapping quadrupole using the LINAC electrodes and re-injected into the ELIT for product ion analysis. Inefficiencies transferring ions back to the trapping quadrupole from the ELIT in our current apparatus makes this method difficult to accomplish as product ions are low in intensities.

6.3.2 Tandem-in-Time

When operated as a tandem-in-time mass spectrometer, a precursor ion is isolated, probed, and mass analyzed in the same mass analyzer. In the device shown in Figure 6.1, ions are injected into the ELIT where a precursor ion is then mass selected using mirror switching. The mass selected ion is then allowed to collide with a gold surface placed behind the rear ion mirror. After colliding with the gold surface ions are then re-trapped for product ion analysis.

Surface induced dissociation using the ELIT has been discussed in-depth previously.[13] In short, the gold surface is electrically connected to the outermost plate electrode. This electrode is pulsed down such that ions can impinge upon the gold surface with an energy corresponding the difference between the energy of the ions (potential plus kinetic) and the potential of the surface. By positioning the gold surface behind the rear ion mirror, most of the ion kinetic energy is converted to potential energy by the ion mirror before fragmentation. Thus, the total energy of the product ions is determined by the electrostatic potential near the surface. Although small changes in fragment ion frequencies do occur (>200 Hz at *m/z* 100 which corresponds to a mass shift of ~0.1 *m/z*), ion energies are still within the focusing range of the current ELIT geometry.

Lipid Analysis

Lipidomics is one potential area in which a high-performance tandem-in-time mass spectrometer would be of interest, as samples can possess many isobaric species.[6,7] The ability to isolate one isobaric lipid species from another simplifies the MS/MS experiment as other stages of separation would likely be needed in lieu high isolation resolution. On our current apparatus, we have demonstrated that phospholipids separated by 57.5 mDa can be isolated from one another using mirror switching (Chapter 4).[15]

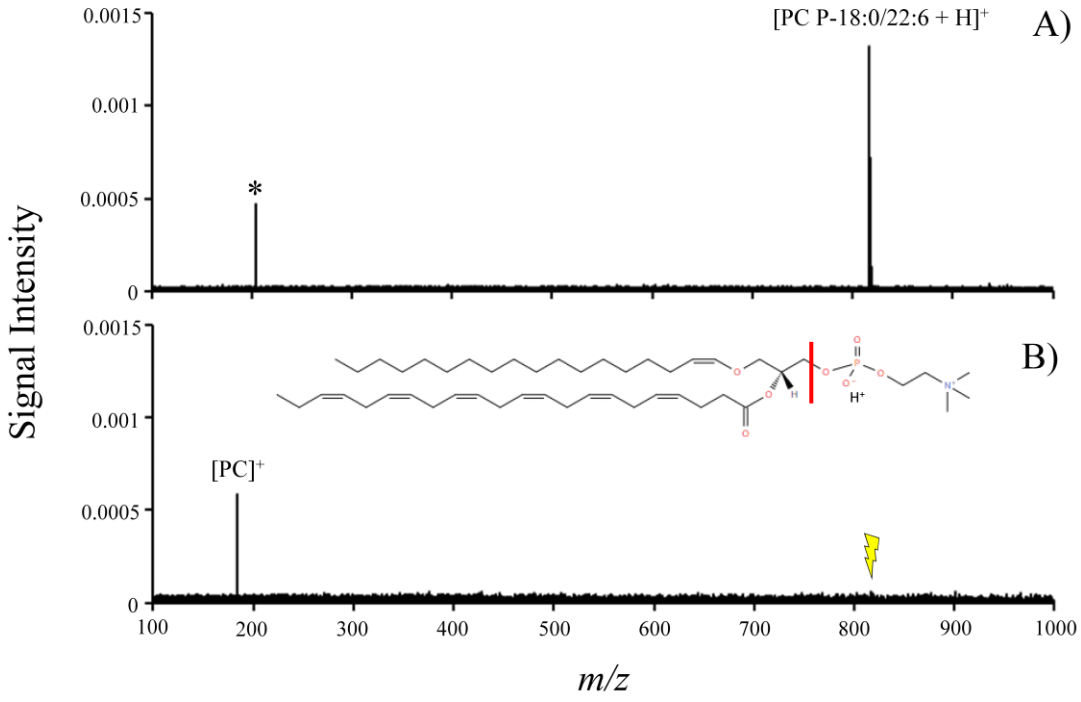

Figure 6.3. Mirror switching isolation of [PC P-18:0/22:6+H]$^+$ after mirror switching isolation.

Figure 6.3 shows tandem-in-time mass spectrometry on [PC P-18:0/22:6]. The precursor ion has been isolated from adducts and in-sources fragments (A). The ion of interest is then allowed to impinge upon the gold surface with an ion energy of ~40 eV to produce a class determinant head group ion which in this case is a phosphocholine (B). When sprayed in positive mode, the

most abundant product ion for a phosphocholine lipid is the phosphocholine head group due to the fixed charge on the quaternary amine. This abundant head group product ion provides useful information on the class of the ion. The class and accurate mass of the lipid can then be used to narrow the possible candidates in a database search.

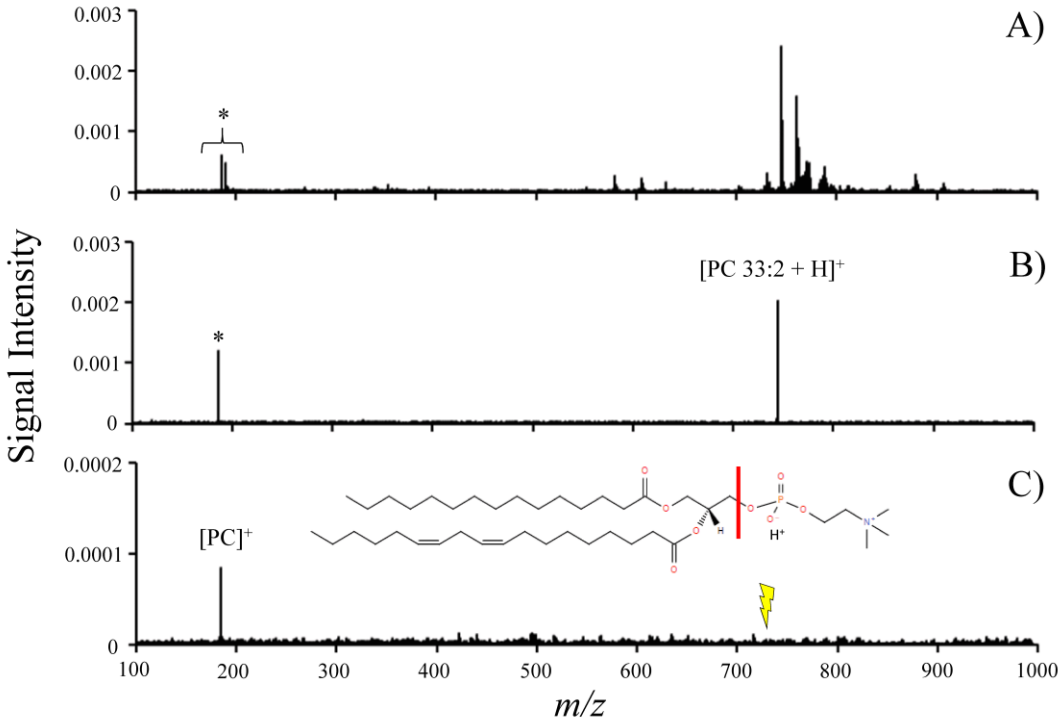

Figure 6.4. Bovine heart extract (polar) prior to isolation (A). Isolation of m/z 744.55 using mirror switching (B). SID of *m/z* 744.55 to produce the class determinant head group ion at *m/z* 184 (C).

Figure 6.4 (A) shows bovine heart extract (polar) prior to ion isolation. A precursor ion can be mass selected (B) before subsequent SID. Based on the appearance of a head group ion at *m/z* 184 we can confirm that this is a phosphocholine and based on the m/z of the precursor ion (*m/z* 744.55), the lipid of interest is most likely [PC 33:2].

Protein Complex Analysis

Structural analysis using SID has become increasing prevalent.[22] For multimeric proteins, the sudden release of energy throughout the ion species leads to dissociation pathways that result in loss of subunits which retain much of their structure. In this way, SID can be used to probe the subunit binding associated with multimeric protein complexes. Figure 6.5 shows a proof-of-concept experiment for multimeric protein complex SID in an ELIT.

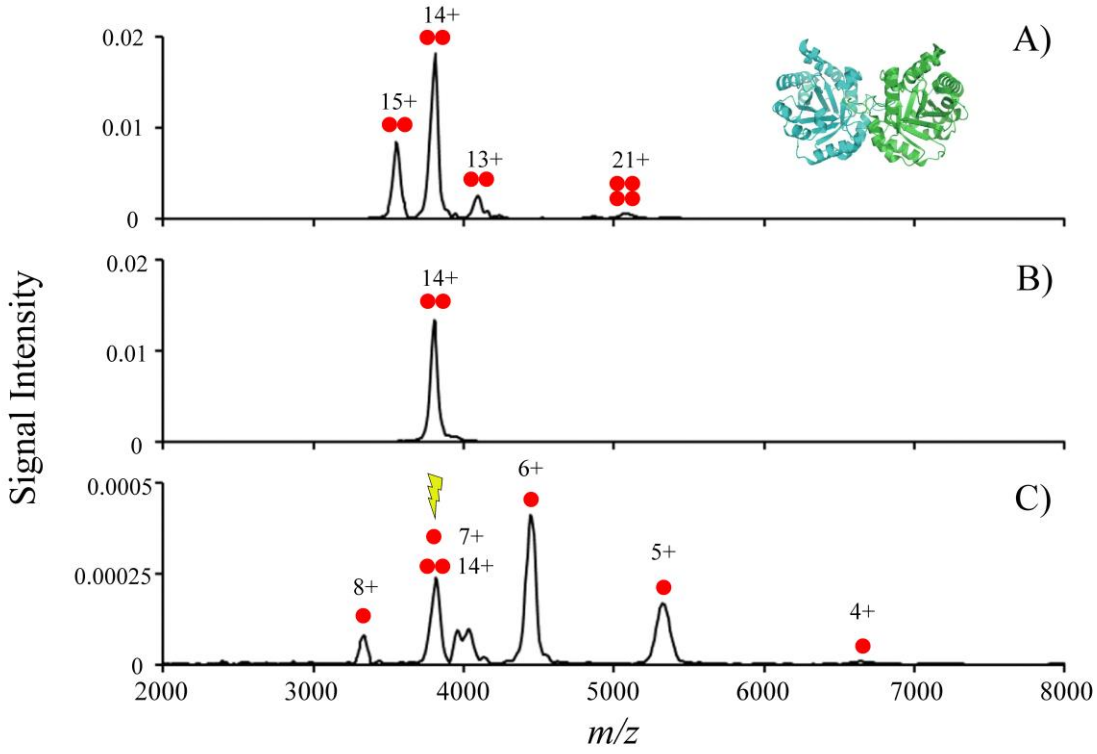

Figure 6.5. Triosephosphate isomerase prior to isolation (A). Isolation of the +14 charge state of the triosephosphate isomerase homo-dimer using mirror switching (B). SID of the isolated charge state to produce monomers (C).

Figure 6.5 (A) shows charge state distributions associated with triosephosphate isomerase which is a naturally occurring dimer (27 kDa per subunit).[10] Using mirror switching, the 14+ charges state of the dimer can be isolated as shown in Figure 6.5 (B). The dimer can then be

subjected to a collision energy of ~1680V to induce fragmentation, producing monomeric species. Thus, demonstrating the utility of the ELIT in probing higher order protein structure.

6.4 Future Directions

In addition to CID and SID, ion activation can occur by radially injecting a beam of light, electrons, atoms, etc. between two plates of an ELIT such that it interacts with the ion packet at the turning point. This form of activation benefits from the fact that both precursor and product ions remain unperturbed, unlike in SID where ion are removed from the trapped. In the case where only a single ion is present in the ELIT after isolation, the beam can be brought down the radial axis of the trap for maximum overlap with the ion population. The method for ion activation is limited by the size of the ion and the amount of energy impart of the population. In the current apparatus, a laser induced dissociation method is being implemented such that a ultraviolet and infrared laser can be brought in between plates 7 and 8 to induce photofragmentation. The final proposed instrument is shown in Figure 6.6 and is capable of CID, SID, UVPD, IRMPD, and ion/ion reaction.

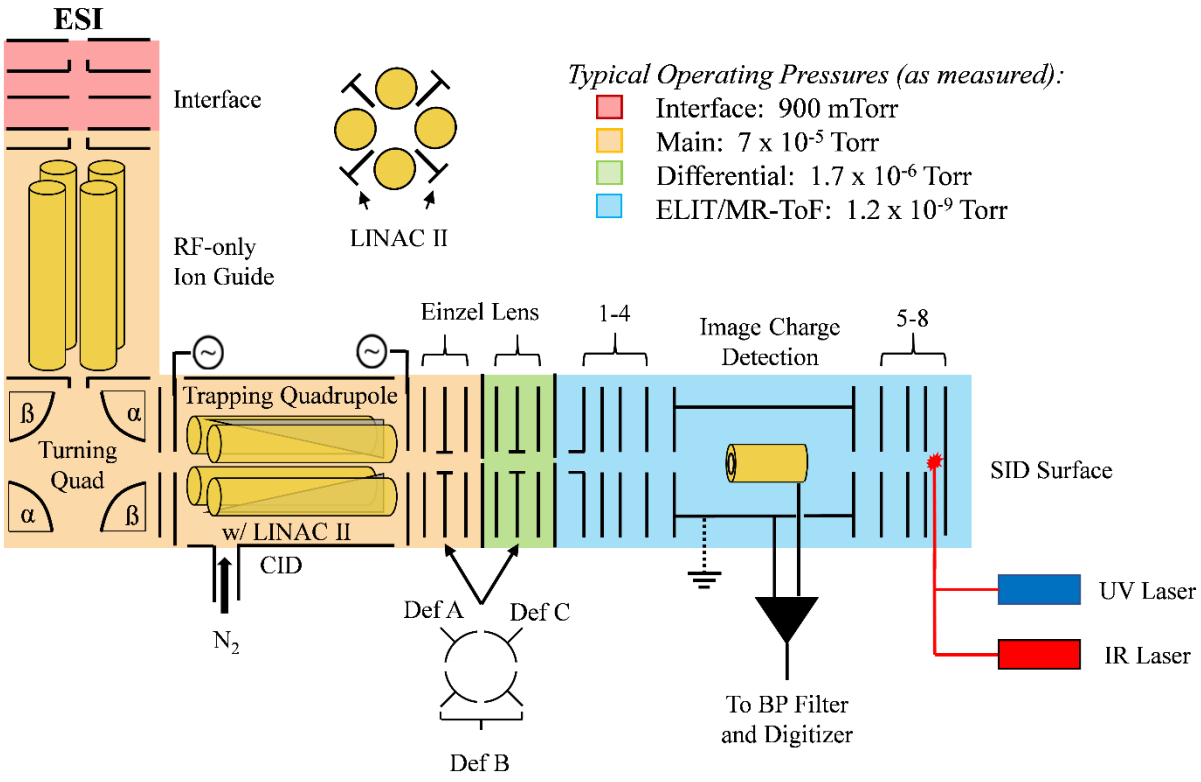

Figure 6.6. Next generation ELIT platform that allows for CID, SID, UVPD, IRMPD, and Ion/Ion reactions.

6.5 Conclusions

The ELIT presented here can operate as both a tandem-in-space and tandem-in-time mass spectrometer. The benefit of utilizing the ELIT as a tandem-in-time device is that high resolution ion isolation can be accomplished via mirror switching prior to generating fragment ions. This is particularly useful when looking at complex mixtures where isobaric compounds are common. Tandem mass spectrometry on lipid mixtures has been shown using mirror switching isolation followed by SID. This provided useful headgroup information which when coupled with the accurate precursor *m/z* was used to determine the identity of a lipid present in bovine heart extract. Structural analysis can also be done using a tandem-in-time approach. A single charge state of a protein complex can be isolated via mirror switching before being subjected to SID. This was demonstrated using the naturally occurring dimer triosephosphate isomerase which produced monomer fragments after interrogation using SID. The ELIT can also be operate as a tandem-in-space mass spectrometer where isolation and CID fragmentation occur in a colinear QLIT. The product ions can then be injected into the ELIT for high resolution mass analysis. Tandem-in-time mass spectrometry was demonstrated with reserpine.

6.6 Reference

1. Gross, J. H. Mass Spectrometry: A Textbook, 2nd Edition; *Springer: New York*, **2011** pp 415−478.

2. Niessen, W. M. A. Fragmentation of toxicologically relevant drugs in negative-ion liquid chromatography-tandem mass spectrometry. *Mass Spectrom. Rev.* **2012**, 31, 626−665.

3. Niessen, W. M. A. Fragmentation of toxicologically relevant drugs in positive-ion liquid chromatography-tandem mass spectrometry. *Mass Spectrom. Rev.* **2011**, 30, 626−663.

4. Hernandez, P.; Müller, M.; Appel, R. D. Automated protein identification by tandem mass spectrometry. *Mass Spectrom. Rev.* **2006**, 25, 235−254.

5. Meng, F.; Forbes, A. J.; Miller, L. M.; Kelleher, N. L. Detection and localization of protein modification by high resolution tandem mass spectrometry. *Mass Spectrom. Rev.* **2005**, 24, 126−134.

6. Cui, Z.; Thomas, M. J. J. Phospholipid profiling by tandem mass spectrometry. *Chromatogr. B* **2009**, 877, 2709−2715.

7. Zehethofer, N.; Pinto, D. M. Recent Developments in tandem mass spectrometry for lipidomic analysis. *Anal. Chim. Acta* **2008**, 627, 62−70.

8. Zhou, W.; Hakansson, K. Structural characterization of carbohydrates by Fourier transform tandem mass spectrometry. *Curr. Proteomics* **2011**, 8, 297−308.

9. An, H. J.; Lebrilla, C. B. Structure elucidation of native N-and O-linked glycans by tandem mass spectrometry. *Mass Spectrom. Rev.* **2011**, 30, 560−578.

10. Harvey, S. R.; Seffernick, J. T.; Quintyn, R. S.; Song, Y.; Ju, Y.; Yan, J.; Sahasrabuddhe, A. N.; Norris, A.; Zhou, M.; Behrman, E. J.; Lindert, S.; Wysocki, V. H., Relative interfacial cleavage energetics of protein complexes revealed by surface collisions. *PNAS* **2019**, 116, 8143-8148.

11. Stiving, A. Q.; VanAernum Z.; Busch, F.; Harvey S. R.; Sarni, S.; Wysocki, V. H., Surface-Induced Dissociation: An Effective Method for Characterization of Protein Quaternary Structure. *Anal Chem.* **2018**, 91, 190-209.

12. Johnson, J. V.; Yost, R. A. Tandem-in-space and tandem -in-time mass spectrometry: triple quadrupoles and quadrupole ion traps. *Anal. Chem.* **1990**, 20, 2162−2172.

13. Hilger, R. T.; Santini, R. E.; McLuckey, S. A. Tandem Mass Spectrometry in an Electrostatic Linear Ion Trap Modified for Surface-Induced Dissociation. *Anal. Chem.* **2014,** 86, 8822-8828.

14. Hilger, R. T.; Santini, R. E.; McLuckey, S. A. Nondestructive Tandem Mass Spectrometry Using a Linear Quadrupole Ion Trap Coupled to a Linear Electrostatic Ion Trap. *Anal. Chem.* **2013,** 85, 5226-5232.

15. Hilger, R.T.; Dziekonski, E.T.; Santini, R.E.; McLuckey, S.A. Injecting electrospray ions into a Fourier transform electrostatic linear ion trap. *Int. J. Mass Spectrom.* **2015,** *378,* 281-287.

16. Dziekonski, E. T., Johnson, J. T., Lee, K. W., McLuckey, S. A. Fourier transform MS and closed-path multireflection time-of-flight MS using an electrostatic linear ion trap. *Anal. Chem.* **2017**, 89, 10965–10972.

17. Lange, O.; Damoc, E.; Wieghaus, A.; Makarov, A. Enhanced Fourier transform for Orbitrap mass spectrometry. *Int. J. Mass Spectrom.* **2014,** 369, 16-22.

18. Johnson, J. T.; Carrick, I. J.; Eakins, G. S.; McLuckey, S. A. Mirror Switching for High Resolution Ion Isolation in an Electrostatic Linear Ion Trap. *Anal. Chem.* **2019**, 91, 8789-8794.

19. Nowicka, A. M.; Hasse, U.; Hermes, M.; Scholz, F. Hydroxyl radicals attack metallic gold. *Angew. Chem., Int. Ed.* **2010**, 49, 1061−1063.

20. Yuan, M.; Zhan, S.; Zhou, X.; Liu, Y.; Feng, L.; Lin, Y.; Zhang, Z.; Hu, J. A method for removing self-assembled monolayers on gold. *Langmuir* **2008**, 24, 8707−8710.

VITA

Joshua Thomas-Keith Johnson was born on April 9th, 1993 in Virginia Beach, Virginia. He is the only son of Sean and Shelley Johnson and has a younger sister named Jade. After moving to Travelers Rest, SC, he graduated from Travelers Rest High School in 2011 before enrolling at Gardner-Webb University. Following his junior year, he spent 10 weeks at Florida State University under the direction of Dr. David Podgorski completing a Research Experience for Undergraduates (REU) program. There his work focused on understanding photochemical oxidation of crude oils with different bulk physical and chemical properties using high resolution mass spectrometry. Joshua graduated from Gardener-Webb University in 2015 with a Bachelor of Science in Environmental Science and minors in Chemistry and Mathematics. He began his graduate studies at Purdue University in August 2015 and joined Dr. Scott McLuckey's Lab that fall where his research focused on the development of an electrostatic linear ion trap. In his time at Purdue, Joshua has been an active member of the Graduate Student Advisory Board where he acted as the Analytical Division Representative, the Blood Drive Coordinator, and the Newsletter Editor. He defended his Ph.D. in March of 2020 and will be working as a research scientist for Corteva Agriscience following graduation.

PUBLICATIONS

1. Dziekonski, E. T.; Johnson, J. T.; Hilger, R. T.; McIntrye, C. L.; Santini, R. E.; McLuckey, S. A. Voltage-induced frequency drift correction in Fourier transform electrostatic linear ion trap mass spectrometry using mirror-switching. *Int J. Mass Spectrom.* **2016**, 410, 12-21.

2. Dziekonski, E. T.; Johnson, J. T.; McLuckey, S. A.; Utility of higher harmonics in electrospray ionization fourier transform electrostatic linear ion trap mass spectrometry. *Anal. Chem.* **2017**, 89, 4392-4397.

3. Dziekonski, E. T.; Johnson, J. T.; Lee, K. W.; McLuckey, S. A. Fourier-transform MS and closed-path multireflection time-of-flight MS using an electrostatic linear ion trap. *Anal. Chem.* **2017**, 20, 10965-10972.

4. Dziekonski, E. T.; Johnson, J. T.; Lee, K. W.; McLuckey, S. A. Determination of collision cross section using a Fourier transform electrostatic linear ion trap mass spectrometer. *J. Am. Soc. Mass Spectrom.* **2018**, 2, 242-250.

5. Johnson, J. T.; Lee, K. L. Bhanot, J. S.; McLuckey, S. A. A Miniaturized Fourier Transform Electrostatic Linear Ion Trap Mass Spectrometer: Mass Range and Resolution. *J. Am. Soc. Mass Spectrom.* **2019**, 4, 588-594.

6. Johnson, J. T.; Carrick, I. J.; Eakins, G. S.; McLuckey, S. A. Mirror Switching for High-Resolution Ion Isolation in an Electrostatic Linear Ion Trap. *Anal. Chem.* **2019**, 14, 8789-8794.

7. Johnson, J. T.; Carrick, I. J.; Eakins, G. S.; McLuckey, S. A. Simultaneous Isolation of Nonadjacent m/z Ions Using Mirror Switching in an Electrostatic Linear Ion Trap. *Anal. Chem.* **2019**, 19, 12574-12580.

International Journal of Mass Spectrometry 410 (2016) 12–21

Contents lists available at ScienceDirect

International Journal of Mass Spectrometry

journal homepage: www.elsevier.com/locate/ijms

Voltage-induced frequency drift correction in fourier transform electrostatic linear ion trap mass spectrometry using mirror-switching

Eric T. Dziekonski, Joshua T. Johnson, Ryan T. Hilger, Catherine L. McIntyre, Robert E. Santini, Scott A. McLuckey*

Department of Chemistry, Purdue University, West Lafayette, IN, 47907-2084, USA

ARTICLE INFO

Article history:
Received 5 July 2016
Received in revised form 21 October 2016
Accepted 24 October 2016
Available online 25 October 2016

Keywords:
Frequency-drift
ELIT
Fourier transform
ESI
Instrumentation
Transient voltage recovery

ABSTRACT

Ion capture from an external nano-electrospray ionization source in a Fourier transform electrostatic linear ion trap has been effected by mirror-switching. This capture method can suffer from time-dependent frequency shifts in the measured ion motion, which compromises mass resolution when using Fourier transform techniques for mass determination. This phenomenon was determined to be a result of the transient voltage recovery of the power supplies used for mirror-switching in response to a pulsed capacitive load, for which several examples are shown. A circuit, based on the AD210AN isolation amplifier, was fabricated to compensate for the voltage perturbation induced by mirror-switching by superimposing the inverted perturbation to the electric field of the opposing reflectron. In doing so, the dependence of the ions path length and frequency on the power supply output was greatly reduced throughout data acquisition. With this circuit enabled, no frequency shifts were observed in the mass spectrum when using mirror-switching, and thus pressure-limited theoretical resolutions were achieved. For example, an absorption mode resolving power of greater than 50,000 M/ΔM FWHM was observed for iodide (m/z 126.9) at a transient length of 300 milliseconds. The use of mirror-switching led to a much greater m/z range than in-trap potential lift for a single ion injection which is demonstrated via simulation and experimental results. This correction method is simple to implement and does not require user intervention once properly tuned.

1. Introduction

In the last two decades, routine polyatomic mass spectrometry (MS) has transitioned to make use of the high resolution, accurate mass analysis offered by Fourier transform ion cyclotron resonance (FT-ICR) and Orbitrap™ mass spectrometers. When the acquisition rate is not a primary concern, these techniques are favored over time-of-flight (TOF) MS and have allowed researchers to probe the isotopic fine structure of molecules to elucidate empirical formulas and determine compound classes [1–3], directly identify post-translational modifications of peptides [4], etc. Today, these platforms are in common use in many '-omic' communities due to their ability to resolve and analyze complex samples where thousands of signals may be present, each of which may have multiple ion forms and isotopologues [5–7]. In order for these Fourier transform (FT) based instruments to perform at such a high level, two criteria must be met: (1) the transient length must be sufficient to obtain the necessary mass resolution for the m/z region of interest, which is a function of the background pressure, packet dephasing [8–12], detection sensitivity, and ion frequency; (2) the experimental ion frequency should not change beyond a specified margin over the course of data acquisition and should not change between runs. With the use of appropriate vacuum techniques, the Orbitrap and FT-ICR can achieve pressures of 10^{-10} and 10^{-12} Torr, respectively, with typical operating pressures being between 10^{-9}–10^{-10} Torr. Even better vacuum may be achieved through the use of specialized pumps and cryogenic cooling [13–15] and as such is not discussed in detail here. In an effort to minimize frequency drift throughout data acquisition and enable the generation of high resolution mass spectra, numerous technologies have been developed by vendors of Orbitrap™ and FT-ICR instruments. These include, but are not limited to, the use of automatic gain control (AGC) [16–19], the dynamically harmonized cell [20–23], the high-field

* Corresponding author at: 560 Oval Drive, Department of Chemistry, Purdue University, West Lafayette, IN, 47907-2084, USA.
E-mail address: mcluckey@purdue.edu (S.A. McLuckey).

http://dx.doi.org/10.1016/j.ijms.2016.10.012
1387-3806/

Orbitrap [24,25], ultra-stable magnets and power supplies, low-noise preamplifiers [19,26,27], and various modes of calibration [19,28–30]. All of these serve to minimize and/or compensate for field effects arising from space charge, analyzer geometry/field homogeneity, and electric/magnetic field drift, which, if left uncorrected, would compromise the mass resolution when using Fourier transform techniques for mass determination.

The Fourier transform electrostatic linear ion trap (ELIT) is another type of FT-based mass analyzer in which ions are reflected back and forth between two opposing reflectrons. Like Orbitrap, the frequency of an ion in an ELIT is inversely proportional to the square root of its mass-to-charge ratio:

$$f_{ion} = \frac{k}{\sqrt{m/z}} + b \tag{1}$$

where k and b are experimentally determined constants. The image charge induced on a pickup electrode is digitized and Fourier transformed to obtain the mass spectrum. Under low resolution conditions (i.e., short transient times), the ELIT has been shown to be capable of performing absorption mode data acquisition [31], surface induced dissociation [32], and ion isolation [33], thereby demonstrating that it can act as a stand-alone tandem mass spectrometer.

Two approaches have been described for the capture of ions that have been axially injected into an ELIT (Fig. 1): mirror-switching [14,34,35] and in-trap potential lift [36–39]. In the former (Fig. 1, left), the entrance reflectron plates are initially held at potentials sufficiently low to allow ions with sufficient kinetic energy (KE) to enter the ELIT (A). Once all ions of interest are within the accepted time-of-flight distance (D), the entrance reflectron is pulsed high to axially confine the ions (B), after which a transient is recorded (C). With in-trap potential lift (Fig. 1, right), all plate potentials are continually held at their respective trapping potentials. Ions are injected with sufficient KE to overcome the electrostatic barrier set by the trapping potentials of the entrance reflectron (A). When the ions of interest enter the repulsive lift electrode, the applied voltage is pulsed to ground, thereby reducing the potential energy of the ions (B) such that they are no longer able to overcome the electrostatic barriers of the reflectrons and a transient can be recorded (C). If the ions are not within the lift electrode when it is pulsed down, they will have sufficient energy to overcome the electrostatic barrier of the rear reflectron and exit the ELIT.

As can be deduced from a comparison of capture methods, for two traps of equivalent geometry, the accepted time-of-flight distance (D), or m/z range, of mirror-switching is much greater than that of in-trap potential lift and is therefore the desired capture method for an axially injected ion packet comprised of ions of significantly different m/z values. This figure of merit is especially important in biological analysis where the various charge states and dissociation channels of peptides and proteins can encompass a wide m/z range. Unfortunately, just as others encountered with the early designs of the ICR [21,40–42] and Orbitrap [24,30,43,44], as we sought to increase the performance of our ELIT using mirror-switching, we discovered that the ion frequency shifts throughout the course of data acquisition. This phenomenon is known to originate from the trapping action of mirror-switching and is the main limiting factor in achieving higher mass resolution [36,38].

Under steady-state conditions, the amount of charge stored on the output capacitance of a power supply is given by the following relationship:

$$Q_T = C_{output} \cdot V_S \tag{2}$$

where Q_T is the total charge in coulombs, C_{output} is the output capacitance in Farads, and V_S is the supply voltage. As ions are injected into the ELIT, the switch, cables, and reflectron plate represent a capacitive load with zero charge stored on them (grounded). When ions are to be trapped, the capacitive load is rapidly connected in series with the output capacitance of the power supply where the stored charge quickly (nanoseconds) establishes a trapping voltage determined by:

$$Q_T = \left(C_{output} + C_{load}\right) \cdot V_{trap} \tag{3}$$

where C_{load} is the total capacitance of the switch, cables, and plate in Farads, and V_{trap} is the initial potential realized on the plate used for mirror switching. The relationship between the initial trapping potential and the set steady-state potential is:

$$V_{trap} = \frac{Q_T}{C_{output} + C_{load}} = V_S \frac{C_{output}}{C_{output} + C_{load}} \tag{4}$$

As the capacitive load will always be greater than zero, the initial trapping potential will always be lower in magnitude than the steady-state power supply voltage. At this point, the power supply will undergo transient voltage recovery wherein the voltage feedback loop of the power supply seeks to increase the output voltage back to the nominally set potential. As this recovery is not instantaneous, and can occur over hundreds of milliseconds, the ions experience a time-dependent trapping potential and thereby have a time-dependent path length and frequency. It should be noted that as the output capacitance of our power supplies are typically on the order of hundreds of nanofarads, and the capacitance of the load is expected to be on the order of hundreds of picofarads, the initial trapping potential is expected to differ from the set potential (~−2500 V) by a few volts. As the capacitance of the load is minimized, the initial trapping potential approaches the nominally set potential of the power supply, and thus the magnitude of the observed frequency shift will become smaller. Increasing the output capacitance of the power supply might be considered as an approach to minimize the time of the voltage adjustment. However, this is not recommended since the in-rush current just after the switch is closed can be hundreds of amperes. Many switches are not rated for such a current; a lower output capacitance limits the in-rush current due to the lower number of stored charges.

While in-trap potential lift does not suffer from frequency shifts associated with the trapping method [39], it suffers from relatively narrow m/z range, lower ion frequencies (see discussion), and a more complex detection scheme. Herein, we describe the fabrication and experimental evaluation of an active circuit that is capable of minimizing changes in the ion path length throughout the recorded transient when using mirror-switching to capture ions in an ELIT. To accomplish this task, the circuit measures the transient voltage recovery of the power supply, inverts it, and adds it to the voltage applied to the opposing plate. In this manner, the turning point of the ion packet in both reflectrons moves concurrently in the same direction, minimizing the observed frequency drift. This approach enables the acquisition of high resolution mass spectra across the wide m/z range offered by mirror-switching. We report our findings with respect to the design of the circuit, its use in measuring the transient recovery of various power supplies in response to a pulsed capacitive load, and its experimental implementation for mass analysis.

2. Experimental

2.1. Materials

A mixture of carboranes consisting of the major components $AgCHB_{11}H_5Cl_6$, and $CsCH_3CB_{11}I_{11}$ (100 μM each) was prepared by dissolving the analytes in 50% H_2O, 50% methanol (v/v). The carboranes were synthesized and provided by Professor C.A. Reed's group at the University of California Riverside, Department of Chemistry. Water and 2-iodopropane were purchased from Sigma-Aldrich

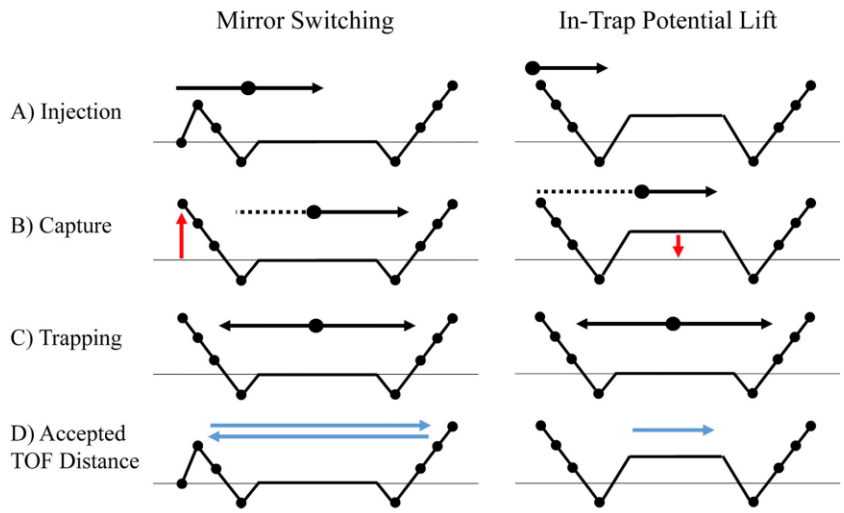

Fig. 1. Pictorial representation of ion injection, capture, and trapping for an ELIT employing mirror-switching (left column) or in-trap potential lift (right column). The y-axis is the potential energy plus the kinetic energy and the x-axis is axial position. The dots represent the individual plates in the ELIT. Only ions that are within the accepted time-of-flight distance (blue arrows) are trapped.

(St. Louis, MO, USA). Methanol was purchased from Malinckrodt (Phillipsburg, NJ, USA).

2.2. Mass spectrometry

A new instrument was constructed (Fig. 2) that includes a differential pumping stage such that the nano-electrospray ionization (nESI) and atmospheric sampling glow discharge ionization (ASGDI) source pressures were decoupled from the ultra-high vacuum (UHV) pressure. For ASGDI, the headspace of a reagent is continuously sampled into the interface region of the mass spectrometer. A glow discharge [45] is initiated by applying a negative potential (−400 V) to the front plate while the focusing lens is floated and the differential lens is grounded. The nESI source and the method by which ions are concentrated and injected into the electrostatic linear ion trap (ELIT) have been described previously [34,46]. In brief, the sample is loaded into a pulled glass capillary and placed in front of the sampling orifice. High voltage is applied to a platinum wire in contact with the solution in order to generate an electrospray [47]. Ions generated via nESI or ASGDI are transported to a trapping quadrupole equipped with LINAC II electrodes [48] where their accumulation and collisional cooling is facilitated by a pulse (10 μs) of helium gas. Once the pulsed gas valve is closed, the instrument is pumped out for one to three seconds prior to injection into the ELIT. This leads to an analysis pressure of 3×10^{-9} Torr (measured with a Granville Phillips 355001-YF ion gauge and displayed on a Granville Phillips 358 Micro-Ion controller). A phase lock circuit was used to trigger both the injection of the bunched ion packet and the start of data collection at a zero crossing of the trapping RF such that a consistent ion energy was sampled.

The ELIT described previously [39] has been replaced with the design depicted in the green region of Fig. 2, which traps ions via mirror-switching and detects the resulting image charge using a central detector. The trap itself is made up of 10 parallel stainless steel plates (5.08 cm × 5.08 cm × 0.635 mm thick, Kimball Physics, Wilton, NH) with holes 6.48 mm in diameter drilled through the center; eight of the plates control ion acceleration, deceleration, and radial focusing (plates 1–8) while the other two are used to enclose the grounded housing for the detector. The spacing between elements (plates 1–3 = 7.62 mm, plate 3 to central housing = 11.43 mm) is maintained by alumina spacers (Kimball Physics). The brass pick-up tube used for image charge detection (8.26 mm i.d., 9.53 mm o.d., 45.72 mm long) is centered within its grounded housing (50.8 mm long, 33.02 mm i.d.) by a polyether ether ketone (PEEK) spacer. Stainless steel tubes (6.35 mm i.d., 10.16 mm o.d., 19.05 mm long) were welded to plates 1 and 8 to make the electric fields in both ion mirrors identical. To trap negative ions, plate 1 is pulsed from ground to −2367 V (ORTEC Model 556, Advanced Measurement Technology, Oak Ridge, TN) using a fast, high-voltage switch (GHTS 30, Behlke Power Electronics, Billerica, MA) at a time defined relative to the ejection of ions from the trapping quadrupole. All other plate potentials are generated by additional ORTEC 556 power supplies with typical trapping potentials being −2367, −1746, −1200, and 2092 V for plates 1–4 respectively; the opposing mirror utilized identical voltages. Daily variations in the output voltages of the power supplies were minimized by leaving the units on at all times. The charge sensitive detection electronics has been described previously [32]. With the detailed trap dimensions, ion energy, and trapping voltages, typical ion frequencies are between 400 kHz and 100 kHz for m/z 100 and 1500, respectively.

2.3. Signal processing

The output of the charge sensitive preamplifier [32] (A250, Amptek) was filtered (band-pass, f_c = 50 and 500 kHz, Krohn-Hite Model 3940, Brockton, MA) and amplified (gain = 5) prior to digitization by a PCI-based digitizer (CS1621, 16-bit, Gage Applied Technologies, Lanchine, Quebec, Canada) at a rate of 10 MS/s (AC coupled, 1 MΩ input impedance). A program written in LabVIEW 13.0 (National Instruments, Austin, TX) was used to acquire and process the transient (fast Fourier transform, average, apodization, absorption mode [31], etc.). A custom program, written in MATLAB

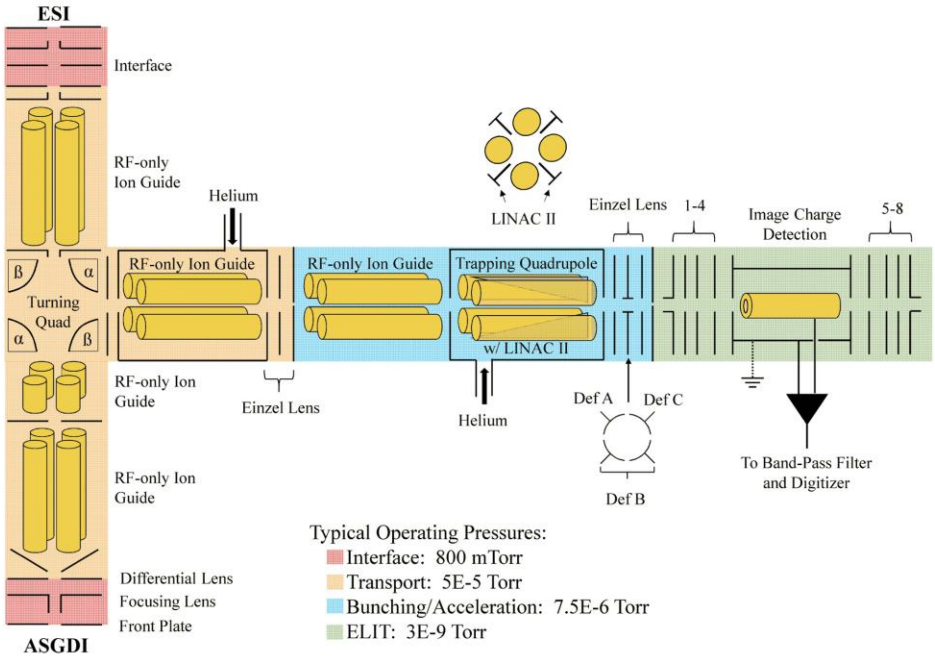

Fig. 2. Schematic of the instrument (not to scale).

2015, was used to generate the enhanced Fourier transform (eFT™) spectrum according to the published procedure [49].

2.4. High voltage decoupler/coupler circuit

The schematic for the high voltage decoupler/coupler used in this work, including component identities and values, is depicted in Fig. 3 (top). The actual experimental implementation is portrayed in Fig. 3 (bottom). The voltage applied to the 'signal in' port of the circuit (trapping potential of plate 1) is divided down by a factor of 100, and subjected to a high-pass RC filter (f_c = 1 mHz). When the potential applied to plate 1 is pulsed high to trap ions in the ELIT, the output of the power supply is rapidly connected in series with a small capacitive load (~350 pF) which introduces a low-voltage, low-frequency transient voltage recovery of the power supply. The very low frequency cutoff of the high-pass filter ensures that the transient voltage recovery of the power supply is accurately reproduced on the output of the input operational amplifier for further processing. After the low-voltage AC components are decoupled from the HV signal, they are amplified by a factor of 100 and inverted such that the overall gain of the input stage is −1. The inverted AC signal and trapping potential for plate 8 ('V_{float}') are coupled via the AD210AN integrated circuit (IC) and applied to plate 8 through the 'HV Out' port. The AD210AN (Analog Devices, MA), is a three-port isolation amplifier (input, output, power) that provides 2500 V_{rms} (continuous) common-mode voltage isolation between any two ports with a bandwidth of 20 kHz. This IC makes it possible to operate using two separate commons (input = power = ground, output = high voltage) with a high enough voltage difference so that the frequency of the ions in the ELIT, and thereby the resolution per unit time, is not compromised. Considering the voltages used in this work, a ground plane was not included near the output port pins of the AD210AN as any arcing will damage the IC.

2.5. Ion optical simulations

A virtual model of the trapping quadrupole, intermediate lenses, and the ELIT was constructed in SIMION 8.1 (Scientific Instrument Services, Ringoes, NJ). All electrodes were modelled within a single potential array with XY symmetry (0.2 mm/gu). One hundred ions of each mass-to-charge ratio (100–5000 m/z, 50 m/z increments) were initialized at random points within a cylindrical distribution (radius = 0.1 mm, length = 1 mm), located near the exit of the trapping quadrupole, with a kinetic energy uniformly distributed between 0.01 and 0.02 eV. All simulations were performed using positive ions. The collisional cross section (CCS) variable of the hard sphere collision model within SIMION was adjusted via the mass of the ion and the equation derived by Tao et al. [50] in order to simulate the collisional cooling process within the quadrupole (15 mTorr helium). The trapping quadrupole was operated at a frequency of 1.09 MHz, with an RF amplitude such that all tested masses had a q of 0.4 on the Mathieu stability diagram. The LINAC II electrodes, rod offset, and exit lens were held at 700 V, 1990 V, and 1978 V respectively during the 2 millisecond step in which ions were allowed to thermalize. Ions were ejected from the trapping quadrupole by pulsing the exit lens from 1978 V to 1690 V at a zero crossing of the RF. Once the ions were injected into the ELIT, the background pressure was set to zero in the entire workbench to avoid collisions that could cause unstable ion trajectories in the ELIT. In the mirror switching simulation, the potential applied to plate 1 was pulsed from ground to 2400 V, 6–12 μs (2 μs increment) after ion injection. For the potential lift simulation, the central lift electrode (brass pick-up tube) was pulsed from 600 V to ground, 5–14 μs

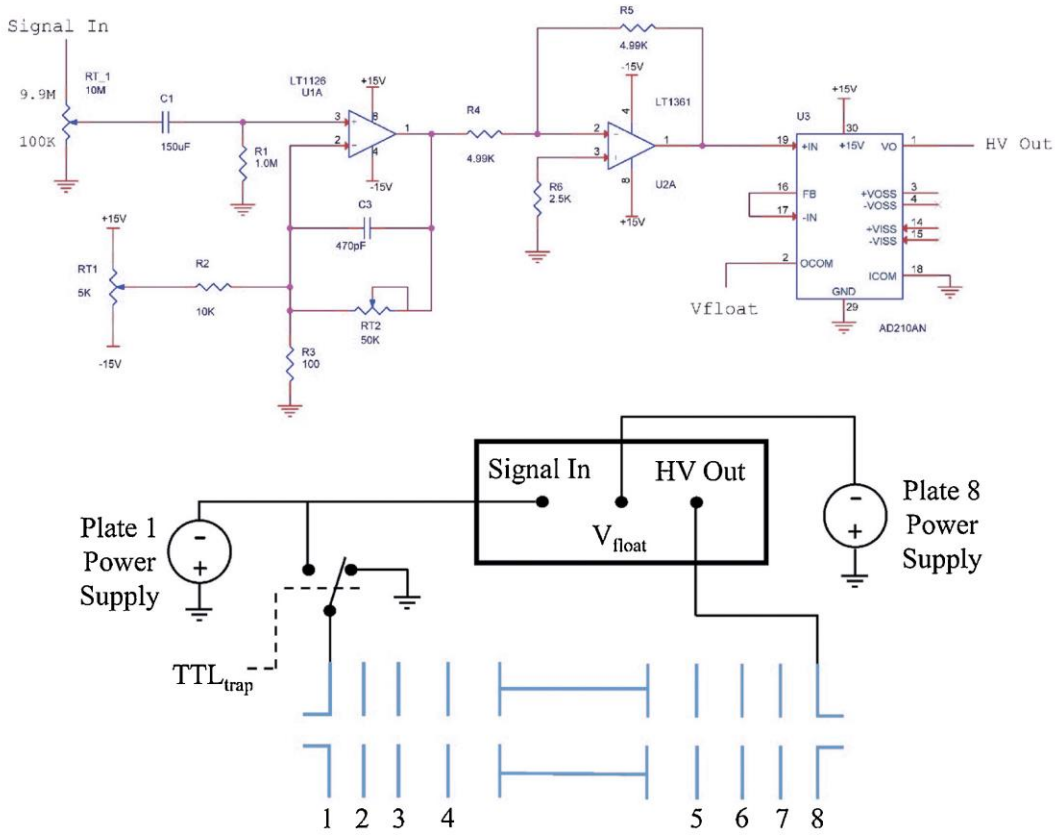

Fig. 3. Top: Schematic of the high voltage decoupler/coupler circuit. Bottom: Experimental setup of the circuit.

(3 μs increment) after ion injection. The trapping potentials applied to plates 1–4 were 2400, 1650, 950, −2060 V respectively (mirror-switching) and 1600, 1200, 800, −1900 V respectively (potential lift) with the trap operated in an axially symmetric manner. The magnitudes of the potentials were chosen to be near the experimental voltages for the two capture methods such that no ions had unstable trajectories in the ELIT if properly captured. The number of ions of each m/z that survived one millisecond in the ELIT were counted and expressed as a percent (Fig. 4).

3. Results and discussion

Mass analysis in an electrostatic linear ion trap (ELIT) may be carried out by in-trap potential lift or mirror-switching. In order to estimate the m/z range of the electrostatic trap utilized in this work, SIMION was used to model our trapping quadrupole, intermediate lenses, and ELIT. The trapping efficiency was simulated for both in-trap potential lift (Fig. 4, top) and mirror-switching (Fig. 4, bottom) across an m/z range of 100–5000 in 50 m/z increments. All simulations were performed using the same injection conditions and ELIT geometry. The time at which the capture event occurred, relative to ion injection, was varied and is indicated by the color code in the legend. The number of ions of each m/z that were successfully trapped and survived for one millisecond were counted and expressed as a percent. As only 100 ions of each m/z were simulated, all coarse features in the graphs are a direct result of limited ion statistics.

As expected from the accepted time-of-flight distance of the two capture methods, mirror-switching yields a much greater mass range than that of in-trap potential lift. When the first plate is pulsed from ground to −2400 V at 12 μs, a simulated m/z range of more than 4000 is observed. In order to match the m/z range of mirror-switching at 12 μs, four or more analyses would be need to be performed with in-trap potential lift. In this respect, mirror-switching is far better suited to acquiring mass spectra with ions present over a wide range of m/z ratios.

In addition to the higher m/z range, it can also be anticipated that for a fixed trap geometry (single detector) and injected kinetic energy (set by the offset of the trapping quadrupole), the highest ion frequency in the ELIT, and thus the highest resolution per unit time, will be achieved using mirror switching. When ions are captured by potential lift, the trapped kinetic energy of the ion packet relative to ground is reduced (trapped kinetic energy = injected kinetic energy − potential lift voltage). In our previous publication [39], the trapped kinetic energy of the ions using potential lift was ~1400 eV versus the ~2000 eV realized here for mirror-

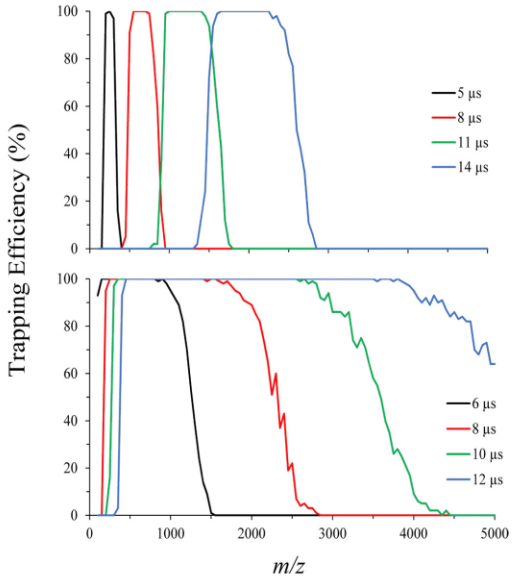

Fig. 4. Simulated trapping efficiency for in-trap potential lift (top) and mirror-switching (bottom) across an m/z range of 100–5000 (50 m/z increment). The time at which the lift electrode or plate is pulsed to trap ions is indicated in the legend. Both simulations were performed using the same trap geometry and injected ion energy.

switching (trapped kinetic energy = injected kinetic energy). Due to the unique trapping potentials for each capture method, the turning points in the reflectrons are actually located at similar positions in space. As it will take ions captured by potential lift longer to traverse the effective path length of the trap, they will therefore have a lower frequency. This issue may be circumvented by changing the injected kinetic energy of the ions by increasing the quadrupole offset, including a pulsed drift tube prior to the ELIT [51], or using multiple detectors. While in principle it is desirable to use the high accelerating and trapping voltages to achieve the highest experimental ion frequencies, there are practical voltage limits associated with a given physical embodiment of the ELIT. The voltages used here approach the highest voltages available to us both to avoid electrical breakdown and to provide sufficient precision for stable operation.

While in theory the observed resolution should be superior for mirror switching, this is only true if the ion frequency is highly stable over the course of data acquisition. Fig. 5 (top) shows the experimental setup for testing the transient voltage response of various power supplies to a pulsed load with the HV decoupler detailed in Fig. 3 (top). For all experiments, the power supplies were held at −2500 V and an additional capacitive load was added directly to the output of the Behlke switch. Due to the intrinsic capacitance of the switch and cables, the total capacitive load is roughly 150 pF higher than the loads specified in the figure. As the decoupled AC recovery of the power supply is being measured on the 'HV out' port of the circuit, it is important to note that it is inverted from the true response. Fig. 5 (bottom left) shows the inverted transient voltage response of the ORTEC 556 (black), Bertan Series 105 (red), and Bertan Model 2918 (blue) to a pulsed 200 pF load (64 averages). Each power supply has a very different response to the pulsed load both in magnitude and form. The ideal power supply for the ELIT would maintain a perfectly constant DC output in response to a pulsed load, however that is not a realistic specification. Of the three power supplies tested, the ORTEC 556 is the most ideal as its output only changes by a few hundred millivolts over the course of acquisition. The polarity of the transient voltage recovery function agrees with expectation. As the power supply voltage is negative, when the load is pulsed, the output capacitance is discharged and the output voltage decreases in magnitude towards ground (positive-going perturbation). The inverting stage of the decoupler turns this into the observed negative-going perturbation. Note that the power supply is still recovering to its nominally set potential after 300 milliseconds, which is often longer than the observed transient length for molecules with a modest collisional cross section in our apparatus.

To determine the effect of a small voltage perturbation on the ion frequency, an ion was started at the center of the ELIT model (SIMION) with 2000 eV, directed straight down the trap axis. All plates were set to their nominal trapping potentials for mirror-switching operation and the voltage on plate 1 was adjusted from −2397 V to −2400 V in two independent simulations. The times at which the ion crossed the center plane of the ELIT were recorded and utilized to calculate the ion frequency. The 3 V change in the trapping potential resulted in a simulated frequency shift of ∼250 Hz for iodide (I^-, m/z 126.904), which corresponds to a 0.186 Da change in the position of the peak in the mass spectrum. In this respect, the resolution that can be achieved when utilizing mirror-switching is directly influenced by the power supply and the magnitude/form of the voltage perturbation. Therefore, when no correction method is used it is likely that higher resolution spectra could be achieved using in-trap potential lift because it does not suffer from perturbations in the output voltage of the power supply.

Since the Bertan Series 105 power supply is equipped with a current limiter, we used it to bound the current to the lowest possible value (∼0.4 mA). Even at this setting, the current limiter was not tripped when the load was pulsed and the transient recovery of the supply did not change. Along with the specifications of the power supplies, this indicates that the output current of the supply is not necessarily the most critical parameter during the recovery, but rather the speed and stability of its voltage regulation. Fig. 5 (bottom right) shows the transient response of the ORTEC 556 power supply to different capacitive loads. It is no surprise that as the capacitance is increased, the voltage perturbation becomes worse, indicating that the stray capacitance of the system needs to be minimized. As any switches, shielding, cables, feedthroughs, chamber, etc. will all contribute to some minimum capacitance, it stands to reason that there will always be some minimum perturbation. If the pressure achieved is sufficiently low, data acquisition could be delayed until the conclusion of the transient voltage response, however this is not conducive to high-throughput analyses and necessitates even lower background pressure. It is also possible to modify or build a power supply in which the feedback loop is highly optimized for pulsed loads and the recovery time is very short, however this requires a very high level of expertise in electrical engineering.

Fig. 6 portrays the simple strategy employed to compensate for the transient voltage recovery of the power supply upon mirror-switching and thereby prevent a change in the fundamental frequency of the ions over the course of data acquisition. With no correction circuit, the turning point between Plates 7 and 8 is fixed in space and the position of the turning point between Plates 1 and 2 varies with time based on the transient voltage recovery of the power supply, thereby inducing a frequency shift. The transient response of the power supply ($V_{perturbation}$) can be measured via the HV decoupler, inverted, and superimposed (AD210AN) on the trapping potential to plate 8 (V_8) such that the turning point located between plates 7 and 8 moves concurrently with the turning point of plates 1 and 2. In doing so, the path length of the ions

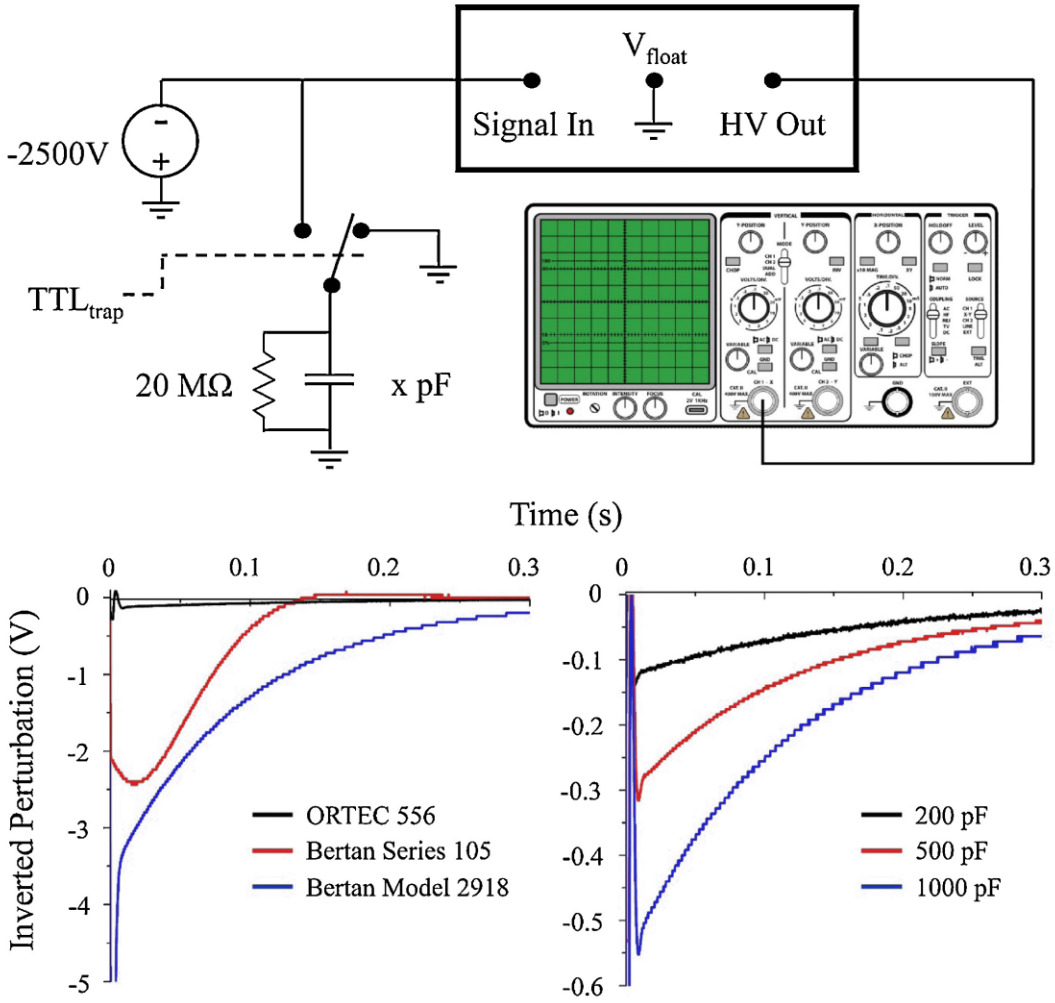

Fig. 5. Top: Setup used to test the transient voltage response of a power supply to a pulsed capacitive load. Bottom Left: Transient voltage response of three different power supplies to a pulsed 200 pF load (64 averages). Bottom Right: Transient voltage response of an ORTEC 556 to a pulsed load of differing capacitance (64 averages). Since the measured AC waveforms would normally be applied to plate 8 of the ELIT, they are inverted from the actual response of the power supply.

at t = a, b, and c are all equal and no change in frequency will be observed. It should be mentioned that while the correction circuit is only used to remedy the transient voltage response of the power supply in this work, this method may also be used to correct for other low frequency interferences due to ion isolation [33], pump noise, line noise, and short-term power supply drift if these effects are found to influence one plate more than another.

The method described above is a broadband correction and is capable of minimizing the drift in the path length of all masses simultaneously. However, as the bandwidth of the correction circuit is limited by the AD210AN (20 kHz), any rapid changes in potential on V_1 will not be able to be accurately reproduced on the output of the circuit (V_8). This effect only occurs when the plate is pulsed to its trapping potentials at the start of the transient (sharp rise and ringing in Fig. 5, bottom). This subtle frequency shift due to the difference in rise times (Behlke vs. AD210AN) will only become apparent at very high resolutions and can be removed by simply deleting, zeroing, or windowing the initial millisecond of the transient.

Fig. 7 shows the mass spectra of iodide (I^-, m/z 126.904) recorded using the Bertan Series 105 power supply to perform mirror-switching in the ELIT (single-shot, 300 ms transient, no zero fills, no apodization). Normally, the ORTEC 556 would be used to perform mirror-switching, however the Bertan Series 105 was chosen as it gave the most interesting voltage response to a pulsed load and to simply prove that even large transient recoveries (frequency shifts) may be corrected. When no correction is applied to plate 8 (blue), the frequency of the ion packet is observed to increase

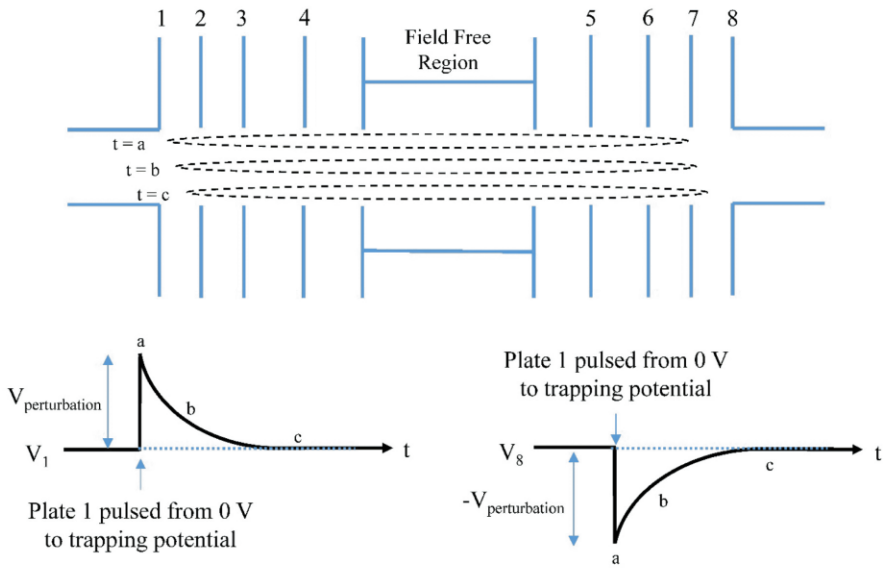

Fig. 6. Cartoon of the voltage recovery correction and its effect on an ion's trajectory (exaggerated). When pulsed, the positive voltage perturbation on plate 1 (V_1 is negative) is inverted and superimposed on the voltage applied to plate 8 (V_8). Throughout the transient voltage recovery of the power supply, the path length of the ion, and therefore its frequency, remains constant.

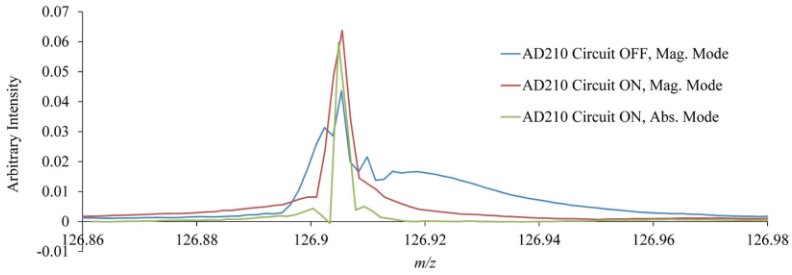

Fig. 7. Mass spectra of iodide (I^-, m/z 126.904) recorded using the Bertan Series 105 power supply to perform mirror-switching (one injection, 300 ms transient, no zero fills, no apodization). With the AD210 circuit off, no correction voltage is applied to plate 8 and a large frequency shift is observed (blue). With the AD210 circuit on, the frequency shift is corrected and higher resolutions may be achieved for both magnitude mode (red) and absorption mode (green). (For interpretation of the references to color in this figure legend, the reader is referred to the web version of this article.)

over time and overshoot the steady-state frequency prior to settling down (confirmed by taking the short-time Fourier transform of the transient, Fig. S1). This correlates well with the measured transient response of the Series 105 in Fig. 5 (bottom left) where the power supply was observed to overshoot the nominally set potential in its recovery. With the AD210 circuit turned on, the inverted transient voltage recovery was applied to plate 8 and the peak was observed to sharpen and increase in intensity. The magnitude mode resolving power (FWHM) was measured to be ~30,000 while the absorption mode [31] resolving power (green) was measured to be greater than 51,000. This corresponds to a resolving power enhancement factor of 1.7 when going from magnitude to absorption mode analysis (Langevin model). For these experiments, mirror-switching was only performed on plate 1 so as to clearly show the effect of the transient response from a single supply and the frequency correction by the AD210 circuit. If multiple plates are involved in mirror-switching, and no correction voltage is applied, the magnitude of the observed frequency shift is expected to be larger. As long as the voltage rating of the AD210AN is not surpassed ($\pm$2500 V_{rms}), a correction circuit could easily be incorporated for each pair of plates, giving the user more flexibility in their experimental setup while maintaining high performance. It should be noted that at these resolving powers, the scan to scan reproducibility of our power supplies becomes an issue. While the resolution remains high for a single scan, the peak position changes from scan to scan and would degrade the observed resolution when averaging.

As illustrated in Fig. 4, the major advantage to using mirror-switching over in-trap potential lift is the mass range of a single injection. Fig. 8 shows the mass spectrum (125 ms transient, 10 averages, eFT™ mode) of a 100 μM mixture of $CHB_{11}H_5Cl_6^-$ (avg. m/z 349.70) and $CH_3CB_{11}I_{11}^-$ (avg. m/z 1541.92) using mirror-switching (plate 1 pulsed high 10 μs after injection). This

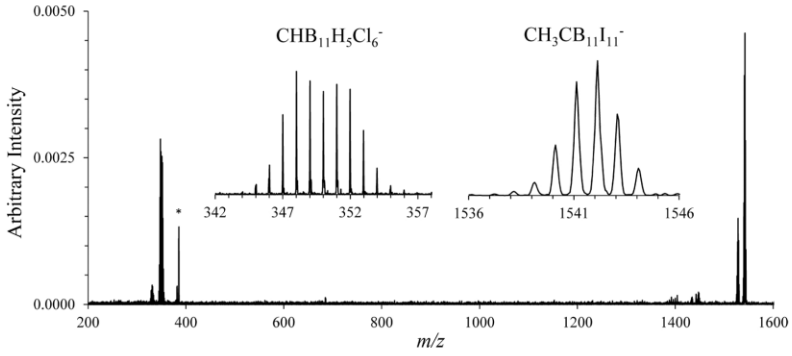

Fig. 8. Mass spectrum of $CHB_{11}H_5Cl_6^-$ and $CH_3CB_{11}I_{11}^-$ (125 ms transient, 10 averages, eFT™ mode) using mirror-switching (10 μs) in the ELIT. The insets are expanded views about the molecular anion distribution of each carborane. The asterisk denotes a harmonic.

demonstrates an experimental *m*/*z* range of nearly 1200, with the resolving power (FWHM) of the base peak in the two distributions being 11,000 and 6000 respectively. In order to record this mass spectrum using potential lift, three or more injections would be necessary in which the lift region is pulsed to ground at different delay times relative to ion injection. According to simulations, mirror-switching at 10 μs can accommodate an even wider *m*/*z* range in the ELIT than is demonstrated in Fig. 8. Indeed, we have previously reported an *m*/*z* range of 1800 using the same injection method [34]. However, the width of the *m*/*z* range in this apparatus may be limited by other factors associated with, for example, ion transmission, ion storage, ion bunching, etc. prior to injection into the ELIT. Through the use of the dynamic compensation approach described here, the mass resolution obtained via mirror-switching in our ELIT is now determined by transient length, which is limited by pressure and the noise floor of our detector, rather than by the magnitude of the voltage drift associated with the pulsed power supply attached to the entrance electrode.

4. Conclusions

We have demonstrated the use of a high voltage coupling/decoupling circuit to correct a time-dependent frequency shift of the ion motion in an ELIT when performing ion capture via the mirror-switching approach. As a result, the expected improvement in mass resolution with transient length was realized. The frequency shift noted in the absence of this circuit was shown to originate from the transient voltage recovery of the power supply used for mirror-switching in response to a pulsed capacitive load. By measuring the transient recovery, inverting it, and superimposing it on the opposing mirror potential, the frequency drift of the ions was reduced to within 10 ppm throughout data acquisition, with the residual drift likely being a result of decreasing space charge. The circuit is capable of correcting the path length of all ions concurrently, no matter the power supply employed. Due to differences in the rise time of the Behlke switch and the AD210AN, the transient response will not be perfectly corrected during the first few milliseconds of the transient, and therefore data acquisition should be delayed to ensure that a frequency shift is not recorded. At present, the useful transient length is limited by the background pressure in the ELIT and the noise floor of our detector. Via simulation and experimental observation, the *m*/*z* range of mirror-switching was shown to be much wider than that of in-trap potential lift and thereby constitutes a major motivation for using this capture method. Furthermore, as there is only one centrally located detector, the mirror switching approach offers a lower noise floor and less complicated frequency spectrum than the dual-detector arrangement recommended for ion capture by in-trap potential lift.

Acknowledgments

This work was supported by AB Sciex. We thank Mark Carlsen, Randy Replogle, Phil Wyss, and Tim Selby of the Jonathan Amy Facility for Chemical Instrumentation for helpful discussions and their help with construction of the mass spectrometer. We also acknowledge Mircea Guna, and Dr. James W. Hager of AB Sciex for helpful discussions and for providing the collision cell with LINAC.

Appendix A. Supplementary data

Supplementary data associated with this article can be found, in the online version, at http://dx.doi.org/10.1016/j.ijms.2016.10.012.

References

[1] S. Kim, R.P. Rodgers, A.G. Marshall, Truly exact mass: elemental composition can be determined uniquely from molecular mass measurement at ~0.1 mDa accuracy for molecules up to ~500 Da, Int. J. Mass Spectrom. 251 (2006) 260–265.
[2] S.D.-H. Shi, C.L. Hendrickson, A.G. Marshall, Counting individual sulfur atoms in a protein by ultrahighresolution Fourier transform ion cyclotron resonance mass spectrometry: experimental resolution of isotopic fine structure in proteins, Proc. Natl. Acad. Sci. 95 (1998) 11532–11537.
[3] A. Gaspar, W. Schrader, Expanding the data depth for the analysis of complex crude oil samples by Fourier transform ion cyclotron resonance mass spectrometry using the spectral stitching method, Rapid Commun. Mass Spectrom. 26 (2012) 1047–1052.
[4] E. Denisov, E. Damoc, O. Lange, A. Makarov, Orbitrap mass spectrometry with resolving powers above 1,000,000, Int. J. Mass Spectrom. 325 (2012) 80–85.
[5] M. Ghaste, R. Mistrik, V. Shulaev, Applications of fourier transform ion cyclotron resonance (FT-ICR) and orbitrap based high resolution mass spectrometry in metabolomics and lipidomics, Int. J. Mol. Sci. 17 (2016) 816.
[6] F. Hernández, J. Sancho, M. Ibáñez, E. Abad, T. Portolés, L. Mattioli, Current use of high-resolution mass spectrometry in the environmental sciences, Anal. Bioanal. Chem. 403 (2012) 1251–1264.
[7] A.C. Peterson, J.D. Russell, D.J. Bailey, M.S. Westphall, J.J. Coon, Parallel reaction monitoring for high resolution and high mass accuracy quantitative, targeted proteomics, Mol. Cell. Proteom. 11 (2012) 1475–1488.
[8] D. Zajfman, O. Heber, M.L. Rappaport, H.B. Pedersen, D. Strasser, S. Goldberg, Self-bunching effect in an ion trap resonator, JOSA B 20 (2003) 1028–1032.
[9] H.B. Pedersen, D. Strasser, B. Amarant, O. Heber, M.L. Rappaport, D. Zajfman, Diffusion and synchronization in an ion-trap resonator, Phys. Rev. A 65 (2002) 042704.
[10] H.B. Pedersen, D. Strasser, O. Heber, M.L. Rappaport, D. Zajfman, Stability and loss in an ion-trap resonator, Phys. Rev. A 65 (2002) 042703.
[11] H.B. Pedersen, D. Strasser, S. Ring, O. Heber, M.L. Rappaport, Y. Rudich, I. Sagi, D. Zajfman, Ion motion synchronization in an ion-trap resonator, Phys. Rev. Lett. 87 (2001) 055001.

[12] M.W. Froese, M. Lange, S. Menk, M. Grieser, O. Heber, F. Laux, R. Repnow, T. Sieber, Y. Toker, R. von Hahn, The decay of ion bunches in the self-bunching mode, New J. Phys. 14 (2012) 073010.
[13] M. Lange, M. Froese, S. Menk, J. Varju, R. Bastert, K. Blaum, J.C. López-Urrutia, F. Fellenberger, M. Grieser, R. von Hahn, A cryogenic electrostatic trap for long-time storage of keV ion beams, Rev. Sci. Instrum. 81 (2010) 055105.
[14] C. Breitenfeldt, M.W. Froese, K. Blaum, S. George, M. Grieser, M. Lange, S. Menk, R. Repnow, D. Schwalm, L. Schweikhard, Spreading times of ion-bunches in the Cryogenic Trap for Fast ion beams, Int. J. Mass Spectrom. (2015).
[15] C. Lin, R. Mathur, K. Aizikov, P.B. O'Connor, First signal on the cryogenic Fourier-transform ion cyclotron resonance mass spectrometer, J. Am. Soc. Mass Spectrom. 18 (2007) 2090–2093.
[16] S.M. Peterman, C.P. Dufresne, S. Horning, The use of a hybrid linear trap/FT-ICR mass spectrometer for on-line high resolution/high mass accuracy bottom-up sequencing, J. Biomol. Tech. 16 (2005) 112.
[17] J.V. Olsen, L.M. de Godoy, G. Li, B. Macek, P. Mortensen, R. Pesch, A. Makarov, O. Lange, S. Horning, M. Mann, Parts per million mass accuracy on an Orbitrap mass spectrometer via lock mass injection into a C-trap, Mol. Cell. Proteom. 4 (2005) 2010–2021.
[18] D.K. Williams, D.C. Muddiman, Parts-per-billion mass measurement accuracy achieved through the combination of multiple linear regression and automatic gain control in a Fourier transform ion cyclotron resonance mass spectrometer, Anal. Chem. 79 (2007) 5058–5063.
[19] A. Makarov, E. Denisov, A. Kholomeev, W. Balschun, O. Lange, K. Strupat, S. Horning, Performance evaluation of a hybrid linear ion trap/orbitrap mass spectrometer, Anal. Chem. 78 (2006) 2113–2120.
[20] E.N. Nikolaev, R. Jertz, A. Grigoryev, G.k. Baykut, Fine structure in isotopic peak distributions measured using a dynamically harmonized Fourier transform ion cyclotron resonance cell at 7 T, Anal. Chem. 84 (2012) 2275–2283.
[21] Y.I. Kostyukevich, G.N. Vladimirov, E.N. Nikolaev, Dynamically harmonized FT-ICR cell with specially shaped electrodes for compensation of inhomogeneity of the magnetic field. Computer simulations of the electric field and ion motion dynamics, J. Am. Soc. Mass Spectrom. 23 (2012) 2198–2207.
[22] E.N. Nikolaev, Y.I. Kostyukevich, G.N. Vladimirov, Fourier transform ion cyclotron resonance (FT ICR) mass spectrometry: theory and simulations, Mass Spectrom. Rev. (2014).
[23] I.A. Popov, K. Nagornov, G.N. Vladimirov, Y.I. Kostyukevich, E.N. Nikolaev, Twelve million resolving power on 4.7 T Fourier transform ion cyclotron resonance instrument with dynamically harmonized cell—observation of fine structure in peptide mass spectra, J. Am. Soc. Mass Spectrom. 25 (2014) 790–799.
[24] A. Makarov, E. Denisov, O. Lange, Performance evaluation of a high-field Orbitrap mass analyzer, J. Am. Soc. Mass Spectrom. 20 (2009) 1391–1396.
[25] D.R. Ahlf, P.D. Compton, J.C. Tran, B.P. Early, P.M. Thomas, N.L. Kelleher, Evaluation of the compact high-field orbitrap for top-down proteomics of human cells, J. Proteome Res. 11 (2012) 4308–4314.
[26] R.A. Zubarev, A. Makarov, Orbitrap mass spectrometry, Anal. Chem. 85 (2013) 5288–5296.
[27] R.J. Rose, E. Damoc, E. Denisov, A. Makarov, A.J. Heck, High-sensitivity Orbitrap mass analysis of intact macromolecular assemblies, Nat. Methods 9 (2012) 1084–1086.
[28] J.J. Savory, N.K. Kaiser, A.M. McKenna, F. Xian, G.T. Blakney, R.P. Rodgers, C.L. Hendrickson, A.G. Marshall, Parts-per-billion Fourier transform ion cyclotron resonance mass measurement accuracy with a walking calibration equation, Anal. Chem. 83 (2011) 1732–1736.
[29] L.K. Zhang, D. Rempel, B.N. Pramanik, M.L. Gross, Accurate mass measurements by Fourier transform mass spectrometry, Mass Spectrom. Rev. 24 (2005) 286–309.
[30] M.V. Gorshkov, D.M. Good, Y. Lyutvinskiy, H. Yang, R.A. Zubarev, Calibration function for the Orbitrap FTMS accounting for the space charge effect, J. Am. Soc. Mass Spectrom. 21 (2010) 1846–1851.
[31] R.T. Hilger, P.J. Wyss, R.E. Santini, S.A. McLuckey, Absorption mode Fourier transform electrostatic linear ion trap mass spectrometry, Anal. Chem. 85 (2013) 8075–8079.
[32] R.T. Hilger, R.E. Santini, S.A. McLuckey, Tandem mass spectrometry in an electrostatic linear ion trap modified for surface-induced dissociation, Anal. Chem. 86 (2014) 8822–8828.
[33] R.T. Hilger, R.E. Santini, S.A. McLuckey, Square wave modulation of a mirror lens for ion isolation in a Fourier transform electrostatic linear ion trap mass spectrometer, Int. J. Mass Spectrom. 362 (2014) 1–8.
[34] R.T. Hilger, E.T. Dziekonski, R.E. Santini, S.A. McLuckey, Injecting electrospray ions into a Fourier transform electrostatic linear ion trap, Int. J. Mass Spectrom. 378 (2015) 281–287.
[35] M.I. Yavor, W.R. Plaß, T. Dickel, H. Geissel, C. Scheidenberger, Ion-optical design of a high-performance multiple-reflection time-of-flight mass spectrometer and isobar separator, Int. J. Mass Spectrom. 381–382 (2015) 1–9.
[36] W.R. Plaß, T. Dickel, C. Scheidenberger, Multiple-reflection time-of-flight mass spectrometry, Int. J. Mass Spectrom. 349 (2013) 134–144.
[37] R.N. Wolf, F. Wienholtz, D. Atanasov, D. Beck, K. Blaum, C. Borgmann, F. Herfurth, M. Kowalska, S. Kreim, Y.A. Litvinov, ISOLTRAP's multi-reflection time-of-flight mass separator/spectrometer, Int. J. Mass Spectrom. 349 (2013) 123–133.
[38] R.N. Wolf, G. Marx, M. Rosenbusch, L. Schweikhard, Static-mirror ion capture and time focusing for electrostatic ion-beam traps and multi-reflection time-of-flight mass analyzers by use of an in-trap potential lift, Int. J. Mass Spectrom. 313 (2012) 8–14.
[39] E.T. Dziekonski, R.E. Santini, S.A. McLuckey, A dual detector Fourier transform electrostatic linear ion trap utilizing in-trap potential lift, Int. J. Mass Spectrom. (2016).
[40] S. Guan, M.C. Wahl, A.G. Marshall, Elimination of frequency drift from Fourier transform ion cyclotron resonance mass spectra by digital quadrature heterodyning: ultrahigh mass resolving power for laser-desorbed molecules, Anal. Chem. 65 (1993) 3647–3653.
[41] X. Xiang, P.B. Grosshans, A.G. Marshall, Image charge-induced ion cyclotron orbital frequency shift for orthorhombic and cylindrical FT-ICR ion traps, Int. J. Mass Spectrom. 125 (1993) 33–43.
[42] M.V. Gorshkov, E.N. Nikolaev, Optimal cyclotron radius for high resolution FT-ICR spectrometry, Int. J. Mass Spectrom. 125 (1993) 1–8.
[43] A. Kharchenko, G. Vladimirov, R.M. Heeren, E.N. Nikolaev, Performance of Orbitrap mass analyzer at various space charge and non-ideal field conditions: simulation approach, J. Am. Soc. Mass Spectrom. 23 (2012) 977–987.
[44] A. Kaufmann, S. Walker, Accuracy of relative isotopic abundance and mass measurements in a single-stage orbitrap mass spectrometer, Rapid Commun. Mass Spectrom. 26 (2012) 1081–1090.
[45] S.A. McLuckey, G.L. Glish, K.G. Asano, B.C. Grant, Atmospheric sampling glow discharge ionization source for the determination of trace organic compounds in ambient air, Anal. Chem. 60 (1988) 2220–2227.
[46] R.T. Hilger, R.E. Santini, S.A. McLuckey, Nondestructive tandem mass spectrometry using a linear quadrupole ion trap coupled to a linear electrostatic ion trap, Anal. Chem. 85 (2013) 5226–5232.
[47] G.J. Van Berkel, K.G. Asano, P.D. Schnier, Electrochemical processes in a wire-in-a-capillary bulk-loaded, nano-electrospray emitter, J. Am. Soc. Mass Spectrom. 12 (2001) 853–862.
[48] A. Loboda, A. Krutchinsky, O. Loboda, J. McNabb, V. Spicer, W. Ens, K. Standing, Novel Linac II electrode geometry for creating an axial field in a multipole ion guide, Eur. J. Mass Spectrom. 6 (2000) 531–536.
[49] O. Lange, E. Damoc, A. Wieghaus, A. Makarov, Enhanced Fourier transform for Orbitrap mass spectrometry, Int. J. Mass Spectrom. 369 (2014) 16–22.
[50] L. Tao, J.R. McLean, J.A. McLean, D.H. Russell, A collision cross-section database of singly-charged peptide ions, J. Am. Soc. Mass Spectrom. 18 (2007) 1232–1238.
[51] R.N. Wolf, M. Eritt, G. Marx, L. Schweikhard, A multi-reflection time-of-flight mass separator for isobaric purification of radioactive ion beams, Hyperfine Interact. 199 (2011) 115–122.

analytical chemistry

Technical Note

pubs.acs.org/ac

Utility of Higher Harmonics in Electrospray Ionization Fourier Transform Electrostatic Linear Ion Trap Mass Spectrometry

Eric T. Dziekonski, Joshua T. Johnson, and Scott A. McLuckey*

Department of Chemistry, Purdue University, West Lafayette, Indiana 47907-2084, United States

Supporting Information

ABSTRACT: Mass resolution ($M/\Delta M$ fwhm) is observed to linearly increase with harmonic order in a Fourier transform electrostatic linear ion trap (ELIT) mass spectrometer. This behavior was predicted by Grosshans and Marshall for frequency-multiple detection in a Fourier transform ion cyclotron resonance mass spectrometer only for situations when the prominent mechanism for signal decay is ion ejection from the trap. As the analyzer pressure in our ELIT chamber is relatively high, such that collisional scattering and collision-induced dissociation are expected to underlie much of the ion loss, we sought to explore the relationship between harmonic order and mass resolution. Mass resolutions of 36 900 (fundamental), 75 850 (2nd harmonic), and 108 200 (3rd harmonic) were obtained for GdO^+ (avg. m/z 173.919) with a transient length of 300 ms. To demonstrate that the mass resolution was truly increasing with harmonic order, the unresolved isotopes at the fundamental distribution of cytochrome c^{+8} ($m/z \sim 1549$) were nearly baseline, resolved at the third harmonic (mass resolution ≈ 23 000) with a transient length of only 200 ms. This experiment demonstrates that, when the ion density is sufficiently low, ions with frequency differences of less than 4 Hz remain uncoalesced. Higher harmonics can be used to increase the effective mass resolution for a fixed transient length and thereby may enable the resolution of closely spaced masses, determination of a protein ion's charge state, and study of the onset of peak coalescence when the resolution at the fundamental frequency is insufficient.

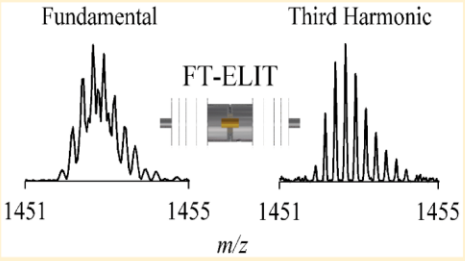

In Fourier transform mass spectrometry (FT-MS), signal harmonics are often regarded as spectral artifacts that provide little to no additional information than that provided by the signals at the fundamental frequencies.[1,2] While the harmonic frequencies can be utilized for higher resolution mass measurements, their presence often leads to more complex mass spectra that make data interpretation more difficult and susceptible to identification errors.[3−5] The origins of harmonics and their unique spectral signatures in both Fourier transform ion cyclotron resonance (FT-ICR) and Orbitrap analyzers have been described in detail elsewhere[1,2,5−12] and can be related to imperfections in the physical device, electric field, or sampling. As the mass resolution at the fundamental frequency is often sufficient, and the harmonics are not related to the chemical identity of the ions, their magnitudes are often minimized via precision machining, shimming the electric field, automatic gain control, balancing of the preamplifier gain, precise initial centering of the ion packet along the symmetry axes of the electric and magnetic fields, etc.

The distinction is made here that the focus of this technical note is on the utility of harmonics, not on the use of frequency-multiplying traps employing frequency-multiple or harmonic detection. For sake of clarification, frequency-multiple detection,[4,12−19] wherein multiple (pairs of) detection electrodes are incorporated in the mass analyzer, can also improve the mass resolution and throughput of an FT-based mass analyzer by moving the detected signal magnitude to a higher harmonic of the fundamental ion motion (reduced cyclotron frequency in ICR, or lap frequency in electrostatic traps). While the idea is decades old, the widespread adoption of frequency-multiplying traps has been limited by the precision to which these traps need to be constructed and operated, without which this detection scheme can produce many higher order, fractional, and/or combination harmonics.[4,17] Additionally, in the case of ICR, because the magnitude of the nth order frequency-multiple signal increases as the nth power of ICR postexcitation radius, it is necessary to excite ions to a large radius to avoid large reductions in the observed signal. Such operation has only been achievable recently with the dynamically harmonized cell, which minimizes nonlinear field effects at large postexcitation radii.

Though they add to spectral complexity and can complicate peak assignment, signal harmonics can be used to elucidate several experimental parameters and improve instrument performance. In an FT-ICR, the relative signal magnitudes of the third harmonic and fundamental can be correlated to the average cyclotron radius and kinetic energies of excited ions

Received: January 4, 2017
Accepted: March 22, 2017
Published: March 22, 2017

DOI: 10.1021/acs.analchem.7b00034
Anal. Chem. 2017, 89, 4392−4397

and thereby can be used to determine the number of coherently orbiting ions.[8,20] Use of unconventional detection electrode geometries, as in the case of the NADEL cell,[11] can induce many higher harmonics. Along with signal processing techniques such as extended basis Fourier transformation (xFT), one can use the harmonics and/or frequency-multiplying traps to achieve higher mass resolution for the same transient length or the same mass resolution with shorter acquisition periods. In charge detection mass spectrometry (CDMS), the sum of the fundamental and second harmonic signal magnitudes can increase the accuracy with which the charge can be assigned, leading to higher resolution mass spectra.[21] Additionally, because the harmonic content is well-correlated to experimental conditions, e.g., clipping the amplifiers produces a series of odd harmonics, the identities and magnitudes of the harmonics provide direct feedback as to how to optimize the performance of a mass analyzer.[2]

The Fourier transform electrostatic linear ion trap (FT-ELIT) is a type of mass analyzer in which ions are trapped between two axially opposing reflectrons.[17,22−30] As the ion packet oscillates back and forth, the image charge induced on a centrally located detector is amplified and digitized. The frequency components are derived from the recorded transient via a fast Fourier transform algorithm and calibrated to generate a mass spectrum. As the detector is located at the center of the ELIT, the frequency at which an ion is detected represents twice the lap frequency and is referred to as the fundamental frequency. Therefore, the term "harmonics" refers to overtones of the fundamental detected frequency that result from nonlinear (noncosine) time-domain signals. Being an FT-based mass analyzer, the ELIT is expected to share many qualities with the FT-ICR and Orbitrap in terms of detection and signal processing. However, as related here, harmonics are not easily suppressed in an ELIT due to its unique geometry and detection scheme. Therefore, it becomes advantageous to utilize the higher harmonics to generate spectra with superior analytical performance and chemical information than is present at the fundamental distribution.

This technical note discusses the origins of harmonics in an ELIT, which is related to the geometry of the trap, image charge preamplifier, and temporal distribution of the ion packet. Strategies for the use of the harmonics as well as their limitations are also presented. Mass spectra are presented to demonstrate a linear gain in mass resolution with harmonic order, as might be anticipated by the major mechanism of signal decay in this apparatus under typical operating conditions being ion loss due to collisions.

EXPERIMENTAL SECTION

Materials. The following chemicals were purchased from Sigma-Aldrich (St. Louis, MO, United States): bromazepam (1 mg/mL methanol), clonazepam (1 mg/mL methanol), chlorprothixene hydrochloride, cytochrome *c* (from horse heart), gadolinium(III) chloride hexahydrate, insulin (from bovine pancreas), oxfendazole, and water. The mixture of bromazepam (m/z 316.0080), clonazepam (m/z 316.0483), oxfendazole (m/z 316.0750), and chlorprothixene HCl (m/z 316.0921) will be referred to as the 316 drug mixture. Methanol was purchased from Thermo Fisher Scientific (Waltham, MA, United States). Glacial acetic acid was purchased from Mallinckrodt (Phillipsburg, NJ, United States). Stock solutions were prepared to indicated concentrations using the following solution conditions: 30 μM 316 drug mixture (50/50 v/v MeOH/H_2O), 20 μM cytochrome *c* (49.5/49.5/1 v/v/v MeOH/H_2O/AcOH), 15 mM gadolinium(III) chloride hexahydrate (49.5/49.5/1 v/v/v MeOH/H_2O/AcOH), and 100 μM insulin (49.5/49.5/1 v/v/v MeOH/H_2O/AcOH).

Mass Spectrometry. The nESI source and the method by which ions are concentrated and injected into the ELIT have been described previously.[23,26] In brief, the sample is loaded into a pulled glass capillary and placed in front of the sampling orifice. High voltage is applied to a platinum wire in contact with the solution to generate an electrospray.[31] Ions generated via nESI are transported to a trapping quadrupole equipped with LINAC II electrodes,[32] where their accumulation and collisional cooling is facilitated by a pulse (250 ms) of helium gas. Once the pulsed gas valve is closed, the instrument is pumped out for five seconds prior to injection into the ELIT. This leads to a pressure of $\sim 3 \times 10^{-9}$ Torr in the analyzer (measured with a Granville Phillips 355001-YF ion gauge and displayed on a Granville Phillips 358 Micro-Ion controller). Relative to the previous instrument design,[27] the differentially pumped region was removed, and the accumulation quadrupole was placed in the main chamber. While this modification led to a greater base pressure in the ELIT, the transmission efficiency of the ion path was greatly increased. A phase lock circuit was used to trigger both the injection of the bunched ion packet and the start of data collection at a zero crossing of the trapping RF such that a consistent ion energy was sampled.

The ELIT utilized in this work has been described previously.[27] Briefly, the ELIT captures ions via mirror-switching and detects the resulting image charge using a central detector. The trap itself is made up of 10 parallel stainless steel plates (5.08 cm × 5.08 cm × 0.635 mm thick, Kimball Physics, Wilton, NH) with holes 6.48 mm in diameter drilled through the center; eight of the plates control ion acceleration, deceleration, and radial focusing (plates 1−8), while the other two are used to enclose the grounded housing for the detector. The spacing between elements (plates 1−3 = 7.62 mm, plate 3 to central housing = 11.43 mm) is maintained by alumina spacers (Kimball Physics). The copper pick-up tube used for image charge detection (8.26 mm i.d., 9.53 mm o.d., 25.4 mm long) is centered within its grounded housing (50.8 mm long, 33.02 mm i.d.) by a polyether ether ketone (PEEK) spacer. Stainless steel tubes (6.35 mm i.d., 10.16 mm o.d., 19.05 mm long) were welded to plates 1 and 8 to make the electric fields in both ion mirrors identical. To trap positive ions, plate 1 was pulsed from ground to 2355 V (ORTEC Model 556, Advanced Measurement Technology, Oak Ridge, TN) using a fast, high-voltage switch (HTS 31-03-GSM, Behlke Power Electronics, Billerica, MA) at a time defined relative to the ejection of ions from the trapping quadrupole. All other plate potentials were generated by additional ORTEC 556 power supplies with typical trapping potentials being 2356 (plate 8), 1639 (plates 2 and 7), 1046 (plates 3 and 6), and −2106 V (plates 4 and 5) as measured with a calibrated 1000× probe and a HP 34401A multimeter. Frequency shifts arising from the transient voltage recovery of the pulsed power supply were compensated for using the published procedure.[27] Daily variations in the output voltages of the power supplies were minimized by leaving the ORTECs on. With the detailed trap dimensions, ion energy, and trapping voltages, typical ion frequencies are between 400 and 100 kHz for m/z 100 and 1500, respectively.

Signal Processing. The charge sensitive detection electronics have been described previously.[24,27] The output of

DOI: 10.1021/acs.analchem.7b00034
Anal. Chem. 2017, 89, 4392−4397

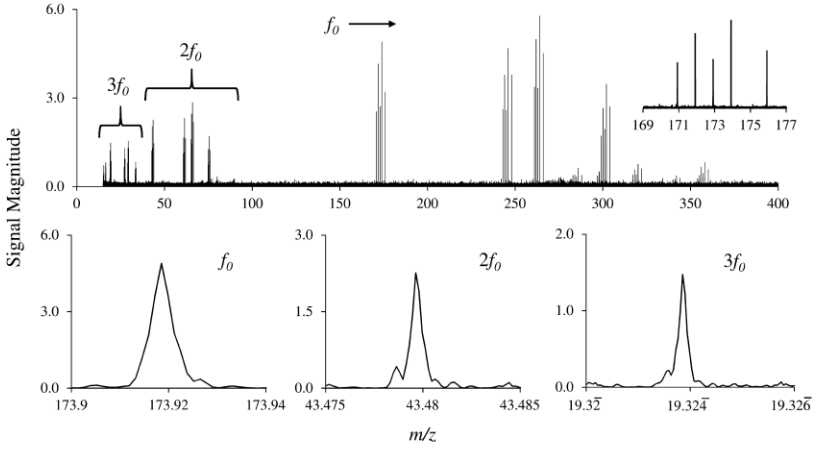

Figure 1. Top: eFT mass spectrum of gadolinium(III) chloride hexahydrate using high-energy interface transfer conditions. The three distributions between m/z 150 and 280 arise from GdO^+, $[GdO{\cdot}4H_2O]^+$, and $[GdO{\cdot}5H_2O]^+$. Inset: expanded view of the GdO^+ isotopic distribution. Bottom: expanded view of the most abundant isotope of GdO^+ (m/z 173.919) at the first (left), second (middle), and third (right) harmonics. The mass resolutions ($M/\Delta M$ fwhm) are 36 900, 75 850, and 108 200, respectively.

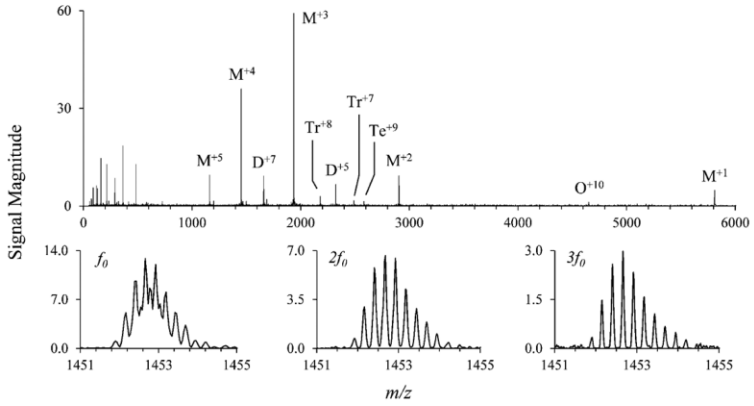

Figure 2. Top: eFT mass spectrum of insulin when the transient is truncated to 75 ms (50 averages). When ions are captured via mirror-switching at 12 μs, $insulin^{+5}$ (m/z 1163) to $insulin^{+1}$ (m/z 5809) is observed, demonstrating an m/z range of greater than 4600 for a single ion injection. M = monomer, D = dimer, Tr = trimer, Te = tetramer, O = octomer. Bottom: $insulin^{+4}$ at the first (left), second (middle), and third (right) harmonics using the full 250 ms transient.

the charge sensitive preamplifier (A250, Amptek) was filtered (band-pass, Krohn-Hite Model 3940, Brockton, MA) and amplified (gain = 5) prior to digitization by a PCI-based digitizer (CS1621, 16-bit, Gage Applied Technologies, Lanchine, Quebec, Canada) at a rate of 10 MS/s (AC coupled, 1 MΩ input impedance, 25 MHz low-pass filter enabled). A program written in LabVIEW 13.0 (National Instruments, Austin, TX) was used to acquire the transient. A custom program written in MATLAB 2015 was used to process the transient and generate the enhanced Fourier transform (eFT) spectrum per the published procedure.[33]

■ RESULTS AND DISCUSSION

Due to the nondifferential detection scheme of the ELIT, ions induce charge on the central pickup tube and can be detected only when in its vicinity, i.e., within the field free region. Outside of the field free region, any image charge induced on the reflectron plates is not detected. With the consideration that the temporal width of the ion packet is less than the time it takes for the packet to turn around, the ion packet can fully leave the detection volume prior to returning. In this manner, the image charge induced on the pickup tube more closely resembles a pulse train than a sinusoid.[21] Using a Keysight 33512B waveform generator, a test signal (pulse train, $f \approx 180$ kHz, width = 1.5 μs, edge time = 1 μs) was run through the

DOI: 10.1021/acs.analchem.7b00034
Anal. Chem. 2017, 89, 4392−4397

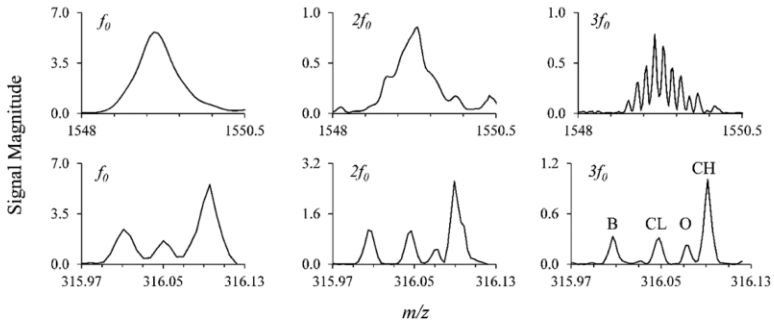

Figure 3. Mass spectra the +8 ion of cytochrome c (top) and the m/z 316 drug mixture (bottom) at the first (left), second (center), and third (right) harmonics. The mass axes have been normalized to the harmonic order. B = bromazepam (m/z 316.0080), CL = clonazepam (m/z 316.0483), O = oxfendazole (m/z 316.0750), and CH = chlorprothixene HCl (m/z 316.0921).

A250 charge sensitive preamplifier, and the experimentally observed harmonic content of doubly protonated angiotensin III (m/z 466.25, $f \approx 180$ kHz) was well replicated on the output (see Supporting Information). Interestingly, even though the test signal was equal in magnitude for the positive- and negative-going edges, the output of the A250 was unequal in amplitude, thus generating an intense second harmonic. If a sinusoid is instead used as the test signal, no amplitude distortion or harmonics are observed on the output. On the basis of these results, we conclude that the harmonics in the present apparatus originate from the A250 preamplifier in response to a pulsed image charge.

A theoretical model published by Grosshans and Marshall[18] suggests that, if the number of ions in the orbiting packet exponentially decreases as a result of scattering collisions with the background gas, the observed mass resolution should increase linearly with harmonic order. (We note that, in addition to scattering, ions can also be lost upon collision-induced dissociation in the ELIT unless the fragmentation takes place in the vicinity of a turning point.) Figure 1 (top) depicts the eFT mass spectrum of gadolinium(III) chloride hexahydrate (300 ms transient, 250 averages) collected using high-energy transfer conditions through the interface region of the mass spectrometer. The inset shows an expanded view of the isotopic distribution of GdO^+ at an average m/z of 173.25. Also observed are $[GdO{\cdot}4H_2O]^+$ (avg m/z 245.31), and $[GdO{\cdot}5H_2O]^+$ (avg m/z 263.33). Figure 1 (bottom) depicts an expanded view of the most abundant isotope of the GdO^+ distribution (m/z 173.919) at the first (left), second (middle), and third (right) harmonics. The m/z axes have been normalized such that an equivalent m/z window is displayed. The mass resolutions of the three peaks are 36 900, 75 850, and 108 200, demonstrating a linear increase in mass resolution with harmonic order ($R^2 = 0.997$). The sidebands that appear at high mass resolution are likely the result of low frequency (1–10 Hz) longitudinal dipolar and quadrupolar bunch oscillations.[34,35]

Figure 2 (top) depicts the eFT mass spectrum of insulin generated from a truncated transient (75 ms, 50 averages) so that large complexes, which decay faster than monomeric ions, were not buried in the noise. Incidentally, this mass spectrum demonstrates that when ions are captured via mirror-switching at 12 μs, an m/z range of greater than 4600 can be accumulated in the quadrupole, and analyzed in the ELIT. Figure 2 (bottom) provides an expanded view of the quadruply protonated insulin signals at the first (left), second (center), and third (right) harmonics using the full 250 ms transient (50 averages). The spacing between the isotopes is 0.25 m/z or 8.8 Hz at the fundamental and a mass resolution of 26 000 is achieved at the third harmonic. Similar harmonic analysis of +3 and +5 charge states (same transient) yields mass resolutions of 24 000 and 31 000, respectively, at the third harmonic. Note that the m/z scales in this case are recalibrated for each harmonic.

Given that higher mass resolution is observed at the higher harmonics in the ELIT, they may be advantageous in determining a protein ion's charge state, resolving isobaric ions, or determining the onset of peak coalescence when the mass resolution at the fundamental is insufficient for such purposes. Figure 3 depicts a narrow region of the mass spectrum of cytochrome c showing the 8^+ charge state (top, 200 ms transient and 1000 averages) and a narrow region of the mass spectrum of the 316 drug mixture described in the Experimental Section (bottom, 150 ms transient and 100 averages) at the first (left), second (center), and third (right) harmonics. All m/z axes are normalized to the harmonic order, as with Figure 2. Under the conditions used here, the isotopic distribution of the ions of the +8 charge state of cytochrome c are unresolved at the fundamental frequency and at the second harmonic. It is therefore not possible to determine the magnitude of the charge associated with the ions from the spacings of the isotope peaks, as is often done with high resolution mass spectrometry. In fact, it is unclear if the merging of closely spaced isotopic peaks, which differ by 4 Hz at the fundamental frequency in this case, might be taking place. At the third harmonic, however, the isotopic peaks are resolved ($M/\Delta M$ fwhm $\approx$ 23 000) with spacings of 0.125 m/z units, which indicates that coalescence of isotope peaks does not occur under these conditions. At higher ion densities (i.e., longer ion accumulation times), little to no change of the peak shape at the fundamental frequency was noted, but the isotopes were not resolved at the third harmonic (data not shown), suggesting a limitation to mass resolution due to space charge effects, which may include peak coalescence.

Isobaric ions may also be resolved at higher harmonics when they are not at the fundamental frequency, as in the case of the 316 drug mixture (Figure 3, bottom). This mass spectrum is comprised of four major, singly protonated components all

DOI: 10.1021/acs.analchem.7b00034
Anal. Chem. 2017, 89, 4392–4397

within 85 mDa (29 Hz) of each other (B = bromazepam (m/z 316.0080), CL = clonazepam (m/z 316.0483), O = oxfendazole (m/z 316.0750), and CH = chlorprothixene HCl (m/z 316.0921)). Though unresolved at the fundamental, all four ions are nearly baseline resolved at the third harmonic with a mass resolution of 41 000. It should also be noted that even though the S/N is lower at the harmonics, the mass accuracy is observed to increase at higher harmonics (Figure 3, bottom), presumably due to the improved mass resolution.

CONCLUSIONS

We demonstrated the use of higher harmonics as an approach to accessing greater mass resolution in a Fourier transform ELIT mass spectrometer. In contrast with typical practice using FT-ICR and Orbitrap mass spectrometers, where harmonics resulting from nonlinear signals are suppressed, there may be incentive to enhance higher harmonics in the FT-ELIT experiment. No hardware or software modifications were necessary to generate the mass spectra presented herein. Rather, the harmonics arise inherently as a direct result of the noncosine signal generated by the charge sensitive preamplifier in response to a pulsed image charge. The harmonics were used to determine a protein ion's charge state and resolve four isobaric drug molecules. A mass resolution of over 108 000 was obtained at the third harmonic of the GdO^+ isotopes. All experimental evidence, including the linear gain in mass resolution with harmonic order and the measured background pressure, indicate that the dominant mechanism for signal loss is via collisions with neutral gas molecules and consequent ion ejection from the trap via either scattering or fragmentation. Given that the major mechanism for signal decay appears to be collisional in nature, improved analytical performance at the fundamental frequency could be achieved with lower analysis pressures. Under conditions in which ion loss due to collisions is no longer the major contributor to signal decay, but rather dephasing and ion cloud dynamics, a linear improvement in mass resolution with harmonic order may no longer be observed.

ASSOCIATED CONTENT

Supporting Information

The Supporting Information is available free of charge on the ACS Publications website at DOI: 10.1021/acs.analchem.7b00034.

Additional figures of time-domain signals, frequency-domain spectra, and synthetic test signals (PDF)

AUTHOR INFORMATION

Corresponding Author

*Phone: (765) 494-5270; Fax: (765) 494-0239; E-mail: mcluckey@purdue.edu.

ORCID

Scott A. McLuckey: 0000-0002-1648-5570

Notes

The authors declare no competing financial interest.

ACKNOWLEDGMENTS

This work was supported by AB Sciex. We thank Mark Carlsen, Randy Replogle, Phil Wyss, and Tim Selby of the Jonathan Amy Facility for Chemical Instrumentation for helpful discussions and their help with construction of the mass spectrometer. We also acknowledge Mircea Guna and Dr. James W. Hager of AB Sciex for helpful discussions and for providing the collision cell with LINAC.

REFERENCES

(1) Mathur, R.; O'Connor, P. B. *Rapid Commun. Mass Spectrom.* **2009**, *23*, 523−529.
(2) Miladinović, S. M.; Kozhinov, A. N.; Tsybin, O. Y.; Tsybin, Y. O. *Int. J. Mass Spectrom.* **2012**, *325*, 10−18.
(3) Delong, S. E.; Mitchell, D. W.; Cherniak, D. J.; Harrison, T. M. *Int. J. Mass Spectrom. Ion Processes* **1989**, *91*, 273−282.
(4) Vorobyev, A.; Gorshkov, M. V.; Tsybin, Y. O. *Int. J. Mass Spectrom.* **2011**, *306*, 227−231.
(5) Jertz, R.; Friedrich, J.; Kriete, C.; Nikolaev, E. N.; Baykut, G. *J. Am. Soc. Mass Spectrom.* **2015**, *26*, 1349−1366.
(6) Eliuk, S.; Makarov, A. *Annu. Rev. Anal. Chem.* **2015**, *8*, 61−80.
(7) Marshal, A. G.; Grosshans, P. B. *Anal. Chem.* **1991**, *63*, 215A−229A.
(8) Grosshans, P. B.; Shields, P. J.; Marshall, A. G. *J. Chem. Phys.* **1991**, *94*, 5341−5352.
(9) Hendrickson, C. L.; Beu, S. C.; Blakney, G. T.; Marshall, A. G. *Int. J. Mass Spectrom.* **2009**, *283*, 100−104.
(10) Makarov, A. *Anal. Chem.* **2000**, *72*, 1156−1162.
(11) Nagornov, K. O.; Kozhinov, A. N.; Tsybin, O. Y.; Tsybin, Y. O. *J. Am. Soc. Mass Spectrom.* **2015**, *26*, 741−751.
(12) Sonalikar, H. S.; Ovhal, A. A.; Mohanty, A. K. *Int. J. Mass Spectrom.* **2016**, *395*, 36−48.
(13) Nikolaev, E. N.; Gorshkov, M. V.; Mordehai, A. V.; Talrose, V. L. *Rapid Commun. Mass Spectrom.* **1990**, *4*, 144−146.
(14) Nikolaev, E. N.; Rakov, V. S.; Futrell, J. H. *Int. J. Mass Spectrom. Ion Processes* **1996**, *157*, 215−232.
(15) Pan, Y.; Ridge, D. P.; Wronka, J.; Rockwood, A. L.; Marshall, A. G. *Rapid Commun. Mass Spectrom.* **1987**, *1*, 120−121.
(16) Pan, Y.; Ridge, D. P.; Rockwood, A. L. *Int. J. Mass Spectrom. Ion Processes* **1988**, *84*, 293−304.
(17) Dziekonski, E. T.; Santini, R. E.; McLuckey, S. A. *Int. J. Mass Spectrom.* **2016**, *405*, 1−8.
(18) Grosshans, P. B.; Marshall, A. G. *Int. J. Mass Spectrom. Ion Processes* **1991**, *107*, 49−81.
(19) Makarov, A.; Denisov, E. V.; Jung, G.; Balschun, W.; Horning, S. R. Electrostatic Trap. U.S. Patent 8198581B2, 2012.
(20) Knobeler, M.; Wanczek, K. *Int. J. Mass Spectrom. Ion Processes* **1993**, *125*, 127−134.
(21) Keifer, D. Z.; Shinholt, D. L.; Jarrold, M. F. *Anal. Chem.* **2015**, *87*, 10330−10337.
(22) Hilger, R. T.; Wyss, P. J.; Santini, R. E.; McLuckey, S. A. *Anal. Chem.* **2013**, *85*, 8075−8079.
(23) Hilger, R. T.; Santini, R. E.; McLuckey, S. A. *Anal. Chem.* **2013**, *85*, 5226−5232.
(24) Hilger, R. T.; Santini, R. E.; McLuckey, S. A. *Anal. Chem.* **2014**, *86*, 8822−8828.
(25) Hilger, R. T.; Santini, R. E.; McLuckey, S. A. *Int. J. Mass Spectrom.* **2014**, *362*, 1−8.
(26) Hilger, R. T.; Dziekonski, E. T.; Santini, R. E.; McLuckey, S. A. *Int. J. Mass Spectrom.* **2015**, *378*, 281−287.
(27) Dziekonski, E. T.; Johnson, J. T.; Hilger, R. T.; McIntyre, C. L.; Santini, R. E.; McLuckey, S. A. *Int. J. Mass Spectrom.* **2016**, *410*, 12−21.
(28) Ring, S.; Pedersen, H. B.; Heber, O.; Rappaport, M. L.; Witte, P.; Bhushan, K. G.; Altstein, N.; Rudich, Y.; Sagi, I.; Zajfman, D. *Anal. Chem.* **2000**, *72*, 4041−4046.
(29) Zajfman, D.; Heber, O.; Vejby-Christensen, L.; Ben-Itzhak, I.; Rappaport, M.; Fishman, R.; Dahan, M. *Phys. Rev. A: At., Mol., Opt. Phys.* **1997**, *55*, R1577−R1580.
(30) Benner, W. H. *Anal. Chem.* **1997**, *69*, 4162−4168.
(31) Van Berkel, G. J.; Asano, K. G.; Schnier, P. D. *J. Am. Soc. Mass Spectrom.* **2001**, *12*, 853−862.
(32) Loboda, A.; Krutchinsky, A.; Loboda, O.; McNabb, J.; Spicer, V.; Ens, W.; Standing, K. *Eur. Mass Spectrom.* **2000**, *6*, 531−536.

DOI: 10.1021/acs.analchem.7b00034
Anal. Chem. 2017, 89, 4392−4397

J. Am. Soc. Mass Spectrom. (2018) 29:242–250
DOI: 10.1007/s13361-017-1720-1

FOCUS: 32nd ASILOMAR CONFERENCE,
NOVEL INSTRUMENTATION IN MS AND ION MOBILITY: RESEARCH ARTICLE

Determination of Collision Cross Sections Using a Fourier Transform Electrostatic Linear Ion Trap Mass Spectrometer

Eric T. Dziekonski, Joshua T. Johnson, Kenneth W. Lee, Scott A. McLuckey

Department of Chemistry, Purdue University, 560 Oval Drive, West Lafayette, IN 47907-2084, USA

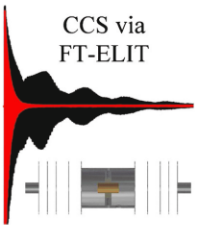

Abstract. Collision cross sections (CCSs) were determined from the frequency-domain linewidths in a Fourier transform electrostatic linear ion trap. With use of an ultrahigh-vacuum precision leak valve and nitrogen gas, transients were recorded as the background pressure in the mass analyzer chamber was varied between 4×10^{-8} and 7×10^{-7} Torr. The energetic hard-sphere ion–neutral collision model, described by Xu and coworkers, was used to relate the recorded image charge to the CCS of the molecule. In lieu of our monoisotopically isolating the mass of interest, the known relative isotopic abundances were programmed into the Lorentzian fitting algorithm such that the linewidth was extracted from a sum of Lorentzians. Although this works only if the isotopic distribution is known a priori, it prevents ion loss, preserves the high signal-to-noise ratio, and minimizes the experimental error on our homebuilt instrument. Six tetraalkylammonium cations were used to correlate the CCS measured in the electrostatic linear ion trap with that measured by drift-tube ion mobility spectrometry, for which there was an excellent correlation ($R^2 \approx 0.9999$). Although the absolute CCSs derived with our method differ from those reported, the extracted linear correlation can be used to correct the raw CCS. With use of $[\text{angiotensin II}]^{2+}$ and reserpine, the corrected CCSs (334.9 ± 2.1 and 250.1 ± 0.5, respectively) were in good agreement with the reported ion mobility spectrometry CCSs (335 and 254.3, respectively). With sufficient signal-to-noise ratio, the CCSs determined are reproducible to within a fraction of a percent, comparable to the uncertainties reported on dedicated ion mobility instruments.

Keywords: Collision cross section, Electrostatic linear ion trap, Fourier transform, Electrospray ionization

Received: 15 April 2017/Revised: 18 May 2017/Accepted: 18 May 2017/Published Online: 11 July 2017

Introduction

Mass spectrometry is widely used for the identification and quantitation of species of interest on the basis of the mass-to-charge (m/z) measurement of their relevant ions. Important information regarding ion structure, such as bond connectivity, can be derived from ion fragmentation. However, the measurement of m/z alone cannot provide information about the three-dimensional gas-phase structure, which is often critical to biological functionality [1, 2]. To obtain such information, instruments containing a dedicated ion mobility spectrometry (IMS) platform may be coupled to a tandem mass spectrometer [3, 4], thereby enabling the user to identify the molecule and elucidate the rotationally averaged collision cross section (CCS) of the ion–neutral pair. It has, however, long been recognized that the spectral linewidth in Fourier transform (FT) mass spectrometry is related to the CCS of the ion–neutral pair [5–9]. Recently, several groups have used FT ion cyclotron resonance (ICR) mass analyzers and linewidth analysis to determine the CCSs of ions derived from amino acids [10], peptides [11], and proteins [12], among others [13]. The process of determining CCSs from the frequency linewidth with an FT-ICR mass analyzer has been given the acronym "CRAFTI," denoting "cross-sectional areas by Fourier transform ion cyclotron resonance" (FT-ICR) [13]. The relative CCSs of very large ions (e.g., those derived from myoglobin, carbonic anhydrase, enolase, bovine serum albumin, and transferrin) have also been reported with use of an Orbitrap mass analyzer. However, the authors were unable to directly measure the pressure in the Orbitrap chamber and therefore were unable to determine the absolute CCSs [14]. It has been proposed, on the basis of theory, that the CCS can be derived in a quadrupole ion trap through a time–frequency analysis method [15].

In an FT electrostatic linear ion trap (ELIT) [16–27], ions are confined between two axially opposing reflectrons. The image charge induced on a central pickup electrode is digitized, subjected to Fourier transformation, and calibrated to generate

Correspondence to: Scott McLuckey; *e-mail:* mcluckey@purdue.edu

a mass spectrum. The rate at which the detected signal intensity decays depends on many factors, including the divergence angle of the injected ion beam, the focal point of the einzel lenses [28], the kinetic energy (KE) focusing characteristics of the reflectrons and einzel lens [29, 30], the CCS of the ion–neutral pair, the background gas density [31, 32], the energy exchanged owing to a collision, space charge [33–36], and any geometric/field imperfections in the trap. Therefore, the source(s) of signal decay on our homebuilt ELIT could be much more complicated than in an FT-ICR mass analyzer, where ions start at the center of the mass analyzer and are excited to radii where field imperfections are minimized by shimming of the electrode potentials. However, all experimental observations point to the fact that, even at the lowest pressures that we have achieved (i.e., approximately 3×10^{-9} Torr), we are operating under a pressure-limited circumstance [24]. Therefore, the collision rate should be the dominant ion loss mechanism such that a CCS may be derived.

Herein we report measurement of the CCSs of six quaternary ammonium cations, $[\text{angiotensin II} + 2\text{H}]^{2+}$, and $[\text{reserpine} + \text{H}]^{+}$ in an ELIT using the energetic hard-sphere collision model proposed by Xu and coworkers [12, 37]. Neither monoisotopic isolation nor high resolution was needed as the frequency-domain spectrum was fit to a sum of Lorentzians, from which the linewidth was extracted. We found there to be good correlation ($R^2 \approx 0.9999$) between the CCS measured in the FT-ELIT and that measured by drift-tube IMS. However, the absolute CCSs differ, which has also been observed in the measurement of the CCSs of ions with an FT-ICR mass analyzer by several different methods [10, 12, 13].

Experimental

Materials

The following chemicals were purchased from Sigma-Aldrich (St Louis, MO, USA): reserpine, angiotensin II (human), tetraethylammonium bromide, tetrapropylammonium bromide, tetrabutylammonium bromide, tetrahexylammonium bromide, tetraoctylammonium bromide, and tetradodecylammonium bromide. Methanol (MeOH) was purchased from Thermo Fisher Scientific (Waltham, MA, USA), glacial acetic acid (AcOH) was purchased from Mallinckrodt (Phillipsburg, NJ, USA), isopropyl alcohol (IPA) was purchased from Macron Fine Chemicals (Center Valley, PA, USA), and high-performance liquid chromatography grade water was purchased from Fisher Scientific (Pittsburgh, PA, USA). Reserpine and angiotensin II were prepared to final concentrations of 100 µM in 49.5:49.5:1 v/v/v MeOH–H_2O–AcOH. All tetraalkylammonium salts were prepared to final concentrations of 100 µM in 50:50 v/v MeOH–H_2O, except for tetradodecylammonium bromide, which was prepared to a final concentration of 100 µM in 45:45:10 v/v/v MeOH–H_2O–IPA.

Mass Spectrometry

The nanoelectrospray ionization (nESI) source and the method by which ions are concentrated and injected into the ELIT have been described previously [18, 21]. In brief, the sample is loaded into a pulled-glass capillary and placed in front of the sampling orifice. High voltage is applied to a platinum wire in contact with the solution to generate an electrospray [38]. Ions generated via nESI are transported to a trapping quadrupole equipped with LINAC II electrodes [39], where their accumulation and collisional cooling is facilitated by the continuous injection of nitrogen gas. Once the ions have cooled, the voltage to all quadrupole elements is ramped to their injection potentials, where the KE of the ions is set by the rod offset. An RF phase-locked circuit was used to trigger both the injection of the bunched ion packet and the start of data collection at a zero crossing of the trapping RF such that a consistent ion energy was sampled. The pressure within the ELIT analysis chamber is continuously variable (manual) between 5×10^{-9} and 5×10^{-6} Torr (N_2) via a VZLVM263R LVM series ultrahigh-vacuum leak valve that is attached directly to the chamber. The pressure is measured with a Granville Phillips 355001-YF ion gauge and displayed on a Granville Phillips 358 Micro-Ion controller. If the controller is out of calibration, in that the response is not 1 V per pressure decade, as it is configured to be, all CCS measurements will suffer from a systematic error and be off by a constant factor from those derived by IMS.

The ELIT used in this work has been described previously [23]. Briefly, the ELIT captures ions via mirror-switching and detects the resulting image charge using a central electrode. The trap itself is made up of ten parallel stainless steel plates (5.08 cm × 5.08 cm × 0.635 mm thick, Kimball Physics, Wilton, NH, USA) with holes 6.48 mm in diameter drilled through the center; eight of the plates control ion acceleration, deceleration, and radial focusing (plates 1–8), and the other two plates are used to enclose the grounded housing for the detector. The spacing between elements (plates 1–3, 7.62 mm; plate 3 to central housing, 11.43 mm) is maintained by alumina spacers (Kimball Physics). The copper pickup tube used for image charge detection [8.26-mm inner diameter (i.d.), 9.53-mm outer diameter (o.d.), 25.4 mm long] is centered within its grounded housing (50.8 mm long, 33.02-mm i.d.) by a polyether ether ketone spacer. Stainless steel tubes (6.35-mm i.d., 10.16-mm o.d., 19.05 mm long) were welded to plates 1 and 8 to make the electric fields in both ion mirrors identical. To trap positive ions, plate 1 is pulsed from ground to 2356 V (ORTEC model 556, Advanced Measurement Technology, Oak Ridge, TN, USA) by a fast, high-voltage switch (HTS 31-03-GSM, Behlke Power Electronics, Billerica, MA) at a time defined relative to the ejection of ions from the trapping quadrupole. All other plate potentials are generated by additional ORTEC 556 power supplies, with typical trapping potentials being 2364 V (plate 8), 1646 V (plates 2 and 7), 1047 V (plates 3 and 6), and -2106 V (plates 4 and 5) as measured with a calibrated 1000x probe and an HP 34401A multimeter. Frequency shifts arising from the transient voltage recovery of the pulsed power supply are minimized by use of the

ORTEC 556 power supply as the power supply from plate 1 [23]. Considering the linewidths (frequency resolution) at elevated background pressures, the frequency correction circuit was not included. Daily variations in the output voltages of the power supplies were minimized by or leaving the ORTEC power supplies on. With the detailed trap dimensions, ion energy, and trapping voltages, typical ion frequencies are between 400 kHz and 100 kHz for m/z 100 and 1500, respectively.

Signal Processing

The charge-sensitive detection electronics have been described previously [19, 23]. The output of the charge-sensitive preamplifier (A250, Amptek) was filtered (band pass, Krohn-Hite model 3940, Brockton, MA, USA) and amplified (gain of 5) before digitization by a PCI-based digitizer (CS1621, 16 bit, Gage Applied Technologies, Lanchine, QC, Canada) at a rate of 10 MS/s (AC coupled, 1-MΩ input impedance, 25-MHz low-pass filter enabled). A program written in LabVIEW 13.0 (National Instruments, Austin, TX, USA) was used to acquire each transient. A custom program, written in MATLAB 2015, was used to process the transients (100 averages, 75 ms, 10 MSa/s, 1 zero fill, rectangular window) and determine the CCS of the ion.

Theory

Signal Decay in an Electrostatic Linear Ion Trap

To measure the CCS of an ion in an FT-ELIT, the relationship between the frequency-domain linewidth and the CCS must be established, which requires the use of an appropriate ion–neutral collision model. Three collision models (i.e., Langevin, hard sphere, and energetic hard sphere) were described by Guo et al. [37] and implemented by Jiang et al. [11] to determine biomolecular CCSs with an FT-ICR mass analyzer. Typically, the appropriate collision model is chosen on the basis of the size of the ion and/or its trapped KE. In a modern Orbitrap or FT-ICR mass analyzer, ions rotate about the trap axis at a constant angular speed and a high ion energy, and it is therefore expected that the energetic hard-sphere collision model is a good description of the ion–neutral collisions so long as the energy exchanged by a single collision is sufficient to dephase or dissociate the ion. Unlike in Orbitrap and FT-ICR mass analyzers, ions trapped within an ELIT have a time-dependent axial KE (KE_z) that can range from 0 to approximately 3.7 keV 7per charge throughout one oscillation of the trap. As such, it is reasonable to presume that the appropriate collision model depends on the location (potential, time) at which the collision occurs. However, for an ion to continue to contribute to the observed signal after a collision has occurred in the ELIT, several criteria must be met:

1. The collision must not lead to fragmentation. The likelihood for this scenario depends on the KEs of the ions, the relative masses of the ion and background gas, and the stability of the ion with respect to fragmentation. The first two factors determine the collision energy in the center-of-mass frame of reference, whereas the latter factor relates to the energies and entropies associated with ion fragmentation as well as the number of degrees of freedom in the ion.
2. The collision must not lead to lateral scattering sufficient for ion loss. In other words, all the KE needs to be retained within the axial motion of the ion ($KE_z >> KE_{xy}$).
3. The postcollision KE (laboratory frame of reference) must be within the focusing capabilities of the reflectrons and einzel lenses to avoid loss of ions in the z-dimension.
4. An extension to criterion 3 is the requirement that the ions maintain the same frequency of oscillation. To achieve this condition, the reflectron potentials must be tuned such that a broad range of KEs exhibit isochronous axial motion. Otherwise, dephasing of the ions leads to loss of signal even when the ions remain trapped.

By definition, if every collision were to lead to fragmentation (i.e., criterion 1 is never met), the energetic hard-sphere collision model can be used to describe the signal decay. If the second or third criterion is not met, the ion will follow an unstable trajectory and be lost from the trap within several oscillations. Smaller ions are especially susceptible to ejection from the trap via criterion 2, where anything but a head-on collision is likely to scatter the ion and partition axial KE into the radial dimensions. As the ion mass increases, the maximum exchange energy [37] is decreased and the collision is less likely to scatter or fragment the ion, as is the case for megadalton-sized complexes [40]. Nevertheless, an ion that does not fragment, is not scattered, and remains within the focusing conditions of the reflectron can still dephase from the packet owing to a change in its total KE if the fourth criterion is not satisfied. As the four plate reflectrons used in the current ELIT do not generate an ideal quadratic electric field, only a small range of KEs will exhibit isochronous motion. Per ion optical simulations performed in SIMION version 8.1 (Scientific Instrument Services, Ringoes, NJ, USA), simply changing the trapped KE of cesium (m/z 132.906, approximately 1960 eV) by 10 eV will change the detected frequency by approximately 80 Hz. If cesium were to undergo a collision with helium in the field-free region, the maximum exchange energy would be approximately 120 eV, causing it to rapidly dephase from the coherent ion packet and/or be ejected from the trap.

From this discussion, even though ions trapped within the ELIT exhibit a time-dependent KE_z, it is expected that a single collision will remove smaller m/z ions from the spatially coherent ion packet by a dephasing mechanism, dissociation, or ejection from the trap. As such, the energetic hard-sphere collision model is used to relate the transient signal decay to the CCS of the ions in this study. Briefly, the number of ions remaining in the coherent packet, $N(t)$, can be described by an exponential decay:

$$N(t) = N_0 e^{-\frac{t}{\tau}}, \quad (1)$$

where N_0 is the initial number of ions in the packet, t is the time, and τ is an exponential damping time constant defined as

$$\tau = \frac{1}{\sigma n v}, \quad (2)$$

in which σ is the CCS of the ion (m^2), n is the neutral gas density (molecules per cubic meter), and v is the ion speed (m/s). The Fourier transformation of the time-domain exponential-damped sinusoid (no apodization) generates a frequency-domain line shape corresponding to a Lorentzian function:

$$A(f) = \frac{2\alpha}{\pi} \frac{\Gamma}{4\cdot(f-f_0)^2 + \Gamma^2} + C, \quad (3)$$

in which $A(f)$ is the signal magnitude at the specified frequency (f), α is the peak area, Γ is the full width at half maximum (FWHM) in hertz, f_0 is the center frequency of the peak in hertz, and C is the offset. The FWHM of a Lorentzian function is related to the exponential decay time constant by

$$\Gamma = \frac{1}{\pi\tau}. \quad (4)$$

Therefore, rearrangement of Eqs. 3 and 5 allows the ion CCS to be calculated:

$$\sigma = \frac{\pi}{v}\cdot\frac{\Gamma}{n}. \quad (5)$$

Given that the ion speed is not constant in the ELIT, the time-averaged ion speed is used instead:

$$\bar{v} = path\_length(KE)\cdot f_0 = path\_length(KE)\cdot\left(\frac{k}{\sqrt{m/z}} + b\right), \quad (6)$$

where path length(KE) is the distance between the turning points (Figs. 1 and 2), which varies with the trapped KE, and f_0 is the center frequency of the ion extracted from a Lorentzian fit of the experimental line shape (Eq. 4). The frequency of an ion within the ELIT is inversely proportional to the square root of the mass-to-charge (m/z) ratio. With use of the ideal trap dimensions, measured plate potentials, injection conditions, and SIMION version 8.1, the potential energy surface along the central axis of the ELIT was extracted (Fig. 2) and the KE of the ion as it passed through the central plane of the ELIT was determined to be approximately 1960 eV per charge. The path length was estimated to be 123.68 mm by linear interpolation of the distance between the turning points (potential energy 1960 V). In part, the experimental error in the absolute CCSs determined with an FT-ELIT can be related to physical imperfections of the ELIT, which could cause accelerated dephasing, or to error in the estimated path length. Both cases lead to systematic errors that are difficult to quantify independently.

Use of Isotopic Information to Improve Performance

Apex ion isolation is relatively inefficient on our homebuilt instrument and causes the intensity of the isotope of interest to be heavily depleted while not providing a monoisotopic isolation.

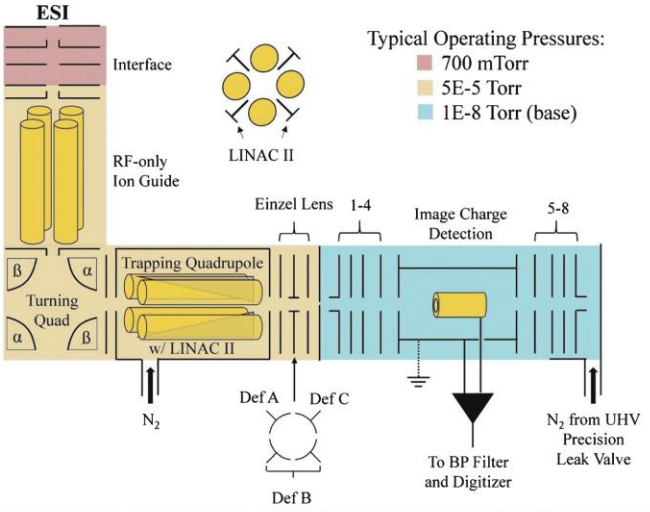

Figure 1. The instrument (not to scale). *BP* band pass, *ESI* electrospray ionization, *UHV* ultrahigh vacuum

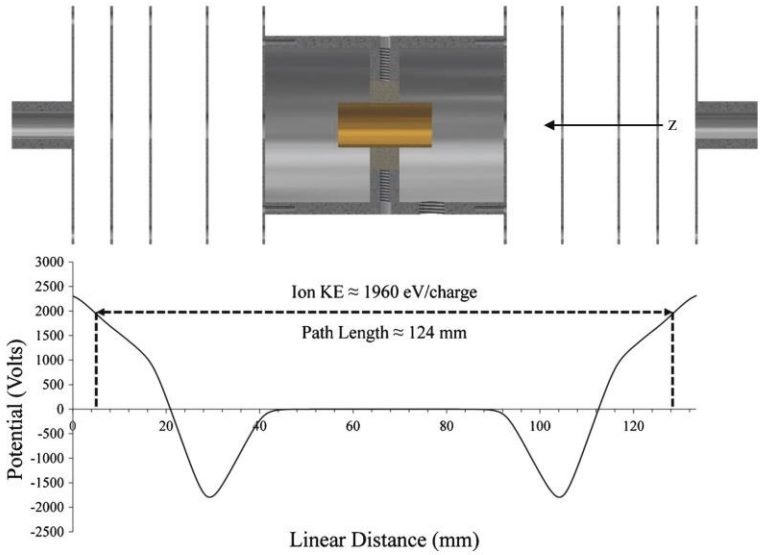

Figure 2. *Top*: AutoCAD assembly of the electrostatic linear ion trap (ELIT). *Bottom*: Potential (in volts) along the central axis of the trap. The effective path length is equal to the distance between the two turning points for a known trapped kinetic energy (*KE*)

If it is used, the signal-to-noise ratio of the frequency-domain spectrum is drastically reduced, leading to a systematically high standard deviation in the extracted FWHM at each pressure and, consequently, a high uncertainty in the calculated CCS. In lieu of monoisotopic isolation, two methods can be adopted: (1) with high-frequency resolution, as is found on an FT-ICR mass analyzer, the FWHM of each individual isotope can be recorded at several pressures before the increasing isotopic linewidths begin to interfere with each other [11, 12]; and (2) if the isotopic distribution of the ions is known, the frequency-domain spectrum can be fit to a sum of Lorentzians (Eq. 7):

$$A(f) = \frac{2\alpha_1}{\pi}\frac{\Gamma}{4\cdot\left(f-f_{0,1}\right)^2+\Gamma^2} + \frac{2\alpha_2}{\pi}\frac{\Gamma}{4\cdot\left(f-f_{0,2}\right)^2+\Gamma^2} + \cdots + C, \qquad (7)$$

in which the subscripts indicate the isotope to which the variables refer. It is assumed that the FWHM of all isotopes are the same and that the areas are proportional to the relative intensities; that is, $\alpha_2 = \frac{R_2}{100}\alpha_1$, where R_2 is the relative intensity of the second isotope.

The second method was used throughout this work, and only those isotopes with a relative abundance greater than 3% were included in the fit.

Results and Discussion

Figure 3 shows eight transients (100 averages each) of tetraoctylammonium (TOA), collected over a pressure range from 4.2×10^{-8} to 7.0×10^{-7} Torr with nitrogen as a buffer gas.

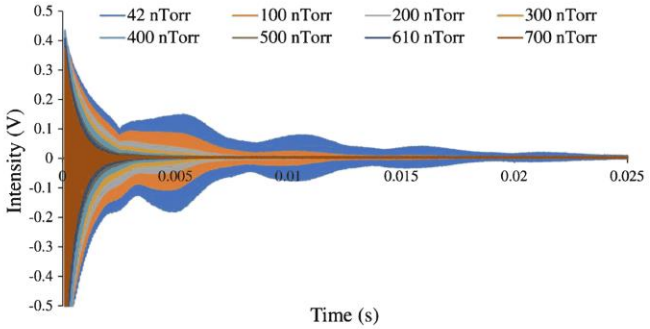

Figure 3. Time-domain signal of tetraoctylammonium (TOA) at different buffer gas pressures. To aid with visualization, only the first 25 ms of the 75-ms transient was plotted. Each trace represents the average of 100 transients

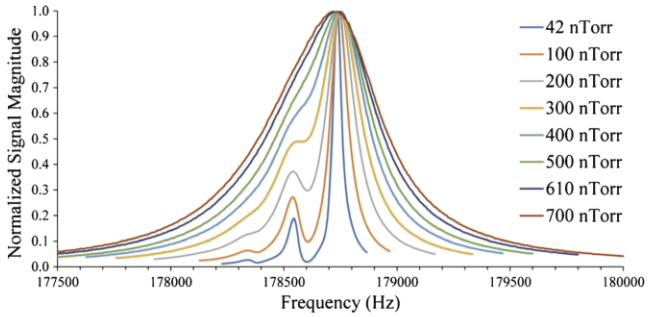

Figure 4. Magnitude-mode frequency-domain spectra of TOA at different buffer gas pressures (power spectra). The corresponding transients (100 averages) are shown in Fig. 3

Considering the high operating pressures and the CCS of the ion–neutral pair, the observed signal decayed very rapidly, and therefore only the first 25 ms of the full 75-ms transients are plotted to aid the reader. At low pressures, a beat pattern was observed in the transient that resulted from isotopic interferences.

The corresponding magnitude-mode fast FTs (power spectrum) of the transients shown in Fig. 3 are plotted in Fig. 4 and expanded about the fundamental distribution of TOA. At low buffer gas pressures, the three major isotopes (relative abundance greater than 3%) were clearly resolved. However, as the pressure was increased, the linewidth of the isotopes increased concurrently to the point that they were no longer resolved (although a shoulder is visible). The frequency-domain spectra were fit to a sum of Lorentzians with use of Eq. 7 and the nonlinear least squares solver in MATLAB (lsqcurvefit). It was assumed that the area of each Lorentzian was proportional to the isotopes' respective relative abundance and that the FWHM of all isotopes was equal. Selected spectra (black trace) and their respective fits (dashed red trace) are shown in Fig. 5. The experimentally observed Lorentzians were asymmetric, an observation made apparent by the seemingly poor fit at 42 nTorr. However, even when the isotopes were unresolved (and uncoalesced), the algorithm could fit the experimental spectrum very well, as is observed at 600 nTorr.

The linewidth at each pressure was extracted from the solver and is plotted against the neutral gas density in Fig. 6 ($n = P/k_BT$, where P is the pressure, k_B is the Boltzmann constant, and T is the temperature). The slope of the linear regression represents the quantity Γ/n in Eq. 5, whereas no physical meaning is attributed to the intercept. As the signal was completely absent by the end of the collected 75-ms transient, no frequency-domain peak broadening (windowing effect) was expected, and therefore no linewidth correction was applied [11]. This procedure was repeated for a total of six different quaternary ammonium cations (five replicate measurements at each pressure) ranging from tetraethylammonium (m/z 130.2) to tetradodecylammonium (m/z 690.8). In all cases, the coefficient of determination (R^2) is near unity. Standard deviations in the measured linewidth were typically within 0.2–2 Hz, and are not represented on the plot as they are unable to be visualized on its scale.

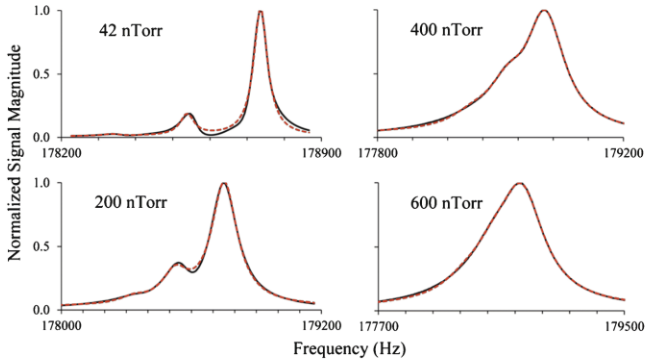

Figure 5. Frequency-domain spectrum (*black*) and Lorentzian fit (*red*) for TOA at selected pressures. When the isotopic information is known, it can be used to fit the spectrum to multiple Lorentzians, thus eliminating the need for isotopic isolation

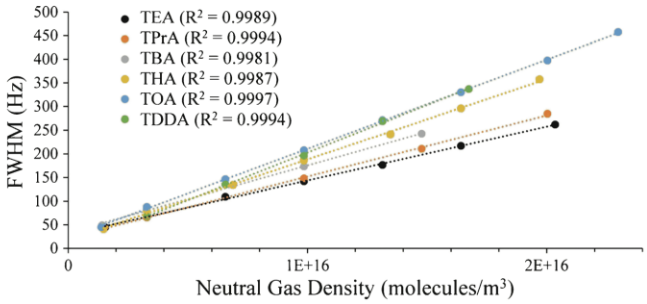

Figure 6. Linewidth (full width at half maximum, *FWHM*) of several tetraalkylammonium cations at different buffer gas pressures. With high signal-to-noise ratio, the coefficient of determination (R^2) is near unity, demonstrating excellent linearity. Error bars have been omitted as they are unable to be visualized on this scale (typically 0.2–2 Hz). *TBA* tetrabutylammonium, *TDDA* tetradodecylammonium, *TEA* tetraethylammonium, *THA* tetrahexylammonium, *TPrA* tetrapropylammonium

From the simulated path length and center frequency of the most abundant isotope, the time-averaged velocity of the ion could be determined (Eq. 6) and used to calculate the CCS via Eq. 5. The CCS of each quaternary ammonium cation, calculated from the FT-ELIT data, is plotted against the reported drift-tube IMS CCS [41, 42] in Fig. 7 (left, dashed line). The solid line represents a 1:1, and therefore perfect, correlation. The FT-ELIT-derived CCS trend correlates very well with that derived from drift-tube IMS measurements ($R^2 \approx 0.9999$). However, the absolute CCSs differ. This observation is not unique to measurements made with an ELIT, and was reported by others when calculating CCSs on an FT-ICR mass analyzer by different methods [10, 12, 13]. Figure 7, right, shows the absolute CCS as a function of the number of carbons in the alkyl substituent. As one could expect from the excellent correlation between the IMS and FT-ELIT CCSs, the trend is observed to be the same in both cases, with only the absolute values differing. Again, the standard deviations of the calculated CCSs in Fig. 7 are smaller than the symbols used for the data points (see Table 1).

The CCSs of $[\text{angiotensin II} + 2\text{H}]^{2+}$ and $[\text{reserpine} + \text{H}]^{+}$ were measured with the ELIT and corrected with use of the relationship derived between the FT-ELIT and IMS CCSs in Fig. 7, left. The experimental (raw) CCS for $[\text{angiotensin II} + 2\text{H}]^{2+}$ was 369.3 ± 2.7 Å^2, whereas the corrected CCS was 334.9 ± 2.1 Å^2, representing less than 0.1% relative error over the reported IMS CCS of 335 Å^2 [41]. For $[\text{reserpine} + \text{H}]^{+}$, the experimental (raw) CCS was 256.8 ± 0.7 Å^2, whereas the corrected CCS was 250.1 ± 0.5 Å^2, representing a 1.7% relative error when compared with the reported IMS CCS of 254.3 Å^2 [43]. It should be noted, however, that Giles et al. [44] reported the CCS (N_2) of reserpine to be between 251.0 and 253.2 Å^2 depending on the instrument used (traveling-wave versus drift-tube IMS), thereby lowering the relative error to within the range of 0.4–1.2%.

The results of all experiments are summarized in Table 1. Generally, the corrected CCSs derived from FT-ELIT mass spectrometry demonstrate relative errors of less than 1% from the reported drift-tube IMS CCSs. As expected, even though the mass of reserpine is approximately 143 Da greater than that of TOA, its measured CCS is smaller. Transients exhibiting a lower signal-to-noise ratio generally have a higher uncertainty in the calculated CCS, as exemplified by the fact that tetradodecylammonium and $[\text{angiotensin II} + 2\text{H}]^{2+}$ had lower

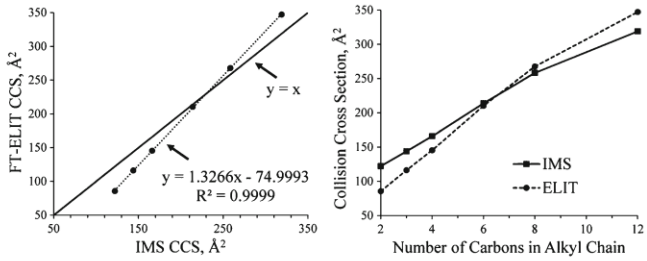

Figure 7. *Left*: Correlation between the collision cross section (*CCS*) measured via Fourier transform (*FT*) ELIT mass spectrometry (MS) and that reported from drift-tube ion mobility spectrometry (*IMS*). The *solid line* represents a 1:1 correlation. *Right*: Collision cross section of tetraalkylammonium cations with dissimilar chain lengths for both IMS and FT-ELIT MS. Error bars for both plots have been omitted as they are unable to be visualized with the corresponding scale (see Table 1)

Table 1. Comparison of collision cross sections derived from drift-tube ion mobility spectrometry (*IMS*) and Fourier transform electrostatic linear ion trap mass spectrometry (*FT-ELIT MS*)

Species	*m/z*	Collision cross section (Å^2)			Relative error (%)
		Drift tube IMS	FT-ELIT MS, raw	FT-ELIT MS, corrected	
TEA	130.2	122.2[a]	85.7 ± 0.2	121.1 ± 0.2	0.9
TPrA	186.2	143.8[a]	116.2 ± 0.5	144.1 ± 0.4	0.2
TBA	242.3	166.0[a]	145.5 ± 0.2	166.2 ± 0.2	0.1
THA	354.4	214.0[a]	210.5 ± 0.2	215.2 ± 0.2	0.6
TOA	466.5	258.3[a]	267.8 ± 0.4	258.4 ± 0.3	<0.1
TDDA	690.8	319.0[b]	347.3 ± 2.6	318.3 ± 2.0	0.2
[Angiotensin II + 2H]$^{2+}$	523.3	335[c]	369.3 ± 2.7	334.9 ± 2.1	<0.1
[Reserpine + H]$^+$	609.4	254.3[a]	256.8 ± 0.7	250.1 ± 0.5	1.7

TBA tetrabutylammonium, *TDDA* tetradodecylammonium, *TEA* tetraethylammonium, *THA* tetrahexylammonium, *TOA* tetraoctylammonium, *TPrA* tetrapropylammonium
[a]From [43]
[b]From [42]
[c]From [41]

signal intensities than the other compounds. Overall, the uncertainties in the measured CCSs and relative errors are comparable to those derived with dedicated IMS instruments. With higher-sensitivity detection electronics, a voltage-controlled leak valve, and lower pressure, fewer averages would need to be recorded to provide the same measurement precision, and therefore the CCS of an ion could be derived in less than 1 min. Currently, no method has been generated or reported that allows one to determine the CCS of an ion in an FT-based mass analyzer if it adopts multiple conformational states; thus, this remains an area of future research.

Conclusions

The FT-ELIT was used to determine the CCS of several molecules in a nitrogen buffer gas. The potentials applied to the reflectron plates are no different from those used during high-resolution analysis, and thus it is trivial to implement this technique during a normal experimental workflow. Owing to the trajectory stability criteria in an ELIT, even though an ion exhibits a KE between 0 and approximately 3.7 keV per charge throughout one cycle of the trap, a single collision can remove an ion from the packet, and therefore the energetic hard-sphere collision model well approximates the transient decay profile. It is not necessary to perform monoisotopic isolation before analysis and, in fact, preservation of the high signal-to-noise ratio provides higher CCS precision even when the isotopic peaks overlap in the frequency domain. Although the absolute CCSs determined via FT-ELIT mass spectrometry deviate from the values reported in the IMS literature, there is a very strong correlation between the two. After correction, this method provides CCSs and relative errors comparable to those generated with dedicated IMS instruments, but cannot determine if multiple conformational states exist for a single *m/z*. The implementation of this measurement, from a hardware perspective, requires only the addition of a precision leak valve compatible with an ultrahigh vacuum. The ability to determine CCSs adds to the capabilities of the low-cost, high-performance, homebuilt, FT tandem mass spectrometer.

Acknowledgements

This work was supported by the Purdue Research Foundation and SCIEX. We thank Mark Carlsen, Randy Replogle, Phil Wyss, and Tim Selby of the Jonathan Amy Facility for Chemical Instrumentation for helpful discussions and their help with construction of the mass spectrometer. We also acknowledge Mircea Guna, and James W. Hager of SCIEX for helpful discussions and for providing the collision cell with LINAC II electrodes.

References

1. Nicholls, A., Sharp, K.A., Honig, B.: Protein folding and association: insights from the interfacial and thermodynamic properties of hydrocarbons. Proteins: Struct. Funct. Bioinf. **11**, 281–296 (1991)
2. Branden, C.I., Tooze, J.: Introduction to protein structure. Garland Science, New York (1999)
3. Kanu, A.B., Dwivedi, P., Tam, M., Matz, L., Hill, H.H.: Ion mobility–mass spectrometry. J. Mass Spectrom. **43**, 1–22 (2008)
4. Lanucara, F., Holman, S.W., Gray, C.J., Eyers, C.E.: The power of ion mobility-mass spectrometry for structural characterization and the study of conformational dynamics. Nat. Chem. **6**, 281–294 (2014)
5. Wobschall, D., Graham Jr., J.R., Malone, D.P.: Ion cyclotron resonance and the determination of collision cross sections. Phys. Rev. **131**, 1565 (1963)
6. Wobschall, D., Fluegge, R.A., Graham Jr., J.R.: Collision cross sections of hydrogen and other ions as determined by ion cyclotron resonance. J. Chem. Phys. **47**, 4091–4094 (1967)
7. Huntress Jr., W.: Ion cyclotron resonance power absorption: Collision frequencies for $CO2^+$, $N2^+$, and $H3^+$ ions in their parent gases. J. Chem. Phys. **55**, 2146–2155 (1971)
8. Dymerski, P., Dunbar, R.: ICR study of nonreactive collision rate constants. J. Chem. Phys. **57**, 4049–4050 (1972)
9. Ridge, D., Beauchamp, J.: The interaction of ions with nonpolar neutrals: The collision broadening of ion cyclotron resonance lines of ions in hydrogen and methane. J. Chem. Phys. **64**, 2735–2746 (1976)
10. Jones, C.A., Dearden, D.V.: Collision cross sections for 20 protonated amino acids: Fourier transform ion cyclotron resonance and ion mobility results. J. Am. Soc. Mass Spectrom. **27**, 1366–1375 (2016)

11. Jiang, T., Chen, Y., Mao, L., Marshall, A.G., Xu, W.: Extracting biomolecule collision cross sections from the high-resolution FT-ICR mass spectral linewidths. Phys. Chem. Chem. Phys. **18**, 713–717 (2016)
12. Mao, L., Chen, Y., Xin, Y., Chen, Y., Zheng, L., Kaiser, N.K., Marshall, A.G., Xu, W.: Collision cross section measurements for biomolecules within a high-resolution Fourier transform ion cyclotron resonance cell. Anal. Chem. **87**, 4072–4075 (2015)
13. Yang, F., Voelkel, J.E., Dearden, D.V.: Collision cross sectional areas from analysis of fourier transform ion cyclotron resonance line width: a new method for characterizing molecular structure. Anal. Chem. **84**, 4851–4857 (2012)
14. Makarov, A., Denisov, E.: Dynamics of ions of intact proteins in the Orbitrap mass analyzer. J. Am. Soc. Mass Spectrom. **20**, 1486–1495 (2009)
15. He, M., Guo, D., Chen, Y., Xiong, X., Fang, X., Xu, W.: Ion collision crosssection measurements in quadrupole ion traps using a time–frequency analysis method. Analyst **139**, 6144–6153 (2014)
16. Zajfman, D., Rudich, Y., Sagi, I., Strasser, D., Savin, D.W., Goldberg, S., Rappaport, M., Heber, O.: High resolution mass spectrometry using a linear electrostatic ion beam trap. Int. J. Mass Spectrom. **229**, 55–60 (2003)
17. Hilger, R.T., Wyss, P.J., Santini, R.E., McLuckey, S.A.: Absorption mode Fourier transform electrostatic linear ion trap mass spectrometry. Anal. Chem. **85**, 8075–8079 (2013)
18. Hilger, R.T., Santini, R.E., McLuckey, S.A.: Nondestructive tandem mass spectrometry using a linear quadrupole ion trap coupled to a linear electrostatic ion trap. Anal. Chem. **85**, 5226–5232 (2013)
19. Hilger, R.T., Santini, R.E., McLuckey, S.A.: Tandem mass spectrometry in an electrostatic linear ion trap modified for surface-induced dissociation. Anal. Chem. **86**, 8822–8828 (2014)
20. Hilger, R.T., Santini, R.E., McLuckey, S.A.: Square wave modulation of a mirror lens for ion isolation in a Fourier transform electrostatic linear ion trap mass spectrometer. Int. J. Mass Spectrom. **362**, 1–8 (2014)
21. Hilger, R.T., Dziekonski, E.T., Santini, R.E., McLuckey, S.A.: Injecting electrospray ions into a Fourier transform electrostatic linear ion trap. Int. J. Mass Spectrom. **378**, 281–287 (2015)
22. Dziekonski, E.T., Santini, R.E., McLuckey, S.A.: A dual detector Fourier transform electrostatic linear ion trap utilizing in-trap potential lift. Int. J. Mass Spectrom. **405**, 1–8 (2016)
23. Dziekonski, E.T., Johnson, J.T., Hilger, R.T., McIntyre, C.L., Santini, R.E., McLuckey, S.A.: Voltage-induced frequency drift correction in fourier transform electrostatic linear ion trap mass spectrometry using mirror-switching. Int. J. Mass Spectrom. **410**, 12–21 (2016)
24. Dziekonski, E., Johnson, J.T., McLuckey, S.A.: Utility of higher harmonics in electrospray ionization fourier transform electrostatic linear ion trap mass spectrometry. Anal. Chem. **89**, 4392–4397 (2017)
25. Zajfman, D., Heber, O., Vejby-Christensen, L., Ben-Itzhak, I., Rappaport, M., Fishman, R., Dahan, M.: Electrostatic bottle for long-time storage of fast ion beams. Phys. Rev. A **55**, R1577–R1580 (1997)
26. Ring, S., Pedersen, H.B., Heber, O., Rappaport, M.L., Witte, P., Bhushan, K.G., Altstein, N., Rudich, Y., Sagi, I., Zajfman, D.: Fourier transform time-of-flight mass spectrometry in an electrostatic ion beam trap. Anal. Chem. **72**, 4041–4046 (2000)
27. Toker, Y., Altstein, N., Aviv, O., Rappaport, M.L., Heber, O., Schwalm, D., Strasser, D., Zajfman, D.: The kick-out mass selection technique for ions stored in an electrostatic ion beam trap. J. Instrum. **4**, P09001 (2009)
28. Verentchikov, A., Berdnikov, A., Yavor, M.: Stable ion beam transport through periodic electrostatic structures: linear and non-linear effects. Phys. Procedia **1**, 87–97 (2008)
29. Vlasak, P.R., Beussman, D.J., Ji, Q., Enke, C.G.: Method for the design of broad energy range focusing reflectrons. J. Am. Soc. Mass Spectrom. **7**, 1002–1008 (1996)
30. Cornish, T.J., Cotter, R.J.: A curved-field reflectron for improved energy focusing of product ions in time-of-flight mass spectrometry. Rapid Commun. Mass Spectrom. **7**, 1037–1040 (1993)
31. Lange, M., Froese, M., Menk, S., Varju, J., Bastert, R., Blaum, K., López-Urrutia, J.C., Fellenberger, F., Grieser, M., von Hahn, R.: A cryogenic electrostatic trap for long-time storage of keV ion beams. Rev. Sci. Instrum. **81**, 055105 (2010)
32. Breitenfeldt, C., Froese, M.W., Blaum, K., George, S., Grieser, M., Lange, M., Menk, S., Repnow, R., Schwalm, D., Schweikhard, L.: Spreading times of ion-bunches in the Cryogenic Trap for Fast ion beams. Int. J. Mass Spectrom. **396**, 1–4 (2016)
33. Pedersen, H.B., Strasser, D., Amarant, B., Heber, O., Rappaport, M.L., Zajfman, D.: Diffusion and synchronization in an ion-trap resonator. Phys. Rev. A **65**, 042704 (2002)
34. Strasser, D., Heber, O., Goldberg, S., Zajfman, D.: Self-bunching induced by negative effective mass instability in an electrostatic ion beam trap. J. Physiol. Biochem. **36**, 953 (2003)
35. Zajfman, D., Heber, O., Rappaport, M.L., Pedersen, H.B., Strasser, D., Goldberg, S.: Self-bunching effect in an ion trap resonator. J. Opt. Soc. Am. B **20**, 1028–1032 (2003)
36. Froese, M.W., Lange, M., Menk, S., Grieser, M., Heber, O., Laux, F., Repnow, R., Sieber, T., Toker, Y., von Hahn, R.: The decay of ion bunches in the self-bunching mode. New J. Phys. **14**, 073010 (2012)
37. Guo, D., Xin, Y., Li, D., Xu, W.: Collision cross section measurements for biomolecules within a high-resolution FT-ICR cell: theory. Phys. Chem. Chem. Phys. **17**, 9060–9067 (2015)
38. Van Berkel, G.J., Asano, K.G., Schnier, P.D.: Electrochemical processes in a wire-in-a-capillary bulk-loaded, nano-electrospray emitter. J. Am. Soc. Mass Spectrom. **12**, 853–862 (2001)
39. Loboda, A., Krutchinsky, A., Loboda, O., McNabb, J., Spicer, V., Ens, W., Standing, K.: Novel Linac II electrode geometry for creating an axial field in a multipole ion guide. Eur. J. Mass Spectrom. **6**, 531–536 (2000)
40. Keifer, D.Z., Alexander, A.W., Jarrold, M.F.: Spontaneous mass and charge losses from single multi-megadalton ions studied by charge detection mass spectrometry. J. Am. Soc. Mass Spectrom. **28**, 498–506 (2017)
41. Bush, M.F., Hall, Z., Giles, K., Hoyes, J., Robinson, C.V., Ruotolo, B.T.: Collision cross sections of proteins and their complexes: a calibration framework and database for gas-phase structural biology. Anal. Chem. **82**, 9557–9565 (2010)
42. May, J.C., Goodwin, C.R., Lareau, N.M., Leaptrot, K.L., Morris, C.B., Kurulugama, R.T., Mordehai, A., Klein, C., Barry, W., Darland, E.: Conformational ordering of biomolecules in the gas phase: nitrogen collision cross sections measured on a prototype high resolution drift tube ion mobility-mass spectrometer. Anal. Chem. **86**, 2107–2116 (2014)
43. Campuzano, I., Bush, M.F., Robinson, C.V., Beaumont, C., Richardson, K., Kim, H., Kim, H.I.: Structural characterization of drug-like compounds by ion mobility mass spectrometry: comparison of theoretical and experimentally derived nitrogen collision cross sections. Anal. Chem. **84**, 1026–1033 (2011)
44. Giles, K., Palmer, M., Richardson, K., Tomczyk, N.: Comparison of CCS(N_2) measurements obtained from two different T-Wave ion mobility systems with direct measurements using a drift tube ion mobility system. (2015) Available at: http://www.waters.com/webassets/cms/library/docs/2015asms_giles_comparison_of_CCS_N2_print.pdf